Characterization and design of coherent optical OFDM transmission systems based on Hartley Transform

PhD Dissertation

Author: Marcin Chochol
Centre Tecnologic de Telecomunicacions de Catalunya (CTTC)
Parc Mediterrani de la Tecnologia B-4
Av. Carl Friedrich Gauss 7 S/N
08860 - Castelldefels (Spain)
E-mail: mchochol@cttc.es

PhD Thesis Advisor: Dr. Josep M. Fabrega
Research Associate
Centre Tecnologic de Telecomunicacions de Catalunya (CTTC)
E-mail: jmfabrega@cttc.es

PhD Thesis Tutor: Prof. Gabriel Junyent
Full-time Professor
Universitat Politecnica de Catalunya (UPC)
Campus Nord UPC, Ed. D5
c/ Jordi Girona, 1-3
08034 Barcelona (Spain)
E-mail: junyent@tsc.upc.edu

Abstract

Nowadays, due to huge deployment of optical transport networks, a continuous increase towards higher data rates up to 100 Gb/s and beyond is observed. Furthermore, an evolution of the current optical networks is forecasted, acquiring new functionalities, e.g. elastic spectrum assignment for the optical signals. The target for these new challenges in transmission is to find techniques ready to deal with a growth of demand for bandwidth continuously asked by network operators, for whom the standard systems do not meet the new functionalities while higher rates are being set up. A solution for covering all of those needs is to adapt techniques capable to deal with such enormous data rates, and ensuring the same high efficiency for long distances and mitigate the optical impairments accumulated along the transmission path. Additionally, these transmission techniques are expected to provide some degree of flexibility, in order to enhance the network flexibility.

A promising technology that can fully cope with those requires is the coherent optical orthogonal frequency division multiplexing (CO-OFDM). CO-OFDM provides several advantages, namely high sensitivity and spectral efficiency, simple integration and possibility to fully recover a signal in phase, amplitude and polarization. These systems are composed by digital signal processing (DSP) blocks that easily process data and can equalize and compensate the main impairments, providing high tolerance for dispersion effects. However, CO-OFDM systems are not free from drawbacks. Their high peak-to-average power ratio (PAPR) reduce their tolerance to nonlinearities. Furthermore, CO-OFDM systems are sensitive to any frequency shift and phase offset.

Hence, a constant envelope optical OFDM (CE-OFDM) is proposed for significantly reducing the PAPR and solving high sensitivity to nonlinear impairments. It consists in a phase modulated discrete multi-tone signal, which is coherently detected at the receiver side. An alternative transform, the discrete Hartley transform, is proposed to speed up calculations in the DSP and eliminate the need to have a Hermitian symmetry. The optical CE-OFDM by its unique flexibility and rate scalability turns out as a great technology applicable to different configurations, ranging from access to core networks. In case of access solutions, several cases are investigated. First, the optical CE-OFDM is applied for radio access network signals delivery by means of a wavelength division multiplexing (WDM) overlay in deployed access architecture. A decomposed radio access network is deployed over an existing standard passive optical network (PON), capable to avoid interference and cross talks with access signals between network clients. The system exhibited narrow channel spacing, while reducing losses fed into the access equipment path. Next, a full duplex 10 Gb/s bidirectional PON transmission over a single wavelength with RSOA based ONU is investigated. The key point of that system is the upstream transmission, which is achieved re-modulating the phase of a downstream intensity modulated

signal after proper saturation. The reported sensitivity performances show a power budget matching the PON standards and an OSNR easy to reach on non-amplified PON. Next, a flexible metropolitan area network of up to 100km with traffic add/drop using WDM is investigated. There the narrowing effect of the optical filters is studied. Finally, an elastic upgrade of the existing Telefonica model of the Spanish national core network is proposed. For that, the transceiver architecture is proposed to be operated featuring polarization multiplexing. Respect to the existing fixed grid, the flexible approach (enabled by the CE-OFDM transceiver) results into reduced bandwidth occupancy and low OSNR requirement.

Resumen

Hoy en día, debido al gran despliegue de las redes de ópticas de transporte, se espera un aumento continuado hacia mayores velocidades de datos, hasta 100 Gb/s y más allá. Por otra parte, la evolución que se prevé para las redes ópticas actuales, incluye la adquisición de nuevas funcionalidades, por ejemplo, la asignación del espectro de forma elástica para las señales ópticas. Por tanto, el claro desafío en cuanto a las tecnologías de transmisión es encontrar técnicas preparadas para hacer frente a un crecimiento de la demanda de ancho de banda; demanda que continuamente se incrementa por parte de los operadores de red, para quienes los sistemas estándar no se acaban de ajustar a las nuevas funcionalidades que esperan para la red. Una solución para cubrir todas estas necesidades es la adaptación de técnicas capaces de hacer frente a estas velocidades de datos enormes, y garantizar el mismo nivel de eficiencia para las largas distancias y mitigar las deficiencias ópticas acumuladas a lo largo de la ruta de transmisión. Además, se espera que estas técnicas de transmisión puedan proporcionar cierto grado de flexibilidad, a fin de mejorar y hacer más eficiente la gestión de la red.

Una tecnología prometedora que puede hacer frente a estos requisitos es lo que se llama multiplexación por división de frecuencias ortogonales, combinado con la detección óptica coherente (CO-OFDM). CO-OFDM ofrece varias ventajas, entre otras: alta sensibilidad y eficiencia espectral y, sobre todo, la posibilidad de recuperar por completo de una señal en fase, la amplitud y la polarización. Estos sistemas están compuestos por bloques de procesado de señales digitales (DSP) que permiten detectar los datos fácilmente así como también compensar las principales degradaciones, proporcionando alta tolerancia a los efectos de dispersión. Sin embargo, los sistemas CO-OFDM no están exentos de inconvenientes. Su alta relación de potencia de pico a potencia media (PAPR) reduce sensiblemente la tolerancia no linealidades. Por otra parte, los sistemas CO-OFDM son sensibles a cualquier cambio de frecuencia y desplazamiento de fase.

Por tanto, se propone un sistema OFDM de envolvente constante (CE-OFDM) para reducir significativamente la PAPR y solucionar la alta sensibilidad a las degradaciones no lineales. Consiste en una señal OFDM modulada en fase, que se detecta coherentemente en el receptor. Una transformada alternativa, la transformada discreta de Hartley, se propone para acelerar los cálculos en el DSP. El sistema CE-OFDM por su flexibilidad y escalabilidad única, resulta una tecnología aplicable a diferentes escenarios, que van desde las redes de acceso hasta las redes troncales. En el caso de las soluciones de acceso, se investigan varios casos. En primer lugar, el CE-OFDM aplica para el desarrollo y soporte de datos de una red radio, reutilizando una red óptica de acceso ya desplegada. A continuación, se investiga la transmisión bidireccional dúplex a 10 Gb / s sobre una sola longitud de onda empleando un RSOA a las unidades de usuario. El punto clave de este sistema es la transmisión en sentido ascendente, que se consigue re-modulando la fase de una señal de intensidad modulada después de saturar de forma adecuada. A

continuación, se estudia una red de área metropolitana flexible de hasta 100 km. Concretamente el efecto de concatenación de filtros ópticos es el objetivo de este estudio. Finalmente, se propone una actualización elástica del modelo de Telefónica I + D para la red troncal española. Por ello, se propone operar el CE-OFDM en multiplexación de polarización. Los resultados muestran que esta combinación reduce sensiblemente el empleo de ancho de banda esto como los requisitos de los enlaces transmisión, reduciendo también los costes tanto de desarrollo como de operación y mantenimiento de la red.

Resum

Avui dia, a causa del gran desplegament de les xarxes de òptiques de transport, s'espera un augment continuat cap a majors velocitats de dades, fins a 100 Gb/s i més enllà. D'altra banda, l'evolució que es preveu per a les xarxes òptiques actuals, inclou l'adquisició de noves funcionalitats, per exemple, assignació de l'espectre de forma elàstica per als senyals òptics. Per tant, el clar desafiament pel que fa a les tecnologies de transmissió és trobar tècniques preparades per fer front a un creixement de la demanda d'ample de banda; demanda que contínuament es fa per part dels operadors de xarxa, per als qui els sistemes estàndard no s'acaben d'ajustar a les noves funcionalitats que esperen per a la xarxa. Una solució per a cobrir totes aquestes necessitats és l'adaptació de tècniques capaces de fer front a aquestes velocitats de dades enormes, i garantir el mateix nivell d'eficiència per a les llargues distàncies i mitigar les deficiències òptiques acumulades al llarg de la ruta de transmissió. A més, s'espera que aquestes tècniques de transmissió puguin proporcionar cert grau de flexibilitat, per tal de millorar i tornar més eficient la gestió de la xarxa.

Una tecnologia prometedora que pot fer front a aquests requisits és el que s'anomena multiplexació per divisió de freqüències ortogonals, combinat amb la detecció òptica coherent (CO-OFDM). CO-OFDM ofereix diversos avantatges, entre altres: alta sensibilitat i eficiència espectral i, sobretot, la possibilitat de recuperar per complet d'una senyal en fase, l'amplitud i la polarització. Aquests sistemes estan compostos per blocs de processament de senyals digitals (DSP) que permeten detectar les dades fàcilment així com també compensar les principals degradacions, proporcionant alta tolerància pels efectes de dispersió. No obstant això, els sistemes CO-OFDM no estan exempts d'inconvenients. La seva alta relació de potència de pic a potència mitjana (PAPR) redueix sensiblement la tolerància a no linealitats. D'altra banda, els sistemes de CO-OFDM són sensibles a qualsevol canvi de freqüència i desplaçament de fase.

Per tant, es proposa un sistema OFDM d'envolvent constant (CE-OFDM) per a reduir significativament la PAPR i solucionar l'alta sensibilitat a les degradacions no lineals. Consisteix en un senyal OFDM modulat en fase, que es detecta coherentment en el receptor. Una transformada alternativa, la transformada discreta d'Hartley, es proposa accelerar els càlculs en el DSP. El sistema CE-OFDM per la seva flexibilitat i escalabilitat única, resulta una tecnologia aplicable a diferents escenaris, que van des de les xarxes d'accés fins a les xarxes troncals. En el cas de les solucions d'accés, s'investiguen diversos casos. En primer lloc, el CE-OFDM s'aplica per al desplegament i suport de dades d'una xarxa radio, reutilitzant una xarxa òptica d'accés ja desplegada. A continuació, s'investiga la transmissió bidireccional dúplex a 10 Gb/s sobre una sola longitud d'ona emprant un RSOA a les unitats d'usuari. El punt clau d'aquest sistema és la transmissió en sentit ascendent, que s'aconsegueix re-modulant la fase d'un senyal d'intensitat modulada després de saturar-la de forma adequada. A continuació, s'estudia una xarxa d'àrea metropolitana flexible de fins a 100 km. Concretament l'efecte de concatenació de filtres òptics

és l'objectiu d'aquest estudi. Finalment, es proposa una actualització elàstica del model de Telefónica I+D per a la xarxa troncal espanyola. Per això, es proposa operar el CE-OFDM en multiplexació de polarització. Els resultats mostren que aquesta combinació redueix sensiblement l'ocupació d'ample de banda això com també els requisits dels enllaços transmissió, reduint també els costos tant de desplegament com d'operació i manteniment de la xarxa.

Acknowledgment

Many years have passed when I realized that a doctorate in optical communication is my target. I have done what really implied to me, my own intuition. I was doing whatever I can in order to commence, go through and successfully complete a PhD, passing all the steps towards final thesis dissertation. The time, years I spent over a doctorate at CTTC belonged to the most experiencing part of my life, of me while I managed myself to deal with a new environment of Castelldefels where I live since the beginning of 2009, new international people whose I met by sharing an apartment and making fun in Barcelona and struggle with problems that you can have anytime during a life. I would not be in trouble if I say that I love Catalunya since it acted as my new home that I like so much until now.

In the first place, I appreciate to CTTC for giving me a chance to work towards my PhD in one of the most beautiful region of Europe.
During my research I participated in several projects and it has to be pointed out that the most important ones related to applications are detailed as follows,

- ✓ the Spanish MINECO projects TEC2009-07995 (DORADO) and TEC2012-38119 (FARO) related to the generation access,
- ✓ the Spanish MINECO projects TEC2009-07995 (FARO) along with the EU-FP7 project IDEALIST (GA-317999) in the part in case of fixed mobile conversion,
- ✓ the DORADO project sponsored by Spanish MICINN (TEC2009-07995) in respect to the filter concatenation for a flexible metropolitan area network,
- ✓ the EU-FP7 integrated project IDEALIST (G.A.317999) and the Spanish MINECO project TEC2012-38119 (FARO) for elastic upgrade of transport network.

Coming back to reality, the old maxim turned out to be up to date. According to it when you are about to do something, let's focus on it, do whatever you want but do not forget about the goal. When you suffer or the problems occupy your mind, try to figure out how something can be fixed and do not panic, try to avoid some misunderstandings and continue keep pushing… here I would like to sincerely thank you – Dr. Josep M. Fabrega.

I am grateful that you were and helped me to understand a lot of issues from the field and from the human nature! Thank you for your supervision, support and motivation to act.
I want to thank all the people from CTTC I have collaborated with during this time. Especial thanks for the chance and positive fervour to work for Dr. Raul Muñoz and Dr. Michela Svaluto Moreolo. I would also like to thank my UPC tutor Prof. Gabriel Junyent for his contribution. I will never forget Fco. Javier Vilchez since I would always count on him in many aspects not only related to work. Laia Nadal, thanks for your attitude and your ideas.
Simo Aliana is and will be the guru of never ending open-minded discussions and good person for sure. I really appreciate his push to work.

In this point I would like also to express that I am really grateful my mum Barbara, father Leszek, sisters Magdalena and Marzena and grandfather Edward for everything what you did to me, all of your selfless support, warm words and continuous belief that I can.

Finally, I figured out that without my attempts and mistakes as well I could not reach the point where I am right now. I keep and will keep trying to make my future world better always focusing on the goal.

Marcin Chochol
Castelldefels, Spain
July, 2013

Contents

Abstract I
Resumen III
Resum V
Acknowledgment VII
Contents IX
List of Acronyms XI
Notation XII
CHAPTER 1: INTRODUCTION ..... - 1 -
1.1 Motivation ..... - 1 -
1.2 Overview and Content of the Thesis ..... - 3 -
CHAPTER 2: RELEVANT THEORY OF OFDM ..... - 4 -
2.1 State of the Art ..... - 4 -
2.1.1 OFDM Systems Classification ..... - 4 -
2.1.1.1 OFDM Principle ..... - 4 -
2.1.1.2 Optical OFDM Systems ..... - 6 -
2.1.2 Transforms applied in Optical OFDM ..... - 10 -
2.1.3.1 Discrete Fourier Transform (DFT) and Discrete Hartley Transform (DHT) ..... - 10 -
2.1.3.2 Discrete Wavelet Transform (DWT) ..... - 11 -
2.1.3.3 Discrete Cosine Transform (DCT) and Discrete Sine Transform (DST) ..... - 12 -
2.1.3 Recent applications in optical-OFDM based on coherent detection ..... - 13 -
2.1.4 Recent applications in Access/Metro Networks and Long Haul Systems ..... - 17 -
2.1.4.1 Optical OFDM in Long Haul applications ..... - 17 -
2.1.4.2 Optical OFDM in Access/Metro Networks applications ..... - 21 -
2.2 Main objectives and description of the architecture ..... - 24 -
2.2.1 Background and description of the research proposal ..... - 24 -
2.2.2 Goals ..... - 26 -
2.2.3 Methodology ..... - 28 -
CHAPTER 3: ANALYTICAL DESCRIPTION OF OPTICAL CE-OFDM SYSTEM ..... - 29 -
3.1 General Principle of Operation for Proposed Scenario ..... - 30 -
3.1.1 DSP at Transmission ..... - 30 -
3.1.2 Optoelectronics at Transmission ..... - 33 -

3.1.3 Channel transmission ..... - 36 -
3.1.4 Optoelectronics at Reception ..... - 36 -
3.2 Chapter Summary ..... - 44 -
CHAPTER 4: CHARACTERIZATION OF OPTICAL CE-OFDM SYSTEM ..... - 45 -
4.1 Impact of Modulator Driving ..... - 45 -
4.1.1 Sensitivity Performance ..... - 45 -
4.1.2 Optical Noise Performance ..... - 52 -
4.2 Impact of Phase Noise ..... - 57 -
4.3 Impact of Frequency Offset ..... - 60 -
4.4 Impact of IQ Imbalance ..... - 64 -
4.5 Impact of Dispersion ..... - 68 -
4.6 Chapter Summary ..... - 71 -
CHAPTER 5: APPLICATIONS IN ACCESS AND TRANSPORT NETWORKS ..... - 73 -
5.1 Applications in Access Networks ..... - 73 -
5.1.1 Next Generation Access ..... - 73 -
5.1.2 Fixed Mobile Conversion ..... - 82 -
5.2 Applications in Optical Transport Networks ..... - 97 -
5.2.1 Flexible Metropolitan Area Network ..... - 97 -
5.2.2 Metro/Regional National Network ..... - 104 -
5.3 Chapter Summary ..... - 109 -
CHAPTER 6: CONCLUSIONS AND FUTURE WORK ..... - 111 -
6.1 Conclusions ..... - 111 -
6.2 Future Work ..... - 112 -
BIBLIOGRAPHY ..... - 114 -

List of Acronyms

ADC	Analog to Digital Converter
ASE	Amplified Spontaneous Emission
BPSK	Binary Phase-Shift-Keying
BER	Bit Error Rate
CD	Chromatic Dispersion
CE	Constant Envelope
CP	Cyclic Prefix
DAC	Digital to Analog Converter
DHT	Discrete Hartley Transform
DFT	Discrete Fourier Transform
DSP	Digital Signal Processing
DWDM	Dense Wavelength Division Multiplexing
GVD	Group Velocity Dispersion
O-E-O	Optical-Electrical-Optical
I-Q	In-phase and quadrature
IDHT	Inverse Discrete Hartley Transform
IM/DD	Intensity Modulation Direct Detection
ITU	International Telecommunications Union
LO	Local Oscillator
MAN	Metropolitan Area Network
MZM	Mach-Zehnder Modulator
OFDM	Orthogonal Frequency Division Multiplexing
OLT	Optical Line Terminal
ONU	Optical Network Unit
OSNR	Optical Signal to Noise Ratio
OTN	Optical Transport Networks
OXC	Optical Cross-Connects
PAPR	Peak to Average Power Ratio
PAM	Pulse Amplitude Modulation
PIN	Positive Intrinsic Negative
PMD	Polarization Mode Dispersion
PM	Phase Modulation
PolMux	Polarization Multiplexing
PON	Passive Optical Networks
RAN	Radio Access Network
R-OADM	Reconfigurable Optical Add-Drop Multiplexers
RSOA	Reflective Semiconductor Optical Amplifiers
SSMF	Standard Single Mode Fiber
TDM	Time Division Multiplexing
TS	Training Symbols
WSON	Wavelength Switched Optical Networks

Notation

A	Signal amplitude
A_{eff}	Effective area of fiber as the area of the guided mode
α	Attenuation factor
β_2	Second-order differentiation of the propagation constant-dispersion velocity dispersion (GVD)
β_3	Third-order differentiation of the propagation constant-dispersion slope
c	Velocity of light in vacuum (c=2.998e8 m/s)
D	Dispersion factor (usual unit=ps/nm/km)
E_k	Phase error component
$erfc$	Complementary error function
F_n	Noise figure
γ	Nonlinear coefficient
h	Planck's constant (6.624e-34 J-s)
H	Modulation index
i_s	Signal current
i_d	Dark current of photodetector
k_B	Boltzmann's constant (1.38e-23 J/K)
L	Length of optical fiber
λ	Operating wavelength
n	Refractive index
N_k	Additive noise component
ϕ_e	Arbitrary phase (phase noise)
ω_S	Optical carrier frequency
ω_{LO}	Optical LO frequency
φ	Phase signal carrying data
P_S	Power of data signal
P_{LO}	Power of local oscillator
q	Electronic charge (1.6e-16 C)
R	Responsivity of photodetector
R_L	Load resistance
S_k,	Signal component
σ_s	Variance of the data signal
σ_φ	Variance of the optical phase
T	Absolute temperature (K)
T_B	OFDM block period
T_S	OFDM symbol period
τ_g	Guard period
θ_i	Arbitrary phase offset
V_π	Driving voltage of π phase change
$*$	Convolution operator

CHAPTER 1: INTRODUCTION

1.1 Motivation

New technological challenges in Optical Transport Networks (OTN) have risen during last years because of the evolution of optical systems towards 100 Gb/s and beyond. Due to the continuous bandwidth demand by the IP traffic growth, the real move towards Dense Wavelength Division Multiplexing (DWDM) was observed. In a first generation, the optical transport in SONET/SDH technology was based on electrical switching, requiring Optical-Electrical-Optical conversion (O-E-O) for re-amplifying, re-shaping and re-timing the optical signal (namely 3R regeneration) [Shen07]. O-E-O regenerators were used to maintain the acceptable level of the signal quality. Moreover, the SONET/SDH technology taking into consideration the bandwidth scalability was completely opaque, and evolved towards all-optical switching networks. The real factor that enabled to deploy optical architecture was based on the use of Optical Cross-Connects (OXC) and Reconfigurable Optical Add-Drop Multiplexers (R-OADM) at network nodes [Hibino07, Shen07]. These last given nodes eliminated the need to make the routing and switching in the electrical domain indicating future benefits as freedom on bit rate, data formats and cost reduction. Therefore, Optical Transport Networks evolved moving from SONET/SDH technology towards end-to-end light-paths and the networks generally called wavelength switched optical networks (WSON) [Hibino07]. Nevertheless, due to the lack of O-E-O regeneration, the accumulation of optical impairments arose. Optical signals that pass through optical links started to be more sensitive to different optical impairments both linear and non-linear; e.g. amplified spontaneous emission (ASE) noise, chromatic dispersion (CD), polarization mode dispersion (PMD) or cross-talk.

Today, the current optical network infrastructure is mostly based on point-to-point virtual connections between the nodes over the network set up in DWDM configuration [Chochol12a]. Continuous demand for bandwidth and various other client needs, reached the point where the existing technology mainly exhibiting the data rate up to 10 Gb/s became insufficient due to the speed that has already attained maturity. In order to cope with these limitations, the network providers install higher bit rates going beyond 100 Gb/s per wavelength [Gerstel12]. The spectral width occupied by data rates greater than 100 Gb/s at standard modulation formats are too broad to fit well into the 50 GHz ITU-T fixed grid. Adopting formats with higher spectral efficiency, the rates can be obliged to fit, however it can benefit only for short distances. So, the challenge is to transmit such a broad spectrum associated with high data rate at high spectral efficiency over long distances [Gerstel12]. In order to address the challenge, new features of transceivers are proposed. The transceivers maximize spectral efficiency by adapting to the actual traffic conditions. In turn, the data rate is properly chosen depending on the demands at each node located across the network. The fixed grid due to its low flexibility and efficiency is being replaced by more dynamic solution with better and easier adaptation to the traffic congestion [Chochol12a, FabregaMch13c]. The shift from rigid optical networks based on fixed properties to spectrally efficient elastic optical networks with flexible bandwidth and adaptive channel spacing is observed. [Jinno12]

The flexible networking [Gerstel12, FabregaMch13c] becomes a sample solution that from one side can help to satisfy better the needs of the clients, and support the network with elastic and intelligent elements from other side.
Hence, based on the evolution of Optical Transport Networks and elastic optical networking as a new dawn for the optical layer [Gerstel12], the challenge is twofold. First to mitigate transmission impairments and second to provide high-data rate transmission evolving towards 100 Gb/s and beyond. All this can be done by adapting the promising Orthogonal Frequency Division Multiplexing (OFDM) technique to optical networks. As a candidate for optical communication and a multicarrier transmission technique itself, OFDM allows the signal transmission over several subcarriers at lower-rate. The subcarriers are orthogonal to each other and, thus, their spectra are able to overlap [Shieh10]. This results in a very high spectral efficiency unique to OFDM. Also, its high tolerance to dispersion impairments reduces the commercially available per-span compensators and offers alternative electronic dispersion compensation (EDC) [Shieh10, Buchali09, Schmidt08]. Basically, its implementation has been framed into two different optical schemes: Intensity modulation with direct detection (IM-DD) [Leibrich09], and coherent detection [Shieh08]. Direct detection proposes the simplest scheme, achievable mostly using off-the-shelf components; whereas coherent systems need more specific hardware but are capable to achieve higher sensitivity and spectral efficiency. Among the properties of coherent optical OFDM systems, it should be highlighted that they are capable to recover the full information of the received optical field (amplitude, phase and polarization), which, combined with digital signal processing, is very promising for compensating the typical optical impairments.

Even the most popular optical OFDM is based on digital signal processing techniques for obtaining the orthogonal subcarriers modulation, an alternative based on all-optical signal processing is currently a very interesting and active field. Precisely, it has recently shown the absolute world record transmitting 26 Tb/s per channel using an all-optical fast-Fourier transform [Hillercuss11]. Nevertheless, the main drawbacks of such systems include poor subcarriers number (yielding to low spectral efficiency), low capabilities capability for system impairments equalization, and reduced granularity. As one of the key features of OFDM to be exploited in the thesis is such a capacity to equalize and compensate the main impairments in optical links, these all-optical OFDM systems fall out of the scope of the thesis and will not be considered.

One of the main drawbacks of OFDM (electrical or optical) is that the modulated waveform has high amplitude fluctuations. Those fluctuations produce large peak-to-average power ratios (PAPRs), which substantially reduces the fiber nonlinearity tolerance [Armstrong09, Jansen08a]. To solve this critical issue about large PAPR and high sensitivity to nonlinear impairments, a novel approach is proposed to be studied in the present thesis. Back in 2008, a new technique called Constant Envelope OFDM (CE-OFDM) was proposed for reducing PAPR based on signal transformation [Thompson08]. Such a technique uses a phase modulation of the OFDM symbols for achieving the lowest PAPR possible; and recently it has been ported to the optical domain [Silva10, Wu10, Huene11]. In our case it is proposed to use a pure optical phase modulation of the each OFDM symbol, and combine it with coherent detection. One of the core functions of the proposed modulation format will be the use of the Hartley transform [Svaluto10, Svaluto11]. Thanks to this alternative transform, it is expected to speed up the signal processing at OFDM

transmitter and receiver while eliminating the constraint to have Hermitian symmetry [Svaluto10, Svaluto12].

1.2 Overview and Content of the Thesis

The dissertation consists of six chapters, where the review material and novel contributions are presented. It presents a novel optical OFDM system based on Hartley transform that works over optical phase modulation and in the regime of coherent detection.
The thesis is organized as follows.

In chapter 2, the state of the art with the main objectives for a PhD research and the description of the initial architecture proposed in the thesis are stated. The state of the art will cover the existing OFDM systems classification, OFDM principle and typical applications corresponding to the coherent optical OFDM, access/metro networks and long-haul. In case of objectives, the goals and an appropriate research methodology will support this section.

In chapter 3, the scheme explanation related to the novel optical CO-OFDM transmission system based on phase modulation and Hartley transform will be given. The system proposed will be explained in detail in terms of properties, functionality and any additional features corresponding to the individual elements of the transmission scheme in which the thesis is focused.

In chapter 4, the theory and simulations supporting theory will be evaluated. In matter of fact, three different impacts stemmed from the system functionality and the transmission itself while the impairments deteriorating propagation will be under investigation. First, the case of modulator driving featured by receiver sensitivity and optical amplification noise [Chochol12, FabregaMCh13a] will be revised. Later on, the impact of individual phase noise, frequency offset and IQ imbalance will be discussed. In both cases, proper sensitivity curves collected at 10^{-3} BER in the function of standard deviation of the transmitted phase will be plotted. At the end, the propagation based on split-step Fourier method will be briefly described. Afterwards, the impact of dispersion as a main impairment while propagating signal featured by special electrical filter to combat dispersion implemented at DSP will be manifested.

In chapter 5, the use cases and several applications with the emphasis to access/metro networks and core optical transport networks will be provided. In the first part, the access networks will be under revision. The applications featuring next generation access based on the phase modulated optical OFDM upstream employing IM/DD downstream for achieving bidirectional transmission along with the fixed mobile conversion by deploying a decomposed radio access network across an optical access network will be presented [FabregaMCh13b, Chochol12b]. Next, the long haul applications supporting an optical transport network will be investigated. The optical transport networks will be addressed in regard to the concatenation effect of optical filters [Chochol12a] together with flexible networking aspects devoted to the existing core network infrastructure deployed within the Telefonica I+D national network model [FabregaMCh13c], where the elastic functionalities are applied.

In chapter 6, the conclusions from individual chapters (from 3 to 5) along with the future plan for investigation will be exhibited. Next to the chapter 6, the bibliography is placed.

CHAPTER 2: RELEVANT THEORY OF OFDM

2.1 State of the Art

The target of the present thesis requires the knowledge of the up-to-date state of the art in several topics. This section gives an overview of the main OFDM techniques that shape the current research scene and particular scenarios of the proposed solutions. This part contains several subsections among which the most important are:

- OFDM systems classification that involves: principle of operation for OFDM systems and different OFDM optical systems;

- Transforms applied in optical communications e.g. Discrete Fourier Transform (DFT), Discrete Hartley Transform (DHT), Discrete Wavelet Transform (DWT), Discrete Cosine Transform (DCT) and Discrete Sine Transform (DST);

- Recent applications of optical OFDM in access/metro networks and long haul transmission systems.

2.1.1 OFDM Systems Classification

Recently, the orthogonal frequency division multiplexing (OFDM) has been proposed as a potential technique for next generation optical systems. In general, the Optical-OFDM (O-OFDM) is based on Fourier transform to attain subcarriers orthogonality and deploy complex digital modulations formats (e.g. QAM, QPSK, DPSK, etc.). The following subsections will deal with the principle of operation for Optical-OFDM systems and their classification.

2.1.1.1 OFDM Principle

In this subsection, the main principle of operation of OFDM systems is going to be introduced. The process of signal generation and detection in OFDM is shown in Fig. 2.1. Fig. 2.1 contains digital signal processing (DSP) blocks at transmitter and receiver part. Additionally the type of the signals that take part in the process is distinguished. The basic concept of OFDM is quite simple. OFDM as a transmission technique transmits high bit data rate over several parallel streams at low bit data rate. So, the incoming data are parallelized and transmitted on a number of different frequencies. As a multi carrier modulation, OFDM employs a large number of closely spaced frequencies called subcarriers. The subcarriers are used to modulate the incoming data at each of this parallel stream. Subcarriers are orthogonal to each other. It means that they are not able to interact each other and are fully independent. So, the cross-talk between the sub-carriers is not possible and hence inter-carrier guard bands are not required [Armstrong09, Buchali09, Shieh08].
So, the parallelized data are first mapped using one of commonly applied modulations like QAM or QPSK. The mapped data in the form of modulated complex symbols go to the inverse transform block, usually an inverse fast Fourier transform (IFFT). IFFT is the main part in the

transmitter and FFT in the receiver. Moreover, since the data is in frequency domain, IFFT is applied at transmitter and FFT used at receiver part. Formally, the input of the IFFT can be written as the complex vector $X_k = [X_0\ X_1\ X_2\ ...\ X_{N-1}]^T$ where N denotes the size of IFFT input and reflects the maximum number of OFDM subcarriers [Armstrong09]. Each of the elements of vector X_k represents the data to be carried on the corresponding subcarrier k. The IFFT produces a complex valued time domain waveform containing the superposition of all the subcarriers.
The output of IFFT is the complex vector $x_n = [x_0\ x_1\ x_2\ ...\ x_{N-1}]^T$. Mathematically, the OFDM signal for $0 \le n \le N-1$ is expressed as [Armstrong09]:

$$x_n = \frac{1}{\sqrt{N}} \sum_{k=0}^{N-1} X_k \cdot \exp(j \frac{2\pi}{N} kn) \qquad (2.1)$$

Afterwards, the training symbols (TS) and cyclic prefix (CP) are added to the IFFT output. Training symbols are dummy OFDM symbols used as a known reference for further equalization and synchronization at the receiver side. Therefore, the more stable a channel is, the less training symbols are required. The overhead of training symbols is dependent on the channel properties. E.g. fluctuations in the channel generated by linear and nonlinear phenomena explain the need to apply more symbols. In the case of optical OFDM systems it oscillates between 2-4 % [Jansen08b].

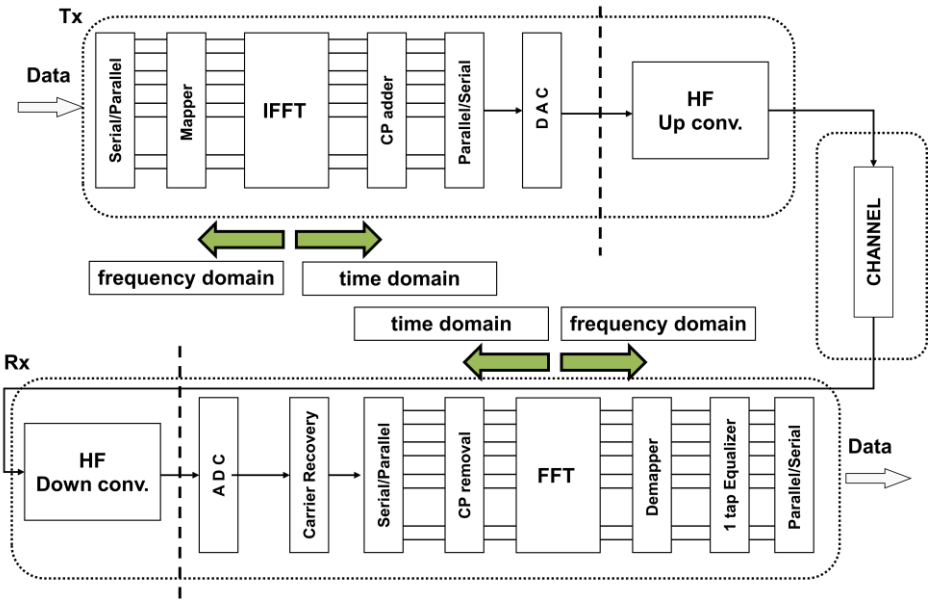

Figure 2.1 Block diagram of OFDM communication system.

Regarding the cyclic prefix, it is applied to prevent the system degradation by inter symbol interference (ISI) and inter carrier interference (ICI). Basically it consists of a cyclic extension of the OFDM symbol coming from the IFFT block [Buchali09, Jansen08b, Peng08]. It is achieved by repeating e.g. at the beginning of the symbol the last part of the OFDM symbol. So, instead of introducing x_k to the system, the sequence $x_{CP} = [x_{N-G}\ ...x_{N-1}\ x_0\ ...\ x_{N-1}]^T$ is transmitted towards optical channel, being G the length of the CP. With such a CP, the OFDM system becomes more resilient to any kind of dispersion during transmission over the optical channel. So, CP depends on the amount of chromatic dispersion (CD) that has to be compensated. By increasing the CP,

the CO-OFDM system is more robust, but as a trade-off it results in a non-negligible data rate overhead. To avoid signal distortion, the CP has to be chosen sufficiently large corresponding to the maximum length of the expected ISI [Buchali09]. However, longer CP could reduce the OFDM data duration and increase the frequency spacing between the subcarriers, that would broaden the signal bandwidth and exaggerate the total CD effect [Peng08]. Since CP typically performs a guard band without carrying information, a longer CP for longer distance will need more optical power to reach the same performance. For easily finding the right length of cyclic prefix at each OFDM symbol x_k, in [Jansen08b] was given that $\tau_{cp} = DB_d c / f^2$, where: D denotes the CD of transmission distance, B_d the effective BW of modulated OFDM signal, c the speed of the light, and f the centre frequency of OFDM band. Obviously it is an approximation, taking into account only the second order dispersion term of the optical fiber.
In turn, OFDM symbols with CP overhead x_{CP} are serialized and processed at digital to analog converter (DAC). DAC is needed after serialization in the transmitter part. Here a discrete time valued OFDM signal is converted to the analog domain [Buchali09]. This converter works at a given sampling rate. So, the maximum subcarrier frequency is equal to the Nyquist frequency $f_{Nyquist}$ that reflects to the half of the sample rate frequency R according to the formula: $f_{Nyquist} \leq R / 2$. Please note that the IFFT size has no impact on data rate. The data rate of OFDM systems depends on the number of bits per OFDM symbol and the symbol duration. Note that discrete signals at both input and output of the IFFT for each symbol have the same total energy and average power.
Next, the analog OFDM signal traverses the channel and is detected at receiver part. Optical channel can be modelled in different ways. The noise sources can be inserted and real optical link emulated. In this combination the general OFDM performances are dependent on the average noise power, unlike the optical systems itself where the noise peak usually limits final system performances [Armstrong09].
By now, let's assume that the channel is ideal and not distorted, in order to make a simple transmission. So, once at the detection part, the received time valued OFDM signal is first digitized by an analog to digital converter (ADC). Further digital OFDM signal (denoted by y_n) is parallelised and the CP removed. The sampled OFDM symbols are then demodulated using the direct form of the Fourier transform for each symbol. So the input of FFT can be written as the vector $y_n = [y_0\ y_1\ y_2\ ...\ y_{N-1}]^T$ and OFDM demodulated symbols Y_k can be expressed as [Armstrong09]:

$$Y_k = \frac{1}{\sqrt{N}} \sum_{n=0}^{N-1} y_n \cdot \exp(-j \frac{2\pi}{N} kn) \qquad (2.2)$$

Being $Y_k = [Y_0\ Y_1\ Y_2\ ...\ Y_{N-1}]^T$. Afterwards, this discrete signal is demapped according to the scheme used at the transmitter and serialized. As the FFT and IFFT are matched transform pairs, Y_k corresponds uniquely to X_k and the bit stream can be recreated [Armstrong09].

2.1.1.2 Optical OFDM Systems

Due to demand for increased data rate and huge development in digital signal processing (DSP), OFDM system has recently been successfully employed to optical communication. The fundamental difference between conventional optical systems and optical OFDM systems are aspects like the type of signals on which system operates, advances in receiver structure or type of applied detection.

Different OFDM systems have been proposed for different kind of applications. Optical OFDM systems can be divided into several groups among which two are the most relevant. These are those based on *linear field modulation* and *intensity modulation* respectively [Armstrong09]. OFDM with linear field modulation is used for single mode optical fibers, where the mapping between each discrete subcarrier of the baseband electrical signal and single discrete frequency in optical domain is realized [Armstrong09]. However, OFDM systems based on intensity modulation are defined for short range applications. There, the OFDM signal is represented by the optical signal intensity. Of course, both types have their own kind of optical transmitters, which are depicted on Fig. 2.2.

In general, electrical OFDM signals normally are complex. So, for the *intensity modulation* first the electrical waveform is modulated onto RF carrier at I/Q electrical modulator, producing real-valued waveform (shown in Fig. 2.2 –up). This waveform is comprised by the subcarriers band displaced from DC. The reason is that intermodulation products from the nonlinear mixing of pairs of OFDM subcarriers due to the photodetection fall there [Lowery06]. Finally, the subcarriers band is modulated onto optical carrier applying a linear optical intensity modulator.

For the *linear field modulation*, optical OFDM signal is attained using an I/Q optical modulator (Fig. 2.2 –down). Here, each branch of the modulator is driven by the real and imaginary parts of the OFDM symbol.

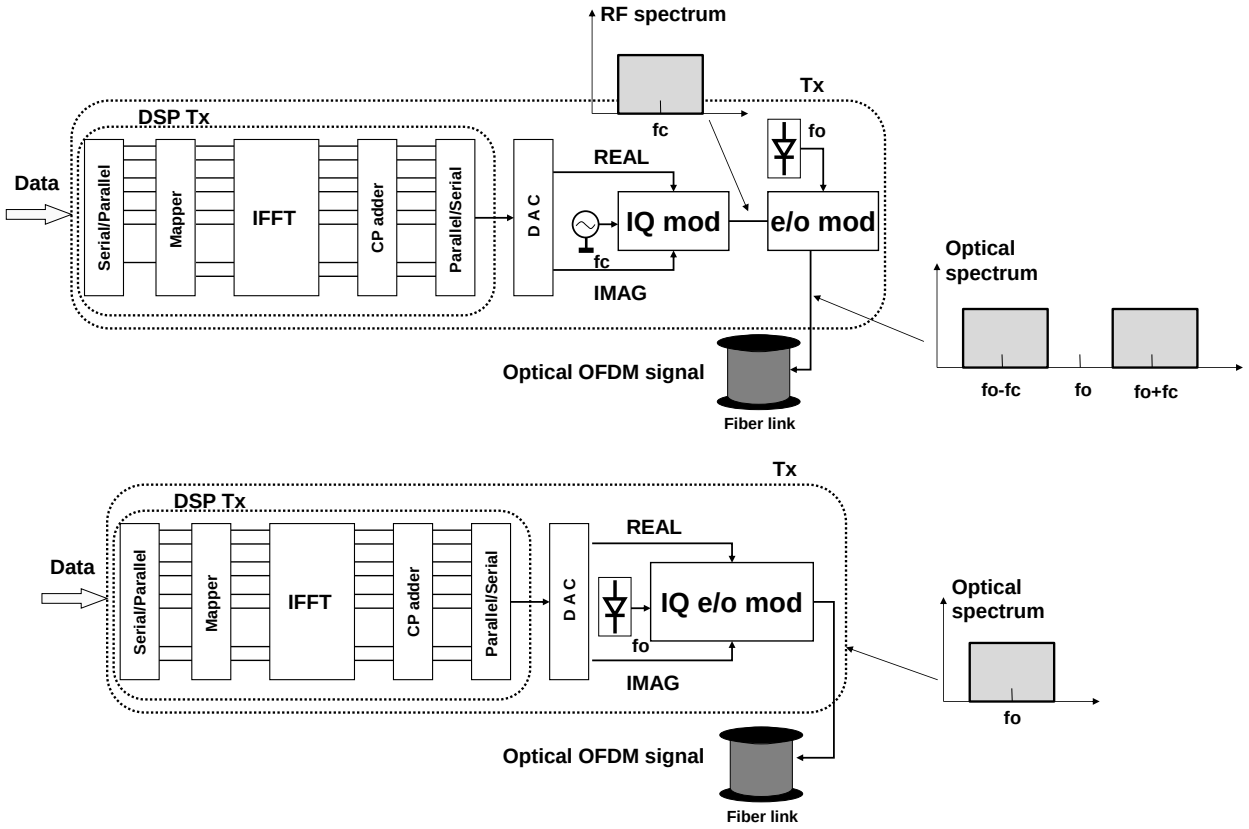

Figure 2.2. O-OFDM transmitter setups with electrical I/Q (up) and optical I/Q mod. (down)

Regarding OFDM optical detection, also two types are used: Coherent detection for linear field modulation and direct detection for intensity modulation.

Basically, the coherent techniques offer higher sensitivity and spectral efficiency together with the capability for link reconfiguration. Fig. 2.3 illustrates different solutions for coherent detection in OFDM: heterodyne detection and homodyne detection.

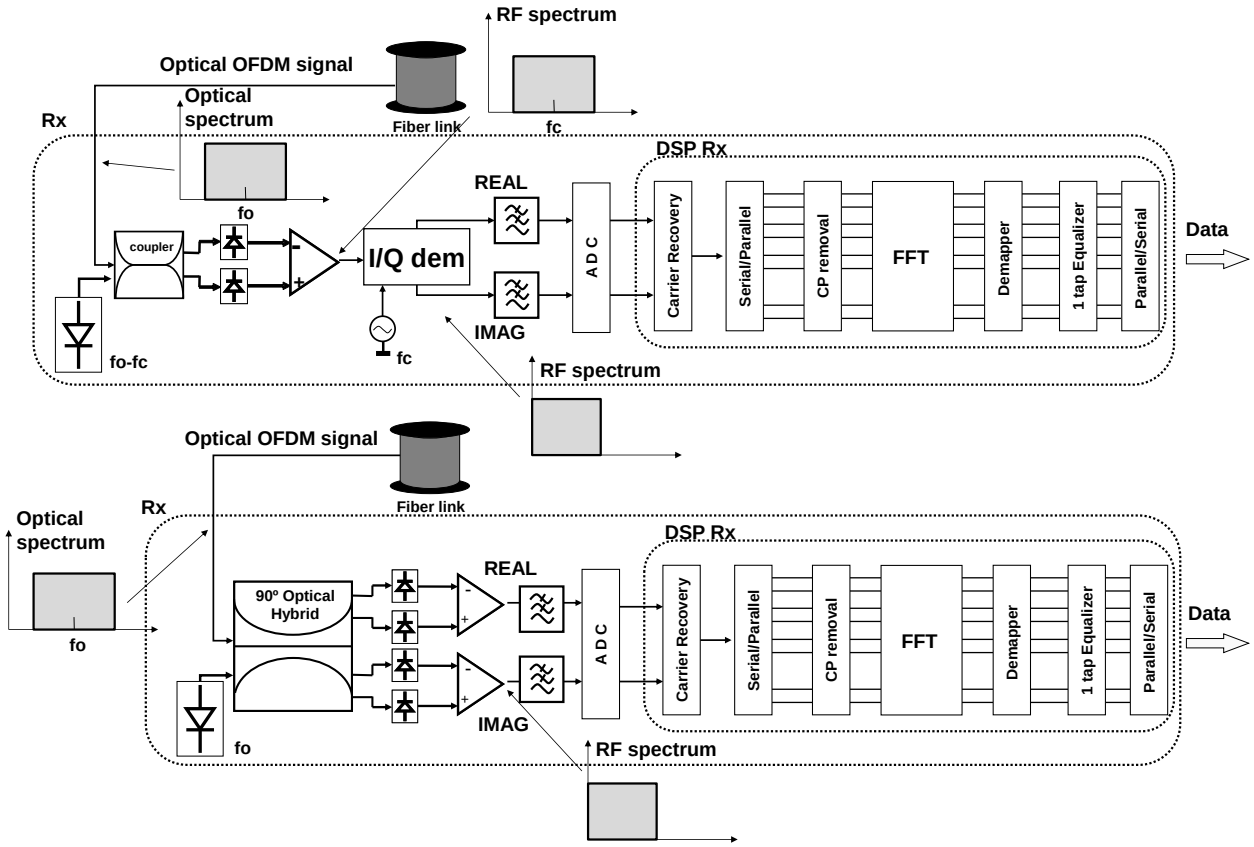

Figure 2.3. CO-OFDM receiver setups with heterodyne (up) and homodyne det. (down)

In the case of homodyne detection, the local oscillator (LO) operates at the same wavelength of the received signal. *I* and *Q* OFDM components are obtained by mixing the received signal with the local oscillator at 90º optical hybrid. The principle of operation for 90º optical hybrid is to combine two incoming optical signals and produce four different optical signals with a 90-degree phase difference that gives 0º, 180º, 90º and 270º phase shifts respectively. These signals drive two pairs of PD acting as balanced detectors. Therefore, the OFDM signal beats with the LO in a 90º optical hybrid obtaining at the output the electrical OFDM signal [Armstrong08, Shieh08].
Please note that both CO-OFDM techniques are sensitive to frequency offset and phase noise (even heterodyne detection is slightly more robust). Hence, very stable lasers featuring narrow linewidth are needed at both transmitter and receiver part in order to overcome such a drawback [Armstrong09, Buchali09, Shieh08]. So, the tracking algorithms to control and track out the laser frequency and phase are crucial. This is the reason why the receiver part at coherent detection case is more complex and the direct synchronization between transmitter and receiver required [Armstrong09].
In the heterodyne scenario, the optical OFDM signal is mixed with the local oscillator (which is oscillating at a near-by wavelength) and downconverted onto an intermediate frequency (*IF*, f_c)

thanks to the non-linearity inherent to the photodetectors [Armstrong09]. After detection the resulting electrical signal is further mixed with an electrical oscillator and I/Q demodulated, giving the real in-phase (*I*) and imaginary quadrature–phase (*Q*) components of the received OFDM symbol. The resulting *I* and *Q* waveforms are located in the baseband signal as the wavelength difference between local oscillator and received signals is forced to be the intermediate frequency.

Compared to coherent systems, direct detection OFDM (DD-OFDM) offers better flexibility and profitability as it uses simple off-the-shelf components [Zhao10]. Nevertheless its performance is limited and shows lower spectral efficiency. In case of some impairments compensation, the OFDM is able to correct for linear distortions using embedded electrical components [Buchali09, Schmidt08]. The standard receiver for direct detection in OFDM is illustrated on Fig. 2.4 [Buchali09]. Here, instead of making a direct detection of pure incoming optical OFDM signal, an optical carrier is delivered by the transmitter. This is a key drawback of DD-OFDM. Hence, the transmitted OFDM signal through the optical link is squared with optical carrier at single photo-detector [Buchali09]. This type of squaring at PD is due to the photodetection fall that is sometimes called square-law detection.

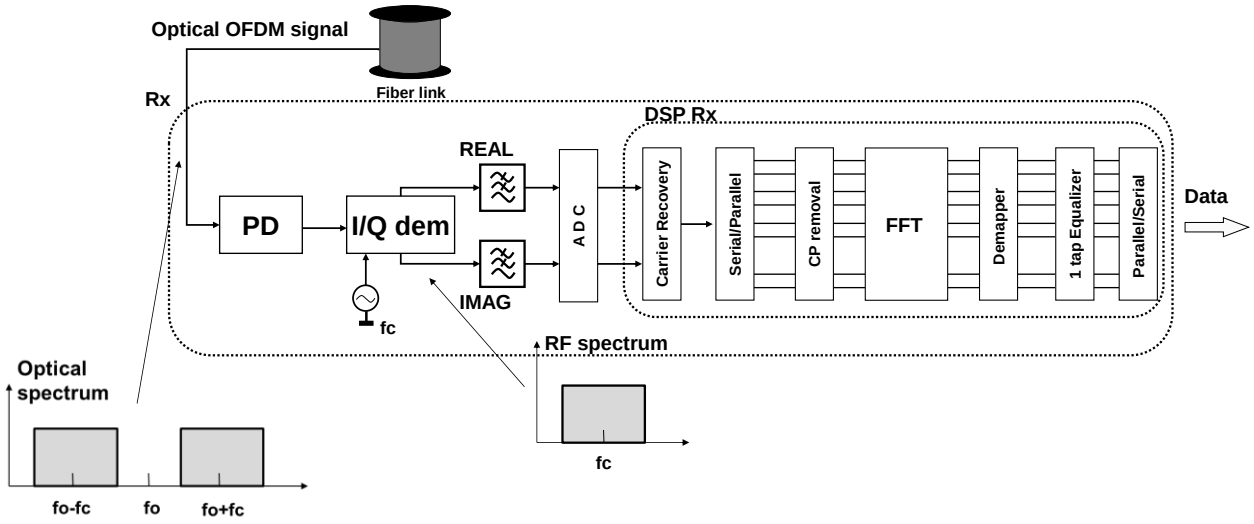

Figure 2.4. Optical standard DD-OFDM receiver setup.

The products of nonlinear mixing between the pairs of OFDM sub-carriers and optical carrier are located in the baseband after detection. So a guard band has to be left unused e.g. by electrically upconverting the signal prior to optical transmission. Additionally, in DD-OFDM more transmitted optical power is needed, because some power is applied to the optical carrier and is not useful for data detection because of these undesired mixing products.
While the modulating baseband OFDM is complex and typically bipolar (has positive and negative part); the input of an intensity modulator should have real and positive values [Armstrong09]. As in DSP at OFDM transmitter an input IFFT is complex and a single real IFFT output is expected, the input of IFFT is constrained to have Hermitian symmetry. This means that imaginary component of IFFT output has been eliminated and is zero. This solves the problem of having real output. For paving the way towards unipolarity, two approaches should

be considered: DC-biasing OFDM (DCO-OFDM) and asymmetrically clipping OFDM (ACO-OFDM).
In the case of DCO-OFDM systems, an appropriate DC offset is added when driving the intensity modulator in order to avoid lower clipping. Nevertheless, as OFDM symbols may have large PAPR, the mentioned bias is not able to avoid some negative peaks [Armstrong09]. This is the reason for the ACO-OFDM. Here any bias nor clipping at zero level were not applied. In order to avoid loosing information, only odd subcarriers should be modulated, achieving a time/amplitude symmetry of the OFDM symbol which results in a redundancy that allows clipping without losing data [Armstrong06, Armstrong08].
In case of DCO-OFDM, all the subcarriers are modulated, but only the odd frequency subcarriers for ACO-OFDM. It is clear that the data rate of the ACO-OFDM is half of the DC-biased OFDM. In general, the average optical power is very much reduced for ACO-OFDM. Thus summarizing, clipped OFDM provides optically power efficient solution at the expenses of only using half of the subcarriers.

2.1.2 Transforms applied in Optical OFDM

In the previous subsections the subsystem architectures have been introduced, mostly using the Fourier transform for achieving the subcarriers orthogonality. Nevertheless, other alternatives can be used, always focused on reducing processing time while increasing transmission performance. Among the best known, we can place discrete Fourier transform (DFT), discrete Hartley transform (DHT), discrete wavelet transform (DWT), discrete cosine transform (DCT) and discrete sine transform (DST). All these will be quickly reviewed in the present subsection.

2.1.3.1 Discrete Fourier Transform (DFT) and Discrete Hartley Transform (DHT)

First of all let's deal with DFT and DHT; which are very similar transforms.
The well-known discrete Fourier transform *F(k)* and its inverse *x(n)* for *k=0,1,.,N-1* can be defined as:

$$F(k) = \frac{1}{N}\sum_{n=0}^{N-1} x(n)\cdot \exp(-j\frac{2\pi kn}{N})$$
$$x(n) = \frac{1}{N}\sum_{k=0}^{N-1} F(k)\cdot \exp(j\frac{2\pi kn}{N}) \qquad (2.3)$$

Similarly, the discrete Hartley transform (DHT) *H(k)* and its inverse *x(n)* for *k=0,1,.,N-1* can be given as [Bracewell83, Svaluto08]:

$$H(k) = \frac{1}{N}\sum_{n=0}^{N-1} x(n)\cdot cas(\frac{2\pi kn}{N})$$
$$x(n) = \frac{1}{N}\sum_{k=0}^{N-1} H(k)\cdot cas(\frac{2\pi kn}{N}) \qquad (2.4)$$

where, $cas(\varphi) = cos(\varphi) + sin(\varphi)$ is an adopted abbreviation.
From the above expressions we can see that DHT is symmetrical, and can be applied to compute DFT, as kernels for both transforms differ only on the imaginary unit [Bracewell83, Svaluto08].

So, it can be said that both transforms are complementary each other. Regarding DHT, the direct and inverse transforms are identical, whereas in DFT one has to keep track of the +j and -j. Also, DFT implies a complex processing, while DHT is a real trigonometric transform. From practical point of view, optimized real-input DFT libraries are freely available, whereas highly optimized DHT libraries are not so common.
Both transforms have been successfully applied to fiber optical transmission. Because of its popularity, DFT appears in the vast majority of research publications related to optical OFDM. Regarding DHT, is a less known transform but it has shown to overcome the efficiency of DFT-based optical OFDM in some cases [Svaluto10, Svaluto12]. Precisely [Svaluto10] presents a fair comparison between DHT and DFT IM-DD optical OFDM systems, showing that the one based on DHT has similar performance to DFT, but with increased efficiency and reduced complexity [Sorensen85, Millane94].

2.1.3.2 Discrete Wavelet Transform (DWT)

Another kind of the transform that has been successfully adapted to optical OFDM is discrete wavelet transform (DWT). In fact, wavelet transform belongs to the family of overlapped transforms, i.e. the beginning of a symbol is transmitted before the previous one ends. The inter-symbol orthogonality is maintained due to the shift orthogonal property of the waveforms [Svaluto08, Bulakci09].
Let consider the signal *x(n)* that is next calculated by passing a series of filters. The samples in general, are passed through a low pass filter *g(n)*, resulting further in a convolution of the two that is given by [Li10]:

$$y(n) = \left(x(n) \otimes g(n)\right) = \sum_{k=-\infty}^{\infty} x(k)g(n-k) \tag{2.5}$$

Also the signal is simultaneously decomposed employing a high-pass filter *h(n)*

$$y(n) = \left(x(n) \otimes h(n)\right) = \sum_{k=-\infty}^{\infty} x(k)h(n-k) \tag{2.6}$$

DWT gives some information about two kinds of coefficients: from the high-pass filter and the low-pass by defined approximation. Both filters are related to each other with a relationship

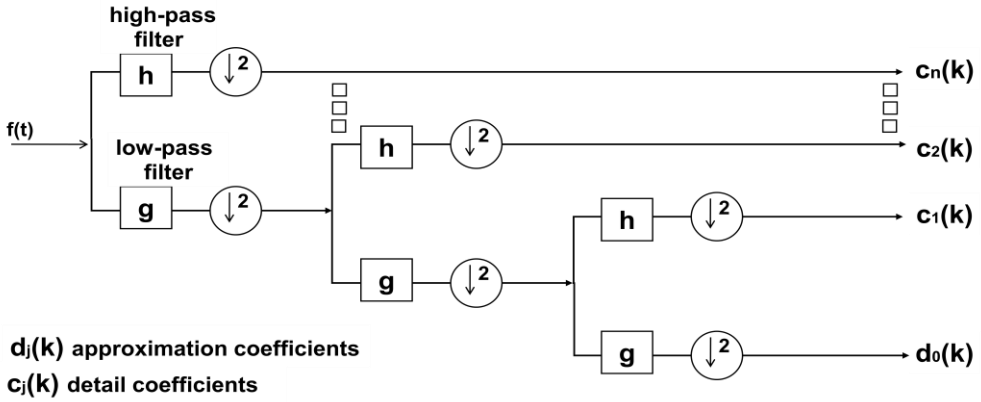

Figure 2.6. Block diagram of DWT with n-level filter banks.

denoted as quadrature mirror filters. The above algorithm implementation can be represented as a lower half binary tree structure as shown in Fig. 2.6.

Notice, that for n-level DWT, the bandwidth is logarithmically divided since only half of the spectrum, the low pass filter outputs are decomposed at each level [Li10].
So, the DWT has become a special case of the WT that provided a compact representation of a signal in time and frequency domain that can be further computed efficiently.
In [Bulakci09] general wavelet transform was first introduced for coherent optical OFDM. Wavelets here were proposed to increase the dispersion tolerance and their performance was compared to FFT-based OFDM. In fact, successful transmission was demonstrated for moderate dispersion and without CP; whereas for the FFT-based OFDM a minimum CP of 10 % was needed. Furthermore, in [Li10] the DWT was applied as an alternative approach to conventional optical OFDM. There, a dual polarization wavelet packet OFDM (WP-OFDM) system featuring coherent detection was investigated in the presence of PMD. PAPR and nonlinearity performance of WP-OFDM were also analyzed, and a comparison with conventional FFT-based OFDM was given. WP-OFDM was proved to be very sensitive to PMD; precisely 1 dB penalty at 5-11 ps DGD for 112 Gb/s dual polarization transmission was obtained. Nevertheless, one of the applied wavelet forms (Haar), improved about 0.9 dB nonlinear power limit compared to FFT-based OFDM systems.

2.1.3.3 Discrete Cosine Transform (DCT) and Discrete Sine Transform (DST)

DCT and DST have been widely used in digital image video processing and signal coding. Both are Fourier-related transforms. Like DHT, they belong to real transforms meaning that a real input gives a real output. In general, DCT is performed using direct or indirect computation, based on DFT or DHT [Svaluto08, Soliman09].
Let define *x(n)* as a discrete signal with length *N* and index *n*. Hence, the DCT $D_c(k)$ and IDCT *x(n)* transform respectively for *k=0,1,2,..,N-1* can be typed as [Soliman09]:

$$D_c(k) = \sqrt{\frac{2}{N}} \sum_{n=0}^{N-1} \beta(n) x(n) \cdot \cos\left(\frac{\pi n(2k+1)}{2N}\right)$$
$$x(n) = \sqrt{\frac{2}{N}} \sum_{k=0}^{N-1} \beta(n) D_c(k) \cdot \cos\left(\frac{\pi n(2k+1)}{2N}\right) \quad (2.7)$$

where, $\beta(n)$ can take $2^{-1/2}$ for *n=0*, and *1* for *n=1,2...N-1*.
Regarding DST, a similar set of expressions can be stated [Soliman09]:

$$D_s(k) = \sqrt{\frac{2}{N}} \sum_{n=0}^{N-1} \beta(n) x(n) \cdot \sin\left(\frac{\pi (n+1)(k+1)}{N+1}\right)$$
$$x(n) = \sqrt{\frac{2}{N}} \sum_{k=0}^{N-1} \beta(n) D_s(k) \cdot \sin\left(\frac{\pi (n+1)(k+1)}{N+1}\right) \quad (2.8)$$

where, $\beta(n)$ can take $2^{-1/2}$ for *n=0*, and *1* for *n=1,2...N-1*.
Even these two transforms are so similar, only DCT transform has been recently reported in optical OFDM transmission systems. First, DCT has been proposed in [Bulakci08] and further studied in [Zhao10]. The former [Bulakci08] proposed it as precoding before the IDFT block for PAPR reduction. In fact, the PAPR could be decreased by >3 dB and the OSNR tolerance at 10^{-3}

BER could be increased in more than 4 dB. The later approach [Zhao10], employed DCT as a way to increase the efficiency in intensity modulated OFDM, but now with coherent reception. In fact, the scheme proposed was similar [Svaluto10], but employing DCT instead of DHT and having a more complex receiver.

2.1.3 Recent applications in optical-OFDM based on coherent detection

Nowadays, a coherent detection in combination with optical OFDM creates a system that emerged by years to be one of the most efficient by means of performances and the way to struggle with potential impairments deteriorating a transmission while increasing the bit rate.
CO-OFDM offers especially innovative tool where the spectra of all the subcarriers partially overlap, resulting in higher spectral efficiency. The system by their advantages became one of the most promising alternatives toward ultrahigh transparent networks [Tang09]. In principle, several undesirable effects over optical CO-OFDM can effectively be monitored and mitigated, from among which the most interesting is the chromatic and polarization mode dispersion. The channel transmission can properly be monitored and estimated using DSP and by the feasibility of the fast Fourier transform and its equivalents, there is an option to scale the OFDM system in case of larger channel dispersion or simply higher data rate [Tang09].
From this point of view, the coherent detection became one of the most useful elements of optical OFDM at receiver side. Several jobs have been done in order to manifest the advantages and benefits of deploying coherent OFDM systems for high speed fiber transmission systems.
According to [Shieh07], the first experiment through the CO-OFDM transmission has been carried out for 1000 km SSMF link at 8 Gb/s. More experiments were quickly reported by investigating the transmission at 50 Gb/s [Jansen07]. Data rates 100 Gb/s [Shieh08a, Kobayash08, Jansen08d] and 1 Tb/s [Shieh09, Ma09, Dischler09] were experimentally demonstrated supporting CO-OFDM as an alternative for 100 Gb/s and future high-capacity networking solutions.
So, taking into account the functionality and feasibility of optical OFDM systems based on coherent detection, the recent work has been grouped depending on technology and features. First, the idea was to present the recent papers with chronological order addressed to the investigation towards performances at the highest bit rate possible. Next, the examples regarding the impact of several factors, as phase noise, frequency offset or simply nonlinearities and CD and PMD dispersion stressing the system will be provided.
So regarding the demand for data rate, Tang in the paper [Tang09] investigated the CO-OFDM performance on the upgrade of 10 Gb/s based DWDM systems with 50 GHz channel spacing to 100 Gb/s per channel. The filter concatenation effect was examined. By assessing above filter cascading due to the high spectral efficiency, 100 Gb/s CO-OFDM signals resulted in a very high tolerance to the filter narrowing effect, and a resilience to the filter cascading ripples.
Chandrasekhar by the paper [Chandrasekhar09] successfully transmitted a novel multi-carrier 1.2 Tb/s super-channel. The channel was comprised of 24 frequency-locked 12.5 GHz spaced PDM-QPSK carriers transmitted over 72x100 km with a channel spectral-efficiency (SE) of 3.7 b/s/Hz. Finally, a record SE-distance product reached 27.000 km·b/s/Hz.
Qi by features in [Qi09] investigated orthogonal band multiplexed OFDM (OBM-OFDM) system. By investigating OBM-OFDM, a successful transmission of 107 Gb/s data rate over 1000 km standard single mode fiber (SSMF) was achieved. Dispersion compensation and Raman amplification were not applied. By real investigation, OSNR sensitivity of 15.8 dB at the data

rate of 107 Gb/s at 10^{-3} BER was achieved. The experimented system based on 2 x 2 MIMO-OFDM provided high electrical spectral efficiency of 3.3 bit/s/Hz.

Benyuan in the paper [Benyuan10] was pursuing transmission of 1.2 Tb/s without any guard intervalusing coherent optical OFDM system over ULAF link. A demonstration of 52x and 72x 100 km of transmission over ULAF was shown by applying hybrid Raman/EDFA and all-Raman amplifier.

Afterwards, Ma by [Ma10] manifested 1 Tb/s OFDM signal transmission over single channel CO-OFDM system. The system consisted of 4104 continuous spectrally-overlapped subcarriers generated thanks to the use of recirculating frequency shifter (RFS). Theoretical and experimental analysis of RFS over CO-OFDM was examined. It has been shown that, the OFDM signal containing 36 uncorrelated bands, with a spectral efficiency of 3.3 bit/s/Hz can be successfully detected after transmission over 600 km SSMF. The link had no any amplification, nor dispersion compensation.

Du by [Du12] provided a tool to combat nonlinearity and wavelength conversion of 604.7 Gb/s OFDM signal. 16-QAM coherent optical OFDM system was investigated. Transmission over 800 km super-channel was tested. Based on tests, the nonlinear threshold has been increased by 4.8 dB, from 4.7 dBm to 9.5 dBm.

Cai in the paper [Cai12] proposed original multiband discrete Fourier transform spread (DFT-S) as a promising technology to reduce peak-to-average power ratio and mitigate the fiber nonlinearity. CO-OFDM system based on DFT-S was investigated in terms of computational complexity and nonlinearity. It has been shown that 450-Gb/s two-band CO-OFDM with DFT-S outperforms conventional CO-OFDM. The new system helped to transmit data over such long distances of 9280 km.

Meanwhile, Liu by [Liu11a] proposed a novel 448-Gb/s Reduced-Guard-Interval RGI-CO-OFDM signal based on16-QAM. The signal occupied a narrow bandwidth of 60 GHz. The signal was transmitted over 2000 km of 100 km low-nonlinearity ULAF spans and five 80 GHz grid wavelength-selective switches (WSS) based on ROADMs. Moreover, it was demonstrated that the WDM transmission of three 80 GHz spaced channels with small penalty provides a spectral efficiency of 5.2 b/s/Hz. Transmission over 1600 km was reached.

In turn, Qunbi in the other paper [Qunbi13a] proposed intra-symbol carrier phase recovery (IS-CPR) for reduced-guard-interval (RGI) CO-OFDM. This approach was made to compensate for the intra-symbol phase shift (ISPS) between subcarriers caused by the dispersion-enhanced phase noise (DEPN). Finally, in comparison to conventional common phase error (CPE) compensation, IS-CPR drastically improved the linewidth tolerance at 1 dB signal-to-noise ratio (SNR) penalty for 10^{-3} BER. The results showed the linewidth tolerance in range of 300 kHz - 2 MHz for 112 Gb/s systems (28 Gbaud QPSK) and 70 kHz - 550 kHz for 448 Gb/s (56 Gbaud 16-QAM) systems with a distance reach after 3200 km and 1600 km respectively.

Moreover, Xiao by [Xiao12] presented a novel implementation of real-time FPGA-based CO-OFDM receiver working at 5.8 Gb/s. A new scheme of self-coherent system with less complexity was proposed. 240 Gb/s multi-band signal over CO-OFDM system was experimentally transmitted over 44 km SSMF. BER floor at 1.74×10^{-5} was notified.

In turn, [Li11] have demonstrated the feasibility of the use of two mode fiber (TMF) using grating based LP_{01}/LP_{11} in dual-mode and dual-polarization coherent OFDM detection at 107 Gb/s. Considering the OFDM signal spectrum width of 19.7 GHz, the spectral efficiency of 5.4 b/s/Hz and reception after 4.5 km two-mode fiber with a grating-based mode converter were achieved.

Afterwards, Caballero by [Caballero12] presented a theoretical model along with simulations of high-capacity wireless signals at millimeter-wave frequencies. The baseband photonic technology was applied. The generation and detection of up to 24 Gb/s CO-OFDM QPSK signals in the 60 GHz and 75–110 GHz band were experimentally achieved.
In turn, Zhanyu by [Zhanyu12] proposed a novel constant envelop minimum CE-MSK-OFDM modulation scheme. This system mitigated the inherent drawbacks of CE-QPSK-OFDM and MSK-OFDM. By means of experiment, 2.5 Gb/s CE-MSK-OFDM signal and 2.5 Gb/s CE-QPSK-OFDM signal were transmitted over 100 km SSMF. The experimental results shown that the proposed system worked pretty well in decreasing ICI and PAPR that proved the theoretical concept deployed in the paper.
In turn, Kaneda in [Kaneda10] experimentally implemented real time receiver based on CO-OFDM system. A field-programmable gate array (FPGA) was employed. The transmission of a OFDM signal with sampling rate of 2.5 Gs/s and reception of a sub-band of 53.3 Gb/s multiband OFDM signal were demonstrated. The measured BER was equal to $3.7x10^{-8}$ and was noted as a record in real-time CO-OFDM demonstration.
Next, nonlinearities with CD/PMD dispersion impact and some techniques for dealing with those effects in optical CO-OFDM systems are highlighted.
So, Ezra by [Ip10] illustrated a digital back-propagation (BP) as a universal method to compensate dispersion and nonlinear impairments in optical fiber at any modulation format. The single carrier (SC) system was compared with OFDM for polarization-multiplexed (PolMux) transmission. It has been shown that at realistic data rates and transmission distances, polarization mode dispersion does not degrade the performance of BP and can be off applying post-BP linear equalizer.
Linglong by [Linglong13] proposed a flexible coherent zero padding OFDM (CO-ZP-OFDM) system for high-speed optical transport networks. The signaling embedded preamble and polarization time frequency (PTF) coded pilot tones were applied. In respect to the commercially available optical OFDM systems, CO-ZP-OFDM system increased payload by about 6.68 %. In this case, the low-density parity-check (LDPC) coded bit error rate suffered from no more than 0.3 dB in reference to the back-to-back case analyzed with high dispersion.
Qunbi by [Qunbi13] made an experimental investigation of the intra-channel nonlinearity effects over single-band 100 G CO-OFDM system. The correlated dual-polarization training symbols (TS's) were applied in order to reduce guard interval CO-OFDM system with short symbol durations. Additionally, employing fewer subcarriers, the intra-channel nonlinearity tolerance in CO-OFDM was demonstrated.
Puntsri in [Puntsri13] reported an ISI tolerance of cyclic prefix free for CO-OFDM system. Experimental results confirmed that the proposed method outperformed the state-of-the-art approaches due to BER and spectral efficiency. Additionally, the proposed method contained no feedback loop and no CD pre-compensation. Experimental results confirmed that the system is bit error free for a fiber length of 320 km.
Meanwhile, Roerich by [Roerich13] studied the impact of nonlinear distortions caused by the external optical MZM in CO-OFDM system. By the analysis of digital pre-distortions of the nonlinear MZM, it can be seen a general improvement of receiver sensitivity in CO-OFDM system. Such improvement of 2.2 dB (1.0 dB) for 64-QAM (16-QAM) with introduced a combined OSNR penalty was noted.
Afterwards, the phase noise and frequency offset investigation will be briefly overviewed.

Hence, Gabriella by [Cincotti12] proposed a novel solution for CO-OFDM based on fractional Fourier transform (FrFT). Here, it has been shown that FrFT would be electronically implemented with a more complex equivalent of FFT. It was concluded that in general planar devices based on FrFT are similar to the passive arrayed waveguide grating (AWG) devices featured by FFT. Finally, several tests were made, among which the most interesting were the analysis of the spectral efficiency, PAPR and the impact of frequency offset.
Nevertheless, Hae in [Hae12] created a novel wide carrier frequency offset (CFO) compensator for CO-OFDM system. The algorithm of offset compensation was based on the combination of the Chinese remainder theorem (CRT) for the integer part of CFO and fine estimation for the fractional part of CFO. This implementation finally provided wide estimation range and high accuracy for the system. Additionally, the results indicated that the range of estimator was as large as the sample rate.
Meanwhile, Karaki by [Karaki12] proposed a simple method to estimate CFO in Pol-Mux CO-OFDM system. The system itself was dominated by chromatic dispersion and PMD. Comparing to existing techniques, this method was based on the determination of the shifted position of the last filled OFDM sub-carrier (located just before the zero or empty sub-carriers area) to compensate large CFO.
In the paper of [Hussin13], A CO-OFDM transmission system with 4-QAM was simulated. The partial pilot filling (PPF) compensation scheme was analyzed and compared to conventional common phase error (CPE) compensation and RF-pilot based phase noise compensation. The PPF method improved a lot the Q factor at an individual laser linewidth of 100 kHz. The simulation results showed also that the PPF technique was robust against laser phase noise for the proposed system based on 1024 carriers. Additionally, better sensitivity is provided.
In turn, in the paper of [Jan13], the impact of laser phase noise (LPN) on DFT-spread CO-OFDM system was investigated. The paper provided that ICI due to LPN significantly degraded the BER of DFT-spread CO-OFDM compared to conventional CO-OFDM. DFT spread of 19 sub-bands yielded better BER than 76 sub-bands for both N-IFFT of 1024 and 2048 points, respectively. Next, two different LPN compensations were studied. The methods featuring CPE compensation and non-iterative interpolation were exhibited. They yielded lower BER for both conventional and DFT-spread CO-OFDM system, respectively.
Finally, an interesting approach for SOA was shown in the paper of [Khaleghi13], where a numerical model of Semiconductor Optical Amplifiers (SOA) was experimentally validated in terms of the alpha factor (αH) and the four wave mixing (FWM). In addition, CO-OFDM system was employed to confirm the good agreement between the real lab results and the simulations of Error Vector Magnitude (EVM). The amplification performances of the SOA for 10.94 Gb/s QPSK CO-OFDM signal were numerically analyzed with respect to the Amplified Spontaneous Emission (ASE) noise, the alpha factor, the output saturation power of the SOA and the bit rate.

Considering all the possible applications during last years, where the coherent detection for optical OFDM can be employed, it is worth to say that due to incredible resilience to CD and PMD, spectral efficiency and simplicity contained in a fast compatibility with DSP, coherent optical OFDM became an especially interesting in different application areas. In case of CO-OFDM, the complexity featured by the requirements for a narrow linewidth local oscillator, an optical phase locked loop or simply a polarization controlling was not only an obstacle, but many times it was a real advantage of their usage in the field of access metro or next generation long-haul. The researchers by years were trying to deploy CO-OFDM typing their viability to

cooperate with existing and future technology or simply deploying the ideal features. Several impact factors from phase noise, frequency offset, nonlinearities and CD and PMD dispersion stressing the system were discussed. The lack of the Raman amplification and even dispersion compensation was not always an important issue to reach high data rate and successfully crossed hundreds of kilometers over optical link [Ma10]. In 2012 in [Xiao12], the innovative implementation of self CO-OFDM based on FPGA with less complexity and supporting such high rate over 240 Gb/s was proposed. The scalability and relevant properties of CO-OFDM contributed to their easy integration to several techniques as e.g. a MIMO with a huge step towards a record back-to-back OSNR sensitivity achieved at roughly 100 Gb/s [Qi09]. Beside the possible applications where the complexity of CO-OFDM is not a main limitation, the CO-OFDM was analyzed in the area of different difficulties as phase noise, frequency drift or nonlinearities. It is worth noting that different techniques were investigated and came up to deal with such troubles. In [Karaki12], it was proposed an original solution for frequency compensation over PolMux CO-OFDM architecture stressed by the dispersion effect and by the paper [Cincotti12], a novel solution based on fractional Fourier transform was delivered to support CO-OFDM. These achievements and even much more typed in the above consideration can easily certificate that CO-OFDM with all rights and bad sides can fully be a great tool and really support a future investigation in high capacity optical networks.

2.1.4 Recent applications in Access/Metro Networks and Long Haul Systems

Now that it has been reviewed the status of Optical OFDM transmission systems and the alternative transforms, recent results for several case studies will be introduced. For easiness, they have been classified in different applications that involved long haul solutions and access/metro networks. So, it was found appropriate to give them in two sections focused on above mentioned applications areas.

2.1.4.1 Optical OFDM in Long Haul applications

In most of the applications with optical OFDM in long haul transmission system, the DD-OFDM was the pioneer and then followed the coherent optical OFDM. The scope of the use of DD-OFDM mainly concerned the problems with dispersion compensation management in such a long optical links. Due to square-law detection in the photodiode, the theoretical model of DD-OFDM was more challenging. Additionally, the receiver sensitivity of DD-OFDM could be tuned in wide range applying proper bias values that differed from other O-OFDM techniques.
M. Mayrock [Mayrock07] reviewed and simulated two types of configurations: DD and CO-OFDM for long haul at 10 Gb/s over both fiber links 2000 km and 4000 km respectively. For both, CD effect was effectively equalized. However, DGD caused some fading. Due to this limitation, both architectures were extended applying new solutions of polarization diversity receiver. This allowed to fully compensate DGD up to the length of cyclic extension.
B. Schmidt [Schmidt08] demonstrated that DD-OFDM with OSSB transmission was able to improve the CD tolerance. Three different transmitter configurations were proposed, that resulted in a very stable channel. Also it was proved that channel estimation from single training sequence could be applied to equalize billions of data symbols that was in contrast to other O-OFDM techniques based on significant overheads for pilot tones and tracking algorithms to follow laser variations. In addition, possible trade-offs between OSNR, DAC speed and

constellation size were shown. Furthermore, the data rates achieved are 10, 12 and 20 Gb/s over the fiber link between 320 and 400 km.

S. Jansen [Jansen08c] proposed a PDM CO-OFDM system as candidate for long haul transmission, achieving a transmission reach of 4160 km of fiber link at 52.5 Gb/s.

In the solution proposed by W. Peng [Peng08], 10 Gb/s data over 340 km of fiber transmission without penalty using virtual single sideband OFDM (VSSB-OFDM) system based on direct detection was investigated. Proposed solution used only half of the electrical bandwidth employing an RF tone at the edge of the signal. Results confirmed the VSSB-OFDM was at least with 2 dB better sensitivity and more robust CD tolerance.

J. Leibrich [Leibrich09] was focused on the impact of modulator bias on the OSNR measurements of DD-OFDM at 20 Gb/s with 7 % forward-error correction overhead. To generate the carrier, an external MZM in push-pull configuration was used. However, the need to set properly the bias was essential. The validity for the linear regime against nonlinear distortions was investigated. The significantly higher robustness towards second order nonlinearity with introduced frequency gap leaded to good agreement of simulations analysis over the wide bias range values.

Afterwards, W. Peng [Peng09] experimentally and theoretically demonstrated RF tone assisted DD-OFDM in two schemes, gapped and interleaved. The proposed system was able to equalize almost all the linear distortions of the optical channel. It was experimentally proven that both DD-OFDM scenarios outperformed the conventional OFDM based on SSB, obtaining negligible penalty after 260 km at 10 Gb/s of transmission over fiber link and 5 dB of improvement in case of back to back transmission.

A. Sano [Sano09] demonstrated 111 Gb/s over 2100 km long haul transmission based on no guard interval 2-subcarrier CO-OFDM. Their scheme improved nonlinear tolerance and CD was successfully compensated. Nonlinear inter-channel interactions were suppressed, achieving 135-channel transmission at 6248 km.

In S. Jansen's paper [Jansen09] 132.2 Gb/s transmission by optically multiplexing three band PDM 8-QAM OFDM was tested. He demonstrated that the nonlinear tolerance is dependent on OFDM symbol length and using 14.4 ns of symbol length at 4 b/s/Hz spectral efficiency, transmission over 1300km of fiber link could be reached.

Y. Qiao [Qiao10] proposed fiber nonlinearity post compensation (FNPC) based on spectral inversion (SI) and a subsequent 80 km compensation high nonlinear fiber (HNLF) sequence that can be applied to post-compensate for fiber nonlinearity impairments in 40 Gb/s CO-OFDM long-haul transmission systems. The link up to 40x80 km SSMF with DCF spans is tested. It was demonstrated that fiber nonlinear impairments can be easy compensated by FNPC configuration for single-channel and WDM systems. Additionally, for single channel system, Q factor is increased by 1.2 dB, however for WDM system with 50 GHz channel spacing 0.7 dB increase in maximum of Q factor is noted.

In M. Ghanbarisabagh's paper [Ghanbarisabagh10] performance analysis of decision feedback time domain equalizer (DF-TDE) for 20.48 Gb/s IM-DD optical OFDM transmission over 2560 km of SMF are performed. DF-TDE was proposed to cancel the residual ISI and ICI caused by both the dispersion and the CP length.

In turn, Xu. Liu [Liu10] numerically studied the effect of inline dispersion compensation for 100 Gb/s polarization division multiplexing PDM CO-OFDM transmission system. Here the investigation is featured by links based on 80 km SSMF spans with and without DCF (in sum up to 1600 km). The input power of DCF was optimized in order to balance the nonlinearity and

dispersion effect. In case of not applying inline compensation, the huge increase of dispersion from 0 to 700 ps/nm is observed.
However, X. Liu [Liu11a] proposed novel CO-OFDM scheme with reduced guard interval (RGI) for high-speed high-spectral-efficiency long-haul optical transmission. The generation of a 448 Gb/s RGI-CO-OFDM signal with 16-QAM through orthogonal band multiplexing was demonstrated. The optical signals occupying the bandwidth of 60 GHz were transmitted over 2000 km of ultra large area fiber (ULAF) and five 80 GHz-Grid ROADMs. A net system spectral efficiency of 5.2 b/s/Hz and a transmission distance of 1600 km of ULAF were additionally attained.
A. Lobato [Lobato12] investigated the nonlinear tolerance of three schemes of coherent detected 50 Gbit/s dual polarization DP-BPSK, 100 Gbit/s DP-QPSK, and 200 Gbit/s DP-QAM for single carrier with pulse shaping and OFDM over the link with and without dispersion management. The optical link is characterized by placing alternately EDFA amplifiers followed by 95 km n-SSMF and 8.45 km n-DCF fiber spans. Comparing to the signal carrier system, the OFDM has shown poor nonlinear tolerance when the link is dispersion managed due to its high PAPR and the highly correlated nonlinearities from span to span.
Afterwards, C. Lin [Lin12] demonstrated the possibility of nonbinary LDPC-coded mode-multiplexed CO-OFDM 1.28 Tbit/s 16-QAM signal transmission over 2000 km of few-mode fiber (FMF) with mode-dependent loss (MDL) by using an advanced mode-coupling compensation scheme. There was indicated that the MDL was the predominant effect in the long-haul optical transmission based on FMFs. The various compensation methods for different pilot-aided OFDM were investigated. Finally, it was shown, that the minimum mean-square estimation with linear interpolation method was the most robust against mode coupling and MDL. Additionally the nonbinary LDPC-coded modulation provided about 1 dB improvement over binary LDPC-coded modulation (MDL of 25 dB).
S. Mirnia [Mirnia12] has shown the analysis of a coupler based NRZ-DQPSK all-optical OFDM system with a rate of 80 Gb/s. The investigation was performed based on 800 km, 1000 km and 1200 km long SSMF link with 21 km DCF for each span. The power tolerance in the function of fiber dispersion ranged from 0, 1, 6 up to 16 ps/nm/km. There is shown, the more dispersion the fibers had, the more power they could tolerate. The maximum power penalty was reached at 15 dB for the case of 800 km link, however the minimum tolerance of 2.7 dB occurred in case of 1200 km link.
E. Giacoumidis [Giacoumidis12] experimentally demonstrated and numerically investigated that dual-polarization multi-band DP MB-OFDM is a great solution for modern DCF-free 100 Gb/s transmission. It has been also verified that DP MB-OFDM is sensitive to the nonlinear inter-band crosstalk effects such as FWM and XPM. Additionally, it was shown that after 1000 km of DCF-free G.652 fiber line, DP MB-OFDM and coherent single carrier DP QPSK system have nearly the same performance.
In turn, C. Li [Li12] proposed the multiband discrete Fourier transform spread (DFT-S) as a novel technology to reduce PAPR and mitigate the fiber nonlinearity. With the nonlinearity improvement, 450 Gb/s two bands DFT-S CO-OFDM were proposed and finally outperformed conventional CO-OFDM. In addition, the successfully transmission over a 9280 km fiber link was carried out.
Finally, S. Zhang [Zhang13] experimentally demonstrated a transoceanic transmission of 40 x 117.6 Gb/s PDM-OFDM-16 QAM over 10 181 km hybrid large core/ultralow-loss fiber link. The error-free transmission has been achieved using following techniques as, in case of hybrid

large-core/ultralow-loss fibers improved received optical-SNR while enhancing fiber nonlinearity tolerance, next the multiband nonlinearity compensation algorithm has been executed to rapidly improve nonlinearity tolerance, and at least the forward error correction (FEC) limit of 5.3 dB was employed by the concatenation of hard-decision and soft-decision FEC codes. This treatment and new functionalities guaranteed to have error-free transmission after turbo equalizer with memory of three symbols, and helped to reach a spectral efficiency of 4.7 b/s/Hz.
Just for a better understanding, the presented achievements for O-OFDM in Long Haul transmission over last years until now, have been plotted on Fig. 2.7.

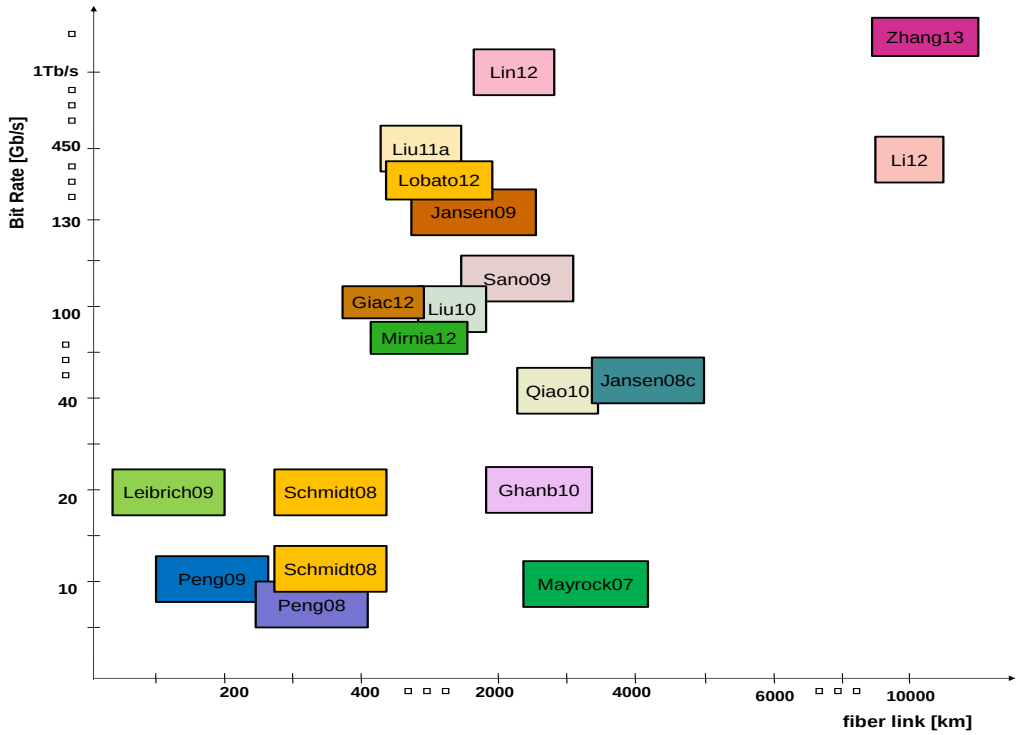

Figure 2.7. Collected achievements for optical OFDM in Long Haul applications.

Analyzing Fig. 1.7 and looking at the detailed examples of proposed optical-OFDM applications for long-haul transmission, some facts with several conclusions have to be stated. First, the presented increase of applications for long-haul follows the number of potential publications created over the last 6 years. Every year brings something new applicable to the transmission towards thousands of kilometers using optical OFDM. The researchers, until when the OFDM has been ported into optical domain, were looking for a robust system and a way itself to deal with optical impairments while the signal is propagated over long distances and provide high rate transmission. The incorporation of OFDM into optics turned out as a novel solution, applicable to optics and with all the drawbacks and advantages more efficient than competitors in terms of sensitivity, spectral efficiency or bandwidth occupancy. The evolution of long-haul applications towards optical OFDM started up since the rate of 10 Gb/s was employed to achieve maximally

4000 km over optical link using direct and coherent detection [Mayrock07]. Over the years the researchers, deploying the functionality of proposed OFDM applied different solutions, from which especially interesting are, the optical links based on ULAF in order to reach more distances, the methods to reduce a high PAPR and mitigate fiber nonlinearity, new kind of transforms (e.g. DFT-S) to simplify and speed up all the calculations performed in DSP; or even the equalizations techniques to struggle with the response of optical channel in case of PMD, CD and losses. Nowadays, the record for long haul applications has been noted in [Zheng13]. There is provided the highest rate close to 5 Tb/s achieved after transmission over 10 000 km of optical link. Hence, evolving during last 6 years, the OFDM came up with a considerable background in order to support long-haul. Note, that the growth in terms of reach versus data speed is quasi-linear, achieving thousands of kilometers at 1 Tb/s.

2.1.4.2 Optical OFDM in Access/Metro Networks applications

Here, couple of applications of optical OFDM in metro and access networks have been selected and described. In today's homes, there is variety of different communication mediums like: coaxial cooper cables for video and radio services, twisted cooper cables pair for telephony and e.g. wireless LAN for IP data transfer. So, single network that is able to integrate and offers general service through the fiber medium, enabling new functionalities and linking different services could be especially interesting. Hence, optical fibers with some benefits like a wide bandwidth and its transparency can be really attractive and appropriate at this case. Let's see the main achievements made thanks to OFDM in access/metro networks scenarios. Of course, in this case the achievements will be intrinsically related to the specific architectures used in each approach.

M. Huang [Huang08] demonstrated a novel approach of WDM-OFDM-PON with centralized lightwave based on direct detection. Downstream signal with 10 Gb/s phase modulated 16-QAM OFDM and upstream signal with 1.75 Gb/s OOK signal have been investigated. Downstream was transmitted over 25 km of fiber link without any OSNR penalty. The power penalty for upstream was less than 0.5 dB.

OFDM as a practical candidate for future access network applications has been proposed also by C. Chow [Chow08]. Here, high spectral efficiency transmission OFDM-PON system over 100 km fiber link was tested. High split ratio of 256 for up and downstream was achieved.

D. Qian [Qian08] was able to provide 11.5 Gb/s DD-OFDM transmission over 640 km fiber applying directly modulated laser (DML). It was proven that the architecture eliminated the need of use of additional elements like, local oscillator, optical phase locked loop and polarization scrambler at receiver side. DML replaced the normal low line width lasers as well. Therefore, the cost and complexity of whole solution were reduced.

A. Koonen [Koonen09] published some solution for in and out building networks. This solution contained the optical OFDM as a promising approach of providing high capacity wireless services over multimode fiber network located in and out of building. Its conclusion was that even CO-OFDM systems gives higher performances in terms of bandwidth efficiency and receiver sensitivity, DD-OFDM systems show some advantages as robustness towards dispersion in fiber links with low effort.

So, W. Rosenkranz [Rosenkranz09] proposed the use of DD-OFDM system for metro networks for 8x80 km of fiber transmission. The receiver and transmitter optimization was performed. The interplay between the strength of DC component and the OFDM signal amplitude was investigated, concluding that bandwidth occupancy could be exchanged for OSNR tolerance and

giving some requirements for DAC and ADC converters. Precisely, 5 bit accuracy for ADC and 4 bit accuracy for DAC were required.
L. Mehedy [Mehedy10] stated that DD-OFDM could be significantly improved using frequency interleaving of neighbouring channels. Two 24 Gb/s DD-OFDM with 25 GHz bandwidth were analyzed. The proposed system was frequency interleaved. This was done by occupying one spectral gap of the one channel by the data band of other one. Finally, this solution resulted in 48 Gb/s system within below 25 GHz bandwidth. So, the spectral efficiency of a single DD-OFDM could be improved applying proposed frequency interleaving mechanism.
In interesting approach given by C. Chow [Chow10], a study of OFDM signal transmission for broadband optical access networks was presented. The authors first quantified the performance of the OFDM signal and proposed carrier distributed OFDM PONs applying dual feeder fiber architecture and wavelength shifting to mitigate Rayleigh backscattering (RB) noise. Finally, 100 Gb/s OFDM-PON including subcarrier multiplexing was proposed and investigated. The results have shown the carrier RB performance is better than signal RB one. In the architecture of heterogeneous optical wired access network, negligible power penalty in 10 Gb/s NRZ signal and 1 dB power penalty in 10 Gb/s OFDM ROF signal were observed. Additional solutions based on 10 Gb/s NRZ signal and 10 Gb/s OFDM on 60 GHz carrier ROF signal were also performed.
In turn, Z. Kang [Kang11] presented a seamless amalgamation full duplex transmission applied to optical access networks supported by two of 2.5 Gb/s 16-QAM OFDM wireless and 10 Gb/s 4-QAM OFDM wired downstream access for clients. The full duplex communication has been realized thanks to the use of wavelength reuse technique (WRT) that supports 2.5 Gb/s upstream service without applying any additional optical sources to ONU and helps in cells distribution. Additionally, 20 km SSMF link was employed to reveal dispersion dependent amplitude attenuation in wireless service unit.
K. Qiu [Qiu11] firstly demonstrated a novel 10 Gb/s OFDM-PON upstream transmission architecture by traffic aggregation based on orthogonal band multiplexing. Presented architecture with 10 Gb/s OFDM signal for four ONUs without laser phase and frequency compensation was experimentally verified afterwards. Next, WPT-OFDM based on real valued transforms, supporting low-cost IM/DD was proposed to study. The experimental evaluation featured WPT-OFDM to be cost effective after successful propagation of 6 Gb/s WPT-OFDM signal over 75 km SSMF link, for PON applications.
L. Zhang [Zhang11] investigated pretty novel approach based on multi-amplitude minimum shift keying MAMSK-OFDM proposed for next generation optical access networks. Here, two signals 5-Gb/s 2AMSK-OFDM along with 2.5 Gb/s upstream OOK signal were transmitted over 20 km SSMF link resulting in OSNR penalties of less than 0.1 dB and 0.2 dB respectively. Next, the comparison between the MAMSK-OFDM signal with 4QAM/8QAM-OFDM and MSK-OFDM signals was given. It translated to the conclusion that the proposed technology based on MAMSK was especially attractive for future access networks applications.
Next, Z. Cao [Cao12] proposed simple, stable and synchronized low-cost signaling insertion and detection scheme for WDM-OFDM access networks with 15 Gb/s per wavelength. The given theoretical studies justified by means of simulations are finally experimentally verified. Overall verification confirmed almost negligible in total of 0.6 dB penalty caused by fiber transmission over 100 km link. This statement exhibited that the proposed signaling scheme had no impact on the system performance by any additional penalty increase and the given scheme could be great monitoring machinery for future WDM-OFDM networks. In 2012, N. Cvijetic [Cvijetic12]

collected different applications already manufactured and proposed for optical access layer with feasibility to optical OFDM. A comprehensive overview of OFDM based on optical access networks was created, covering practical examples and demonstrations with real challenges and features. The following conclusions supporting the sense of usage of optical OFDM in access confirmed that OFDM as a multilevel modulation with easy dispersion compensation could forward high-speed, spectrally efficient long-reach access, and due to mainly DSP implementation, the silicon technology can be employed in order to reach cost-efficient profile.
Next, R. Llorente [Llorente12] implemented cost and energy efficient multi-standard OFDM integrated optical access and in-building network architecture. The proposed architecture supported a large number of users with flexible bandwidth aggregation based on elastic optical comb generation. A tunable 5 GHz and 2.5 GHz frequency spacing with double and quadruple number of wavelengths were physically tested. Finally, the transmission of high bitrate OFDM data over 100 km SSMF and DVB-T signals over up to 500 m of in-building SSMF were demonstrated resulting in great flexibility.
E. Giacoumidis [Giacoumidis12a] presented an extensive comparison between a recently proposed novel technique of fast FOFDM and conventional OFDM for Local and Access Networks. It has been shown that, both systems working in OFDM nomenclature were able to support up to 20 Gb/s over 500 m worst-case multimode fiber (MMF) links with 3 dB effective bandwidth. The special power-loading (PL) algorithm was adopted featuring almost 4 dB improvement in case of FOFDM. The only 1 dB deviation between both systems is noted in case of optimum DAC/ADC parameters. D. Clausen [Clausen12] made experimentally an investigation through the bit and power loading in 10 Gb/s next generation optical OFDM for access networks. It was demonstrated that the approach based on the bit and power loading prevents the further need to apply optical single sideband filters. By OSNR penalty of 1.75 dB, it reduces the cost of expense hardware as an important factor for future cost-efficient PON.
Finally, taking the note that the ONU does not have to fully support OFDM band, low-bandwidth and low-speed devices have features to be applied in order to reduce ONU cost, C. Lei [Lei13] proposed novel sub-band access scheme with subcarrier-level bandwidth allocation implementing 1 Tb/s WDM-OFDM-PON system. It has to be said that the granularity of the bandwidth allocation was as small as the bandwidth of single subcarrier. Assuming the lack of band limitation, the ONUs were receiving the only desired subcarriers. The proposed scheme provided a promising solution for the realistic high-speed OFDM-PON deployment with cost-effective applications in PONs.

The optical OFDM emerged here over last 5 years as an architecture that pretty well deals with variety of multimedia communications services from video, radio or telephony, easily integrates with the existing building fiber infrastructure and supports high capacity wireless solutions for IP traffic. The OFDM addressed in case of access to short distances (typically less than 500 km) came up with some of the wisdom where their robustness towards dispersion, the flexibility to implement a traffic aggregation based on the full duplex transmission or at least the simplicity to retransmit e.g. a DVB-T signal over in-building network revealed the potential possibilities and facility to be integrated with current PON infrastructure. The direct detection employed in OFDM helped to reduce the cost and the complexity of the architecture devoted to cost-sensitive access or even metro networks. IM/DD OFDM also eliminated the difficulties reflected to the receiver phase noise or frequency offset by employing DFB or DML lasers without affecting so much performances. These treatments became especially relevant for future effective solutions

for PON networks. The multiple access exhibited by OFDMA-PON came up as an alternative from the cost and spectrum efficiency point of view giving the possibility for downstream transport of services based on 10 Gb/s. The latest solution promoted in [Lei13], positively supported high-speed OFDM-PONs in case of ONU's drawbacks. It was featuring special sub-band access with special subcarrier allocation which finally provided a way to fix the inherent problems with supporting OFDM band from ONUs.

2.2 Main objectives and description of the architecture

2.2.1 Background and description of the research proposal

Beside many of advantages, coherent optical OFDM transmission has also some drawbacks. The most important are the high peak to average power ratio (PAPR), the sensitivity to the phase noise, frequency offset and I/Q imbalance.

One of the most important constraints is large PAPR of transmitted signal. For a large number of subcarriers, the signal samples at the transmitter output have Gaussian distribution [Shieh10]. Once the large number of signals from different subcarriers is added together, the signals with the same time instants produce high amplitude peaks, leading to the PAPR figure. In particular, the high PAPR makes OFDM system sensitive to nonlinear distortions caused by the amplifier which drives the optical modulator of the transmitter. The output of such amplifier should be linear over a wide range of signal levels. However, the power of these peaks is high at this case. This transfers the amplifier output towards nonlinear range and the system performances are degraded [Armstrong09]. Additionally, in case of intensity modulation (and linear field modulation), the most popular modulators are Mach-Zehnder modulators (or the nested Mach-Zehnder modulators), which are linear only in the vicinity of the bias voltage used, which usually corresponds to the $\pm\pi/2$ voltage [Kaminow97]. So, at the output of the optical transmitter one can have serious limits due to PAPR. Moreover, in a long-haul scenario (transmission over >500 km of fiber) several impairments due to fiber nonlinearities are increased because of signal PAPR; seriously limiting the proper data detection at the receiver side [Jansen08a]. Several methods such as partial transmit sequence (PTS), selected mapping (SLM), clipping, tone reservation, signal mapping, block coding and trigonometric transforms have been proposed to address the PAPR level problem in OFDM applications [Rushdi07, Nadal11]. These different techniques provide different tradeoffs and effectiveness levels and can cause to reduce spectral efficiency, limit performance and increase system complexity.

Likewise, the sensitivity to phase noise and frequency offset of CO-OFDM systems is a general difficulty that disrupts real-time transmission. Even some of these effects can be digitally compensated by applying compensation in the digital domain [Shieh10]; the laser sources tolerated are still limited to those featuring linewidths in the order of 100 kHz. This leaves as potential sources only few of them, with complex (and expensive) device architecture.

An alternative solution to mitigating all the previously mentioned problems can be a coherent optical OFDM system based on a different modulation scheme. The idea is to overcome PAPR by using a phase modulation at the transmitter. With an OFDM signal processing similar to the one used for intensity modulation, the signal driving the phase modulator would be real-valued. As most popular phase modulators are based on exploiting the Pockels effect in a crystal (usually $LiNbO_3$ [Kaminow97]), the voltage applied is linearly translated as a refractive index change, giving in turn a linear phase change of the optical field. Thus, optical power remains unchanged

(except for the insertion losses of the device itself) and after transmission over fiber, the system is expected to become more insensitive to fiber nonlinearities. Nevertheless, for proper data reception, coherent detection is needed. But for the case proposed the phase noise would be additive (instead of multiplicative) respect to the OFDM signal, which gives more chances to make signal processing more easy.

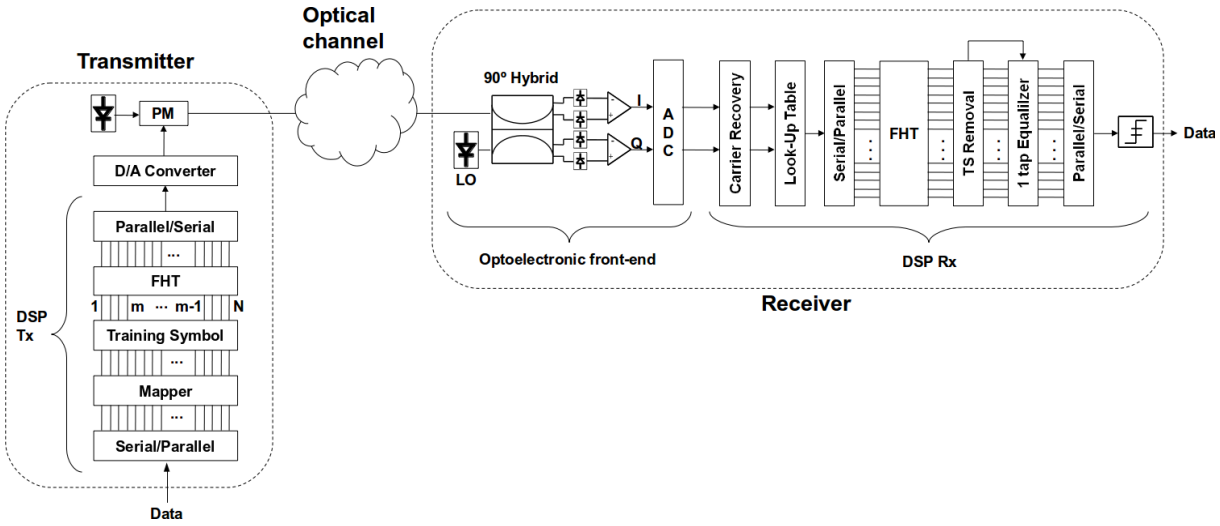

Figure 2.8. Simplified scheme of constant envelope optical CO-OFDM based on FHT.

The proposed transmission system scheme is shown in Fig. 2.8. The transmitter has two main parts: the Digital Signal Processing (DSP) and the optoelectronic hardware modules. The input data is first parallelized and mapped onto a real constellation (e.g. BPSK, multilevel PAM) by the DSP. Then, a training symbol sequence is added and the inverse transform is performed using the same routine of the direct transform, thanks to the self-inverse property of the Hartley transform. The resulting OFDM symbol is serialized. After the DSP, a Digital-to-Analog converter (DAC) drives a Phase Modulator (PM) excited by a laser.

Similarly, the optical receiver can be divided into two main blocks: the optoelectronic front-end and the digital signal processing. The optoelectronic front-end is a standard intradyne receiver featuring phase diversity, where the optical input signal is interfered with a local laser (LO) in a 2x4 90º hybrid. The local laser is assumed to be locked in polarization and wavelength with the received optical signal by means of the corresponding automatic frequency and polarization controls (not shown). The output signals of the hybrid are detected by two balanced detectors, whose I and Q outputs are digitized by an Analog-to-Digital Converter (ADC). Then, the DSP module parallelizes the incoming samples and performs the OFDM demodulation and data detection. This block first performs a carrier recovery to compensate phase and frequency errors, and then it extracts the argument of the received signal from its I and Q components by means of a look-up table. Afterwards, the OFDM demodulation is performed. After performing the Hartley transform, the training symbol (TS) is removed and the channel can be estimated in order to efficiently equalize the received signal. After equalization, the received signal is serialized, driving the data decider.

Regarding the previous work in similar topics, several articles have to be taken into account. In early 1990s *Casas* [Casas91] suggested using frequency modulation (FM) infrastructure over mobile OFDM. There, a thorough study was carried out but excluding the exploration of

improvement on the PAPR. More recently, in 2008, *Steve C. Thompson* [Thompson08] et al. proposed a signal transformation of each OFDM symbol to a phase magnitude, with the clear target to overcome PAPR in wireless OFDM communications. In that article a valuable study of the technique was provided, mostly from the theoretical point of view. Since then, some approaches have tried to port such a technique to optical OFDM systems [Silva10, Wu10, Huene11].

First, in [Silva10] the technique was proposed for IM-DD optical OFDM, showing a great improvement while driving the Mach-Zehnder modulator, and drastically reducing PAPR to values nearby 3 dB.

In turn, in the transmitter architecture proposed in [Wu10], a complex electrical OFDM signal was first up-converted to an RF carrier. The resulting signal was driving a phase modulator. At the receiver side a coherent detector was used, in order to recover the optical phase information. The RF up-conversion was claimed to be for overcoming the phase noise, but in fact it was decreasing the spectral efficiency and increasing the bandwidth (and the price) of the components used in reception. The performances when transmitting over a single mode fiber could be improved with respect to an IM-DD OFDM system.

Finally, in [Huene11] was proposed a constant envelope OFDM system based on coherent detection, similar to the one proposed for being developed in this thesis. Nevertheless, as the main requirement is that the signal driving the phase modulator has to be real, and they used the IFFT, they were limited by the Hermitian symmetry needs of the OFDM symbol generation. Their study showed simulation results, giving as main outcome a clear improvement in the phase noise tolerance and the tolerance of accumulated OSNR over a long haul link.

As seen, the proposed topic is found to be growing in the optical OFDM systems research line, but there are still many missing points to cover. In fact, only few simulations and experiments on sub-optimum solutions have been found among the literature. Thus, the main objective of this thesis will be to find an optimum solution to the PAPR mitigation based on alternative modulation schemes. The basic system will be the one featuring phase modulation, which is going to be thoroughly studied and optimized.

2.2.2 Goals

Once defined a starting architecture and seen the technical achievements of the previous work, it is time to define which will be the goals of the thesis. They are detailed in the following list:

1. **Use the Hartley transform**. As a first improvement of the system, it is proposed to use the Hartley transform, instead of the Fourier transform. Precisely the most interesting features of the Hartley transform are its no need for Hermitian symmetry; the fact that direct and inverse transforms are identical; and that its output is real when its input is also real. Additionally and as seen in the previous section, it will fully improve the power efficiency of the transmission system, because it can be computed much faster than standard Fourier transform.

2. **Propose alternative devices for phase modulation**. When starting the present work, only phase modulation using a standard external phase modulator has been reported. But also an interesting feature is that phase modulation can be achieved in a variety of other

devices. For example, it is achieved by using the inherent chirp of reflective semiconductor optical amplifiers (RSOA).

3. **Assess the effects of the several impairments in a back-to-back system** and propose alternative and innovative solutions. Most of them are directly related to the reception part and some of them can be:
    a. Modulation index optimization. As a main parameter of the phase modulator, its optimum point has to be found, as until now only timid simulation approaches have pointed that the higher the modulation index is, the better the performance of the system is [Huene11]. Nevertheless, its limit has to be reached and determine the reasons for such a limit.
    b. Phase noise. This is one of the main problems that arise when dealing with coherent detection. Even laser's phase noise is additive and not multiplicative for the case presented, it cannot be neglected.
    c. Frequency mismatch and symbol synchronization. As in every OFDM system, it is expected to have a key technical problem with the symbol synchronization in reception and the frequency estimation.
    d. IQ imbalance. For the architecture proposed in Fig. 2.8 it is evident that the 90º optical hybrid used in reception has to be as perfect as possible. Nevertheless, perfect devices do not exist and the goal is to evaluate the tolerances for different imbalances between branches of the hybrid.
    e. Impact of dispersion for propagation over the fiber link. Even it has not been highlighted on the system description, dispersion is the main impairment that can really deteriorate a transmission via fiber.

4. **Use cases/Application scenarios**, mainly covered by two lines of action:
    a. Extended reach access networks
        i. *Bidirectional transmission over a single fiber*. It is mostly limited by scattering and reflections [VanDeventer96, Lazaro07]. Nevertheless, it has never been studied for modulation formats similar to the one presented in this thesis. Thus this will be one of the most active technical points.
        ii. *Dispersion penalties up to 100 km transmission*. As the maximum reach of these networks is usually forecasted to be around 100 km, the main contributing fiber impairment is dispersion.
        iii. *Explore its use for delivering new services on a deployed PON infrastructure.* Precisely, a fixed-mobile convergence solution is proposed in the form of an overlay of a decomposed radio access network by means of WDM with narrow channel spacings. In short, a distribution based on wavelength per each pair of radio management and remote units is achieved providing the virtual links between central office and radio units incorporating *C*-band for investigation.

b. Long-haul transmission in core networks

i. *Proposed upgrade for core network* while enabling elastic functionalities. The PolMux structure for doubling the spectral efficiency was investigated. A potential deployment within the model of Telefonica I+D national network is manifested.

ii. *The dispersion penalties study extended to longer distances* and considered in case of digital equalization and optical compensation.

iii. *Accumulated OSNR effects in amplified systems*. The initial strategy to follow was to work with spans from tens to 100 km between optical amplifiers and find the limits for the proposed transmission system. Nevertheless, depending on the results, other working strategies were briefly proposed and studied.

iv. *Filter narrowing effects*. In flexible optical core networks a main limitation arises when cascading optical filters corresponding to different nodes. As all these filters may have slightly different central wavelengths and a certain error on their bandwidth, the resulting filtered signal will have large transition bands with irregular slopes. Thus impact of this effect had to be studied for the case the transmission system is applied to core networks.

2.2.3 Methodology

For all the research action points mentioned in the previous subsection, the working methodology has been achieved comprising two different parts:

1. Theory. Here the main goal was to develop mathematical models at each case. Basically, it involved the mathematical signal description of the signals at each point of the transmission system for each of the cases previously mentioned. The main figures of merit evaluated at this point were the Bit Error Ratio (BER) and the associated penalties for each of the impairments analyzed.
2. Simulations. At this point, the mathematical models developed in theory section were validated by means of numerical simulations. Prior to simulations, first the work from reference articles [Thompson08, Silva10, Huene11] was properly replicated. Afterwards, the conclusions coming from references and novel ideas became critical for the solutions attached to the thesis. Steps that were initially performed, helped to develop completely new own models in Matlab. The models deployed within simulations corresponded to the novel transmission system with all the features proposed in the thesis. Those models were especially useful for assessing the goals presented in the thesis and evaluating specific case studies detailed in theory.

CHAPTER 3: ANALYTICAL DESCRIPTION OF OPTICAL CE-OFDM SYSTEM

In this chapter, the general description and principle of operation for the proposed optical phase modulated CO-OFDM technique based on Hartley transform is given. The technique utilizing coherent intradyne detection with some new functionalities can also be called optical constant envelope OFDM (CE-OFDM).

This section covers the architecture description and scheme explanation of proposed CE-OFDM system with novel functionalities As has been shown in chapter 2, the scheme of the proposed novel optical CE-OFDM system is shown in Fig. 3.1.

The system is composed of two Digital Signal Processing (DSP) blocks, one at the transmitter and another at the receiver, an optical pure phase modulator, a 90º optical hybrid driven by local

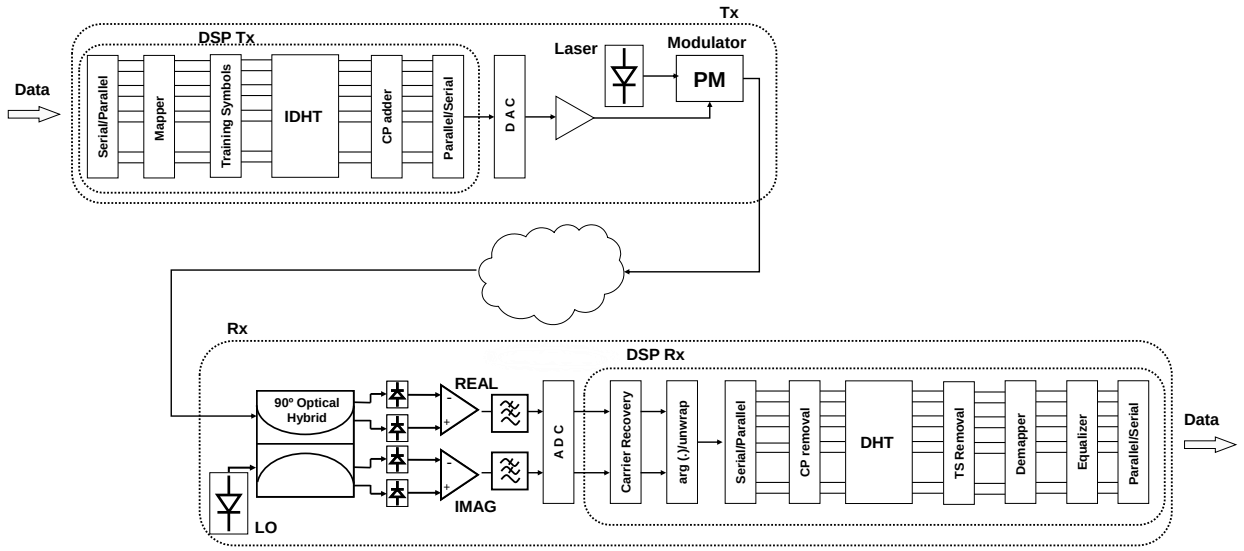

Figure 3.1. Schematic of the proposed Optical Phase Modulated CO-OFDM (CE-OFDM).

oscillator (LO) block, and a channel. For a formal description, the optical channel is neglected, considering only a back-to-back configuration. DHT is going to be used because of simplicity and power efficiency and as a consequence of that, the modulation format is restricted to BPSK and real-valued constellations (e.g. MPAM).

The use of discrete Hartley transform (DHT) speeded up the signal processing and simplified all the calculations behind the scenario. DHT is a real trigonometric transform. The direct and inverse transforms are identical and the transform of real signal is real [Bracewell83, Svaluto11].

New pure optical modulation in terms of phase is proposed to substitute commonly used amplitude modulation in OFDM system proposed for an optical domain. Phase modulation replaced the module of intensity modulation and overcomes the problems with high peak-to-average power ratio (PAPR) level.

3.1 General Principle of Operation for Proposed Scenario

At this section a more detailed description for individual parts of the proposed optical CE-OFDM system is exhibited. The section is split into four subsections supporting every stage of signal generation, transmission and reception.

3.1.1 DSP at Transmission

First of all, let's struggle with a generation and signal processing for an OFDM data signal. The basic idea behind any OFDM system is to transmit the high data bit rate using several parallel streams at lower bit rate. The proposed partial scenario associated with DSP processing and digital-to-analog converter (DAC) is shown in Fig. 3.2. Hence, according to the following Fig. 3.2, data is generated at 1 bit per symbol.

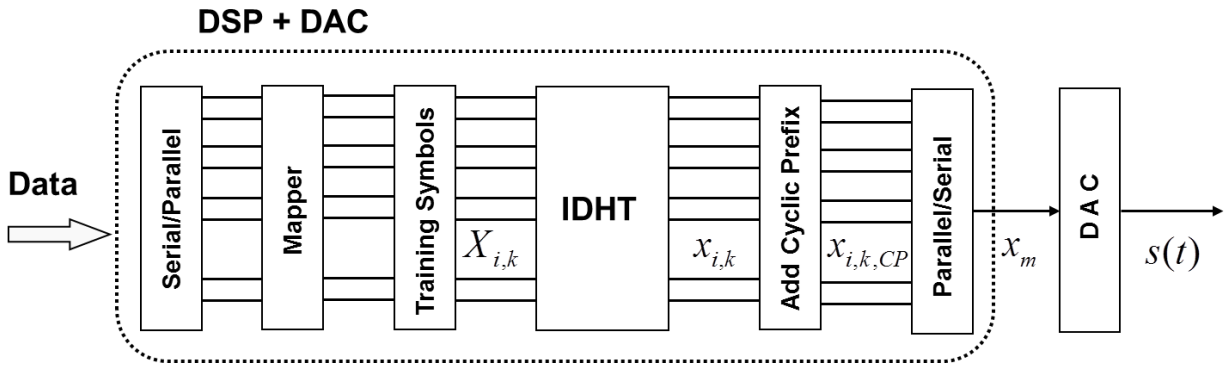

Figure 3.2. DSP with DAC block as a part of transmitter scheme.

Then data is parallelized and transmitted in each of parallel streams. Afterwards, the parallelized data is being mapped onto real constellation symbols referred to binary phase-shift-keying (BPSK) symbols. In BPSK nomenclature, the phase of a constant amplitude carrier signal is switched between two values according to the two possible signals that correspond to binary 1 and 0, respectively. A training symbol sequence is then inserted for channel equalization. The training symbols are associated to the data symbols and their length respond to the number of sub-carriers used in the scenario.

Next, the OFDM modulation is performed. In this scenario the inverse discrete Hartley transform (IDHT) is proposed to perform base-band modulation.

IDHT transform is equivalent of DHT and both are giving the same mirrored output [Bracewell83, Svaluto11]. Employing IDHT, all the carriers support data. IDHT is a real transform and by this has a lower computational complexity. This is a reason why only one-dimensional modulation format featured by BPSK was applied. Furthermore, lower hardware cost along with lower power consumption and reference to simplified scenarios for optical modulation and detection, became an advantage to use IDHT=DHT inside the proposed solution [Svaluto11, Svaluto12]. Inside IDHT block, the mapped BPSK symbols are OFDM modulated by proper number of subcarriers using the proposed transform. Comparing to the DFT, it does not require doubling the symbol rate since the Hermitian symmetry is not needed to support a real output.

The input of the IDHT is the real vector $X_{i,k} = [X_{i,0}\ X_{i,1}\ X_{i,2}\ ...\ X_{i,N-1}]^T$. The vector has a length N where N implies the size of the IDHT. Each of the elements of vector $X_{i,k}$ represents the data to be carried on the corresponding subcarrier k.
As BPSK mapping is employed, N real data symbols are transmitted during the ith OFDM block. The OFDM, instead of sending all the symbols serially, sends N symbols as an OFDM block. The block period is $T_B = NT_S$, where T_S denotes the individual symbol period.
The output of IDHT is the real vector $x_{i,k} = [x_{i,0}\ x_{i,1}\ x_{i,2}\ ...\ x_{i,N-1}]^T$. Based on the definition of IDHT, a single discrete OFDM symbol for $0 \le m \le N-1$, can be given as [Svaluto08],

$$x_m = \frac{1}{\sqrt{N}} \sum_{k=0}^{N-1} X_{i=1,k} \cdot \left[\cos(\frac{2\pi}{N} f_k m) + \sin(\frac{2\pi}{N} f_k m) \right] = \frac{1}{\sqrt{N}} \sum_{k=0}^{N-1} X_{i=1,k} \cdot \left[cas(\frac{2\pi}{N} f_k m) \right] \qquad (3.1)$$

where, k denotes subcarrier index, m is the discrete time domain index and f_k is the center frequency of each kth subcarrier per OFDM symbol. The subcarrier frequency $f_k = k/T_B$, where the subcarrier spacing, $1/T_B$ defines the orthogonality of all the subcarriers over the ith block interval.
In (3.1), the sum of modulated subcarriers $cas(2\pi/N\, f_k m)$ with associated N data symbols $X_{i=1,k}$ at one block are given.
Afterwards, cyclic prefix (CP) is added to the IDHT output at each ith block. Hence, let consider $x_{i,k}(j) = [x_{i,0}(j)\ \ x_{i,1}(j)\ \ x_{i,2}(j)\ ...\ \ x_{i,N-1}(j)]^T$ is the output of IDHT in the jth symbol period. In common cases, the CP is appended to the start of each OFDM symbol. So, instead of sending $x_{i,k}(j)$, the sequence $x_{i,k,CP}(j)$ with included CP [Armstrong09],

$$x_{i,k,CP}(j) = \left[x_{i,N-G}(j) ... x_{i,N-1}(j), x_{i,0}(j) ... x_{i,N-1}(j) \right]^T \qquad (3.2)$$

is transmitted towards optoelectronic part at transmitter; where, G is the length of the CP.
In general, CP prevents the system degradation by inter symbol interference (ISI) and inter carrier interference (ICI) due to chromatic dispersion. ISI is a consequence of a time shift of subcarriers in OFDM band [Buchali09] and ICI highlights a cross-leakage between the subcarriers [Jansen08c], mainly due to the impact of phase noise in OFDM. Properly large length of added CP, corresponding to the maximum length of the expected ISI would combat for signal distortion [Buchali09]. In addition, as long as the chromatic dispersion is less than the length of CP, the OFDM subcarriers rotate, what can easily be equalized after reception [Schmidt08].
Moreover, CP introduces some redundancy, reduces the data rate and makes a system more resilient to any kind of dispersion.
For simplicity, the CP is neglected at this case, leaving the example of CP usage at baseband signal to be discussed later.
Next, OFDM symbols with/without included CP overhead $x_{i,k,CP}(j)$ are serialized and converted to the analog domain by a digital-to-analog converter (DAC). DAC operates at a given sampling rate, where the sampling frequency is determined to be equal or simply greater than twice the maximum subcarrier frequency (the Nyquist frequency) in OFDM spectrum [Buchali09, Shieh10].
Inside DAC block, the superposition of all the subcarriers is performed. Here, the real time valued OFDM signal is formed. In ideal case, the DAC conversion convolves each discrete time sample $\{x_m\}$ by a *sinc* representation of individual carrier in frequency domain [Shieh10].
The discrete time OFDM samples $\{x_m\}$ clearly reflect to the real time OFDM values $\{s(t)\}$. The baseband OFDM signal $s(t)$ in continuous time domain for $0 \le t < T_B$, can be expressed as [Proakis89],

$$s(t) = \frac{1}{\sqrt{N}} \sum_{i} \left[\sum_{k=0}^{N-1} X_{i,k} \cdot \left[\cos(2\pi f_k t) + \sin(2\pi f_k t) \right] \right] g_k \left(t - iT_B \right) \tag{3.3}$$

where, *i* implies ith OFDM block, *N* is the total number of subcarriers and *g(t)* is the pulse shape. The pulse shaping along with oversampling takes part in DAC conversion process.
The *g(t)* is rectangular in most of the cases [Proakis89]:

$$g(t) = \begin{cases} 1, \Leftrightarrow 0 \le t < T_B \\ 0, \Leftrightarrow t < 0 \wedge t \ge T_B \end{cases} \tag{3.4}$$

and reflects to the ideal low-pass pulse shaping filter that removes aliasing generated due to the sampling process. By oversampling, the OFDM vector is increased by proper factor locating *n-1* zeros (un-modulated carriers) in the middle of samples. The oversampling was used to prevent high frequency distortions and noise components from being mirrored into the baseband OFDM signal [Lowery06]. Then, square root raised cosine finite-impulse-response (FIR) filter fitting the ideal low-pass filter is applied. Roll-off factor, characteristic for FIR filter, catching the value in range of *0-1*, became important parameter of addressed filter. It determines the excess bandwidth above the maximum frequency of the signal.
Looking at (3.3), it has to be clear that the signal *s(t)* is composed of several *i*th OFDM blocks. The OFDM block period T_B is *N* times longer than the symbol period T_S.
In continuous time domain, the subcarriers orthogonality can be explained mathematically by following,

$$\begin{aligned} &\frac{1}{T_B} \int_0^{T_B} \left[\cos(2\pi f_{k_1} t) + \sin(2\pi f_{k_1} t) \right] * \left[\cos(2\pi f_{k_2} t) + \sin(2\pi f_{k_2} t) \right] dt \\ &= \frac{1}{T_B} \int_0^{T_B} \left[cas(2\pi \left(f_{k_2} - f_{k_1} \right) t) \right] dt = \begin{cases} 1, \Leftrightarrow k_1 = k_2 \\ 0, \Leftrightarrow k_1 \ne k_2 \end{cases} \end{aligned} \tag{3.5}$$

where, *(*)* represents the convolution. Similar evidence of subcarrier orthogonality can be made in frequency domain.
Next, a small cyclic prefix explanation for the baseband OFDM signal is given.
It is claimed that the guard interval allows to mitigate the ISI/ICI impact and the cyclic prefix is transmitted during the defined interval. So, the guard interval can be defined between the range of $-\tau_g \le t < 0$, where τ_g is the guard period. The CP can be transmitted if the last τ_g of the *i*th block is forwarded within the guard interval. This condition is based on OFDM baseband definition and for one OFDM block can be written by,

$$s_{CP}(t) = \sum_{k=0}^{N-1} X_{i=1,k} \cdot \left[\cos(2\pi f_k (t + T_B)) + \sin(2\pi f_k (t + T_B)) \right] \tag{3.6}$$

Employing Euler's formula, (3.6) can easily be simplified to,

$$\begin{aligned} s_{CP}(t) &= \sum_{k=0}^{N-1} X_{i=1,k} \cdot \left[\frac{e^{j2\pi f_k (t+T_B)} + e^{-j2\pi f_k (t+T_B)}}{2} + \frac{e^{j2\pi f_k (t+T_B)} - e^{-j2\pi f_k (t+T_B)}}{2j} \right] \\ &= \sum_{k=0}^{N-1} X_{i=1,k} \cdot \left[\frac{e^{j2\pi f_k t} e^{j2\pi k} + e^{-j2\pi f_k t} e^{-j2\pi k}}{2} + \frac{e^{j2\pi f_k t} e^{j2\pi k} - e^{-j2\pi f_k t} e^{-j2\pi k}}{2j} \right] \\ &= \sum_{k=0}^{N-1} X_{i=1,k} \cdot \left[\cos(2\pi f_k t) + \sin(2\pi f_k t) \right] \end{aligned} \tag{3.7}$$

Hence, for $-\tau_g \leq t < T_B$, the OFDM signal with the guard interval/CP included is defined as,

$$s_{CP}(t) = \sum_{k=0}^{N-1} X_{i=1,k} \cdot \left[\cos(2\pi f_k t) + \sin(2\pi f_k t)\right] \tag{3.8}$$

In general, OFDM is commonly called a multicarrier modulation (MCM) being opposed to a single carrier modulation (SCM) where data symbols after bits mapping are transmitted serially. The signal waveform of such modulation $s_{scm}(t)$ can be defined as,

$$s_{scm}(t) = \sum_i X_i g(t - iT_S) \tag{3.9}$$

where, X_i are the data symbols in SCM system and g is rectangular.

The SCM signal $s_{scm}(t)$ can be approximated as the constant envelope while $|X_i| = 1$. Going into more details, in case of MCM system, the bandwidth is split into several narrow bands at different modulated frequencies. Whereas, the data symbols are divided into several parallel data streams where each is transmitted at separate modulated subcarrier (band) [Armstrong09]. Hence, the symbol duration $T_S = N/BR$, where BR accounts for the reciprocal baud rate [Buchali09, Thompson08].

Meanwhile, in case of SCM system, the signal representing each symbol is addressed to the full available signal bandwidth [Thompson08], so the symbol duration T_S depends only on BR and possess $1/BR$.

However, there are more differences between both systems. SCM transmits the same number of bits per each frequency band irrespective of the amount of noise per band, while MCM transmits more bits where there is less noise, and less bits in case of the bands with more noise. For a signal separation, MCM uses the orthogonality of employed DHT/DFT, but SCM has to apply one complex filter per transmission band. Nevertheless, the advantages of MCM over SCM are definitely higher, since MCM offers more efficient bandwidth, better spectrum utilization and more flexible implementation in case of frequency bands [Ramirez12].

Farther, a transmitted baseband OFDM signal $s(t)$ is upshifted onto optical domain using the optoelectronic front-end, that will be explained in the next subsection.

3.1.2 Optoelectronics at Transmission

At this subsection, the generated OFDM data signal is upshifted onto optical domain. This step is entirely performed using optoelectronics front-end.

So, here the optical PM modulator is employed. The scenario of proposed modulator is shown in Fig. 3.3 below. The phase modulator adapts the baseband OFDM signal to be transmitted over the channel in sense of back-to-back or fiber link connection. In case of PM modulator, the incoming baseband electrical OFDM signal is used to drive it and optical phase of the constant wave laser becomes phase modulated.

From practical point of view, the PM modulator can be realized on a strip waveguide where two electrodes are placed and are equally driven by applied electrical field. The phase change $\delta\phi$ provided by PM modulator can optimally be calculated using [Kaminov97],

$$\delta\phi = \frac{\pi}{\lambda} n^3 r \frac{V \cdot L}{d} \tag{3.10}$$

where, λ is the operating wavelength, n is the refractive index, r denotes the electro-optic coefficient featured by, V is the applied voltage, d is the distance between electrodes and

L accounts for the length of the electrodes.

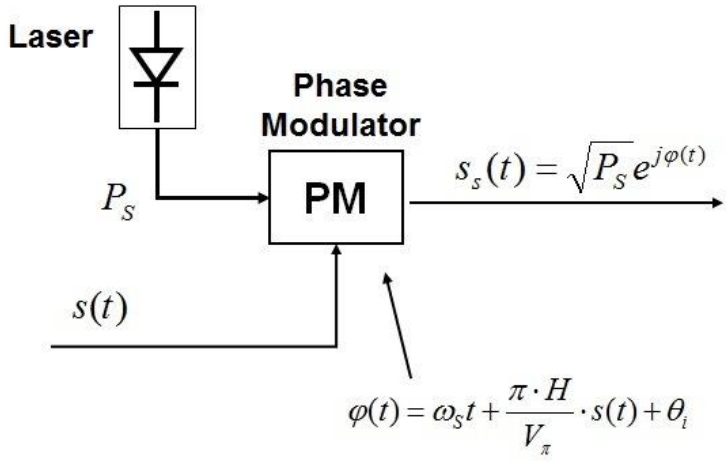

Figure 3.3. Scheme of optoelectronic front-end featured by Phase Modulator.

For an example, this device can be manufactured in laboratory environment based on the diffusion of sample *Nb* units into $LiTaO_3$ crystal, whose refractive index is a function of the driving voltage applied to the modulator electrodes. In that way, a phase shift of π radians between both electrodes along with applied voltage can be notified [Shieh10, Kaminov97].
Indeed, while the modulator is exposed to an electric field from the driving voltage, optical waveform moves slowly through it. The phase of the optical field at the modulator output becomes directly proportional to the period of time needed to pass over it [Binh10, wiki12]. Hence, it stems from that, the phase of optical signal at the output of PM modulator can easily be controlled varying the driving voltage at modulator input (see 3.12).
This way, the up-converted constant envelope OFDM (CE-OFDM) signal is generated.
Thus, the signal at the output of the modulator as a baseband constant envelope (CE) signal is formulated as,

$$s_S(t) = Ae^{j\varphi(t)} = \sqrt{P_S} e^{j\varphi(t)} \tag{3.11}$$

where, A and P_S are the signal amplitude and the data signal power respectively, and $\varphi(t)$ is the phase signal carrying information.
CE waveform at (3.11) forwards a main advantage. The instantaneous power is constant by the following assumption while $|s_s(t)|^2 = A^2$.
CE-OFDM signal $s_s(t)$ generated in phase modulator, combines baseband OFDM signal (3.3) and constant envelope signalling (3.11). CE-OFDM signal has a form of (3.11) where the phase component reflects to the OFDM waveform. Here, the phase modulation has been performed in optical domain. Due to the phase modulation, the typically large PAPR of any OFDM signal is no longer present, and an optimum PAPR of 0 dB is obtained.
The phase component of CE-OFDM at each *i*th block in the baseband can be defined as,

$$\begin{aligned} \varphi(t) &= \omega_S t + \frac{\pi \cdot H}{V_\pi} \cdot s(t) + \theta_i \\ &= \omega_S t + \frac{\pi \cdot H}{V_\pi} \cdot \frac{1}{\sqrt{N}} \sum_i \left[\sum_{k=0}^{N-1} X_{i,k} \cdot \left[\cos(2\pi f_k t) + \sin(2\pi f_k t) \right] \right] g_k\left(t - iT_B\right) + \theta_i \end{aligned} \tag{3.12}$$

where, *s(t)* is the OFDM real time waveform, *H* denotes an amplitude factor (driving voltage), ω_S is the optical carrier frequency, V_π accounts for the voltage to provide a π phase change at PM output and θ_i indicates an arbitrary phase offset. θ_i as a memory component, it is also modelled to perform phase-continuous modulation [Thompson05].
Let σ^2_X assume to be the variance of identically distributed data symbols. So, the variance can easily be calculated by $\sigma_X{}^2 = E\left\{\left|X_{i,k}\right|^2\right\}$. To achieve the final value, additional contribution has to be appended. As we are limited by a real valued transform, only real constellations are going to be considered, e.g. BPSK (M-PAM). Since, a multiple pulse amplitude modulation (M-PAM) can occur while *X(t)* is taking symmetrically distributed values of $\alpha_j = 2j-1-M$ addressed to each symbol interval $T_s = T_b log_2 M$, where $j = \pm 1, \pm 3, \ldots, \pm(M-1)$.
Hence, in terms of the symmetrical M-PAM, the average symbol energy σ^2_X, can be computed as [Simon00, Proakis89],

$$\sigma_X{}^2 = E\left\{\left|X_{i,k}\right|^2\right\} = \frac{1}{M}\sum_{j=1}^{M}(2j-1-M)^2 = \frac{M^2-1}{3} \tag{3.13}$$

assuming constellation points referred to $P(X_{i,k}=l)=1/M$, for all *i* and *k*. σ^2_X is fixed when a constellation is chosen.
The modulation index *H* defines the variance of the optical phase $\sigma_\varphi{}^2 = (\pi H/V_\pi)^2$. Since, the signal *s(t)* (3.3) is performed as a Gaussian process and is normalized making an assumption that the variance of the data signal $\sigma_x{}^2 = 1$ [Huene11, Thompson05], the factor $(M^2-1)/3$ at $\sigma_\varphi{}^2$ can be avoided.
Thus, the variance of the phase signal is given by [Proakis89, Thompson05],

$$\begin{aligned}
&\sigma_\varphi{}^2 = E\left\{\frac{1}{T_B}\int_{iT_B}^{(i+1)T_B}\left[\varphi(t)-\theta_i\right]^2 dt\right\} = \left(\frac{\pi\cdot H}{V_\pi}\right)^2 \frac{1}{T_B}\frac{2}{N\sigma_X{}^2}\cdot\ldots \\
&\ldots\cdot\int_{iT_B}^{(i+1)T_B}\sum_{k1=1}^{N}\sum_{k2=1}^{N}E\left\{X_{i,k1}X_{i,k2}\right\}\cdot\left[\cos(2\pi f_k t)+\sin(2\pi f_k t)\right]\cdot g_{k1}(t-iT_B)g_{k2}(t-iT_B)dt\ldots \\
&\ldots = \left(\frac{\pi\cdot H}{V_\pi}\right)^2 \frac{1}{T_B}\frac{2}{N\sigma_X{}^2}\sum_{k=1}^{N}\int_0^{T_B}\sigma_X{}^2 g_k{}^2(t)dt = \left(\frac{\pi\cdot H}{V_\pi}\right)^2
\end{aligned} \tag{3.14}$$

As a consequence of (3.14), the variance of the phase signal strongly depends only on modulation index.
The phase of the entire optical signal $s_s(t)$ behaves in the same way, but with the variance of $(\pi H/V_\pi)^2$ when $\sigma_x^2 = 1$ [Huene11, Thompson05].
Meanwhile, combining the full optical CE-OFDM property for *s(t)* (3.3) at PM modulator output, the signal $s_s(t)$ (3.11) can be expressed as follows as,

$$s_S(t) = \sqrt{P_S}\exp\left(j\varphi(t)\right) = \sqrt{P_S}\exp\left(j\omega_S t + j\frac{\pi\cdot H}{V_\pi}\cdot s(t)+\theta_i\right) \tag{3.15}$$

where $s_s(t)$ fully stands for the up-converted optical OFDM signal.
Hence, optical phase modulated output $s_s(t)$ (3.15) referred to (3.11) is finally characterized by a constant power and a varying phase. Next, the optical signal $s_s(t)$ is transmitted over the channel.

3.1.3 Channel transmission

At this subsection the channel transmission is briefly explained. After propagation, in non-ideal case, $s_s(t)$ can interact with a channel itself and can suffer from the channel noise. Hence, in huge simplicity, the received signal can be written as,

$$r(t) = s_S(t) * h(\tau) + n(t)$$
$$= \sqrt{P_S} \int_{-\infty}^{+\infty} h(\tau) e^{\left(j\omega_S t + j\frac{\pi \cdot H}{V_\pi} \frac{1}{\sqrt{N}} \sum_i \left[\sum_{k=0}^{N-1} X_{i,k} \cdot \left[\cos(2\pi f_k (t-\tau)) + \sin(2\pi f_k (t-\tau)) \right] \right] g(t - iT_B - \tau) + \theta_i \right)} d\tau + n(t) \quad (3.16)$$

where, $h(\tau)$ is the time channel impulse response and $n(t)$ is an additive noise term.
At this case, the noise source and channel itself are omitted and the phase modulated OFDM signal $s_s(t)$ traverses out of distortions in a back-to-back system. The data sent $\{X_{i,k}\}$ reflects to the received data $\{Y_{i,k}=X_{i,k}\}$ that are equal in case of back-to-back analysed system.

3.1.4 Optoelectronics at Reception

At the receiver side, the optical data signal $s_s(t)$ is entirely processed in both, optoelectronic front-end and DSP manifested in Fig. 3.4 and Fig. 3.6 respectively. First, the optoelectronics front-end is overviewed. According to the attached Fig. 3.4, phase-diversity receiver is employed for intradyne detection.
In case of coherent detection, the transmitter is fully synchronized with the receiver. The scheme of phase diversity receiver with electrical filters is depicted in Fig. 3.4.

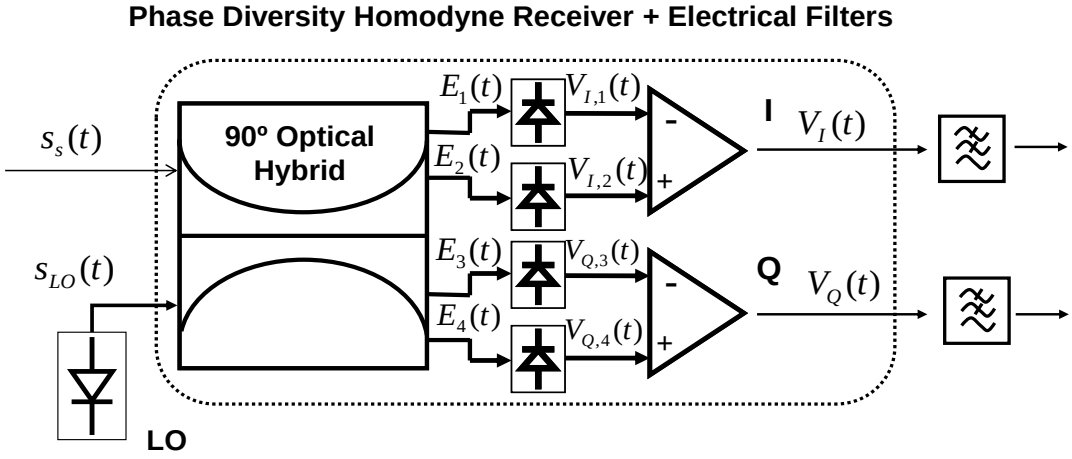

Figure 3.4. Configuration of the phase-diversity homodyne receiver with filters.

Therefore, at phase-diversity receiver, the signal $s_s(t)$ is first coupled with the local oscillator (LO) in a 90º optical hybrid. The local oscillator is featured by tunable optical laser frequency locked with transmitter optical laser [FabregaMCh13a]. Both are usually dominated by the phase noise due to improper set of the linewidth. In common OFDM systems, the impact of phase noise generates a common phase rotation (CPR) of all the subcarriers per symbol from one side, and a cross-leakage easily named ICI from another [Jansen8c]. So, consequently in order to limit the ICI, the OFDM symbol are short and in practice, the linewidth of the LO must be sufficiently narrow, minimized to about a few kHz that will eliminate such a destructive impact of phase

noise. In general, the optical LO is a model of semiconductor continuous-wave external cavity laser (ECL) with good dynamic range of min 100 dB, high wavelength accuracy, usually set < 20 pm and tuning range up to 200 nm. In terms of dynamics, the LO output normally exhibits fluctuations in intensity, phase or frequency chirp while biasing at constant current. Those fluctuations are due to some internal noise mechanisms as the spontaneous emission and the shot noise reflected to the recombination of the electrons and holes [Binh10] and they can lead to a certain spectral linewidth. Thus, some facts have to be stated, so that, LO dealing with high data bit rate first, needs to have a narrow spectral width and minimizes the impact to OFDM signal [Binh10].

The principle of operation of 90º optical hybrid is to combine two incoming interfering optical signals: the optical data (the received optical signal $s_s(t)$) and the reference local oscillator signal $s_{LO}(t)$ and then to produce four different optical signals with a 90º phase difference that gives 0º, 180º, 90º and 270º phase shifts respectively.

Such a LO signal can be written as,

$$s_{LO}(t) = \sqrt{P_{LO}} \exp\left(j\omega_{LO}t + j\phi_e(t)\right) \tag{3.17}$$

where, P_{LO} is the local oscillator optical power, ϕ_e describes an arbitrary phase (including phase noise) and ω_{LO} stands for the LO optical frequency.

In practical approach, the main task for a 90º optical hybrid is to recover optical incident signals assuming full synchronization just before their detection. Following the scheme in Fig. 3.5, first, the received incoming optical signal (by the assumption in case of back-to-back, $r(t) = s_s(t)$) is split into two identical signals using 3 dB coupler.

A 90º phase shift is added to one of its line. The same situation is applied to the LO signal $s_{LO}(t)$ (3.17). It is split into two the same signals by using second 3 dB coupler with enclosed 90º phase shift placed at one of its arm. Next, these four signals are combined together applying two more 3 dB couplers that lead them to the detection input afterwards.

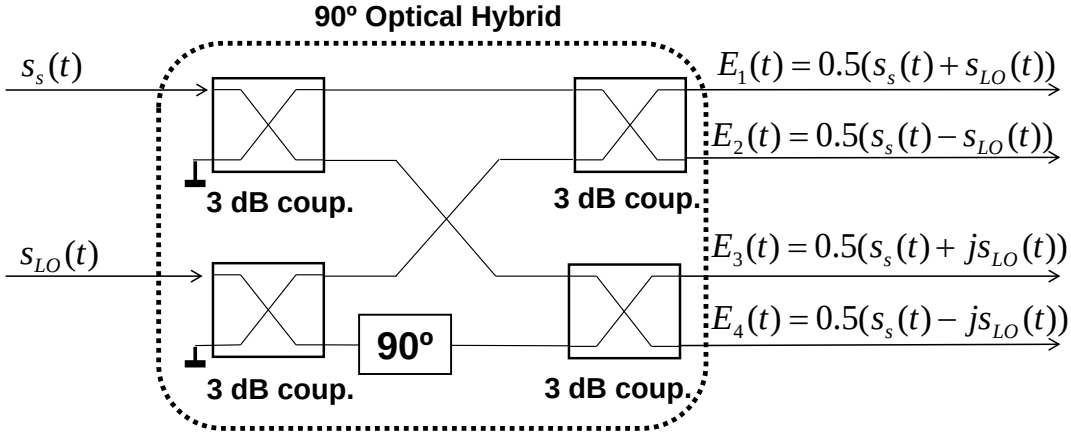

Figure 3.5. Detailed scheme of a 90º optical hybrid.

After a 90º optical hybrid, the resulting combination between received signal $s_s(t)$ and LO $s_{LO}(t)$ in terms of 4 outputs $E_{1\text{-}4}(t)$, drives two pairs of photo-diodes (PD) acting as balanced photo-detectors. In ideal case of a 90º optical hybrid, neglecting imbalance and losses, the output signals $E_{1\text{-}4}(t)$ can be expressed as,

$$E_1(t)=\frac{1}{2}\{s_S(t)+s_{LO}(t)\},\quad E_2(t)=\frac{1}{2}\{s_S(t)-s_{LO}(t)\} \tag{3.18}$$

$$E_3(t)=\frac{1}{2}\{s_S(t)+js_{LO}(t)\},\quad E_4(t)=\frac{1}{2}\{s_S(t)-js_{LO}(t)\} \tag{3.19}$$

Accordingly with a Fig. 3.4, those signals on detection inputs reflect to the complex detected representation where upper $E_{1\text{-}2}(t)$ and lower $E_{3\text{-}4}(t)$ input optical signals give the real $V_{I,1\text{-}2}(t)$ and imaginary $V_{Q,3\text{-}4}(t)$ components respectively.
Photo-detectors used at this scheme usually are positive intrinsic negative (PIN) diodes.
Due to photoelectric effect, PIN photodiodes work to convert the incoming light into electricity. The electrical signal generated on PIN output is directly proportional to the optical intensity of the coupled signal on PIN input [Binh10]. In practice, a PIN diode is integrated with bias resistor circuit, capacitor operating as DC block or low-noise electrical pre-amplifier on the right side of a diode. The bias resistor limits the electrical current that goes from PIN diode. Moreover, the pre-amplifier converts square-current into the voltage providing the electrical version of the information from the source. The PIN diode provides sufficient level of sensitivity to detect the signals highly attenuated [Binh10, BBrown94]. Unlike avalanche photodiodes (APDs), it ensures 5-10 dB less sensitivity, but it is cheaper without additional complexity (no stable power supply) and can easily be used and operated in a printed circuit board in the range of 5-15 V of power supply [Ciscoweb]. Thus, APDs are not used as a LO, ensures enough power and photodiode sensitivity becomes less critical.

The output current is given as a sum of individual components, photocurrent, dark current, shot noise and thermal noise and can be exhibited by,

$$i(t)=i_S(t)+i_{sh}(t)+i_{th}(t)+i_d(t) \tag{3.20}$$

where elementary components features as follows, $i_s(t)$ denotes the current due to the optical signal equal to $i_S(t)=R\cdot P_{in}$ with R as a the responsivity of PIN photodiode and P_{in} related to the input signal power and $i_d(t)$ stands for the dark current flowing across the junction and can be defined as, $i_d(t)=i_{sat}\left(\exp\left(qV_d/k_BT\right)-1\right)$, where, $i_{sat}(t)$ is the temperature that depends on reverse saturation current, k_B is the Boltzmann constant, q describes an electronic charge , T is the absolute temperature and V_d stands for the forwarded voltage to PIN diode.
In turn, $i_{sh}(t)$ features the shot noise current that in case of PIN diode describes the particular nature of the photons and can be denoted by the spectral density of, $N_{sh}=\sqrt{2q\cdot\left(i_S(t)+i_d(t)\right)}$. Moreover, $i_{th}(t)$ denotes the thermal noise due to electron random motion and can be featured using the spectral density as, $N_{th}=\sqrt{4k_BT/R_L}$, with R_L as the load resistance.
Continuing the scheme on Fig. 3.4, two PDs on each I and Q branch generate the following voltages of $V_{I,1\text{-}2}(t)$ and $V_{Q,3\text{-}4}(t)$. The I component featured by upper PDs can be described in the following way,

$$V_{I,1}(t)=\left|E_1\right|^2=\frac{1}{2}\left\{\left|s_S(t)\right|^2+\left|s_{LO}(t)\right|^2+2\,\mathrm{Re}\left\{s_S(t)s_{LO}^*(t)\right\}\right\} \tag{3.21}$$

$$V_{I,2}(t)=\left|E_2\right|^2=\frac{1}{2}\left\{\left|s_S(t)\right|^2+\left|s_{LO}(t)\right|^2-2\,\mathrm{Re}\left\{s_S(t)s_{LO}^*(t)\right\}\right\} \tag{3.22}$$

The voltages at Q component can easily be derived accordingly.

Afterwards, each pair of PDs characterized by $V_{I,1\text{-}2}(t)$ and $V_{Q,3\text{-}4}(t)$ responds to the one electrical substractor featuring finally balanced detection with the outputs of $V_I(t)$ and $V_Q(t)$. In case of balanced detection, the individual intensity contributions resulting from the mixing of optical fields in 90º optical hybrid are rejected and the useful beat intensities only stored [Painchaud09]. The beat signal bears the useful data unlike the photons that are featured by the sum of different intensities. After beating, only beats out of phase of π are differentially detected. Therefore, at the outputs, the individual intensities are subtracted, but the beats carrying an useful information added, resulting in the highest signal photocurrent at each I and Q branch featured by $V_I(t)$ and $V_Q(t)$ [Painchaud09]. Hence, due to this fact the balanced detection eliminates DC component and doubles the photocurrent [Kikuchi10a].
Using (3.21-3.22), the outputs of balanced detection determined by the I and Q components of photocurrents featured by $V_I(t)$ and $V_Q(t)$ respectively can be derived as,

$$V_I(t) = V_{I,1}(t) - V_{I,2}(t) = 2\,\mathrm{Re}\left\{s_S(t)s^*_{LO}(t)\right\} \tag{3.23}$$

$$V_Q(t) = V_{Q,3}(t) - V_{Q,4}(t) = 2\,\mathrm{Im}\left\{s_S(t)s^*_{LO}(t)\right\} \tag{3.24}$$

Next to the PIN diodes, each balanced detector is followed by a low pass electrical filter. Electrical filters are located on two branches of the intradyne receiver outputs called: In-phase (I) and Quadrature-phase (Q). They are matched in order to have the same response.
As an extension to (3.23-3.24), the voltage signals present at the output of both I and Q branches each are better described by the following expressions (3.25), where the output of the top branch *I* of phase-diversity receiver is,

$$\begin{aligned} V_I(t) &= R_L R\sqrt{P_S P_{LO}}\cos\left(\left(\underbrace{\omega_S - \omega_{LO}}_{\Delta\omega}\right)t + \frac{\pi\cdot H}{V_\pi}\cdot s(t) + \theta_i - \phi_e(t)\right) \\ &= R_L R\sqrt{P_S P_{LO}}\,\ldots \\ &\ldots\cdot\cos\left(\begin{array}{l}\Delta\omega\cdot t + \dfrac{\pi\cdot H}{V_\pi}\cdot\ldots \\ \ldots\cdot\dfrac{1}{\sqrt{N}}\displaystyle\sum_i\left[\sum_{k=0}^{N-1} X_{i,k}\cdot\left[\cos(2\pi f_k t) + \sin(2\pi f_k t)\right]\right]g_k\left(t - iT_B\right) + \theta_i - \phi_e(t)\end{array}\right) \end{aligned} \tag{3.25}$$

In a similar fashion to (3.25), the output of the bottom branch *Q* is generated, depending only on *sin(·)*.

$$V_Q(t) = R_L R\sqrt{P_S P_{LO}}\sin\left(\left(\underbrace{\omega_S - \omega_{LO}}_{\Delta\omega}\right)t + \frac{\pi\cdot H}{V_\pi}\cdot s(t) + \theta_i - \phi_e(t)\right) \tag{3.26}$$

The frequencies of LO ω_{LO} and transmitter laser ω_S are equal, so for simplicity let the frequency difference $\Delta\omega$ between both signals be,

$$\Delta\omega = \omega_S - \omega_{LO} = \omega_{LO} - \omega_S = 0 \tag{3.27}$$

So, indeed taking into consideration all the simplifications contained in (3.19-3.27), $V_I(t)$ and $V_Q(n)$ can be rearranged as,

$$V_I(t) = R_L R\sqrt{P_S P_{LO}} \cdot \cos\left(\frac{\pi \cdot H}{V_\pi} \cdot \frac{1}{\sqrt{N}} \sum_i \left[\sum_{k=0}^{N-1} X_{i,k} \cdot \left[cas(2\pi f_k t) \right] \right] g_k\left(t - iT_B\right) + \theta_i - \phi_e(t) \right) \quad (3.28)$$

$$V_Q(t) = R_L R\sqrt{P_S P_{LO}} \cdot \sin\left(\frac{\pi \cdot H}{V_\pi} \cdot \frac{1}{\sqrt{N}} \sum_i \left[\sum_{k=0}^{N-1} X_{i,k} \cdot \left[cas(2\pi f_k t) \right] \right] g_k\left(t - iT_B\right) + \theta_i - \phi_e(t) \right) \quad (3.29)$$

So, thanks to the combination of above 90° optical hybrid and PIN diodes, acting all together as phase-diversity optical front-end. The optical incoming signal is down-converted while translating it to the electrical domain.
The resulting two signals on two parallel I and Q branches (3.28-3.29), are then pointed to the

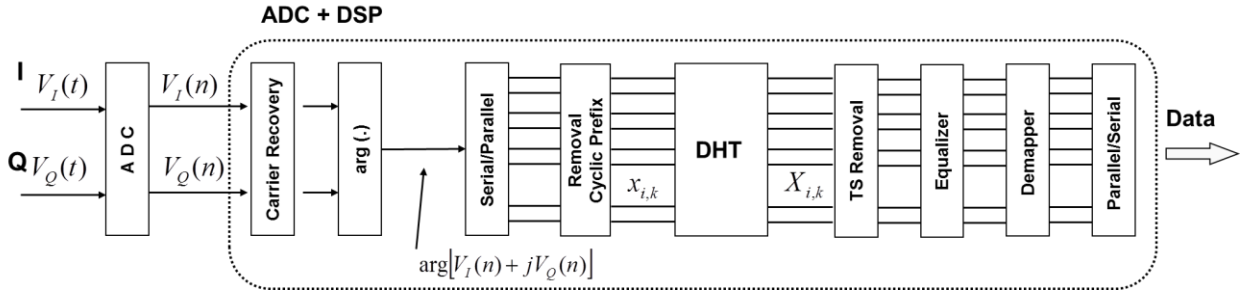

Figure 3.6. ADC block with DSP as a part of receiver scheme.

analog-to-digital converter (ADC). The ideal principle of operation for ADC conversion along with DSP processing at receiver side is shown in Fig. 3.6.
Here in Fig. 3.6, the down-converted to baseband signals for both *I* and *Q* branches $V_I(t)$ and $V_Q(t)$ are operated in ADC module. ADC operates as in case of DAC at a given sampling frequency. Within ADC, the signals are down-sampled, converting continuous received signals $V_I(t)$ and $V_Q(t)$ to discrete samples $V_I(n)$ and $V_Q(n)$. Down-sampling, commonly named sub-sampling is applied to alias a high frequency input down to a lower frequency [Proakis89]. Finally, the continuous received signals (3.28-3.29) are easily digitized converting to their discrete representation shown by (3.30-3.31). The real time values $\{t\}$ clearly reflect to discrete time samples $\{n\}$. The processed information has a following form,

$$V_I(n) = R_L R\sqrt{P_S P_{LO}} \cdot \cos\left(\frac{\pi \cdot H}{V_\pi} \cdot \frac{1}{\sqrt{N}} \sum_i \left[\sum_{k=0}^{N-1} X_{i,k} \cdot \left[cas(\frac{2\pi}{N} f_k n) \right] \right] g_k\left(nT_s - i\right) + \theta_i - \phi_e(n) \right) \quad (3.30)$$

$$V_Q(n) = R_L R\sqrt{P_S P_{LO}} \cdot \sin\left(\frac{\pi \cdot H}{V_\pi} \cdot \frac{1}{\sqrt{N}} \sum_i \left[\sum_{k=0}^{N-1} X_{i,k} \cdot \left[cas(\frac{2\pi}{N} f_k n) \right] \right] g_k\left(nT_s - i\right) + \theta_i - \phi_e(n) \right) \quad (3.31)$$

where, T_s reflects to the sampling period as the reciprocal of the sampling rate.
Next, the digitized OFDM baseband at $V_I(n)$ and $V_Q(n)$ enter the DSP block.
First, the carrier recovery is performed. In a purpose of coherent demodulation, a carrier recovery in general is made to compensate for phase and frequency errors between the received carrier and LO laser. As was already implied, in the transmitter, an optical carrier was phase modulated by a baseband OFDM signal. Meanwhile, at the receiver the baseband signal is retrieved from the incoming modulated carrier. So, the idea behind the carrier recovery is to employ the equivalent low-pass linear phase FIR filter with a raised cosine transition band at the carrier frequency [Barry03]. The filter of even order is specified by cut-off frequency, sampling

frequency F_S and transition bandwidth always typed in range of (0, $F_S/2$). The cut-off frequency of the filter is smaller than subcarrier spacing, as it is detailed in chapter 4. After digital filtering, the angle of extracted signals $V_I(n)$ and $V_Q(n)$ addressed as $\Theta_{I,Q}$ is computed. Next to this operation, the complex signal composed from each $V_I(n)$ and $V_Q(n)$ signals is multiplied by exponential equivalent depended on retrieved angle Θ, given by,

$$V(n) = \left(V_I(n) + jV_Q(n)\right) \cdot e^{-j \cdot \Theta_{I,Q}} \tag{3.32}$$

Next, the argument of the complex received OFDM signal taken from *I* and *Q* components is extracted. The extraction is executed unwrapping the phase. This approach is transparently manifested performing electrical phase demodulation. The phase demodulation is processed by computing the argument of incoming both $V_I(n)$ and $V_Q(n)$ signals respectively. The argument is formulated by the angle between individual complex components $V_I(n)$ and $V_Q(n)$. The way of computing the angle is approximated by employing inverse tangent function. Hence, the arctangent function supporting the angle extraction is proposed.

The arctangent function can be realized on two ways, employing following one-argument inverse tangent (arctan) and two-argument inverse tangent (arctan2) functions. The arctan is a multivalued function that requires a branch cut defined as a curve with ends possibly open, closed, or half-open in the complex plane [Abramowitz72, Weisstein]. The branch cut determines the range of real arguments typed between ($-\pi/2$, $\pi/2$) or in most cases taken from (0, π). Being plotted above the complex plane, the arctan can take the following values, e.g. arctan($-\infty$)= $-\pi/2$, arctan(0)= 0, arctan(∞)= $\pi/2$ [Weisstein]. So, in a purpose of arctan application, the complex argument of a sample complex number $z=x+i \cdot y$ can often be rewritten as $\phi=arctan(y/x)$, where ϕ corresponds to the counterclockwise angle from the positive real axis [Weisstein]. Whereas, the one-argument arctan is not able to correctly distinguish between opposite directions, the arctan2 takes into account the signs of both *x* and *y* coordinates, placing the angle in the correct quadrant. Thus, in terms of standard arctan2 in range of ($-\pi/2$, $\pi/2$), the arctan2 can be expressed as [Zwillinger95, Abramowitz72],

$$\arctan 2(y,x) = \arg(z) = \begin{cases} \arctan(y/x) \Leftrightarrow x > 0 \\ \arctan(y/x) + \pi \Leftrightarrow y \geq 0, x < 0 \\ \arctan(y/x) - \pi \Leftrightarrow y < 0, x < 0 \\ +\pi/2 \Leftrightarrow y > 0, x = 0 \\ -\pi/2 \Leftrightarrow y < 0, x = 0 \\ undefined \Leftrightarrow \{y,x\} = 0 \end{cases} \tag{3.33}$$

Thence, the argument featured by arctan2 function between complex components is calculated and the phase un-wrapper is used to minimize the effect of phase ambiguities.

Since, the OFDM receiver operates in the discrete time domain, the following formulas (3.30-3.32) have been used.

Thus, the argument of complex OFDM signal formulated as $s(n)=arg(\cdot)$ for both *I* and *Q* branches, using Euler's formula can be expressed by,

$$s(n) = \arg\left[V_I(n) + jV_Q(n)\right] =$$
$$\ldots = \arg\left[\begin{array}{l} R_L R\sqrt{P_S P_{LO}} \cdot \ldots \\ \ldots \cdot \exp\left(j\frac{\pi \cdot H}{V_\pi} \cdot \frac{1}{\sqrt{N}} \sum_i \left[\sum_{k=0}^{N-1} X_{i,k} \cdot \left[cas(\frac{2\pi}{N} f_k n) \right] \right] g_k(nT_s - i) + \theta_i - \phi_e(t) \right) \end{array}\right] \quad (3.34)$$

Following phase components as θ_i and $\phi_e(t)$ are assumed to be constant. Forasmuch the OFDM signal is known to behave as a Gaussian process, such phase factors can be neglected for simplicity. By applying the property of argument for complex signal, $arg(Ae^{j\varphi}) = s(n)$, expression (3.34) can be approximated in time domain yielding,

$$p(t) = \frac{\pi \cdot H}{V_\pi} \cdot \frac{1}{\sqrt{N}} \sum_i \sum_{k=0}^{N-1} X_{i,k} \cdot \left[\cos(2\pi f_k t) + \sin(2\pi f_k t)\right] g_k(t - iT_B) \quad (3.35)$$

Next, by deploying the discrete samples, constant time values $\{t\}$ (3.35) lead to discrete values $\{n\}$. The final $arg(\cdot)$ is arranged as,

$$p(n) = \frac{\pi \cdot H}{V_\pi} \cdot \frac{1}{\sqrt{N}} \sum_i \sum_{k=0}^{N-1} X_{i,k} \cdot \left[\cos(\frac{2\pi}{N} f_k n) + \sin(\frac{2\pi}{N} f_k n) \right] g_k(nT_s - i) \quad (3.36)$$

Further, the resulting samples are parallelized and the cyclic prefix removed. The resulting real signal is handled like an usual OFDM discrete signal including DHT, training symbols removal, linear equalization, subcarrier demapping and serialization stage.

So, let $x_{i,k} = [x_{i,0}\ x_{i,1}\ x_{i,2} \ldots\ x_{i,N-1}]^T$ be the vector representing the sampled time domain signal at the DHT input and $X_{i,k} = [X_{i,0}\ X_{i,1}\ X_{i,2} \ldots\ X_{i,N-1}]^T$ the discrete frequency domain vector at DHT output. Therefore, from the definition, DHT performs the forward transform of x_m discrete samples for each ith OFDM block resulting in,

$$X_{i=1,k} = \frac{1}{\sqrt{N}} \sum_i \left[\sum_{m=0}^{N-1} x_m \cdot \left[\cos(\frac{2\pi}{N} f_k m) + \sin(\frac{2\pi}{N} f_k m) \right] \right] \quad (3.37)$$

Here, DHT was applied to perform OFDM demodulation process.

Hence, (3.36) is compared with general DHT equation (2.37) that has been finally proved and satisfied (3.1).

After completing DHT, the training symbols are removed and equalization of the received signal is pursued.

Normally, the sense of linear equalization in theory is translated into the transversal filter equipped with a tapped delay line [Kaminow97]. That line in principle sums the incoming copies of many delayed inputs. Each input is separately adjusted by a proper weight. Generally, the tap spacing is desired to be less than one symbol period. In turn, a proper number of taps to be taken while equalization is chosen once the channel spread is surpassed by the single span [Kaminow97].

In matter of fact, the applied equalization combat channel impairments and help to adjust data after transmission. The data is estimated in feasible way by using training symbols.

In principle of operation for the proposed equalization scheme, the training symbols are allocated at each subcarrier. Total number of symbols transmitted over the system is enlarged by the number of training symbols added for estimation. The equalization is based on complex I and Q components of data symbols retrieved from data at phase-diversity receiver outputs and tailored for estimating a channel.

In principle, the idea for equalization matched DHT is to generate the training symbols and by sending them over the channel, to evaluate the impact of impairments that can deteriorate the data transmission. To satisfy this goal, the equalization complex matrix for both I and Q branches is constructed. Initially, the complex matrix is equipped with zeros. Next, once the training symbols have been inserted in all the subcarriers [Wang05, Wang00], the correction coefficients represented by data and training symbols are properly ported into the correct place of equalization matrix M_{eq}, expressed for $i= 0,1,2,...,N-1$ as,

$$M_{eq}=\begin{bmatrix} \frac{d(1\quad 1:nts)}{ts(:\quad 1)} & 0 & \cdots & 0 & 0 & \cdots & 0 & 0 \\ 0 & \frac{d(i\quad 1:nts)}{ts(:\quad i)} & 0 & \vdots & \vdots & 0 & 0 & \frac{-d(N-i+1\quad 1:nts)}{ts(:\quad i)} \\ \vdots & 0 & \ddots & 0 & 0 & 0 & \iddots & 0 \\ 0 & \vdots & 0 & \ddots & 0 & \iddots & 0 & \vdots \\ 0 & 0 & 0 & 0 & 1 & 0 & \vdots & 0 \\ \vdots & \vdots & 0 & \iddots & 0 & \ddots & 0 & \vdots \\ 0 & 0 & \iddots & 0 & \vdots & 0 & \ddots & 0 \\ 0 & \frac{d(N-i+1\quad 1:nts)}{ts(:\quad i)} & 0 & \cdots & \cdots & \cdots & 0 & \frac{d(N/2-i+2\quad 1:nts)}{ts(:\quad N/2-i+2)} \end{bmatrix} \tag{3.38}$$

where, d stands for the received data symbols, ts denotes the received training symbols for estimation and nts is the number of training symbols.

The size of the M_{eq} matrix is equal to the number of carriers in a row and a column. Hence, once M_{eq} is filled by the data and training symbol coefficients, the channel information can be featured later on by the subcarrier response a_i and the interference factor b_i as [Wang05],

$$\begin{aligned} a_i &= \frac{d_i \cdot ts_i + d_{N-i} \cdot ts_{N-i}}{|ts_i|^2 + |ts_{N-i}|^2} \\ b_i &= \frac{d_{N-i} \cdot ts_i - d_i \cdot ts_{N-i}}{|ts_i|^2 + |ts_{N-i}|^2} \end{aligned} \tag{3.39}$$

Having the way to estimate data sent through the channel, such symmetry properties of equalization coefficients as $a_i = a_{N-i}$ and $b_i = -b_{N-i}$ need to be taken into account [Wang05].

Due to above assumption, only $\{a_i\}$ and $\{b_i\}$ can be used for estimation. Then, if zeros are inserted to the $N/2,N/2+1,...,N-1$, for each N as a real division, (3.39) becomes simplified to [Wang05],

$$\begin{aligned} a_i &= \frac{d_i}{ts_i} \\ b_i &= \frac{d_{N-i}}{ts_i} \end{aligned} \tag{3.40}$$

, from whose the recover data symbols can easily be equalized.

Approaching to the end of this consideration, data is reconstructed by means of BPSK symbols demapping. Subsequently, the serialization stage is executed and data totally recovered.

3.2 Chapter Summary

At this chapter the full explanation of the scheme used in the PhD research is given.
The explanation is based on the general description supported by the theoretical consideration of signal processing in the proposed optical OFDM transmission system.
The proposed architecture is carefully characterized and each of the elements properly detailed at the end of each transmission stage.
The scheme presents the novel approach to the well-known CO-OFDM system widely explored in mobile/wireless communication and finally fed into optical domain with some new functionality. The functionality is addressed to demand for high bandwidth service and potential architecture possibilities. The demand for bandwidth lately increases at exponential rate and architecture possibilities are mainly featured by intelligent phase-diversity coherent receiver alongside advanced DSP. DSP provides easy way to mitigate optical impairments and increase the total transmission capacity not yet attained based on RF transmission model [Gerstel12].
Furthermore, some new feasibilities of the proposed system were manifested.
A new kind of totally real transform was applied to DSP. The discrete Hartley transform replaced a traditional discrete Fourier transform and overcame the need to have a Hermitian symmetry. These attempts simplified and speeded up all the calculations in DSP at transmitter and receiver side, making them faster and easier to process and evaluate [Svaluto12].
Meanwhile, an additional pure phase modulation fully performed in optical domain helped dealing with amplitude fluctuations of OFDM signal and lowered such a huge PAPR level till 0 dB [Huene11, Svaluto12].
The phase diversity receiver equipped with functionality of homodyne detection became a main detection method and part of the proposed system. It involved the 90^0 optical hybrid with the balanced detection featured by four PIN photo-detectors.
The digital processing at receiver side reflects the full functionality of the processing at transmitter side. The main difference concerns the carrier recovery, electrical phase demodulation and equalization totally deployed at frequency domain.

CHAPTER 4: CHARACTERIZATION OF OPTICAL CE-OFDM SYSTEM

In this chapter, theory and simulations are discussed. Furthermore, for the first time a phase modulated CO-OFDM system based on Hartley transform is characterized in terms of different impacts from the transmission and system point of view.

First, impacts of sensitivity featured by thermal and shot noises and optical amplification noise exhibited by amplified spontaneous emission (ASE) noise are investigated. Moreover, the impact of additional effects from among of phase noise, frequency offset and IQ imbalance are studied. At the end, the impact of dispersion is analysed, as well as its mitigation by means of a digital filter placed at the receiver side.
The main figures of merit used to evaluate the system performance are the probability of error and the bit error ratio.

The chapter is organized as follows. Section 4.1 deals with the impact of the modulator driving and the theoretical model is proposed and validated by means of simulations. Next, in section 4.2 the impact of phase noise is investigated by means of simulations. Section 4.3 struggles with the impact of frequency offset and section 4.4 presents the impact of IQ imbalance. For both sections, a numerical analysis is carried out. The last section 4.5 covers the impact of dispersion featuring a transmission over the fiber link and a filter compensation using a digital filter to combat dispersion.

4.1 Impact of Modulator Driving

In this section, the impact on the modulator driving is going to be studied. That in fact, it supposes a problem, as the performance of the system is being limited by the impact of noise generated on electrical and optical way. The electrical noise featured by shot and thermal noise refers to the one generated during photo-detection process and electrical amplification. Meanwhile, the optical noise is usually contributed by amplified spontaneous emission (ASE) of optical amplifiers. Hence, at this section the full theoretical description and its validation by means of simulations in case of sensitivity performance related to the electrical noise (shot and thermal noises) and the optical noise characterized by optical amplification is manifested.

4.1.1 Sensitivity Performance

At this sub-section, the performance of the proposed system illustrated in chapter 3, in terms of receiver sensitivity is assessed. First, a theoretical model is developed. Afterwards, the analytical model is validated with numeric simulations. Please note that when testing the receiver sensitivity, the dominating noises are relative to the photo-detection and the electrical amplification, i.e. shot and thermal noises. Thus, a back-to-back configuration with no optical link is under investigation.

A. Theoretical model

Hence, deploying analytical model from 2nd chapter, let $\varphi(t)$ consider as an useful received OFDM signal for a single OFDM symbol at kth subcarrier. The scheduled OFDM signal is given by,

$$s(t) = \frac{1}{\sqrt{N}} \sum_{k=0}^{N-1} Y_{1,k} \cdot \left[\cos(2\pi f_k t) + \sin(2\pi f_k t)\right] \tag{4.1}$$

The further analysis regarding the sensitivity performance is studied in time domain featured by $\{t\}$ rather than in digital domain represented by $\{n\}$. All the mathematical study is based on the general description related to the generation of the CE-OFDM signal discussed in chapter 3 (3.1-3.15). The present analysis exhibits the features of the receiver in terms of complex additive noises once the CE-OFDM signal (3.15) is received.

Thus, since the baseband signal, represented by (3.11) and (3.12), is up-converted and transmitted, the optical phase modulated OFDM signal in this configuration can be written as in (3.15),

$$s_s(t) = \sqrt{P_S}\exp\left(j\varphi(t)\right) = \sqrt{P_S}\exp\left(j\omega_S t + j\frac{\pi \cdot H}{V_\pi} \cdot s(t) + \theta_i\right) \tag{4.2}$$

After reception, the general optical CE-OFDM received signal is so equal to,

$$r(t) = s_s(t) + n(t) \tag{4.3}$$

where, *n(t)* refers to the noise components defined by (4.5).
Going further, the voltages present at the output of the balanced detectors at I and Q branches respectively can be defined as,

$$\begin{aligned} V_I^{'}(t) &= V_I(t) + n_I(t) \\ V_Q^{'}(t) &= V_Q(t) + n_Q(t) \end{aligned} \tag{4.4}$$

where, both $n_I(t)$ and $n_Q(t)$ refer to the complex additive noise (thermal and shot noise) at individual *I* and *Q* branches respectively.
As, it was already implied in chapter 3, substituting the real (3.19, 4.1) into (4.2), the voltages present at the output of balanced detectors (4.3), including noise information can be deployed as,

$$\begin{aligned} &V_I^{'}(t) \cong R_L R\sqrt{P_S P_{LO}} \cdot \ldots \\ &\ldots \cdot \cos\left(\frac{\pi \cdot H}{V_\pi} \cdot \frac{1}{\sqrt{N}} \sum_i \left[\sum_{k=0}^{N-1} Y_{i,k} \cdot \left[\cos(2\pi f_k t) + \sin(2\pi f_k t)\right]\right] g_k\left(t - iT_B\right) + \theta_i - \phi_e(t)\right) + n_I(t) \end{aligned} \tag{4.5}$$

$$\begin{aligned} &V_Q^{'}(t) \cong R_L R\sqrt{P_S P_{LO}} \cdot \ldots \\ &\ldots \cdot \sin\left(\frac{\pi \cdot H}{V_\pi} \cdot \frac{1}{\sqrt{N}} \sum_i \left[\sum_{k=0}^{N-1} Y_{i,k} \cdot \left[\cos(2\pi f_k t) + \sin(2\pi f_k t)\right]\right] g_k\left(t - iT_B\right) + \theta_i - \phi_e(t)\right) + n_Q(t) \end{aligned} \tag{4.6}$$

The shot and thermal noise are the dominating noises, as they are relative to the photo-detection and further electrical amplification, they are. The thermal noise is assumed to be the most dominating one and it behaves as a Gaussian noise.

So, the variance of the processes $n_I(t)$ and $n_Q(t)$ at individual I and Q branches each in photocurrents can be exhibited by,

$$\sigma^2 = \sigma^2{}_{thermal} + \sigma^2{}_{shot} = \left\langle i^2{}_{thermal} \right\rangle + \left\langle i^2{}_{shot} \right\rangle \cong \left\langle i^2{}_{thermal} \right\rangle \tag{4.7}$$

where, individual $\sigma_{thermal}$ and σ_{shot} components account for both thermal and shot noise respectively. Here, we consider that the shot noise is neglected and the thermal noise is only one dominating noise term to be considered.
Consequently, $n(t)$ (4.3) can be represented by individual $n_I(t)$ and $n_Q(t)$ components as the projections of a noise polar signal,

$$n(t) = n_I(t) + jn_Q(t) = A_n(t)e^{j\Theta(t)} \tag{4.8}$$

where, $A_n(t)$ is the noise envelope and $\Theta(t)$ stands for the noise phase signal.
At this case, if $n_I(t)$ and $n_Q(t)$ accounted as Gaussian process are far from 0, $A_n(t)$ is a Ricean process with a standard deviation of σ and may be explained as,

$$A_n(t) = \sqrt{n_I{}^2(t) + n_Q{}^2(t)} = \sqrt{N_I(\sigma) + N_Q(\sigma)} \tag{4.9}$$

Regarding $\Theta(t)$, it has a uniform distribution between $\{-\pi, \pi\}$ [Papoulis02] and can be defined as,

$$\Theta(t) = \arg\big(n(t)\big) = \arg\big(n_I(t) + jn_Q(t)\big) = \arctan\left[\frac{n_Q(t)}{n_I(t)}\right] \tag{4.10}$$

Substituting (4.9-4.10) into (4.8), the noise $n(t)$ at the input of the receiver can be represented in a total polar form as,

$$n(t) = \sqrt{n_I{}^2(t) + n_Q{}^2(t)}\, e^{j\arctan\left[\frac{n_Q(t)}{n_I(t)}\right]} = A_n(t)e^{j\Theta(t)} \tag{4.11}$$

Next, the phase demodulation process is going to be executed. The phase demodulation featured as a$rg(\cdot)$ is processed by unwrapping the phase of single complex input, including the useful signal $s(t)$ and the noise $n(t)$. The approach to calculate final a$rg(\cdot)$ is based on the properties of arctan function along with arctan2 featured in chapter 3 (see 3.26). The function of arctan2 is an extended version of the arctan in the range of $(-\pi, \pi)$ and both can equally be employed to find the phase term.
Hence, using the voltages at the output of the balanced detectors (4.5-4.6), the phase of the received signal $\theta(t)$ can be retrieved as,

$$\theta(t) = \arg\left[V_I'(t) + jV_Q'(t)\right] = \arctan\left[\frac{V_Q'(t)}{V_I'(t)}\right] \tag{4.12}$$

Further, substituting (4.5-4.6) into (4.12), the final $\theta(t)$ = a$rg(\cdot)$ is featured as,

$$\theta(t) = \arg\left[V_I'(t) + jV_Q'(t)\right] = \arctan\left[\frac{V_Q'(t)}{V_I'(t)}\right] = \arctan\left[\frac{R_L R\sqrt{P_S P_{LO}}\cdot\sin\big(\varphi(t)\big) + n_Q(t)}{R_L R\sqrt{P_S P_{LO}}\cdot\cos\big(\varphi(t)\big) + n_I(t)}\right] \tag{4.13}$$

Simplifying the following (4.13), the received phase signal is finally given by,

$$\theta(t) = \arctan\left[\frac{A\sin\left(\frac{\pi \cdot H}{V_\pi} s(t)\right) + n_Q(t)}{A\cos\left(\frac{\pi \cdot H}{V_\pi} s(t)\right) + n_I(t)}\right] = \frac{\pi \cdot H}{V_\pi} s(t) + \theta_e(t) + \theta_n(t) \tag{4.14}$$

where, $\theta_e(t) = \theta_i(t) - \phi_e(t)$ denotes the phase error term, which can depend on the phase noise, frequency offset or IQ imbalance; and $\theta_n(t)$ stands for the phase term including noise components at $n_I(t)$ and $n_Q(t)$.

Subsequently, several assumptions are taken. The binary data symbols $\{X_{1,k}\}$ (3.30) take the following values of ±1 and the phase pulses $\{g(t)\}$ turn out as orthogonal OFDM subcarriers defined for $nT \leq t < (n+1)T$.

Hence, after some algebra, $\theta_n(t)$ in terms of noise components at $n_I(t)$ and $n_Q(t)$ is written as,

$$\theta_n(t) = \arctan\left[\frac{\sqrt{n_I^{\,2}(t) + n_Q^{\,2}(t)} \cdot \sin\left[\Theta(t) - \frac{\pi \cdot H}{V_\pi} s(t) - \theta_e(t)\right]}{R_L R\sqrt{P_S P_{LO}} + \sqrt{n_I^{\,2}(t) + n_Q^{\,2}(t)} \cdot \cos\left[\Theta(t) - \frac{\pi \cdot H}{V_\pi} s(t) - \theta_e(t)\right]}\right] \tag{4.15}$$

Then, assuming high signal-to-noise ratio (SNR) it turns that $R_L R\sqrt{P_S P_{LO}} >> A_n(t)$, and (4.15) becomes,

$$\theta_n(t) \approx \arctan\left[\frac{\sqrt{n_I^{\,2}(t) + n_Q^{\,2}(t)} \cdot \sin\left[\Theta(t) - \frac{\pi \cdot H}{V_\pi} s(t) - \theta_e(t)\right]}{R_L R\sqrt{P_S P_{LO}}}\right] \tag{4.16}$$

Analysing the worst case, the argument of $\sin(\cdot)$ can behave as a uniform random process, taking values inside $\{-\pi, \pi\}$, varying at much higher speed than data rate.

Hence, assuming that phase error $\theta_e(t)$ is constant and equal to $-\pi/2$ (one taken at $\sin(\cdot) = \sin(E\{\cdot\})$), that translates to the phase term of (4.14) neglected, (4.16) can be finally approximated to,

$$\theta_n(t) \approx \arctan\left[\frac{\sqrt{n_I^{\,2}(t) + n_Q^{\,2}(t)}}{R_L R\sqrt{P_S P_{LO}}}\right] \approx \frac{\sqrt{n_I^{\,2}(t) + n_Q^{\,2}(t)}}{R_L R\sqrt{P_S P_{LO}}} \tag{4.17}$$

Indeed, the output of phase demodulator in terms of noises $\theta_n(t)$ is defined in 4.17.

At this point, the digitizing, argument extraction and OFDM demodulation can be considered as a correlator bank plus sampling. So, the kth OFDM receiver block correlates noisy input with the data subcarriers and the demodulated phase can be expressed as,

$$\theta_k(t) = \frac{1}{T_B}\int_0^{T_B} \theta(t) T_k(t) dt = \frac{1}{T_B}\int_0^{T_B}\left[\frac{\pi \cdot H}{V_\pi} s(t) + \theta_e(t) + \theta_n(t)\right] T_k(t) dt \ldots \tag{4.18}$$

$$\ldots \equiv S_k + E_k + N_k$$

where S_k stands for the useful signal, E_k corresponds to the phase error term $\theta_e(t)$, and N_k is the noise term due to $\theta_n(t)$. In turn, $T_k(t)$ refers to the transform of the k-th subcarrier formulated as,

$$T_k = cas\left(\frac{2\pi f_k t}{N}\right) = \cos\left(\frac{2\pi f_k t}{N}\right) + \sin\left(\frac{2\pi f_k t}{N}\right) \tag{4.19}$$

being,

$$\int_0^{T_B} T_k(t) T_k(t) dt = T_B .$$

Hence, the useful signal component can be calculated as [Thompson08],

$$S_k = \frac{1}{T_B}\int_0^{T_B} s(t) T_k(t) dt = \frac{2\pi h}{T_B}\int_0^{T_B}\left[\sum_{n=1}^{N} Y_n s_n(t)\right] T_k(t) dt = \frac{\pi \cdot H}{\sqrt{N} V_\pi} Y_k \tag{4.20}$$

Similarly to [Thompson08], E_k can be assumed to be constant and due to periodicity of the OFDM subcarriers, such a phase error can be neglected.
So, assuming $E_k = 0$, the noise component is the only remaining term and can be defined as,

$$N_k = \frac{1}{T_B}\int_0^{T_B} \theta_n(t) T_k(t) dt \tag{4.21}$$

Afterwards, the approximation by taking (4.19) leads to the Fourier coefficients of $\theta_n(t)$ at $f_k = k/(2T)$ Hz. While T_B goes to the infinity, the variance of the coefficient is proportional to the spectrum evaluated at $f_k = k/2T$.
Looking for the noise value, when assuming $R_L R\sqrt{P_S P_{LO}} >> A_n(t)$, $\theta_n(t)$ will behave as a very small Rician random process [Papoulis02], varying around levels of signal much larger than itself.
Thence, in this case, N_k can be approximated by a zero mean Gaussian variable [Davenport58].
In case of $n_I(t)$ and $n_Q(t)$ are independent and identically distributed Gaussian noises with variance σ^2, it is pretty straight forward to get the variance of N_k as,

$$\mathrm{var}\{N_k\} = E\left[N_k{}^2\right] = \frac{N_0}{8T_B R^2 P_S P_{LO}} = \frac{\sigma^2}{8T_B R^2 P_S P_{LO}} \tag{4.22}$$

where, $2T_B$ defines considered bandwidth and the number *4* confirms the number of *2* Fourier coefficients instead of only 1.
For the case proposed where the dominating noise is the thermal noise, σ is then calculated as [Agrawal02],

$$\sigma = \sqrt{\frac{2k_B T F_n}{R_L}} \tag{4.23}$$

Where, k_B is the Boltzmann constant, T stands for the room temperature and F_n defines the noise figure.
Afterwards, note that (4.20) and (4.22) pave the way to the calculus of the signal-to-noise ratio (SNR) of the received data symbols just before demapping, given by,

$$SNR = \frac{P_{signal}}{P_{noise}} = \frac{S_k^{\,2}}{\mathrm{var}\{N_k\}} = \frac{\pi^2 H^2}{N V_\pi^{\,2}} \cdot \frac{8 T_B R^2 P_S P_{LO}}{\sigma^2} \ldots$$
$$\ldots = \frac{8\pi^2 H^2 R^2 P_S P_{LO} T_B}{N V_\pi^{\,2} \cdot \sigma^2} \tag{4.24}$$

where, P_{signal} denotes the linear signal power and P_{noise} is the linear noise power.
So, taking into account the SNR as defined in (4.24) and assuming the Gaussian statistics, the theoretical probability of error in case of BPSK signal can be reached by applying [Proakis89],

$$Pe = \frac{1}{2}\left[erfc\left(\sqrt{\frac{SNR}{2}} \right) \right] = \frac{1}{2}\left[erfc\left(\frac{2\pi HR}{V_\pi \sigma} \cdot \sqrt{\frac{P_S P_{LO} T_B}{N}} \right) \right] \tag{4.25}$$

where, *erfc* features the complementary error function.

Afterwards, the theoretical investigation in case of thermal noise featured by (4.25) is summarized by plotting the BER waterfalls and validating the theoretical scheme by means of extensive simulations. Fig. 4.1 shows sample theoretical BER curves as function of useful received signal power P_S and at different values of the standard deviation of the phase at the output of the transmitter ($\pi H/V_\pi$). Taking into account that the OFDM signal at the output of the DAC can be modelled as a gaussian noise, the optimized parameter became its standard deviation ($\sigma_{mod} \approx \pi H$) such that has been normalized to the V_π of the phase modulator. In turn, there, it can be observed that, according to the theoretical model, the higher the standard deviation is, the lower the needed power is at the input of the receiver for attaining the same BER. The validity of this model is assessed by means of simulations and, in the next subsection, it is featured and further discussed.

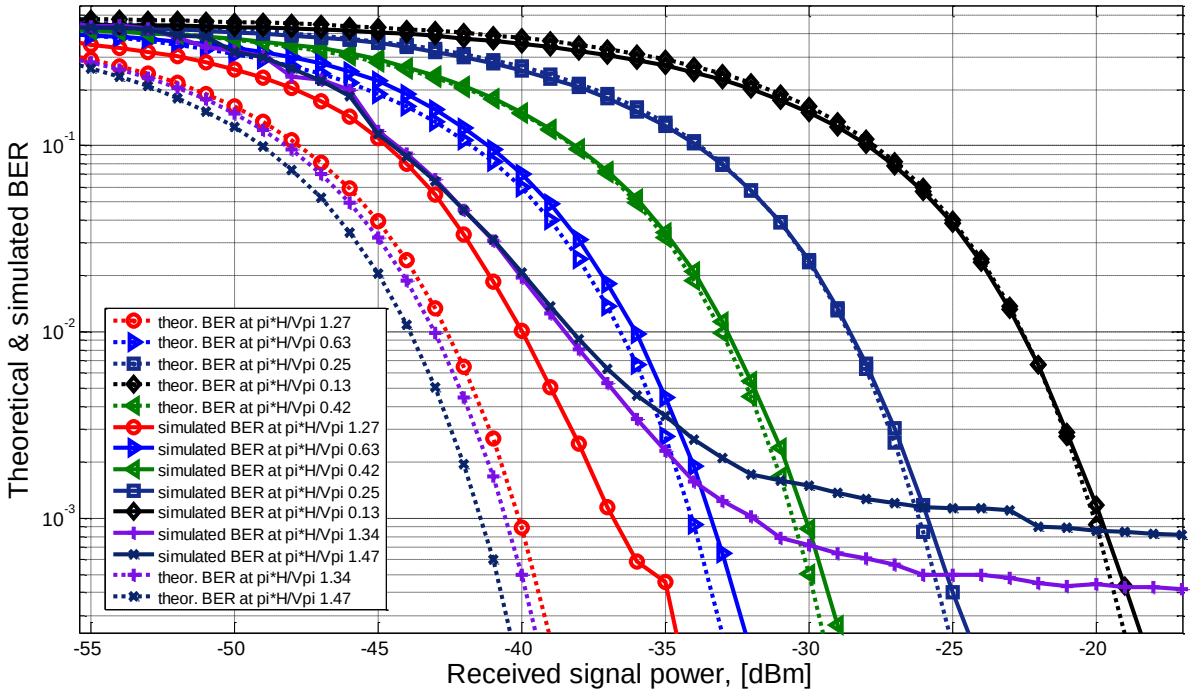

Figure 4.1. Sample theoretical and simulated BER curves in the function of received signal power at 10 Gb/s.

B. *Simulations*

All the simulations have been performed using Matlab software. A set of 2^{15}-1 pseudorandom bits are generated at 10 Gb/s using a sequence of length 2^{16} bits. The bit sequence was BPSK encoded and OFDM modulated to 64 carriers by applying IFHT. Next, the resulting signal was up-sampled using 8 samples per bit and directed to the phase modulator, excited by a continuous wave (CW) laser centered at 1550 nm with output power of 0 dBm. At the receiver, the local oscillator was also modeled as a CW laser centered at 1550 nm with output power of 1 mW. The photo-detectors are modelled as PIN diodes at room temperature of 290 K with responsivity of 0.7 A/W, impedance of 50 Ohm, dark current of 1 Pa and thermal noise of 9.2 $pA\sqrt{Hz}$. The noise factor is considered of 2 dB. OFDM decoding and data demodulation are performed after intradyne detection.

Using these parameters, extensive simulations are carried out varying the standard deviation of the phase at the output of the transmitter ($\pi H/V_\pi$) and measuring the sensitivity at the receiver side. In order to perform this, the signal between transmitter and receiver was attenuated in steps of 1 dB maximum, and the BER is calculated by counting errors at the receiver output. Results are shown in Figs. 4.1-4.2.

On Fig. 4.1, sample BER waterfall curves are exhibited. There it can be observed that for low standard deviation of the transmitted phase (< *0.79 rad*), theory and simulations match almost perfectly. However, when increasing the standard deviation, there is a penalty between theory and simulations.

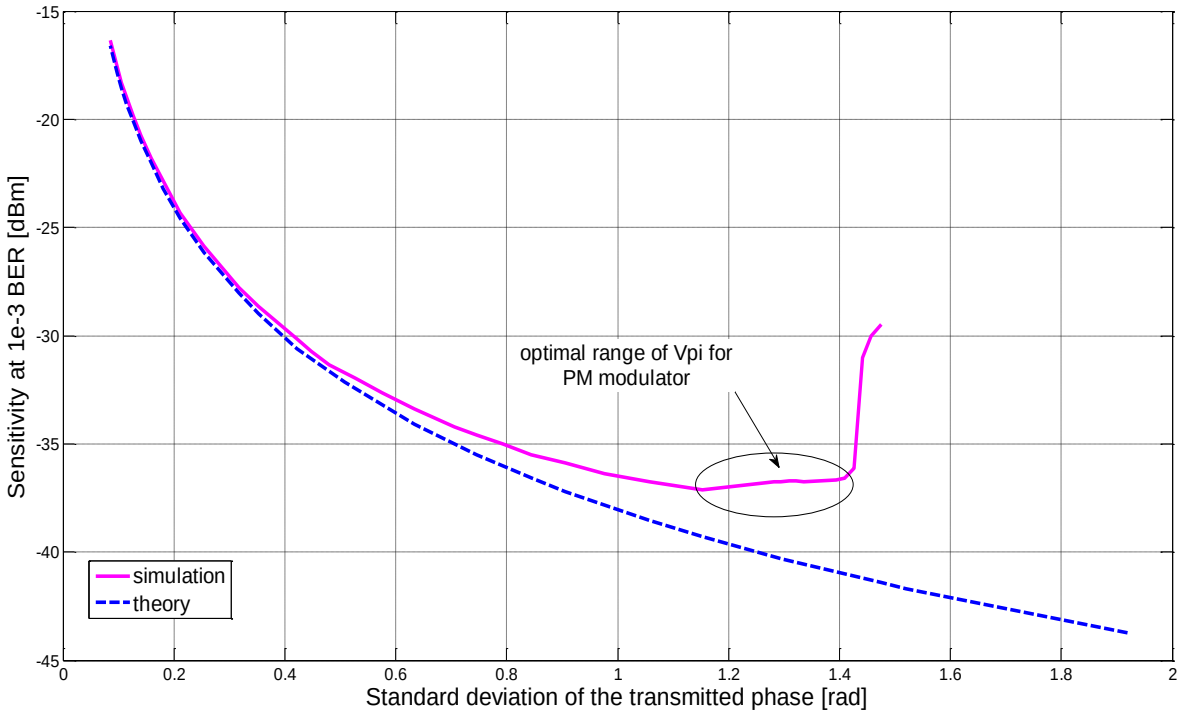

Figure 4.2. Theoretical and simulated sensitivity curves vs. standard deviation of the transmitted phase.

For evaluating the difference between theory and simulations when increasing $\pi H/V_\pi$, Fig. 4.2 shows the sensitivity at 10^{-3} BER as a function of the standard deviation of the transmitted phase.

There, it is shown that for $\pi H/V_\pi$ values around $\pi/4 \approx 0.79$ and beyond, the system sensitivity at 10^{-3} BER experiences a non-negligible penalty.
Precisely, a minimum optimal sensitivity value of -37 dBm is reached in the marked region of $\sigma_{mod} \in$ 1.2-1.4 rad. This is consistent with the observations reported by [Thompson08] where an optimum σ_{mod} of 1.3 rad was found. Furthermore, near $\pi/2$, the penalty between simulations and theory increases and beyond that point it is not possible to achieve 10^{-3} BER. That is due to the arctan function used for retrieving the phase at the reception side. The property of arctan function was deployed in chapter 3 (3.26). As it is implied in the simulations, the angle extraction is performed by the angle function of Matlab, which is based on the two argument arctan2(r_{Qn}, r_{In}) function [Matlab10]. The arctan2(r_{Qn}, r_{In}) is a typical function limited within the range $(-\pi, \pi]$, and for the first and fourth quadrants ($r_{In} > 0$) it can be defined as arctan2(r_{Qn}, r_{In}) = arctan(r_{Qn}, r_{In}). This is the reason why, when using an enhanced angle extraction, the results show the behavior expected according to the mathematical models discussed.
Finally, from the results, the arctan function results in a non-defined value at $\pi/2$, whereas it tends to $+\infty$ when approaching to it from the left side. This leads to an additional noise which depends on the standard deviation of the transmitted phase, as a sigmoid-like clipping affects the signal.

4.1.2 Optical Noise Performance

In previous sub-section, photo-detection noise and its model were discussed and investigated. However, for optically amplified systems, the most dominant noise is the optical one mainly contributed by amplified spontaneous emission (ASE) of optical amplifiers [Agrawal02]. In the present sub-section, a theoretical model is developed and briefly describes the effects of ASE noise in the proposed OFDM system. Next, as in the previous section, the theoretical model is compared against simulations and further discussed.

A. *Theoretical model*

In this sub-section, a theoretical model of the impact of optical amplification noise is going to be discussed. In fact, this noise is modeled as a Gaussian process, and it is additive in terms of the optical field. Hence, when employing coherent detection, the resulting currents after photodetection behave as a Gaussian process at the output of each balanced detector [Seimetz09]. That is the reason why the developments performed in case of sensitivity performances are applicable to describe the performance of the proposed system for the amplification noise.
Nevertheless in the optical domain, the noise of applied optical amplifier is complex and defined as,

$$n(t) = n_{\parallel}(t)e_{\parallel} + n_{\perp}(t)e_{\perp} \tag{4.26}$$

where, both components $n_{||}(t)$ and $n_{\perp}(t)$ are co-polarized orthogonally polarized with respect to the incoming signal.
Since the noise is considered to have a much higher contribution than the noise due to the photo-detection, the variance of the noise processes can be approximated to the one due to ASE. Hence, once $Re\{n_{||}(t), n_{\perp}(t)\}$ and $Im\{n_{||}(t), n_{\perp}(t)\}$ are considered, the following noises at I and Q branches are featured by the total variance σ^2 given by,

$$\sigma^2 = \sigma^2{}_{thermal} + \sigma^2{}_{shot} + \sigma^2{}_{ASE} \cong \sigma^2{}_{ASE}$$
$$\sigma^2_{ASE} = \sigma^2{}_I = \sigma^2{}_Q = \frac{N_O \cdot B_n}{2} \tag{4.27}$$

where B_n is the optical noise bandwidth.
In the following development, the shot and thermal noises are neglected and the ASE noise is only one dominating noise term to be analysed.
Indeed, based on (4.4-4.6) the outputs of 90º optical hybrid referred as $V_I(t)$ and $V_Q(t)$ including ASE noise components are defined as,

$$V_I^{'}(t) \cong V_I(t) + n_{ASE,I}(t)$$
$$V_Q^{'}(t) \cong V_Q(t) + n_{ASE,Q}(t) \tag{4.28}$$

where, both $n_{ASE,I}(t)$ and $n_{ASE,Q}(t)$ refer to the complex additive ASE noise at individual I and Q branches each.
Substituting the real (3.19) into (4.4) in terms of ASE noise, (3.28) is becoming,

$$V_I^{'}(t) \cong R_L R\sqrt{P_S P_{LO}} \cdot \ldots$$
$$\ldots \cdot \cos\left(\frac{\pi \cdot H}{V_\pi} \cdot \frac{1}{\sqrt{N}} \sum_i \left[\sum_{k=0}^{N-1} Y_{i,k} \cdot \left[\cos(\frac{2\pi}{N} f_k t) + \sin(\frac{2\pi}{N} f_k t) \right] \right] g_k\left(t - iT_B\right) \right) + n_{ASE,I}(t) \tag{4.29}$$

$$V_Q^{'}(t) \cong R_L R\sqrt{P_S P_{LO}} \cdot \ldots$$
$$\ldots \cdot \sin\left(\frac{\pi \cdot H}{V_\pi} \cdot \frac{1}{\sqrt{N}} \sum_i \left[\sum_{k=0}^{N-1} Y_{i,k} \cdot \left[\cos(\frac{2\pi}{N} f_k t) + \sin(\frac{2\pi}{N} f_k t) \right] \right] g_k\left(t - iT_B\right) \right) + n_{ASE,Q}(t) \tag{4.30}$$

Meanwhile, taking into account that the ASE noise has a Gaussian distribution and is additive in nature, the theoretical analysis deployed for ASE noise fully reflects to the sensitivity performance discussed in previous section. By (4.8-4.11), the noise distortion $n(t)$ in a presence of optical noise of ASE is represented by individual $n_{ASE,I}(t)$ and $n_{ASE,Q}(t)$ components as,

$$n(t) = n_{ASE,I}(t) + jn_{ASE,Q}(t) = \sqrt{n_{ASE,I}{}^2(t) + n_{ASE,Q}{}^2(t)}\, e^{j \arctan\left[\frac{n_{ASE,Q}(t)}{n_{ASE,I}(t)}\right]} = A_{ASE,n}(t) e^{j\Theta(t)} \tag{4.31}$$

where, $A_{ASE,n}(t)$ is the envelope of optical noise and $\Theta(t)$ stands for the noise phase signal.
Nevertheless, next based on (4.12-4.17), the phase demodulation by unwrapping a phase is performed. The $arg(\cdot)$ of demodulation input, including the useful signal $s(t)$ interfered with $s_{LO}(t)$ and the noise $n(t)$ reflecting ASE noise limit is calculated. In fact, similarly to (4.17), the phase term in case of optical noise components $\theta_n(t)$ is approximated by,

$$\theta_n(t) \approx \frac{\sqrt{n_{ASE,I}{}^2(t) + n_{ASE,Q}{}^2(t)}}{R_L R\sqrt{P_S P_{LO}}} \tag{4.32}$$

(4.32) deals pretty well with the theory behind sensitivity performance manifested in previous section. Here, $\theta_e(t)$ defines the phase error term depending on phase noise, frequency offset or IQ imbalance, and $\theta_n(t)$ is the noise component regarding $n_{ASE,I}(t)$ and $n_{ASE,Q}(t)$.
In general, in presence of ASE noise, $\theta_n(t)$ will only be dominated by optical noise featured by ASE.

Hence, taking into account (4.18-4.19), the *k*th OFDM receiver noisy input with data subcarriers and ASE noise element can be denoted as,

$$\theta_k(t) = \frac{1}{T_B}\int_0^{T_B}\theta(t)g_k(t)dt = \frac{1}{T_B}\int_0^{T_B}\left[\varphi(t)+\theta_e(t)+\theta_n(t)\right]g_k(t)dt \equiv S_k + E_k + ASE_k \qquad (4.33)$$

where, ASE_k reflects to the ASE noise in N_k.
Here, the variance of optical noise has to be properly calculated. The approach to compute the proper value for the variance of ASE goes by the noise analysis of ASE for electrical fields and photocurrents of PDs within balanced detection.
The way to calculate the optical noise component is widely overviewed in [Seimetz09].
According to chapter 3 (3.18-3.19), the two higher sample outputs of a 90º optical hybrid of $E_1(t)$ and $E_2(t)$ in terms of optical noise (4.26) can be featured by the following electrical fields,

$$\begin{aligned} E_1(t) &= \frac{1}{2}\left(s_S(t)+s_{LO}(t)+n(t)e^{j\omega_S t}\right) \\ E_2(t) &= \frac{1}{2}\left(s_S(t)-s_{LO}(t)+n(t)e^{j\omega_S t}\right) \end{aligned} \qquad (4.34)$$

where, $s_S(t)$ and $s_{LO}(t)$ stand for both useful signal and LO respectively and ω_s is the operating frequency of useful signal. For both *I* and *Q* branches, the consideration of optical ASE noise power is identical. So, the studies regarding the only one *I* (In-phase) branch were performed.
In the balanced detector, photocurrents at upper and lower PD are obtained. The polarizations of useful signal and LO are assumed to be identical. In practice the polarization controller located at input of 90º optical hybrid keeps tracking both polarizations to maintain them in the same regime.
Hence after photo-detection, combining (4.34) first the individual photocurrent for upper I branch input is calculated as,

$$V_{I,1}(t) = R_L \cdot E_1(t)\cdot E_1^*(t) = R_L \cdot \left(s_S(t)+s_{LO}(t)+n(t)e^{j\omega_S t}\right)\cdot\left(s_S^*(t)+s_{LO}^*(t)+n(t)^* e^{-j\omega_S t}\right) \qquad (4.35)$$

After simplicity, including the properties (3.21-3.22) and (4.26), (4.35) becomes,

$$\begin{aligned} V_{I,1}(t) = {} & \frac{R_L}{2}\left|s_S(t)\right|^2 + \frac{R_L}{2}\left|s_{LO}(t)\right|^2 + \frac{R_L}{2}\underbrace{\left[s_S(t)s_{LO}^*(t)+s_S^*(t)s_{LO}(t)\right]}_{A}\ldots \\ & \ldots+\frac{R_L}{2}\underbrace{\left[s_S(t)n_{\parallel}^*(t)e^{-j\omega_S t}+s_S^*(t)n_{\parallel}(t)e^{j\omega_S t}\right]}_{B}+\frac{R_L}{2}\underbrace{\left[\left|n_{\parallel}(t)\right|^2+\left|n_{\perp}(t)\right|^2\right]}_{C}\ldots \\ & \ldots+\frac{R_L}{2}\underbrace{\left[s_{LO}(t)n_{\parallel}^*(t)e^{-j\omega_S t}+s_{LO}^*(t)n_{\parallel}(t)e^{j\omega_S t}\right]}_{D} \end{aligned} \qquad (4.36)$$

where, *A* is the signal/LO beating, *B* stands for the signal/ASE noise power, *C* is the ASE/ASE noise power and *D* features a dominant LO/ASE noise power.
Afterwards, the photocurrent for the lower PD input is computed as,

$$V_{I,2}(t) = R_L \cdot E_2(t)\cdot E_2^*(t) = R_L \cdot \left(s_S(t)-s_{LO}(t)+n(t)e^{j\omega_S t}\right)\cdot\left(s_S^*(t)-s_{LO}^*(t)+n(t)^* e^{-j\omega_S t}\right) \qquad (4.37)$$

Further simplifying (4.37), $V_{I,2}(t)$ can be deployed in,

$$V_{I,2}(t)=\frac{R_L}{2}\left|s_S(t)\right|^2+\frac{R_L}{2}\left|s_{LO}(t)\right|^2+\frac{R_L}{2}\left[-s_S(t)s^*_{LO}(t)-s^*_S(t)s_{LO}(t)\right]\ldots$$
$$\ldots+\frac{R_L}{2}\left[s_S(t)n^*_{\parallel}(t)e^{-j\omega_S t}+s^*_S(t)n_{\parallel}(t)e^{j\omega_S t}\right]+\frac{R_L}{2}\left[\left|n_{\parallel}(t)\right|^2+\left|n_{\perp}(t)\right|^2\right]\ldots \quad (4.38)$$
$$\ldots+\frac{R_L}{2}\left[-s_{LO}(t)n^*_{\parallel}(t)e^{-j\omega_S t}-s^*_{LO}(t)n_{\parallel}(t)e^{j\omega_S t}\right]$$

The calculations for lower Q branch $V_{Q,3\text{-}4}(t)$ can be derived accordingly.
Furthermore, the noise at both upper and lower *I* branches is assumed to be correlated and all the noise components excepting the LO/ASE noise mitigated.
However, combining (4.37) and (4.34), the overall photocurrent of both upper and lower *I* branches is evaluated as,

$$V_I(t)=V_{I,1}(t)-V_{I,2}(t)\ldots$$
$$\ldots=R_L\underbrace{\left[s_S(t)s^*_{LO}(t)+s^*_S(t)s_{LO}(t)\right]}_{A}+R_L\underbrace{\left[s_{LO}(t)n^*_{\parallel}(t)e^{-j\omega_S t}+s^*_{LO}(t)n_{\parallel}(t)e^{j\omega_S t}\right]}_{D} \quad (4.39)$$

where, symbols *A* and *D* are related to (4.36). Here, the power of useful signal and LO signal were eliminated. The *A* element includes useful data, but the real information about the optical noise is featured by *D*.
Next, accounting *D* element for LO/ASE noise power *n(t)* and combining (4.39) with (3.21-3.24), the element D can easy be simplified to,

$$\underbrace{D}_{LO/ASE}=n(t)=2R\cdot\mathrm{Re}\left[s^*_{LO}(t)n_{\parallel}(t)e^{j\omega_S t}\right] \quad (4.40)$$

Then, using (4.26), the equation (4.40) employing LO/ASE noise *n(t)* is expressed as,

$$n(t)=2R\cdot\mathrm{Re}\left[s^*_{LO}(t)n_{\parallel}(t)e^{j\omega_S t}\right]=2R\cdot\mathrm{Re}\left[s^*_{LO}(t)e^{j\omega_S t}\cdot\left\{\mathrm{Re}\left\{n_{\parallel}(t)\right\}+j\,\mathrm{Im}\left\{n_{\parallel}(t)\right\}\right\}\right]$$
$$...+2R_L\sqrt{P_{LO}}\cdot\mathrm{Re}\left\{n_{\parallel}(t)\right\}\cdot\sin\left(\omega_{LO}t+\phi_e(t)\right)\ldots \quad (4.41)$$
$$\ldots+2R_L\sqrt{P_{LO}}\cdot\mathrm{Im}\left\{n_{\parallel}(t)\right\}\cdot\cos\left(\omega_{LO}t+\phi_e(t)\right)$$

Nevertheless, it has to be assumed that LO signal $s_{LO}(t)$ is free from the phase noise. So, then the final expression for the optical ASE noise *n(t)* is derived in (4.42), Finally, the optical ASE noise in terms of Gaussian distribution can be manifested by the power spectral density (PSD) described as,

$$N_{LO/ASE}=\frac{R_L\cdot R^2\cdot P_{LO}\cdot P_S}{\Delta f\cdot OSNR}\cong{\sigma_{ASE}}^2 \quad (4.42)$$

where, Δf is the measurement OSNR bandwidth (12.5 GHz corresponding to 0.1nm). OSNR is expressed in linear units and computed by subtracting a real ASE noise value from the output power of the link.
Thus, by substituting equations (4.27)-(4.42) into equation (4.24), the performance of the receiver in presence of ASE noise can be evaluated using a Gaussian approximation.
So, the SNR can be straightly computed as,

$$SNR=\frac{{S_k}^2}{\mathrm{var}\left[N_k\right]}=\frac{{S_k}^2}{\mathrm{var}\left[ASE_k\right]}=\frac{\pi^2H^2\cdot 8T_B\Delta f\cdot OSNR}{N{V_\pi}^2R_L} \quad (4.43)$$

However, for low OSNR values, $A_n(t)$ starts being comparable to $R_L R\sqrt{P_{LO}P_S}$, and $\theta_n(t)$ behaves as a Ricean process [Papoulis02]. Thus, in this case, the problem is no longer a BPSK detection with Gaussian noise. Instead, it is similar to the envelope detection of a binary signal, reported in [Schwartz66]. Therefore the final probability of error can be written as,

$$Pe = \frac{1}{2}\left[1 - Q\left(\sqrt{\frac{SNR}{2}}, \sqrt{\frac{S_k^2}{2}}\right)\right] = \frac{1}{2}\left[1 - Q\left(\frac{2\pi H}{V_\pi}\sqrt{\frac{T_B \Delta f \cdot OSNR}{NR_L}}, \frac{\pi H}{V_\pi}\sqrt{\frac{1}{2N}}\right)\right] \qquad (4.44)$$

where, Q features the Marcum's Q function.
On Fig. 4.3, required OSNR values for 10^{-3} BER at different standard deviation of the transmitted phase ($\pi H/V_\pi$) are plotted. There, it can be seen, for the BER models developed, the higher the standard deviation is, the lower the required OSNR is. The validity of this model is assessed by means of simulations, presented in the next subsection and further discussed. In that figure, it is possible to observe that the expected behavior does not match with the simulations when assuming Gaussian behavior of the noise, whereas a theoretical limit is well established when assuming Ricean statistics.

B. *Simulations*

For this case, all the simulations have been performed using the same Matlab software and based on the same parameters retrieved from previous sub-section 4.1 where the thermal noise analysis was explored.

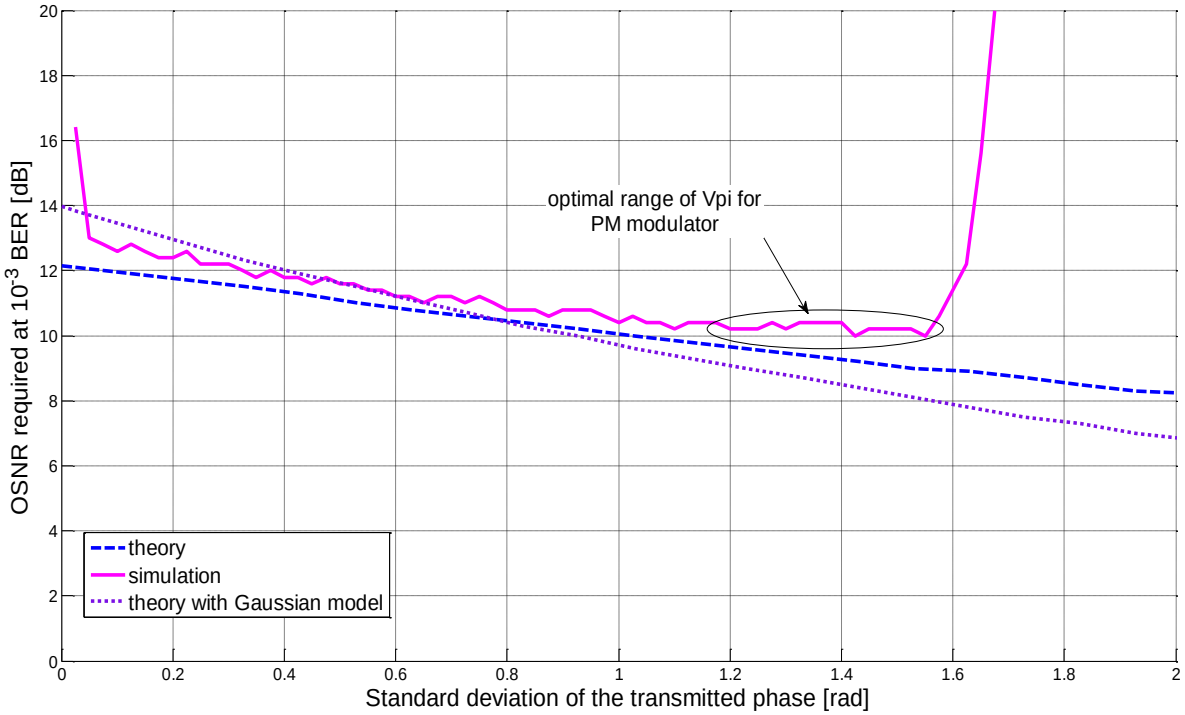

Figure 4.3. Theoretical and simulated OSNR curves vs. standard deviation of the transmitted phase.

Additionally, optical amplifiers effects were modelled by adding white optical noise just before the receiver, to obtain a certain OSNR in a 0.1 nm bandwidth.
Also, the standard deviation of the phase at the output of the transmitter ($\pi H/V_\pi$) was varied when evaluating BER waterfalls vs. OSNR.
All the results are plotted on Fig. 4.3. It shows the optimization in the phase modulator driving. The optimal range of chosen driving amplitudes was properly placed in the circle. Precisely, it can be observed that the minimum OSNR required at the receiver side is of 10 dB for a BER of 10^{-3} and was achieved in the region between 1.35-1.55 rad. Also, the behavior of the curve for the theory model corresponding to equation (4.44) explains the limit of the performance with less than 0.8 dB of error for standard deviations of the transmitted phase below *0.79 rad*.
As it could be expected after characterizing the performance in terms of sensitivity, results also show a disagreement between theory and simulations when standard $\pi H/V_\pi$ approaches to $\pi/2$. This is due to a BER-floor caused by the arctangent function used for retrieving the phase at the reception side.
After looking to the results grouped in BER waterfalls and sensitivity either OSNR curves, retrieved from both parts of modulator driving analysis, several conclusions were made.
First, the proposed OFDM system based coherent detection with pure phase modulation and Hartley transform in DSP was fully characterized in terms of sensitivity and optical amplification noise. For both cases, a theoretical model has been developed and validated by means of numerical simulations.
It has been demonstrated that the standard deviation of the transmitted phase (controlled by the amplitude of the signal driving of the phase modulator) is an extremely important parameter for optimizing the system. However, a limit has been found on the neighborhood of $\pi/2$, limited by the function of argument extraction. Precisely saying, a 10 Gb/s system has been simulated, achieving an optimum sensitivity of -37 dBm at 10^{-3} BER, for standard deviations of 1.2-1.4 rad. For the same system the minimum OSNR required at the receiver side has been found to be of 10 dB for obtaining a 10^{-3} BER and within the region of 1.35-1.55 rad.

4.2 Impact of Phase Noise

From among various effects associated to the optoelectronic front-ends at transceiver and receiver side of proposed OFDM system, the phase noise became one of the especially interesting phenomena and first to be investigated.
Hence, in this section, the performance of the system proposed and illustrated in chapter 3, in terms of phase noise impact is assessed. From practical point of view, the phase noise is an important issue during transmission over optical OFDM systems. In a coherent transmission, the local oscillator is beaten with incoming received optical signal and after detection, down-mixed to the baseband form. The phase noise of the lasers used at transmitter and receiver has an extremely high impact on the overall performance of the system and must be controlled and compensated [Jansen10]. In ideal case in terms of simulations, the linewidth of both lasers can slightly be avoided and set up to zero. In case of more sophisticated solutions based on solid-state lasers working with single frequency pump diodes which can use Er/Yb co-doped fiber (e.g. telecommunication fiber SMF-28), the coherence length is much longer and the linewidth range much narrower. Latest improvement towards lasers equipped with possibly narrow linewidths resulted in the reduction of linewidth for those lasers from 10 kHz to about 1 kHz [Geng05]. These facts exhibit such conclusion that in case of our proposed CE-OFDM system with

coherent detection, the narrower the linewidth range is, the better performance of the system is achieved.
Behind the theory, OOFDM system in case of coherent detection was especially sensitive to the phase noise. The key point is a coherent detection itself. The homodyne coherent detection requires full synchronization between both sides of transmitter and receiver and needs to especially struggle with the problem of linewidth associated to the lasers at both sides.
In general, the case of phase noise in OFDM is twofold. It can generate a common phase rotation (CPR) of all the subcarriers per symbol and a cross-leakage between the subcarriers, commonly called inter-carrier interference (ICI). Both destructive effects can easily be neglected using appropriate techniques to compensate for. This is a reason why the case of linewidth impact became an interesting issue for investigation.
In fact, the shot, thermal and ASE noises were turned off and the phase noise by the mean of phase error was the only one dominating noise to be considered in this approach.
Based on the noise analysis through the previous subsection, all of defined noises as: shot, thermal and ASE noise were additive with proper Gaussian distribution.
In the presence of phase noise, both lasers at transmitter and receiver side are affected by the phase noise. For simplicity, only the LO signal with phase noise was under investigation. The phase noise at data signal was neglected.

Considering the theoretical model for the phase noise impact, it has been assumed that the phase noise of the laser is featured as an uniform random variable. The characteristic of the phase noise has different nature than data and can be modelled as the finite power Wiener-Levy process detailed in [Fabrega10, Pollet95]. However, the analytical model that was under investigation turned out to be too complex, especially due to the way to compute the probability error and further relations of the sensitivity in terms of another parameters: e.g. varying the laser linewidth in case of several subcarriers suppressed from OFDM band. Hence, the analysis in case of phase noise was limited to the simulations.

All the simulations at this section were executed in Matlab environment. The simulating model was developed based on the same data used for validating theory behind additive noises (e.g. in case of receiver sensitivity and optical amplification noise).
Evaluating this model, different characteristics were performed. First, the investigation of the sensitivity taken at optimal BER at 10^{-3} versus standard deviation of transmitted phase for simulation is given. The results are presented in Fig. 4.4. Solid line represents the changes of penalty in case of simulations. The curve was plotted for the entire amount of 1 kHz laser linewidth. For simulations, 1st carrier from OFDM band has been suppressed. Focusing on the curve, the smooth decrease of the sensitivity caught at BER at 10^{-3} for $\pi H/V_{\pi}$ up to 1.15 rad is observed. In that region, almost slight curve slope is reported. Exploring the range of standard deviation, beyond 1.2 rad, the slope of the characteristic starts to vary experiencing a significant increase of the sensitivity of about 2 dB with respect to the trend of the curve. Precisely, a minimum sensitivity of -36 dBm is attained in the range of marked values of 1.3-1.5 rad. Moreover, close to $\pi/2$, the sensitivity value suddenly grows up. Beyond $\pi/2$, the lack of appropriate sensitivity values is notified. In addition, while spreading the penalty distance beyond $\pi/2$, there is no way to achieve BER at 10^{-3}. This is happening due to the feasibility of arctangent function used to retrieve the phase towards electrical phase demodulation at DSP.
In matter of fact, as in previous cases regarding the analysis of additive noises, it tends to $+\infty$ when forthcoming from the left side.

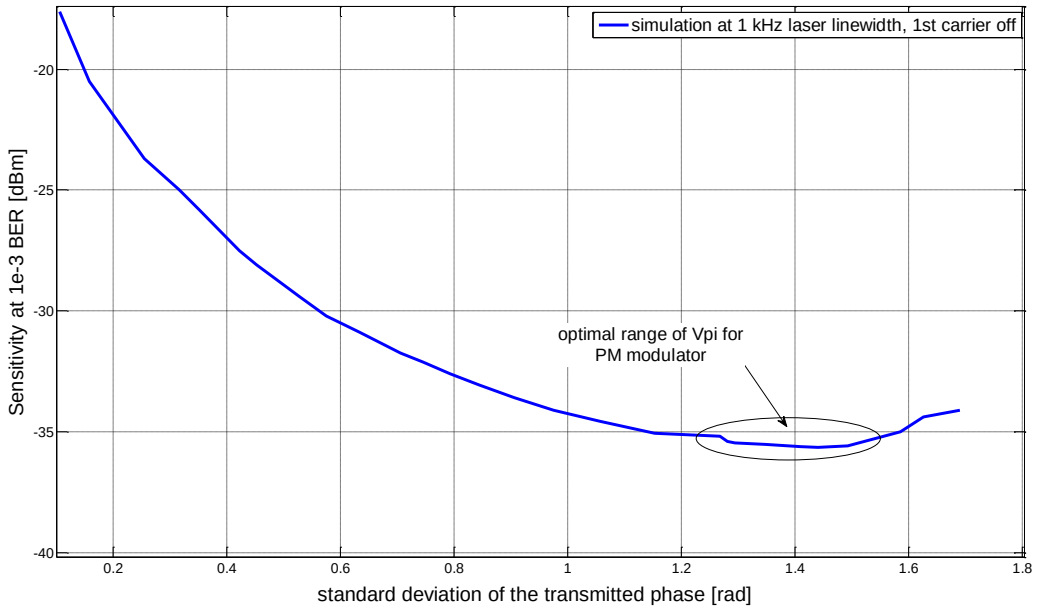

Figure 4.4. Sensitivity at BER at 10^{-3} vs. standard deviation of the transmitted phase in case of 1st carriers off and 1 kHz laser linewidth.

In Fig. 4.5, the results obtained by suppressing various carriers in terms of sensitivity penalty over laser linewidth are shown.

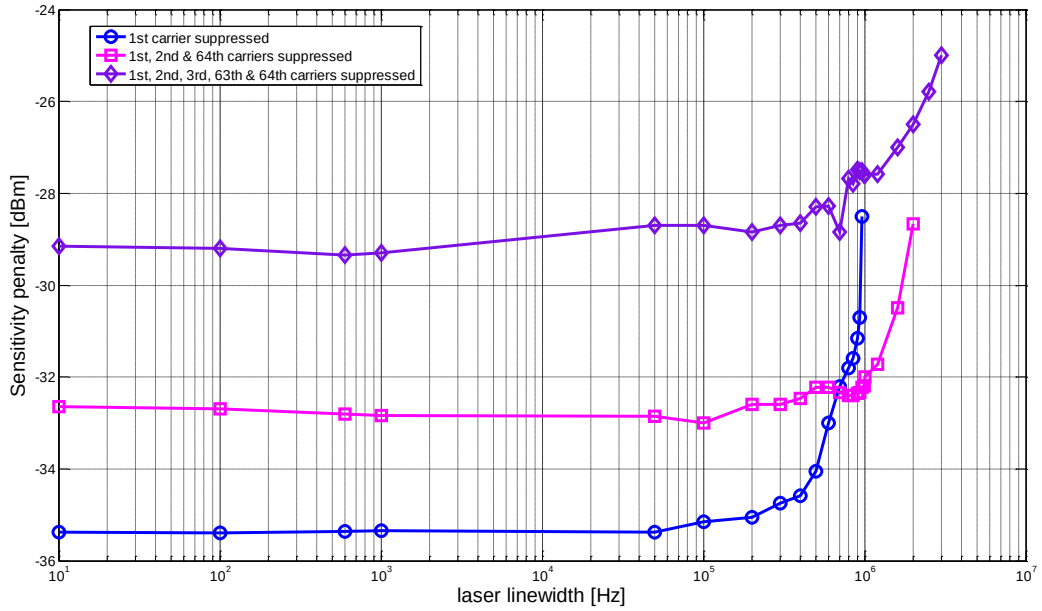

Figure 4.5. Sensitivity penalty vs. laser linewidth in case of 1/3/5 carriers off.

The range of laser linewidth spreads from 10 Hz up to couple of MHz. Between presented curves, there is a significant penalty that grows up while increasing the number of subcarriers to be suppressed. For all the curves, the higher the laser linewidth is, the higher sensitivity achieved at optimal level of BER at 10^{-3} is. Cutting more subcarriers from OFDM band, higher penalty is experienced. In all the cases, when approaching to 1 MHz of linewidth, the penalty between the resulted values is almost constant. The non-changeable 3 dB penalty between 1 and 3 carriers off is notified up to 100 kHz. In case of 5 carriers suppressed, the spread between the penalties in comparison to the rest is higher. Here, 6 dB and 3 dB penalties are attained between 5-1 and 5-3 carriers off respectively. While approaching to ten of MHz, the penalties vary for all the cases. This helps to conclude, there is connection between the number of carriers to suppress and acceptable level of the linewidth. The possible linewidth is getting higher tending to $+\infty$ when more carriers are programmed to be off.

4.3 Impact of Frequency Offset

At this section the assessment of the impact of frequency offset is overviewed.
The frequency offset likely as the phase noise is the one of most important disadvantages of optical OFDM systems based on coherent detection. It results in ICI and successively breaks the orthogonality of individual OFDM subcarriers. In presence of frequency offset, the received signal can be frequency shifted in respect to the LO, what results that subcarriers start to interact by beating with others. The frequency offset sometimes called handling offset, can really affect the system while the lasers at transmitter and receiver side are not oscillating at the same carrier frequency. This means the lack of full synchronization between both sides of the studied system. Finally, the frequency offset implies the increase in error probability and degrades the performance [Shieh10, Zhou12].
In case of frequency offset impact, both the theory analysis and theory validated by simulations were performed.
Featuring the frequency offset, the same system from previous subsections, the optical OFDM with coherent detection was under investigation.
Over current analysis the case of frequency offset is discussed as the only one source of dominating effect excluding additive (thermal/shot and ASE) and phase noise that are switched off and out of consideration.
In the presence of frequency offset, the phase differential algorithm is deployed. Differences in the frequency between LO at the receiver and the carrier of the received data truly degrade system performance. Both lasers at transmitter and receiver side were affected by the frequency offset change. For simplicity, only the LO signal with frequency offset is under investigation.

Next, the analytical model deployed for the impact of frequency offset was going to be presented. In matter of fact, the frequency offset could be modelled as a variable that affects only the data signal transmitted over the system, what easily differs it from other approaches where the impact factor is considered as a noise with Gaussian distribution. However, due to the complexity of mathematical approximations in the theory consideration towards the final exact probability error function, the simulations turned out the best way to exhibit the feasibility of the frequency shift influence on the system performance.

The simulation model at this subsection was performed using Matlab software. The data and simulation parameters applied for assessing the impact of frequency offset were related to the parameters in case of previous model featuring phase noise influence and additive noises.
So, the simulation results in respect to the reminded factor are shown in Fig. 4.6.

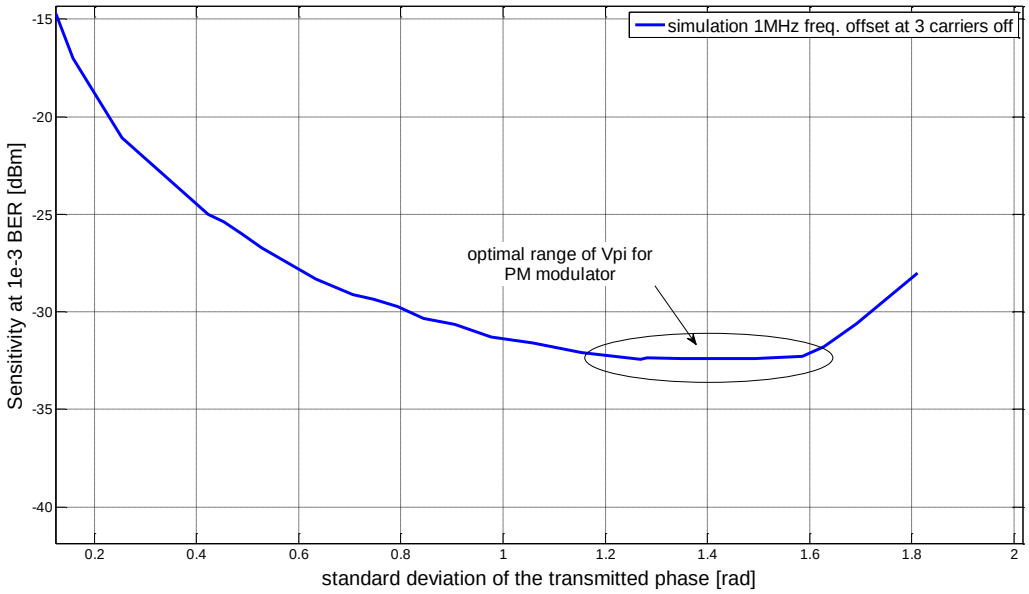

Figure 4.6. Sensitivity at BER at 10^{-3} vs. standard deviation of the transmitted phase in case of 1MHz frequency offset and 3 carriers off.

Here, the sensitivity values extracted at BER at 10^{-3} in the function of standard deviation of the transmitted phase are plotted. The results are highlighted for 1 MHz of frequency offset. The curve reflected to the simulations is illustrated to be a solid line. The dependence provides almost liner decline of sensitivity values over the standard deviation up to 0.25 rad. Next, while further increasing the standard deviation of modulator, the sensitivity values also decrease, however the gentle slope of the curve up to roughly 1.1 rad is observed. Afterwards, the dependence curve becomes linear justifying the optimal range for modulator sensitivity. Thus, the minimal range of optimal sensitivity is maintained in the marked region of 1.2-1.6 rad. Moreover, the sensitivity values near $\pi/2$, starts to grow up again, where there is no chance to achieve the optimal level of BER at 10^{-3}. This is because of the feasibility of arctangent function applied to extract argument in phase demodulation at DSP on receiver side. Finally, beyond the optimal range of sensitivity, the curve with simulation results approaches to $+\infty$ what can be translated to the additional noise correlated with amplitude factor of phase modulator.
In Fig. 4.7, the results for sensitivity penalty in the function of frequency offset are demonstrated. At this case, prior to the sensitivity curve, the BER values at 10^{-3} were captured at various amounts of frequency offset. The range of the scanned frequency offset accounts for the region of 10 Hz - 1GHz. It can be figured out, that close to 100 MHz, the dependence between sensitivity at BER = 10^{-3} and frequency offset experiences some penalty. The penalty is indicated in almost exponential grow up of the curve towards GHz. The most optimal penalties at 1 dB and 3 dB are successfully notified at 400 MHz and 640 MHz respectively. It is concluded that increasing the range of the offset in frequency, the penalties start to play important role in the

system featured by pure optical phase modulation. The penalties occur for the offsets tending to GHz.

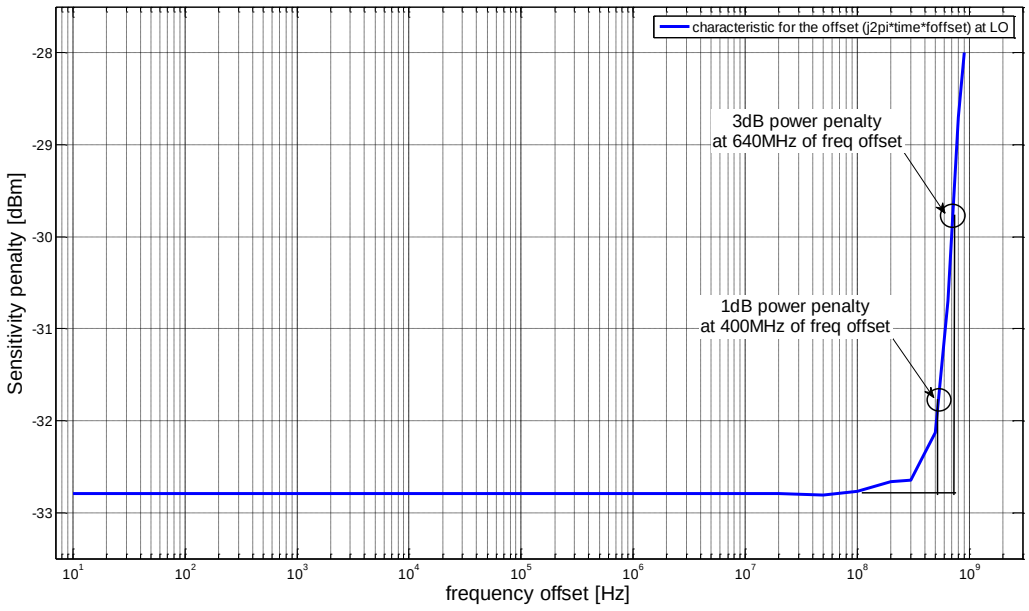

Figure 4.7. Sensitivity penalty in the function of frequency offset.

Next, the impact of Moving Average Filters (MAF) in case of the system with frequency offset presence was investigated. The sample picture featuring the transfer functions for the proposed MAF filter is shown in Fig. 4.8. Here, amplitude characteristic for the proposed filters at various orders of 21, 201 and 407 were designed.
It has to be noticed, that in all three cases, the frequency response of the MAF filter has a low-pass characteristic. Furthermore, the filter is un-attenuated at zero frequency. Some higher frequencies are completely removed applying proposed filter.
MAF filter, sometimes called running or rolling filter, provides simple implementation and is commonly used to solve many problems among which e.g. the reduction of white random noise is very well known. It can also be used to smooth out some fluctuations and distortions as in case of investigated offset [Berkleyweb, [AnaDevweb].
The filter is designed by averaging the proper number of elements from input signal and generating each point at output signal.
The principle of operation of the filter can be shortly exhibited by employing [AnaDevweb],

$$y(n)=\frac{1}{M}\left[\sum_{m=0}^{M-1}x(n-m)\right] \tag{4.45}$$

where, both *x(n)* and *y(n)* features the input and output signal respectively and *M* accounts for the number of points to average (order of the filter).
Applying the proposed M-MAF filter into the frequency offset application, the dependence of sensitivity penalty versus frequency offset was plotted in Fig. 4.9. The impact of number of carriers from OFDM spectrum to suppress along with the order of the filter was discussed.

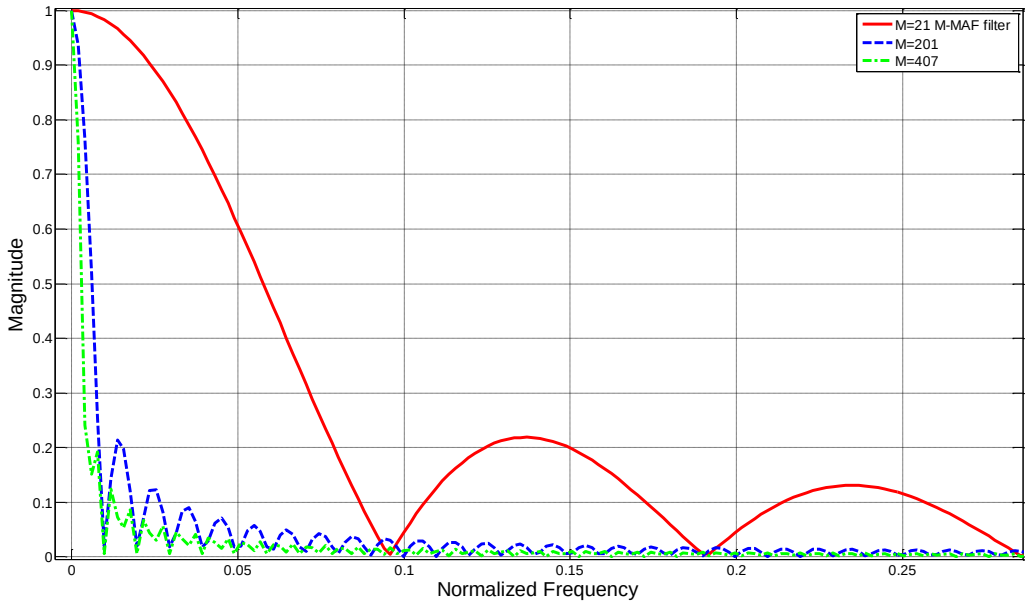

Figure 4.8. Frequency Response of M-point Moving Average Filter (M-MAF).

All the curves featuring the penalties over the range of frequency offset experience similar effect to that shown in Fig. 4.7. Since around 10-100 MHz of offset, all of the curves exhibited characteristic exponential increase limited to 400 MHz.

In case of 3 carriers off and approximately 199 and 407 points to average, the system experiences a negligible penalty up to 10 MHz of offset in respect to the case without filter. The filter eliminates higher frequencies than 400 MHz which became the last acceptable threshold for the system on frequency shift.

Meanwhile, in case of 3 carriers off and only 21 points to average, the valuation by the filter is not so precise as in previous case and it seems to be only coarse. The penalty occurred over whole range of the frequency offset is around 3 dB in reference to the example without the filter.

The case with only 1 carrier suppressed and 201 points to average provides almost 2.5 dB of penalty to the case without filter in range of the frequency offset up to 10 MHz. While increasing the offset, the sensitivity penalty gets higher limiting acceptable range of the frequency shift.

Finally, in case of 5 carriers off and 201 points, the penalties attained in this configuration seemed to be the highest possible in relation to the rest of the curves and the case without filter. 400 MHz also in this point became the maximum offset to whose the systems works.

4 dB of penalty up to 10 MHz of offset differs it from the case without applied filter and with 3 carriers off and 199 and 407 points respectively. In turn, almost 1 dB of penalty was noticed with 3 carriers off and 21 points. The highest penalty on a distance to 10 MHz was occurred with 1 carrier off and 201 average points.

The results accomplished to the MAF filter applied for dealing with the frequency offset, ensured that this filter was not a really good choice and was simply worse than expectations. The right filter employed to struggle with the impact of reminded offset is the baseband digital filter employed into the phase diversity receiver just before down-sampling in ADC. The filter characteristic had to be preceded by zeros in order to remove the characteristic filter transient.

The filter was designed in the way of one-dimensional digital filtering. The proposed baseband filter could handle with both FIR and IIR filters. The filter coefficients of the numerator and denumerator respectively, have been retrieved from the low-pass raised cosine FIR filter with linear phase implemented in the receiver. The bandwidth of such digital filter with original transition and distinctive roll-off was mainly depended on bit rate, as the objective was to filter below the first baseband subcarrier.

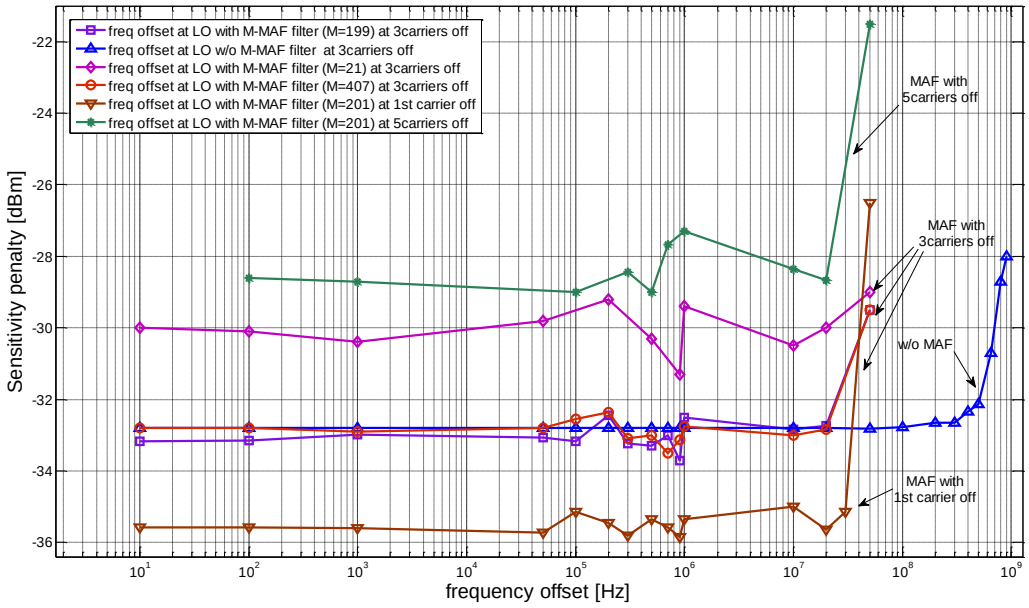

Figure 4.9. Sensitivity penalty in the function of frequency offset in case of M-MAF filters with various points to average and in case of 1-3-5 carriers suppressed.

4.4 Impact of IQ Imbalance

In this subsection, the impact of destructive IQ imbalance effect on OFDM system proposed in this consideration is characterized.
IQ imbalance became next crucial point in the theory analysis and the general assessment of effects reflected to front-end non-idealities at innovative system proposed in the thesis.
In fact, the provided OFDM system with optimal performances is sensitive to that effect.
In this analysis, IQ imbalance in contrast to the models of previous front-end effects is generated at only receiver side. It does not concern LO laser itself and plays main role right after balanced photo-detection at phase-diversity receiver. IQ imbalance is performed just before down-sampling of both I and Q components. IQ imbalance is realized on two ways, in particular incorporating power and phase unbalancing respectively. The IQ imbalance is modelled as power and phase errors associated with the optical carrier used for up-conversion at transmitter and the LO applied for down-conversion at receiver. IQ imbalance can deteriorate the overall system performance due to ISI/ICI effects incorporating mismatch between I and Q components as it was explained in previous cases regarding other impairments. This degradation can be induced by different parts of the system, including the imperfection of ADC/DAC converters,

modulator either the 90º optical hybrid where the power of LO and received optical signal is redistributed. At any side, this effects provides the image beating between the adjacent symmetrical subcarriers from OFDM band and LO and constellation spread as well [Fyath11, Jansen09a].
However, only the solution with IQ unbalance assessment at receiver side is investigated in this section.
Preserving the shape of IQ imbalance model, it can be concluded that IQ imbalance can shortly be characterized by two parameters. As was said, there are the power imbalance factor $k \in (0, 1)$ between I and Q branch and the phase orthogonality mismatch called phase unbalancing factor $\Delta\vartheta$. Nevertheless, the phase factor $\Delta\vartheta$ is featured by unbalancing the arbitrary phase between both I and Q streams.
For simplicity, the rest of front-end effects is out of theoretical consideration in case of IQ mismatch.
Thence, based on the step-by-step algorithm of IQ imbalance, both power and phase unbalancing factors respectively are discussed and overviewed later on.

Moreover, the analytical model of those factors of power and phase unbalancing was properly analysed and resulted in similar conclusions as those in respect to the rest of the impact factors e.g. the phase noise or the frequency shift. Hence, the simulations came up as the final possibility for evaluating the impact of phase and power unbalance factors on system performance.
So, studying the imbalance impact, several simulations were executed.

The simulation parameters for the system tested in case of IQ imbalance reflects to the same values from the impact of additive noises and others. All the simulations, as in previous cases were investigated using Matlab software.
First, the dependence of sensitivity penalty versus the deviation of phase modulator in case of both power and phase unbalance was plotted.

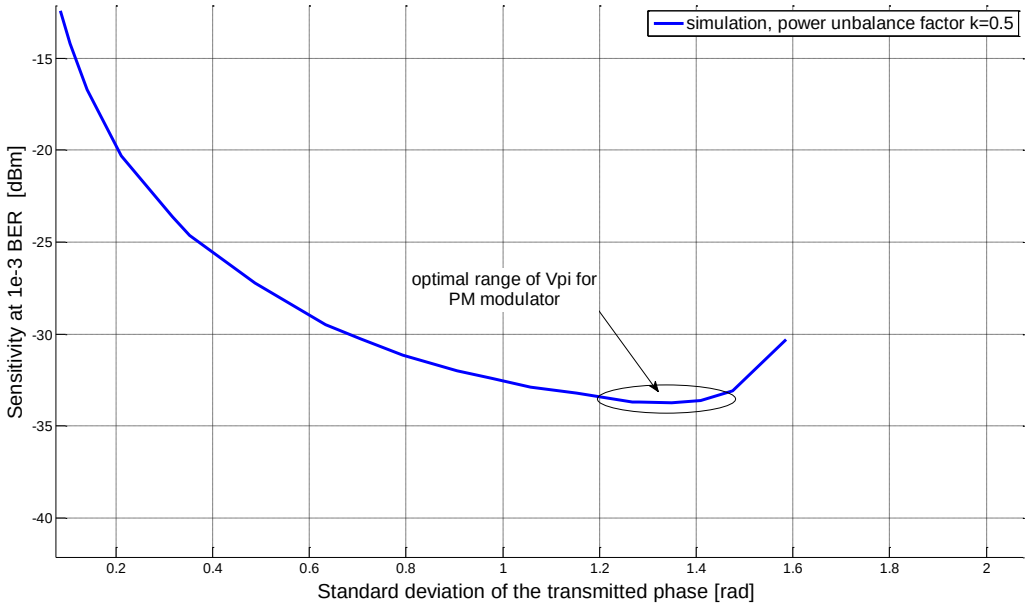

Figure 4.10. Sensitivity penalty vs. standard deviation of the transmitted phase in case of power unbalance (k).

The results employing power unbalance factor are seen in Fig. 4.10 above. The case with *k* factor varied in the range of (0, 1), finally set-up to 0.5 was analysed. Solid curve represents the sensitivity values achieved at each BER at 10^{-3}. As in respect to the previous cases e.g. analysing the impact of frequency offset, alike at this case, increasing the standard deviation values of the transmitted phase, the decrease of the system sensitivity is observed. The almost linear decline of sensitivity is only noted up to 0.2 rad. Above the value of 0.2 rad, the relation between the sensitivity vs. standard deviation shows a nature of the curve with minimal slope.
The slight decrease of the sensitivity is featured up to 1.2 rad. Next, increasing the standard deviation, the sensitivity curve gets more stability resulting in the optimal range for driving voltage of the modulator. Thus, a minimum optimal sensitivity of -34 dBm is reached in the optimal range of 1.25-1.4 rad. Beyond 1.4 rad, the sensitivity suddenly grows up, what can easily be explained by the properties of arctangent function applied for the phase demodulation. Moreover, tending to $+\infty$ from the left side, the sensitivity penalty is getting higher up to the level where, there is no way to retrieve any BER at 10^{-3}.

For the case of phase unbalance, the same type of sensitivity dependence in the function of the standard deviation was plotted and is shown in Fig. 4.11. At this case, the phase factor $\Delta\vartheta$ was set up to 0.05 rad. As in previous case of power unbalance, the solid curve covered the simulation results. The sensitivity vs. standard deviation behaves alike in respect to the power unbalance characteristic. Getting higher with the standard deviation, the parallel decrease of the sensitivity values is notified up to 1.2 rad. From this value, the sensitivity curve becomes linear resulting in the optimal range for phase modulator. The optimal sensitivity values keep the same level of -34 dBm as in case of power unbalance and feature the range of 1.2-1.4 rad. The conclusions reported for power unbalance regarding the sudden increase the sensitivity above the optimal range and the nature of arctangent function close to $\pi/2$ fully support this case.

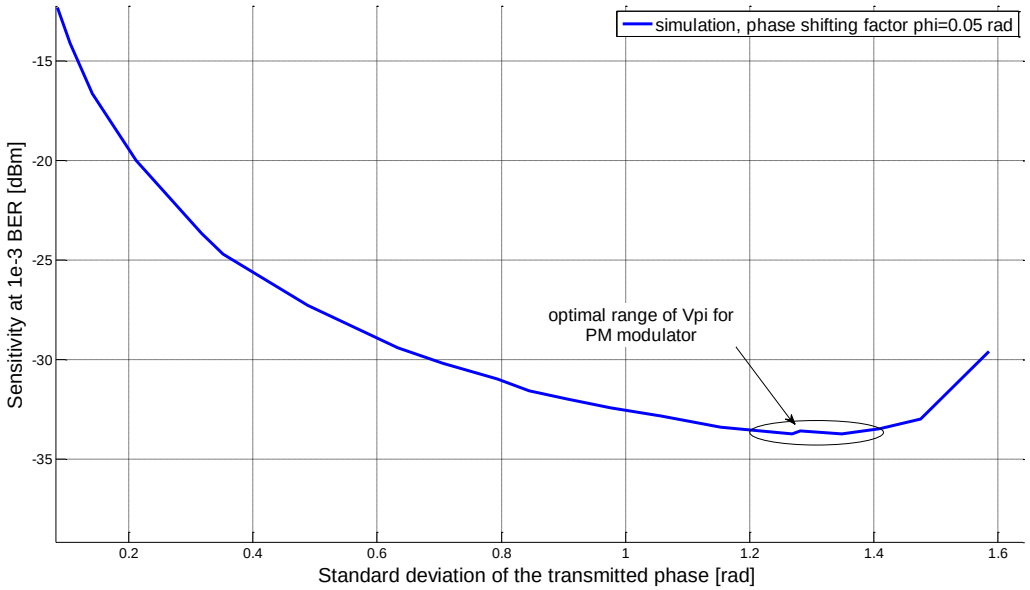

Figure 4.11. Sensitivity penalty vs. standard deviation of the transmitted phase in case of phase unbalance ($\Delta\vartheta$).

Next, in Fig. 4.12, the relation between sensitivity penalty and power unbalancing factor *k* is reported.
The sensitivity curve was plotted based on 3 OFDM sub-carriers suppressed. The curve was executed varying the power factor *k* in the range of (0, 1). Looking to the curve, it is simple to conclude that minimum and maximum values for factor *k* reached 0.35 and 0.64 respectively. Beyond those values, there is no possibility to achieve 10^{-3} BER and only between min and max values, the unbalance can be demonstrated. The reported values satisfy the assumed range for *k* of (0, 1). The optimal values for the power factor *k* oscillated in the range of 0.45-0.55. There, it is featured that the system sensitivity at optimal BER at 10^{-3} experiences a negligible penalty. The following penalties of 1 dB and 3 dB occurred at *k* of 0.57 and 0.6 respectively.

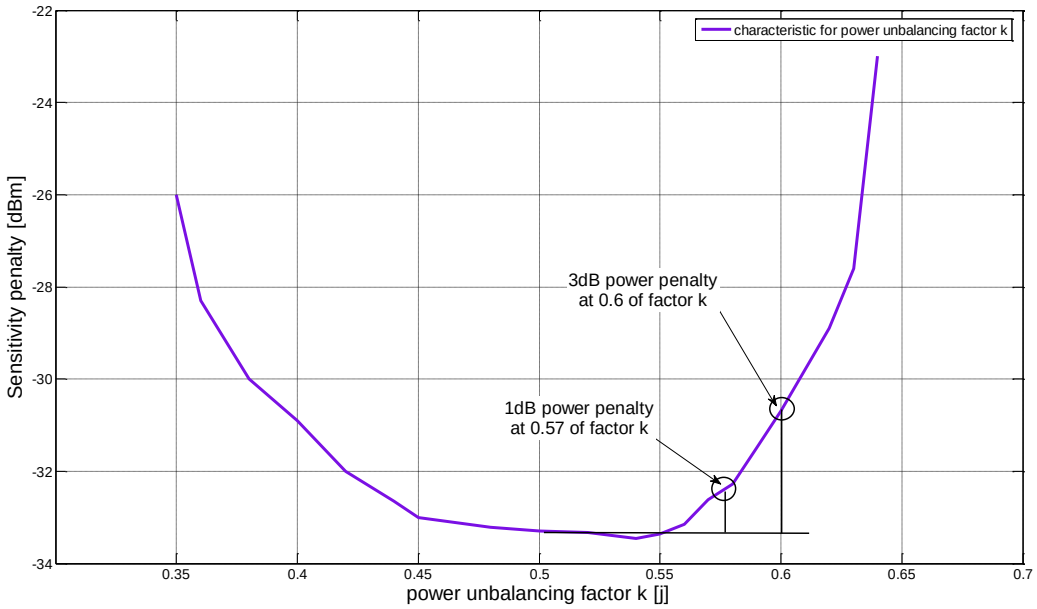

Figure 4.12. Sensitivity penalty vs. power unbalancing factor k at 3 carriers off.

Finally, in Fig. 4.13, the sensitivity penalty in the relation to the phase shifting factor $\Delta\vartheta$ is shown.
The curve was executed using 3 sub-carriers off. It is reported that 0.05 grad is an optimal minimum value for phase factor to maintain phase unbalancing. While increasing the phase unbalancing factor, the system sensitivity performed at BER at 10^{-3} experiences some penalties. The penalties grow up with the increase of the phase unbalance parameter. The dependence in the function of the phase shifting factor meets some penalties of 1 dB and 3 dB at 0.2 grad and 0.28 grad respectively.

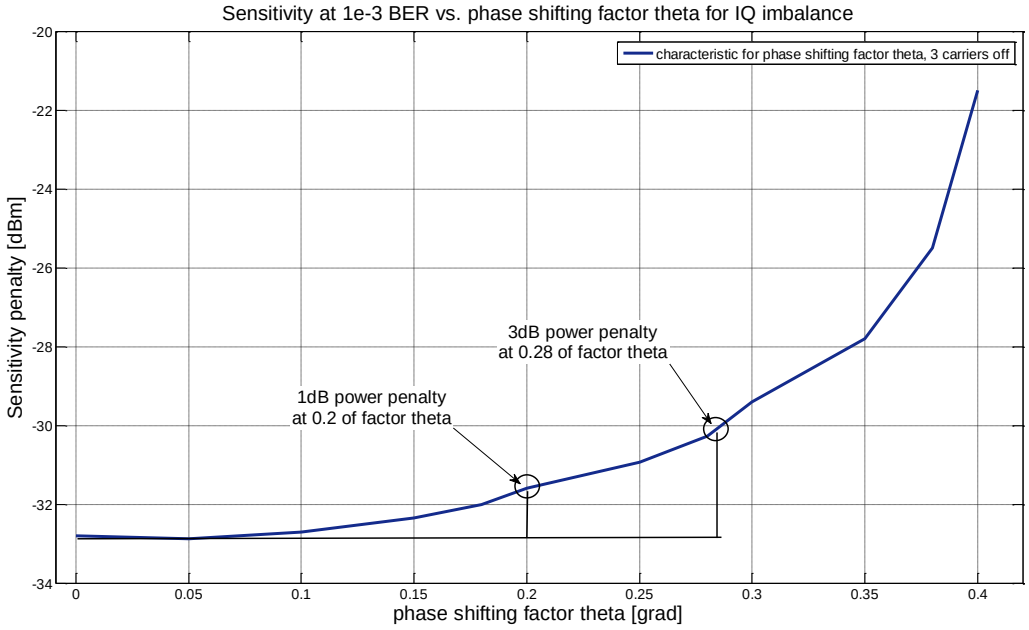

Figure 4.13. Sensitivity penalty vs. phase shifting factor $\Delta\vartheta$ at 3 carriers off.

4.5 Impact of Dispersion

In this section, the impact of destructive dispersion effect on OFDM system performance and the consideration of digital filter to combat dispersion proposed in the thesis are discussed. In order to support this section, first the brief description of lightwave propagation over the link implied to the simulations of proposed novel optical OFDM system is given. Then, the dispersion effect is overviewed. The last part accounts for the new filter proposed to deal with the phase and amplitude conversion problems due to dispersion effect.

So, the link associated with the system is typically chosen standard single mode fiber (SSMF).

The transmission over the SMF link was featured by the proper script carried out in Matlab software. In order to simulate the propagation of light in optical fiber, the popular split-step Fourier method (SSFM) [Agrawal07, Jaworski07] was proposed. The method was described by nonlinear Schrodinger equation (NLSE) and originally designed for soliton transmission,

According to the method, the fiber length has been divided into a large number of segments of small step size δz. Additionally, it was assumed that during propagation through each segment δz, the dispersion and nonlinearities are treated separately [Binh10].

The NLSE has easily been rewritten with the linear operator calculated in frequency domain and nonlinear in time domain, respectively. The formal notation is given by,

$$\frac{\partial A}{\partial z} = (D + N) \cdot A \tag{4.46}$$

where, D denotes a differential linear operator including dispersion and power losses and N accounts for a nonlinear operator employing fiber nonlinearities [Agrawal01, Binh10].

Moreover the following operators D and N are simplified and exhibited as,

$$D = \frac{-j\beta_2}{2}\frac{\partial^2}{\partial T^2} + \frac{\beta_3}{6}\frac{\partial^3}{\partial T^3} - \frac{\alpha}{2} \qquad (4.47)$$
$$N = j\gamma|A|^2$$

where, $A(z,t)=A$ is a complex envelope over time t and distance z, β_2 and β_3 represent 2nd and 3rd order factors of dispersion, γ is the nonlinear coefficient, α is a fiber attenuation and $T=t-z/v_g$ accounts for the reference time frame at group velocity dispersion (GVD).

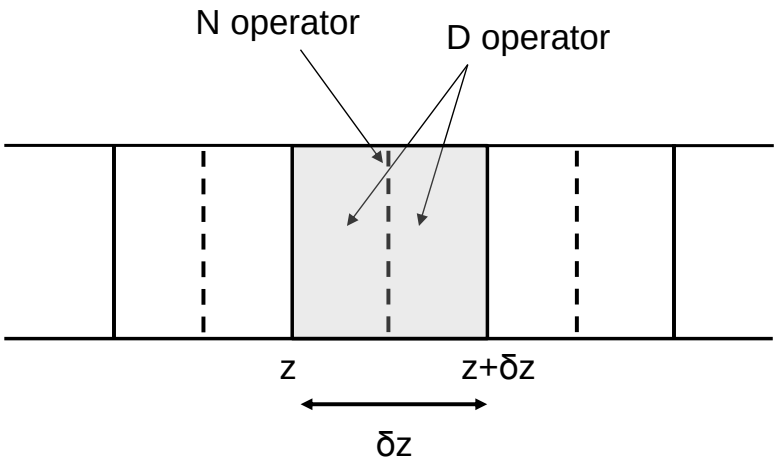

Figure 4.14. Illustration schematic of the SSFM [Binh10].

In matter of fact, the nonlinearity and dispersion act together over the fiber length. As shown in Fig. 4.14, the nonlinearity is situated in the middle of the segment δz.
The propagation from z to $z+\delta z$ is demonstrated, first by performing nonlinearity when $D=0$ and later on executing dispersion while $N=0$ [Agrawal07, Binh10].
Fulfilling the above assumption, (3.46) can be finally approximated using the following form,

$$A(z+\delta z,T) \approx \exp(\delta z D)\cdot \exp(\delta z N)\cdot A(z,T) \qquad (4.48)$$

where, each of D and N component is considered separately, what completes the proof about SSFM and propagation over the fiber based on this method.

All the parameters required for the transmission over fiber are given below and in the next chapter with use cases and applications. The propagation algorithm as was reminded is modelled in Matlab.

Today in different applications, where the proposed novel OFDM system can be employed, the main thought is to increase the data bit rate what always is a challenge for a transmission itself. While increasing the bit rate, the intensity of operating optical light is getting higher. The level of interactions between the light and fiber environment grows up. Various effects can deteriorate the transmission itself and the system can suffer from them. From among well-known effects, the power losses, dispersion and nonlinearities are the one of most important during a transmission.
Although, the attenuation over SSMF can totally be combatted using proper amplification associated with proper length of fiber span and attenuation parameter, the case with dispersion is a little bit harder.

The dispersion over SSMF can be featured by chromatic dispersion or simply polarization mode dispersion depending on the distance reach. At this consideration effect of only the chromatic dispersion is overviewed.
The chromatic dispersion called sometimes GVD during propagation causes pulse spreading such that the pulse spreads across several slots of the other pulses [Ciscoweb]. Pulse broadening makes the system more difficult to carry out the proper reception. Going with a bit rate, the higher dispersion, the longer bit interval must be applied. The longer bit interval, a lower bit rate has to be set up and fewer bits can be propagated per unit of time.
The dispersion sufficiently degrades the performance generating ISI and power penalty. E.g. considering the case with fiber dispersion of 16 ps/(nm·km), it can be observed that a signal at 10 Gb/s with a pulse width of 100 ps, spreads for about 16 ps at every 1 km. Taking into account, that every 1 km generates a spread of 16 ps, the maximum dispersion cumulated in the SSMF link attains 1600 ps/nm [Ciscoweb].
In case of the treatment for the dispersion impact, the filter to combat chromatic dispersion was applied.
Behind the theory, it has to be taken into account that dispersion can be emulated as a filter with band-pass characteristic. Furthermore, the filter will belong to the group of narrow-bands filters where filter bandwidth is approximately equal to the useful signal bandwidth.
The proposed filter struggles with phase and amplitude conversion due to dispersion over dispersive channel [Ho05].
The transfer function of the filter placed on the output of phase-diversity receiver can be expressed as [Plant12],

$$TF(f) = \exp\left(-2j\pi^2 f^2 \beta_2 L\right) \Leftrightarrow \exp\left(j\left(\frac{\beta_2 f^2}{2} + \frac{\beta_3 f^3}{6}\right)\cdot\frac{\delta z}{2}\right) \tag{4.49}$$

where, β_2 denotes a GVD parameter and L accounts for the length of SSMF.
So, it is straightforward that *TF(f)* is fully dependent on the basic properties of the fiber link.
Moreover, in fact for a dispersive SSMF, the received optical field can be computed by [Ho05],

$$E_{rx}(f) = E_{tx}(f)\cdot TF(f) \;\Rightarrow\; E_{tx}(t)\otimes TF(t) = E_{rx}(t) \tag{4.50}$$

where, $E_{rx}(f)$ and $E_{tx}(f) = fft(I+jQ)$ are the received and transmitted signal field representations in the frequency domain, I and Q features complex down-sampled components.
So, indeed in the time domain, $E_{rx}(f)$ is approximated as a convolution between $E_{tx}(f)$ and the frequency selective response of the dispersive SSMF [Shieh10, Ho05].
The frequency response of the dispersion filter at various lengths of the fiber link is presented in Fig. 4.15.
Therefore, the OFDM signal at 10 Gb/s equipped with 8 samples per symbol and at sample rate of 80 GHz was fed into the SSMF link.
The calculations for the further propagation over the fiber link with included filter were performed including the following parameters of the link as, attenuation factor α of 0.29 dB/km, central wavelength λ_0 of 1550 nm, dispersion parameter D of 16.5 ps/(nm·km), dispersion slope S of 0.06 ps/(nm^2·km), non-linear silica index n_2 of 2.4e^{-20} m^2/W and effective core area A_{eff} of 80e^{-12} m^2.
The rest of the fiber coefficients were computed using the following equations,

$$\beta_2 = -D\frac{\lambda_0^2}{2\pi c}$$
$$\beta_3 = S\frac{\lambda_0^4}{4\pi^2 c^2} - \beta_2\frac{\lambda_0^2}{2\pi c} \qquad (4.51)$$
$$\gamma = \frac{2\pi \cdot n_2}{A_{eff}\lambda_0}$$

where, *c* accounts for the speed of light (≈ $3e^8$ m/s).

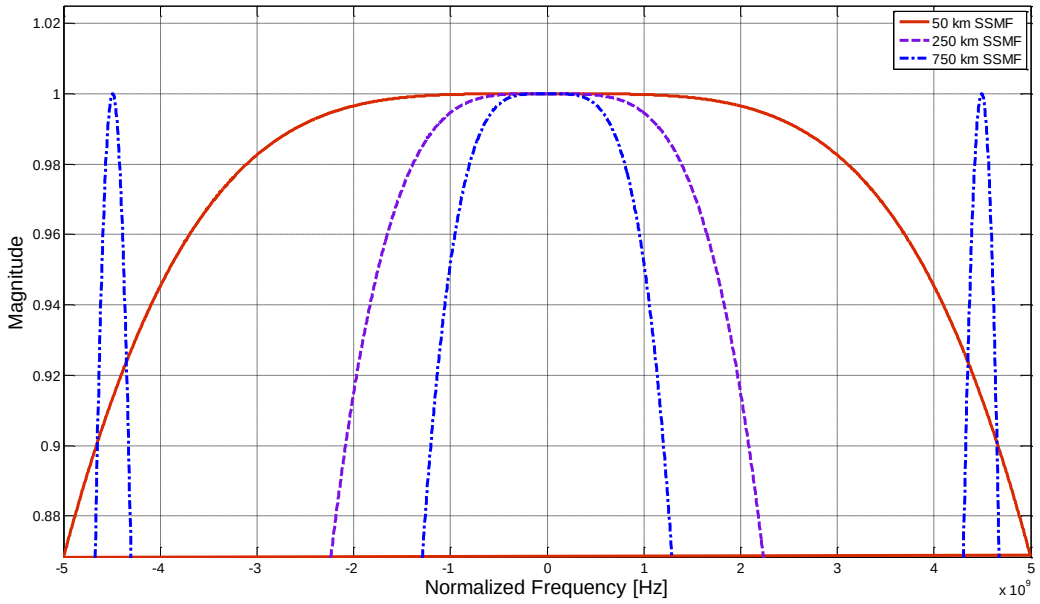

Figure 4.15. Frequency response of filter to combat dispersion.

So, the frequency responses of the filter for compensating an accumulated dispersion shown in Fig. 4.15, were optimally normalized. Sample transfer functions were drawn for 3 different lengths of the fiber (50 km, 250 km, and 750 km) whose characteristic with all the parameters was analysed based on (4.48). As there was implied, the higher the distance is, the narrower the filter spectrum can be attained. While increasing the fiber distance, close to 750 km, the filter exhibits strong ripples within the band. The overshoots are seen on the edges of filter transfer function and the filter indicates twice less bandwidth than in case of shorter distance. Hence, The length of the fiber is still an important parameter of the filter to vary the filter bandwidth.

4.6 Chapter Summary

At this chapter, the theoretical and numerical characterization of proposed CE-OFDM system, all executed in Matlab environment was given.
The study of two classes of the noises deteriorating the transmission aspects and principle of operation of individual elements of transmitter and coherent detector was under of investigation. The mentioned noises belonged to the additive and multiplicative group. The additive one was

covered by the photo-detection noise (thermal and shot noise) and optical amplification noise (ASE). Meanwhile, the multiplicative group was featured by the following impacts of the phase noise, frequency offset and IQ imbalance respectively. Additionally, the review of the propagation over the fiber link together with the impact of chromatic dispersion was investigated.

In case of additive and multiplicative noises and its impact on the system performance, the analytical consideration has been deployed and mainly the sensitivity curves in the function of the standard deviation of the transmitted phase were plotted.

The simulations curves fitted almost perfectly with the linear model for the standard deviation values below 45º for all of the executed noises. Increasing deviation beyond 45º, the trend followed by most of the simulations was different. While approaching to 90º from the left side, the soft envelope- clipping effect become dominant and the system was not able to properly work manifesting only the BER above 10^{-3}.

Moreover, the impact of chromatic dispersion along with the description of the way to propagate the light over the fiber link was shortly explained. The propagation itself was based on the SSFM and concerned mainly the links featured by SSMFs.

Providing the digital filter to combat chromatic dispersion, it turned out the cyclic prefix is not the only one factor to deal with the dispersion impact, so deteriorating the propagation over long distances. The transfer function of the proposed filter given by (4.49) strongly addicted the filter feasibility from the assumed propagation distance and the rest individual parameters of the fiber under test, like central wavelength and GVD.

CHAPTER 5: APPLICATIONS IN ACCESS AND TRANSPORT NETWORKS

In this chapter, the possible applications to translate the OFDM system into several use cases are manifested. For the first time, the system supported by novelties featuring Hartley transform and all-optical pure phase modulation was employed in various potential areas. The possible application resources were addressed to access and optical transport networks. For those two possible applications, the system solutions were proposed and endorsed by 5 technical papers overviewed in the text.
Next, each type of applications referred to access and optical transport networks was properly shared into two possible destinations.
The destinations associated to the access networks were featured by the next generation access and the fixed mobile conversion. In turn, the optical transport networks were exhibited by the filter concatenation effect and the metro-regional network.
The content of proposed application schemes is shown below at paragraph 5.1 and 5.2.

5.1 Applications in Access Networks

5.1.1 Next Generation Access

In this section, the practicability of a phase modulated optical OFDM upstream transmission employing IM/DD downstream for attaining a bidirectional transmission with symmetric data rate of 10 Gb/s over a single wavelength is assessed by means of simulations for a passive optical access network scenario. First, an upstream modulation is performed using a reflective semiconductor amplifier. Next, the coherent detection is employed at the central office. Afterwards, the bidirectional transmission over a single wavelength with RSOA based ONU is validated with numeric simulations of distance reach, phase optimization and any possible back-reflections.

A. Behind the research

Point to multi-point access Passive Optical Networks (PONs) have emerged as effective platforms to deploy bandwidth demanding advanced services [Girard2005]. In those networks, a Central Office (CO) is connected through a tree-branched passive distribution network to the Optical Network Units (ONUs). In these schemes the different user signals are usually multiplexed in time, leading to the time division multiplexed PONs (TDM-PONs) standardized by the IEEE and ITU-T [Girard05]. This means that next generation PONs have to solve several challenges, including high bit rate delivery to a high users' density, opening the door to the wavelength division multiplexed (WDM) TDM-PONs. In order to avoid limiting the available wavelength number, the same wavelength can be employed for upstream and downstream. Also, a mandatory specification is the use of a single fiber for both the upstream and downstream transmission for reducing the size of the external plant and the complexity of the ONUs, leading to the use of reflective colorless ONUs. A promising solution is the use of different magnitudes (e.g. amplitude and phase) to carry upstream and downstream data for minimizing their mutual crosstalk [Hung03].

An interesting property of Semiconductor Optical Amplifiers (SOAs) is their capability of being modulated in phase [Schrenk11, Jung09]. Precisely, a binary phase shift keying (BPSK) system for upstream transmission in PONs, using Reflective SOA (RSOA) and employing coherent detection at the central office has been demonstrated [Jung09]. Commercially available RSOA devices are known to have a poor modulation bandwidth, limiting their effective data rate. The use of intensity modulation and direct detection (IM/DD) optical orthogonal frequency division multiplexing (OFDM) has demonstrated to be effective on delivering data rates of 9 Gb/s over a PON system using commercial RSOAs of 1.25 GHz bandwidth [Wei10].
In this paper the authors investigate the feasibility of a bidirectional transmission with symmetric data rate of 10 Gb/s for downstream and upstream over a single wavelength. Downstream transmission is performed using standard IM/DD [ITU-T G.987.2]. Upstream transmission is achieved re-modulating the phase of the downstream signal. It is attained saturating the RSOA, modulating its phase with a Discrete Multi-Tone (DMT) signal using the Fast Hartley Transform (FHT) and employing coherent reception at the CO. Its performance and limits are investigated by means of numerical simulations.

B. Network scheme and signal delivery strategy

A simplified network scheme is shown in Fig. 5.1. At the CO, 10 Gb/s downstream data is intensity modulated according to the standard [ITU-T G.987.2]. This signal is then distributed among the network to *N* end users by means of an optical power splitter. In order to properly adjust the RSOA input power, at the ONU an optical coupler drives a standard direct-detection receiver (for downstream reception) and the RSOA (for re-modulation with upstream data).

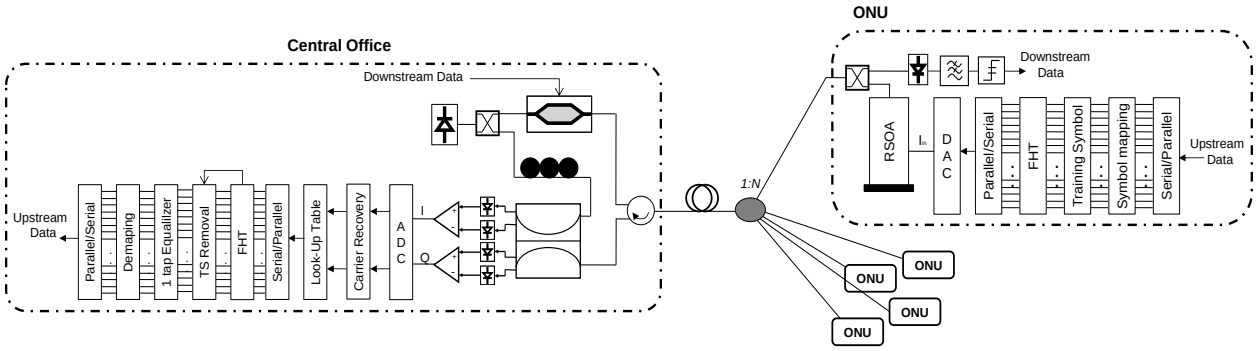

Figure 5.1. Simplified network scheme and proposed CO-ONU design.

In the RSOA, changes in the refractive index of its active region, caused by modulation of the carrier density of the active waveguide, will affect the phase velocity of the optical wave and, therefore, the optical phase [Jung09, Manning94]. To avoid possible crosstalk between downstream and upstream data, a continuous wave holding beam on another wavelength can be used to control the energy due to the optical input signal [Manning94], saturating it and extinguishing the effects on a carrier density change. Under these conditions, the carrier density and, thus, the optical phase changes will be proportional to the modulation of the RSOA bias current. Then, a DMT signal generated using the fast Hartley transform modulates the RSOA bias current and consequently its output optical phase.
To generate the DMT signal, data is first parallelized, mapped into a BPSK constellation and a training symbol sequence is inserted. Next the resulting symbols are OFDM modulated using the

fast Hartley transform, which is equal to its inverse [Bracewell00]. Subsequently, the obtained real-valued OFDM symbols are serialized and converted into an analog signal by a Digital-to-Analog Converter (DAC). The generated upstream signal is propagated back to the CO, where it is coherently detected employing phase diversity and using the downstream carrier as a local oscillator to ensure a wavelength match with the received signal.

So, the upstream data signal is first coupled with the downstream carrier in a 90o optical hybrid. It combines both signals producing four different optical signals with 0^o, 90^o, 180^o and 270^o phase difference respectively. These signals drive two pairs of photo-diodes acting as balanced detectors. Next, the resulting In-phase (I) and Quadrature (Q) outputs are digitized by an Analog-to-Digital Converter (ADC). Next, the signal passes through a carrier recovery block in order to compensate for phase and frequency errors. The argument of the complex received signal recovered from I and Q components is afterward extracted. Next, the fast Hartley transform is carried out, the training symbols are conveniently extracted and equalization is performed. Finally, data are detected after symbols demapping and serialization.

Even fiber is usually modeled as a reciprocal component and polarization changes underwent along downstream propagation would be cancelled when performing upstream path, in practice a polarization control must be placed between the laser and the optical hybrid for a correct data reception [Cho11].

An interesting feature of the proposed transmission system is that a single wavelength is used for achieving upstream and downstream communication. Thus, the network can implement wavelength division multiplexing either including a WDM demultiplexer at the external plant between the feeder fiber and the power splitting stage; either using a photo-detector jointly packaged with a tunable thin-film filter at the receiver side of the ONUs, just after the optical duplexer [Murano08, Raharimanitra11]. As a coherent detection is used at the CO, no optical filters are needed at that receiver and its central wavelength corresponds to the one provided by the local laser (i.e. the laser source used for downstream). So, the CO transceivers can be tuned from one channel to another by modifying the wavelength of their laser source. A lot of progress has been done in fast tunable lasers and tuning times in the order of hundreds of picoseconds have been demonstrated [Schrenk11]. Therefore, a WDM upgrade of the proposed network is possible and it can be easily reconfigured in case the network includes a control layer/plane.

C. Upstream performance

The performance of the proposed system is assessed by means of numerical simulation using Matlab software. First, a downstream data set of 2^{17} pseudorandom bits is generated using a sequence of 2^{15}-1 at 10 Gb/s. Next it is transmitted at 1550 nm using intensity on-off keying with an extinction ratio of 10 dB and transmitter output power of 5dBm, according to the XGPON standard [ITU-T G.987.2].

The transmission link includes a Standard Single Mode Fiber (SSMF) and a variable optical attenuator. This last is placed for emulating also the losses associated to the 1:*N* power splitting element of Fig. 5.1. The split-step Fourier method is used to model the propagation over the SSMF [Agrawal07]. In the fiber model, all the relevant elements with the corresponding values are selected in Tab. 5.1 below,

SSMF link	
effective area	80 m^2
power losses	0.2 dB/km
dispersion factor	17.0 ps/(km·nm)
dispersion slope	0.07 ps/(km·nm^2)

Table 5.1. The values for individual parameters of used SSMF link.

After downstream transmission, the signal is amplified, saturated and the upstream DMT signal is modulated in the phase. Upstream signal is generated from a decorrelated set of 2^{17} pseudorandom bits using a sequence of 2^{15}-1 running at 10 Gb/s. Next, the bit sequence is parallelized, BPSK encoded and DMT modulated to 64 carriers using the fast Hartley transform. The resulting signal is injected to the phase of the RSOA. The resulting ONU output power is 5 dBm.
After upstream transmission, at the coherent receiver of the CO, the local oscillator is modeled as a CW laser centered at 1550 nm with output power of 1 mW, giving -6 dBm to each photodetector after the 90^o optical hybrid. The photodetectors are modeled as PIN diodes with the parameters distinguished in the Tab. 5.2 below,

PIN diode	
responsivity	0.7 A/W
load resistance	50 Ω
dark current	1 pA
thermal noise	11.51 $pA/\sqrt{Hz}$

Table 5.2. The values of individual elements of PIN diode.

OFDM decoding and data demodulation are performed after intradyne detection.
In all the analyzed cases the output parameter measured is the statistical counting of received bits, which provides the best measure of the system Bit Error Ratio (BER). A RS(1023,1007)/BCH(2047,1952) super FEC code can be used, making possible to consider a BER of 10^{-3} with only 7 % overhead [ITU-T G.975.1].
Prior to run any analysis, the output phase of the RSOA is set to its optimum to obtain maximum performance in terms of system sensitivity. As the OFDM signal modulating the optical phase can be modeled as a gaussian noise [Shieh10], its amplitude is varied until the standard deviation of the optical phase is set to the optimum. According to [Chochol12], this value is set at 0.4π.

C.1. Parasitic impact

First of all the effects of RSOA packaging parasitics are evaluated for a back-to-back configuration. The unequalized electro-optic modulation bandwidth of commercial RSOAs is

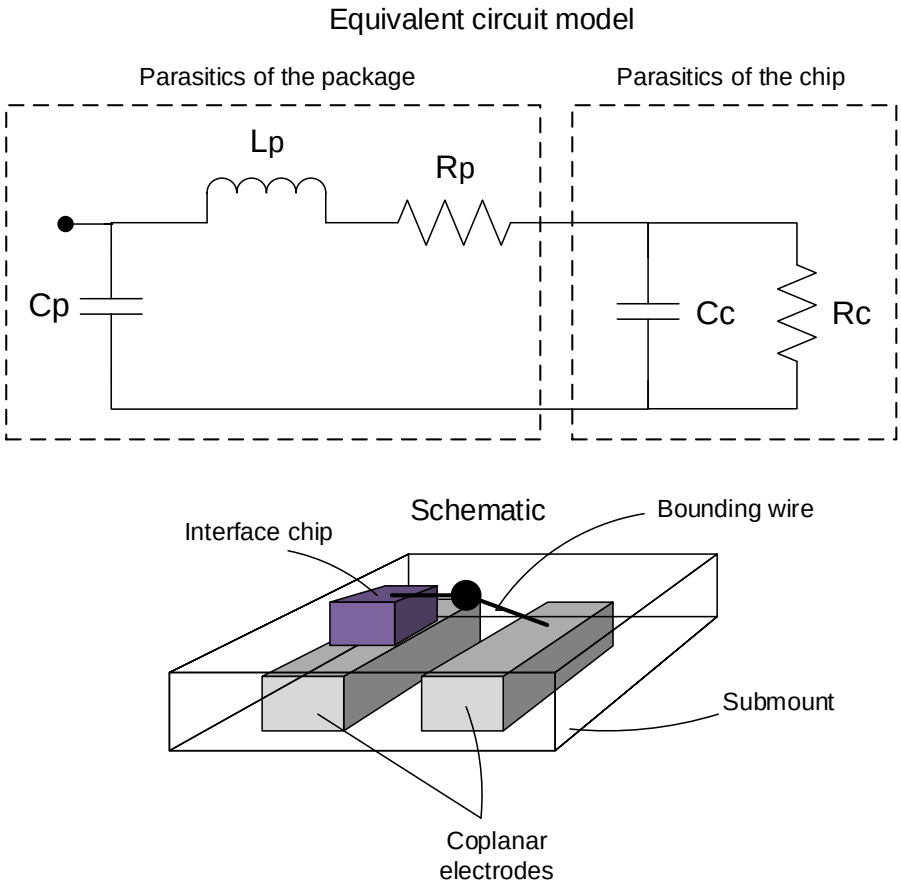

Figure 5.2. The schematic and equivalent circuit for the electrical interface to the RSOA including the parasitic effects of the device packaging.

known to be very poor and with smooth quasi-linear slope [Wei2010]. In case of the pure phase modulation proposed, this effect is highly contributed by the electrical interface of the package, which introduces a natural low-pass transfer function for the electrical signal [Wei10]. The electrical circuit model of the package interface is shown in Fig. 5.2. The electrical interface to the RSOA consists of two parasitics blocks referred to the package and the chip. The parasitic components of RSOA interface are independent from the bias current impact. The subtraction between the frequency response of the RSOA interface and various bias currents leads to the calculation of intrinsic response of the RSOA interface [Zhu05].

In turn, according to the Fig. 5.2, the equivalent circuit model of the RSOA interface was mounted on the submount pad. The submount is composed of extrinsic parasitic network and intrinsic RSOA interface. In practical model, two coplanar electrodes are applied to the submount. The analysing interface is attached to the one of electrodes. The connection between the chip and electrode is established by the bounding wire. In detail, referring to the circuit in Fig. 5.2, the parasitic of the chip consists of two parallely situated elements of an equivalent resistance *Rc* and a capacitance of the RSOA electrode Cc respectively. The parasitic of the package is composed of the bonding wire and the submount layer. The bonding wire introduces an inductive element *Lp* and a resistance *Rp*. Meanwhile, the submount pad of the packaging is characterized by its capacitance *Cp*.

With a simple analysis, the response of the filter featured by its transfer function is given by,

$$H(s) = \frac{1}{1 + C_c\left(R_p + R_c\right)\cdot s + L_p C_p \cdot s^2} \tag{5.1}$$

where, *s* parameter features the Laplace transform.
Since RSOAs are commercialized with a standard through-hole (TO) packaging, its typical values are used for taking into account these effects. According to [Chen07], the individual values of elements applied into the RLC circuit featured in Fig. 5.2 are given in Tab. 5.3 specified below,

RLC elements	
submount capacitance *Cp*	0.77 pF
bonding wire inductance *Lp*	0.30 nH
bonding wire resistance *Rp*	1.93 Ω
chip capacitance *Cc*	12.9 pF
chip resistance *Rc*	8 Ω

Table 5.3. The values for RLC elements of equivalent circuit of RSOA interface.

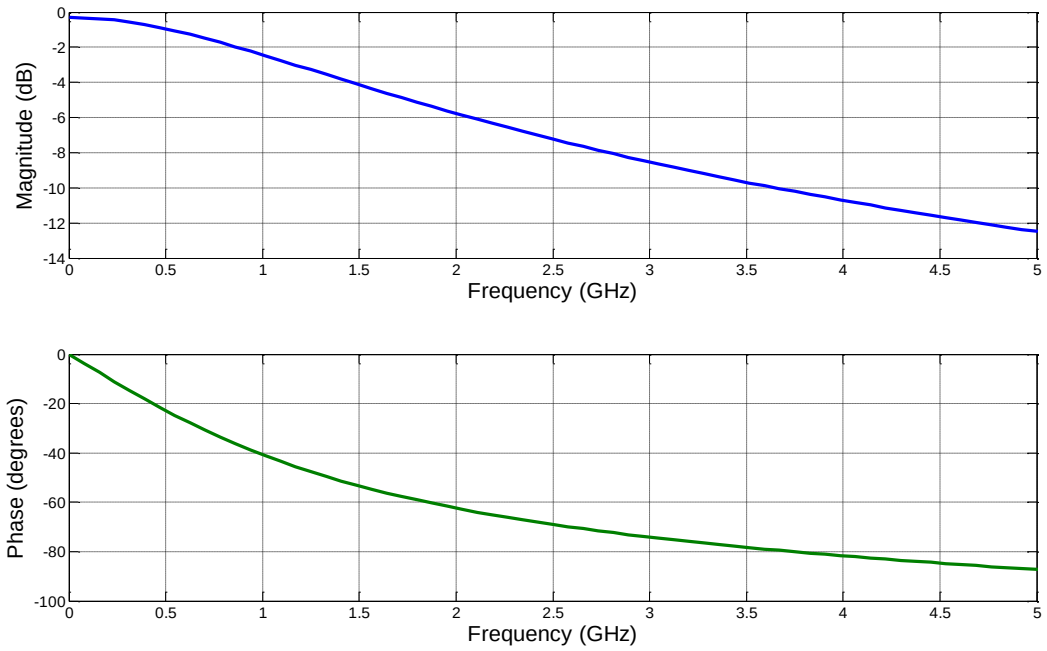

Figure 5.3. The frequency response in magnitude and phase of the parasitic filter.

Fig. 5.3 seen above shows the frequency response of the filter using these values typed in Tab. 5.3. There it can be observed that the 3 dB bandwidth is of only 1.3 GHz, as expected [Wei10].

For higher frequencies the magnitude smoothly decreases at about 3 dB per GHz. Regarding the phase, it is quasi-linear within the pass band and tending to -90^{o} according to equation (5.1), which is a two-pole configuration.
A first set of simulations is carried out to evaluate the penalty due to the packaging. Fig. 5.4 below shows the results. There, the back-to-back sensitivity at 10^{-3} BER for the ideal configuration (without packaging) is found at -37.8 dBm.

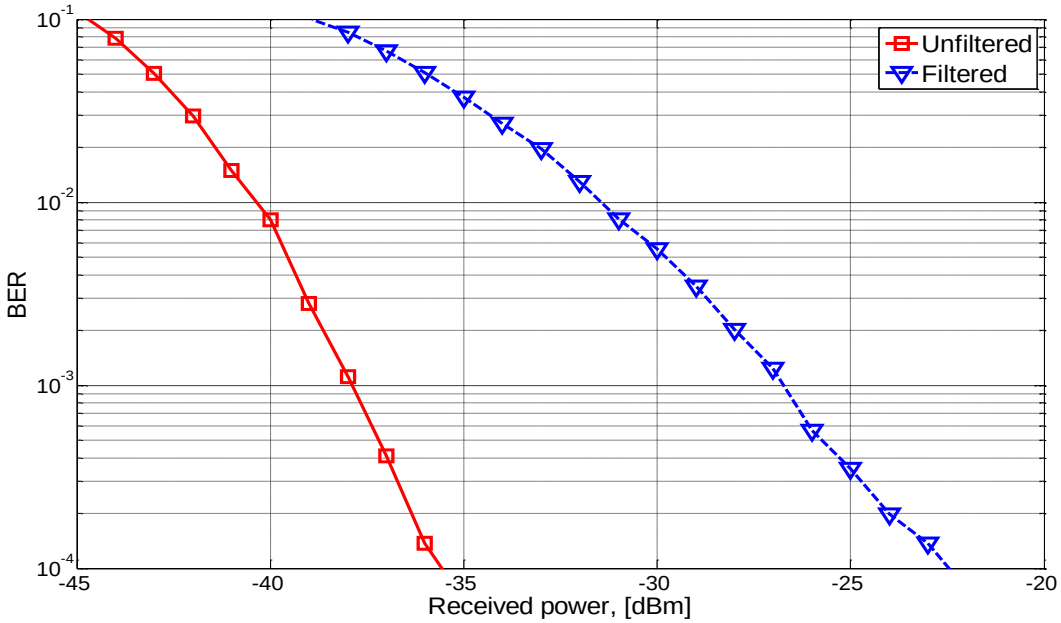

Figure 5.4. Sensitivity penalty at 10^{-3} BER as function of the parasitic.

When the filtering effects due to the package interface are included, the sensitivity at 10^{3} BER turns to be -26.5 dBm, 11.3 dB away from its ideal value. As it is a non-negligible effect, it has been included in the following evaluations.

C.2. Reflections

Afterward, the performance against back-reflections is evaluated for a back-to-back transmission. For that, a portion of the downstream signal is coupled to the upstream signal and varied its power. So, different optical signal to reflection ratios (OSRR) are obtained and their impact in terms of sensitivity penalty is analyzed.
Results are given in Fig. 5.5 below. There it can be observed that 9.5 dB OSRR can be tolerated with a penalty of less than 1 dB at 10-3 BER. For a sensitivity penalty of 3 dB at 10^{-3} BER, the minimum OSRR tolerated decreases down to 5.5 dB.

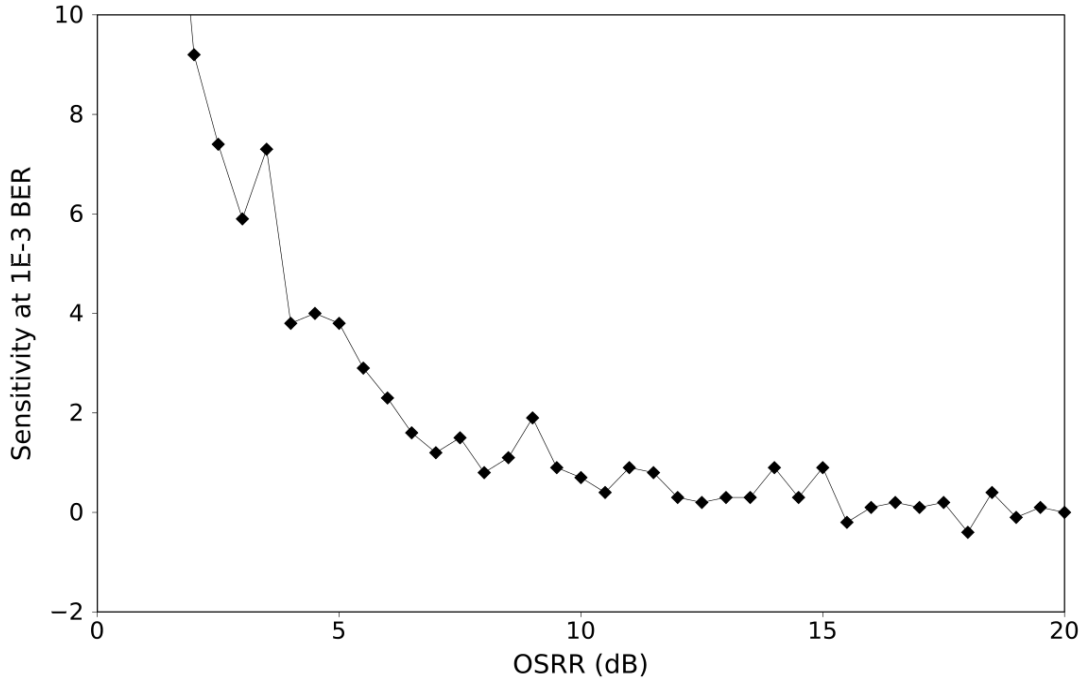

Figure 5.5. Sensitivity penalty at 10^{-3} BER as function of optical signal to reflection ratio (OSRR).

C.3. Transmission

Finally, the fiber transmission performance is evaluated in terms of system sensitivity and OSNR required at the output of the RSOA. Optical noise is modeled by adding white optical noise just after modulating the optical phase, to obtain a certain Optical Signal to Noise Ratio (OSNR) in 0.1 nm bandwidth.

As the application framework are access PONs, a maximum distance of 50 km is assumed. A training symbol is inserted every 2048 OFDM symbols for equalization, resulting in a 0.05 % of associated overhead. An additional overhead of only 11.3 % is considered, due to FEC and carrier suppression for phase noise tolerance enhancement.

Results can be seen in Fig. 5.6 and Fig. 5.7. Fig. 5.6 shows that the sensitivity at 10^{-3} BER for the back-to-back is -26.5 dBm and after 50 km is -25.6 dBm, only 0.9 dB away. Since the ONU output power is 5 dBm, the obtained upstream power budget is 31.5 dB for the back-to-back and 30.6 dB after 50 km. Similarly, Fig. 5.7 shows that the OSNR required at the output of the RSOA for achieving a 10^{-3} BER is 16.8 dB for the back-to-back and 17.7 dB after 50 km.

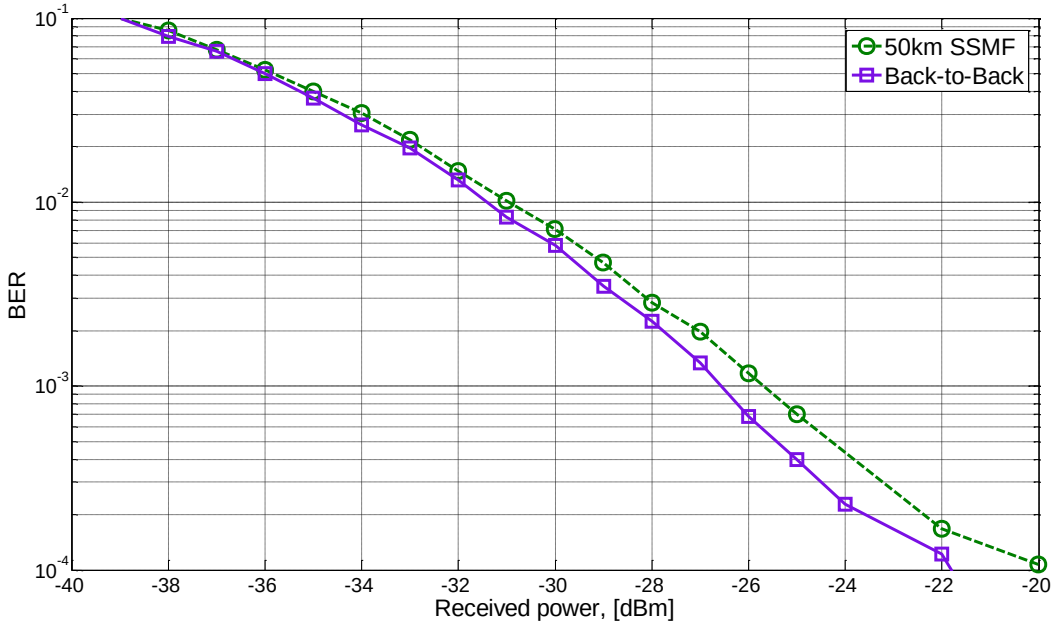

Figure 5.6. BER as function of the received power for back-to-back and after 50km.

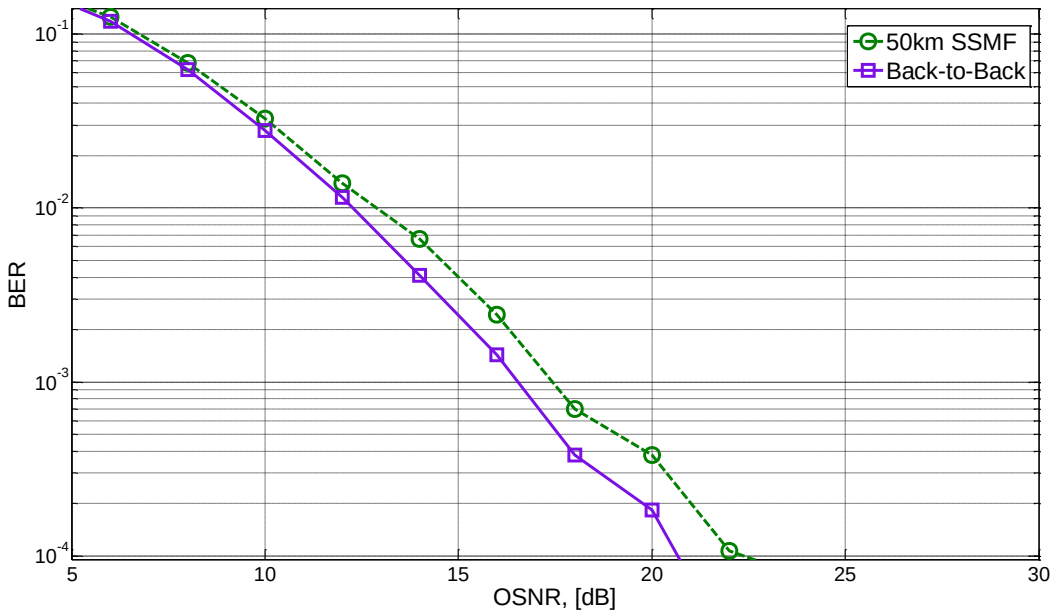

Figure 5.7. BER as function of the OSNR at the RSOA output for back-to-back and after 50km.

5.1.2 Fixed Mobile Conversion

In this section, it is proposed to take advantage of the deployed passive optical network (PON) infrastructure by overlaying a decomposed radio access network (RAN) using a very dense WDM. Coherent optical orthogonal frequency-division multiplexing technology is investigated for achieving the desired narrow channel spacings while minimizing the impact on the performance of legacy equipment. A practical implementation is evaluated using simulations. Within the analyzed configurations, a trade-off is found between time-division multiplexed (TDM)-PON and RAN performance. The optimum balance is found for additional losses in the TDM-PON path of less than 1 dB, ensuring simultaneous service to a maximum of 145 metro cells together with the PON customers and within a reach of 24 km.

A. Behind the research

Point to multi-point Passive Optical Networks (PONs) are popular architectures for supporting fiber-based broadband access to a set of customers [Girard2005]. Thus, an optical line terminal (OLT), which is part of a central office (CO), is connected through a tree-branched passive distribution network to the optical network units (ONUs), which are located at the customer premises equipment (CPE). In these schemes, the different user signals are usually multiplexed in time, leading to the time-division multiplexed (TDM)-PONs standardized by the ITU-T [ITU-T G.984.2] and the IEEE [IEEE 802.3ah]. Along a different line, mobile data traffic is expected to grow exponentially due to the emergence of smart mobile devices, asking for capacities of up to 25 Gb⁄s⁄km^2 [CiscoVNI11–Liu11]. The latest developments of mobile technologies use bandwidths of only 100 MHz for targeting data rates in the range of hundreds of megabits per second [3GPP TR 25.912]. Thus, in densely populated areas, a small cell deployment is needed for coping with the required capacities, which increases the intercell interference. Within this scenario, joint signal processing would be desirable for mitigating these interferences [Liu11]. A possible solution is the decomposition of each base station into a radio resource management unit (RRM) and radio units, which allow moving the radio units to a remote location while keeping the signal processing centralized at a central office. Furthermore, the remote radio units (RRUs) would be substantially simpler and new joint processing techniques, requiring multiple base station antenna signals, could be implemented in a centralized pool of RRMs [Liu11–CPRI11]. This decomposed radio access network (RAN) can be implemented over different infrastructures. Among them, those based on optical fibers are the ones that can offer true broadband communication encompassed with an enhanced reach. The common public radio interface (CPRI) is one of the most popular standards used for RAN implementation, thanks to its compatibility with common optical transceivers [CPRI11]. In case the optical infrastructure is dedicated to the radio signal delivery, communication can be achieved by means of optical Ethernet [Segel11a, Segel11b] or even over a dedicated hybrid TDM/WDM-PON [Liu11]. A more practical solution is the overlay of the decomposed RAN over existing TDM-PONs, as there is no need of deploying new network infrastructure.

Nevertheless, this solution is challenging, as it has to satisfy the needs of the optical access network subscribers while supporting the decomposed radio access. Several approaches have been proposed to support the wireless signal delivery over optical access networks while serving a set of fixed customers. The techniques employed were either radio-over-fiber techniques combined with WDM [Koonen08, Othman11], either suggesting novel network architectures [Madamopoulos12], or more advanced solutions in combination with optical orthogonal frequency division multiplexing (OFDM) [Cartaxo11, Milosavljevic11]. Precisely, [Koonen08]

and [Othman11] proposed to deliver a single mobile carrier per user, reusing the deployed infrastructure, whereas the last conceive an alternative coexistence between wireless and broadband access signals in future deployments. In [Cartaxo2011], a different set of transceivers is used for accommodating a single mobile carrier per customer within a network infrastructure similar to the one already deployed. Reference [Milosavljevic11] proposes CPRI delivery over an access network concept based on orthogonal frequency division multiple access. In [Madamopoulos12], a new tree-ring converged network architecture is discussed for achieving fixed and mobile signal delivery. Thus, from these approaches, [Koonen08, Othman11] and [Cartaxo11] may not be able to support the target mobile capacities, whereas [Madamopoulos12]

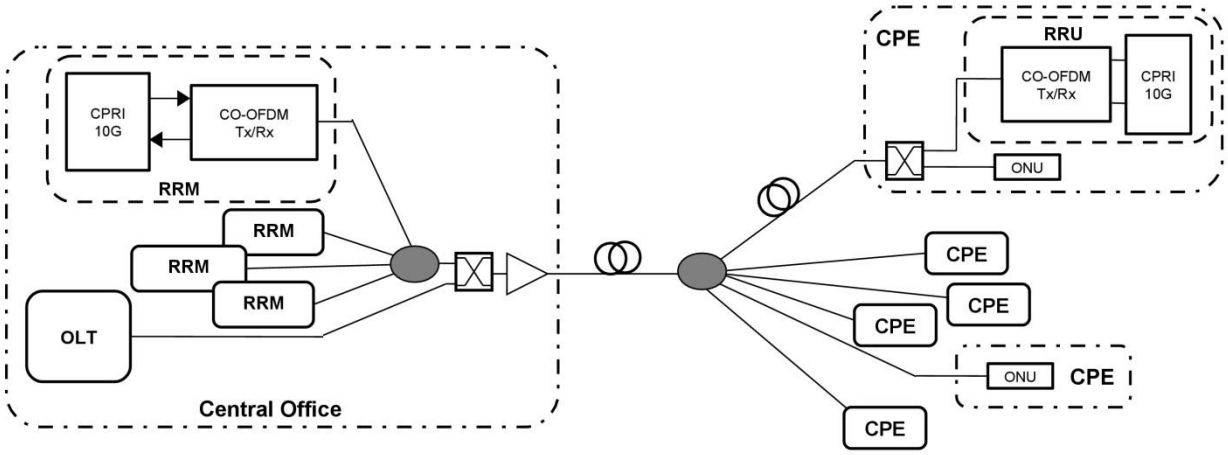

Figure 5.8. Generic network architecture. The customer premises equipment (CPE) can also contain a remote radio unit (RRU), while the radio resource management units (RRMs) are kept at the central office (CO).

and [Milosavljevic11] would not ensure backward compatibility with inherited PON systems.
In this section, we propose to overlay a decomposed RAN on an existing deployed TDM-PON infrastructure. As each base station would be decomposed into RRM and RRU, the idea is to keep the first in the CO, while the last are located at selected customers' premises. A wavelength schedule is detailed for assigning an exclusive wavelength per RRM–RRU pair, and crosstalk with PON signals is mitigated by using a dense WDM plan. As the distribution network is to be kept passive, coherent optical OFDM technology is used for minimizing the impact on the performance of TDM-PON equipment in terms of power budget. Precisely, a transceiver design is discussed, based on phase-modulated optical OFDM, which improves sensitivity and enables narrow channel spacings while featuring low overhead and simplified signal processing [Fabrega11]. Furthermore, the case of a practical implementation based on 10 Gb⁄s CPRI data streams is analyzed by means of simulations. The remainder of the paper is organized as follows. Section B deals with the signal delivery strategy with a wavelength plan proposed for a generic network topology. Afterward, in Section C, a transceiver scheme is proposed for RAN deployment, and its implementation is discussed. Next, Section D details and reports the results of the system simulations performed, whereas Section E evaluates the possible-use cases from the simulation results. Finally, the main conclusions are drawn in Section F.

B. Network Topology and Signal Delivery Strategy

A generic network scheme is shown in Fig 5.8 above. It is based on a tree-branched outside plant with a single splitting stage, which distributes the signals to the N users connected to the network. Using this topology, the deployed TDM-PONs can be compliant with the IEEE and ITU-T standards, sharing many common parameters.

As a WDM overlay is envisioned, the wavelength plan specified by these standards is shown in Fig. 5.9 for the third window.

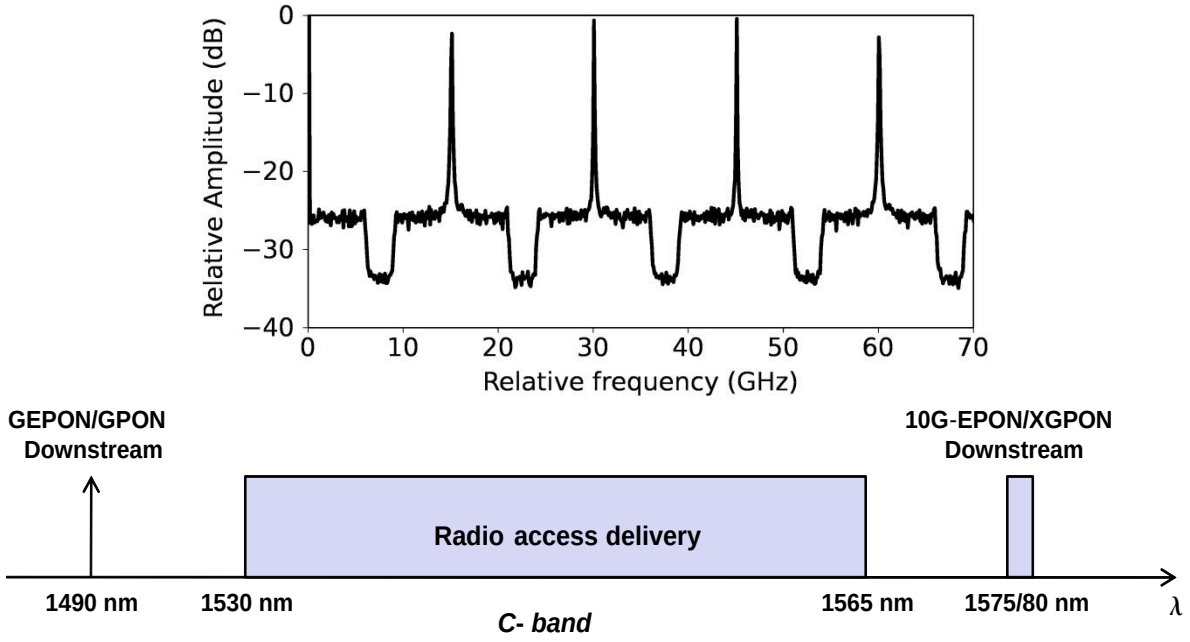

Figure 5.9. Wavelength plan. Inset shows a sample portion of the optical spectrum occupied by the proposed RAN deployment, each channel running at 12.1 Gb⁄s with channel spacing of 15 GHz.

Legacy standards (e.g., GEPON, GPON) use 1490 nm for downstream and 1310 nm for upstream [ITU-T G.984.2, IEEE 802.3ah], while the newest standards (10G-EPON and XGPON) [IEEE 802.3av, ITU-T G.987.2] recommend using the range of 1575–1580 nm for downstream and the range of 1260–1280 nm for upstream. The other wavelengths are not used except when some optional services are delivered, such as CaTV services, which are placed at 1550 nm. In this topology, the 1530–1565 nm range (C band) is proposed for RAN communication, from a converged CO, to each of the M RRUs. The M RRUs would be included at a selected customer premises ($M \leq N$), as shown in Fig. 5.8. Note that an optical amplifier is needed at the CO for ensuring a certain power level at its output and compensating the losses when aggregating the contributions of each RRM and the TDMPON OLT. Thus, the proposed wavelength range is also suitable for amplification because commercial optical amplifiers mostly operate in the C band. When the optional PON services are given, the neighborhood of 1550 nm would not be used for wireless delivery.

In order to prevent PON equipment detecting RAN traffic, a photodetector jointly packaged with a (tunable) thin-film filter can be used at the receiver side at the ONU, just after the optical

duplexer [Murano2008]. The optical filters demonstrated in [Murano2008] present a 3 dB bandwidth of 0.3 nm (~37.5 GHz) and a 10 dB bandwidth of 0.6 nm (~75 GHz), enough to keep free the targeted band for the RAN signal delivery. The same configuration (packaged photodetector and filter) has demonstrated optical budgets above 25 dB while operating at data rates as high as 10 Gb⁄s when combined with electronic equalization [Rahar11]. Furthermore, the employed optical filter technology has reported tunable bands beyond 40 nm and finesse higher than 1500 [Domash2002].
For the radio signal delivery, the coherent optical OFDM transceiver shown in Fig. 5.10 is proposed to be included at the RRMs and RRUs as an interface with the optical domain.

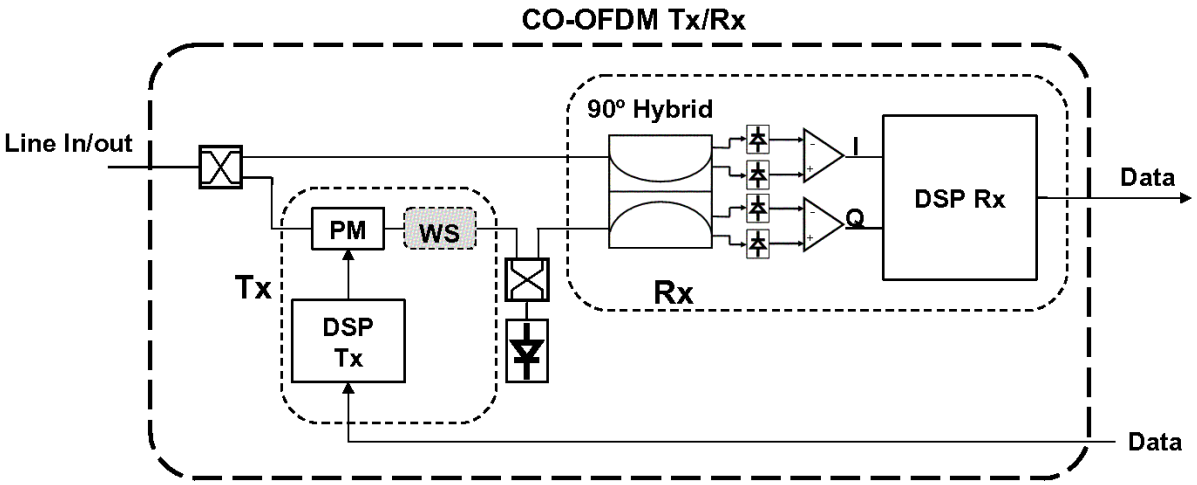

Figure 5.10. Transceiver architecture. Details of digital signal processing (DSP) of the transmitter and the receiver are shown in Figs. 4.11 and 4.12, respectively.

The signal contributions are aggregated by means of optical couplers. At the CPE, an asymmetrical coupler with x:y splitting ratios is used. It must be noted that the branch featuring less insertion losses (e.g., x when $x \geq y$) will be connected to the legacy ONUs in order to minimize the impact of including the RAN transceiver. Thus, transmission losses are increased on the RRM–RRU path. Coherent optical OFDM is used for overcoming this problem, as it offers much better sensitivity than direct detection systems. At each transceiver, the tunable local oscillator selects the assigned channel (λ_U or λ_D, depending if the direction of the communication is upstream or downstream), and transmits or receives the OFDM signals following the steps detailed in Section C. A direct detection scheme at the CPE side in combination with coherent detection at the CO would be useful to overcome the power budget limits; nevertheless, optical (tunable) filters would be needed to avoid crosstalk from neighboring channels, featuring lower selectivity at the GHz scale and thus limiting the number of RRM–RRU pairs to serve. Regarding the dimension of the decomposed RAN to support, it is forecasted that two types of cells will be needed to deliver mobile traffic in an urban scenario [Segel2011]. The first of them is a 1 km diameter three-sector macro cell, giving support to the global system for mobile communications (GSM), wideband code division multiple access (W-CDMA) and long term evolution (LTE) signals. The other cell is a metro cell with 250 m diameter and a single sector, which is used to deload the macro cells in the urban spots with high traffic. This last would mainly support W-CDMA, LTE and WiFi. As stated in the Introduction, our interest is the use of the CPRI to ensure communication between RRMs and RRUs. The CPRI is standardized to work

up to 10 Gb⁄s [9]. For the proposed cases, a 10 Gb⁄s CPRI data stream is to be guaranteed per cell sector. Thus, a macro cell is expected to ask for an equivalent CPRI traffic of 30 Gb⁄s (3 × 10 Gb⁄s), whereas a metro cell is expected to need 10 Gb⁄s. Further details on such dimensioning can be found in [Segel11b].

C. Transceiver Scheme

The proposed transceiver scheme is shown in Fig. 5.10. Details of the digital signal processing (DSP) blocks are depicted in Figs. 5.11 and 5.12. At the DSP block of the transmitter (Fig. 5.11), data is first parallelized and mapped into a binary phase shift keying (BPSK) constellation, and a training symbol sequence is inserted. Next, the resulting symbols are OFDM-modulated using the fast Hartley transform (FHT), which is equal to its inverse [Bracewell2000]. As the Hartley transform is a real transform, it is used to simplify the transform implementation (i.e., no complex operations are needed) and thus reduce the delay associated with the DSP. Nevertheless, noncomplex modulation formats are to be used when employing
FHT. This limits the mapping of the input symbols to unidimensional modulation formats, e.g., BPSK or multilevel pulse amplitude modulation (M-PAM). Thus, BPSK is used because of its robustness and simple implementation. The obtained real-valued OFDM symbols are serialized and converted into an analog signal by a digital-to-analog converter (DAC). Afterward, the

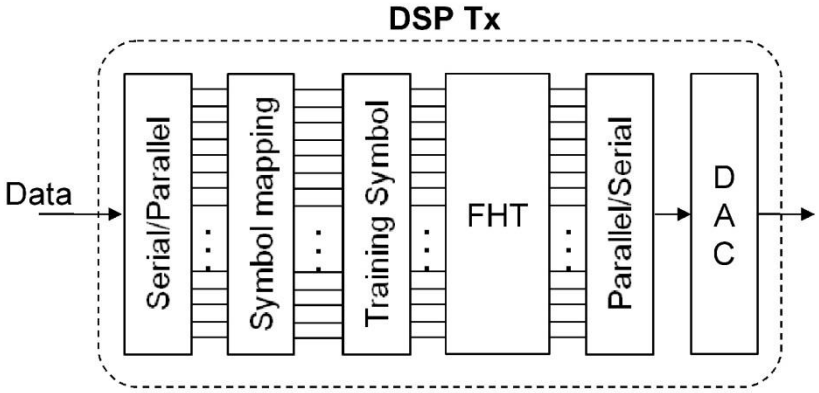

Figure 5.11. Scheme of the digital signal processing block on the transmitter's side. Insets show samples of time and spectrum representations of the signal at the output of the DAC V_i.

resulting OFDM analog waveform is injected into an optical phase modulator (PM) and transmitted. On the receiver's side, the optical data signal is first coupled with the local oscillator signal in a 90° optical hybrid. It combines both signals, producing four different optical signals with 0°, 90°, 180° and 270° phase differences. These signals drive two pairs of photodiodes acting as balanced detectors. Next, the resulting in-phase (I) and quadrature (Q) outputs are digitized by an analog-to-digital converter (ADC). At the DSP block (Fig. 5.12), the signal passes through a carrier recovery block to compensate for phase and frequency errors. The phase of the complex received signal recovered from the I and Q components is afterward extracted. Next, the FHT is carried out, the training symbols are conveniently extracted and equalization is performed. Finally, data are detected after the symbols' demapping and serialization. The local laser at each transceiver is used as a transmission source and as a local oscillator at reception. In

case of high Rayleigh backscattering, the use of the same wavelength for downstream and upstream is not recommended ($\lambda_U \neq \lambda_D$). Therefore, a wavelength shifting (WS) device can be

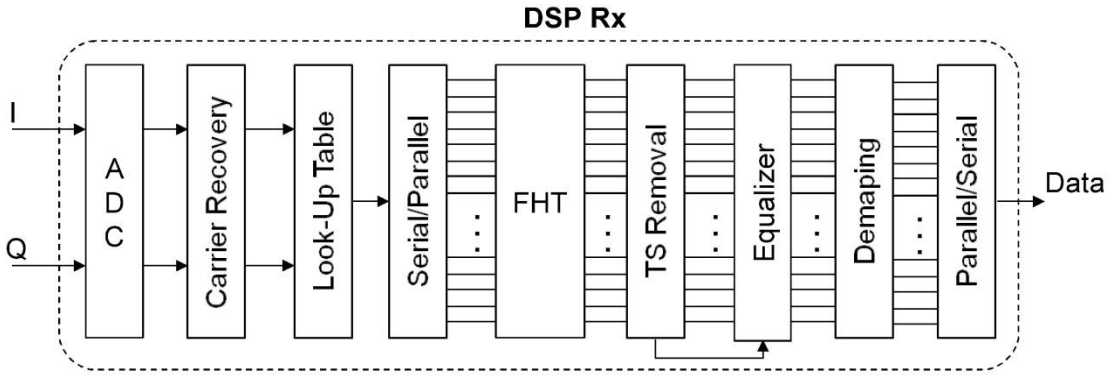

Figure 5.12. Scheme of the digital signal processing block on the receiver's side. Inset shows a sample of the received constellation before data demapping.

used to detune, e.g., transmission from reception [Omella09].

A much better implementation, featuring higher sideband suppression, could include the use an optical single side band modulator [Kawanishi02, Savchenkov09]. Moreover, a tunable laser can be used for dynamically adapting the optical carrier frequency. This feature becomes especially relevant when using the proposed intradyne detection, as no optical filters are needed at the receiver. Thus, for each channel, the central wavelength corresponds to the one provided by the local laser. The transceiver can be tuned from one channel to another by modifying the wavelength of the local laser. A lot of progress has been made in fast tunable lasers, and tuning times on the order of hundreds of nanoseconds have been demonstrated [Buus06, Fabrega11qe]. Therefore, the proposed WDM overlay could be quickly reconfigured in case the network includes a control layer/plane. One of the main properties of the proposed transmission system is that the phase noise only affects the central OFDM subcarriers of the transmitted/received signal [Fabrega11]. As the OFDM signal is modulated on the optical phase, phase noise results are additive instead of multiplicative, affecting only the central subcarriers and not all the OFDM symbols. Thus, if these subcarriers are suppressed, the effects of the lasers' phase noise are mitigated without any specific digital processing [Fabrega11]. Nevertheless, subcarriers suppression leads to an increased overall signal overhead.

Since the changes in the polarization state of the optical signals are expected to be very slow for the targeted distances [Shieh10], they are not taken into account in the scheme of Fig. 5.10 for the sake of simplicity.

D. Simulations and Results

The performance of the proposed signal delivery strategy is assessed by means of numerical simulation using Matlab software and employing the parameters of Table 5.4. A data set of 2^{17} pseudo-random bits is generated using a sequence of $2^{15} - 1$. The target net data rate is Rb = 10 Gb⁄s plus overhead due to forward error correction (FEC; ϵ_f = 7 %), linewidth reduction (ϵ_l, to be fixed after the first set of simulations), and training symbols (ϵ_s = 0.05 %). The resulting bit sequence is parallelized, BPSK encoded and OFDM modulated to 64 carriers using the FHT. As

transmission is forecast in relatively short distances, the cyclic prefix has been avoided, substantially reducing the signal overhead. A training symbol is inserted every 2048 OFDM symbols for equalization, resulting in ϵ_s = 0.05 % of associated overhead. The resulting signal is injected into the phase modulator and excited by a laser of variable output power. The output power of the transceiver is set to +5 dBm, which is also set as a condition at the CO output. At the receiver, the local oscillator is also modeled as a CW laser with output power of 16 dBm, giving 0 dBm to each photodetector after the 90:10 coupler and the 90° hybrid. OFDM decoding and data demodulation are performed after intradyne detection. The parameters for the PIN diode correspond to a commercially available
device [DSCR401HG]. As a phase-modulated OFDM system is proposed, a preliminary set of simulations has been carried out to find the optimum phase-modulation index for distances of up to 50 km. The optimum value was found for an optical phase standard deviation of 54°.

Simulation parameters	
Net data rate	10 Gb⁄s
PRBS length	$2^{15} - 1$
Total number of bits	2^{17}
FEC overhead	7%
Training symbol overhead	0.05%
Number of OFDM subcarriers	64
Modulation format of all subcarriers	BPSK
Samples per OFDM symbol	512
Number of training symbols	1
OFDM transmission	
Transmitter laser	CW laser
Central wavelength	1550 nm
Optical phase standard deviation	54°
Transceiver output power	5 dBm
OFDM reception	
Local oscillator	CW laser
Local oscillator wavelength	1550 nm
Local oscillator output power	16 dBm
Photodiode type	PIN
Photodiode responsivity	0.7 A⁄W
Photodiode dark current	10 nA
Photodiode thermal noise	15 $pA/\sqrt{Hz}$

Table 5.4. Simulation parameters for the proposed coherent optical OFDM system.

In all the analyzed cases, the output parameter measured is the statistical counting of received bits, which provides the best measure of the system bit error ratio (BER). A target BER of 10^{-3} is considered, as a super FEC code can be effectively used for the ϵf = 7 % overhead assumed, for example the RS(1023,1007)/BCH(2047,1952) code found in [ITU-T G.975.1].

D.1. Back-to-Back characterization of the transceiver

Prior to performing the transmission simulations over the network, a back-to-back characterization of the proposed transceiver is carried out.

As phase noise is an important impairment of coherent systems, the first point to evaluate is the laser linewidth tolerance of the system. As pointed out in Section C, the phase noise is additive, instead of multiplicative, for the proposed receiver. Thus, only suppressing the central subcarriers of the transmitted signal is sufficient for compensating it at the expense of increasing the overhead. Several overheads are tested in the simulations, corresponding to the suppression of the 2 (ϵ_l = 3.1 %), 4 (ϵ_l = 6.3 %), 6 (ϵ_l = 9.4 %) and 8 (ϵ_l = 12.5 %) central subcarriers. Thus, the gross data rate analyzed at each simulation is of

$Rg = Rb(1 + \epsilon_l)(1 + \epsilon_f)(1 + \epsilon_s)$, ranging from Rg = 11.04 Gb⁄s (ϵ_l = 3.1 %) up to Rg = 12.04 Gb⁄s (ϵ_l = 12.5 %).

As the total overhead is to be kept as lowas possible, nohigher values of ϵl are analyzed. Regarding the phase noise, the total linewidth (corresponding to the transmitter plus local

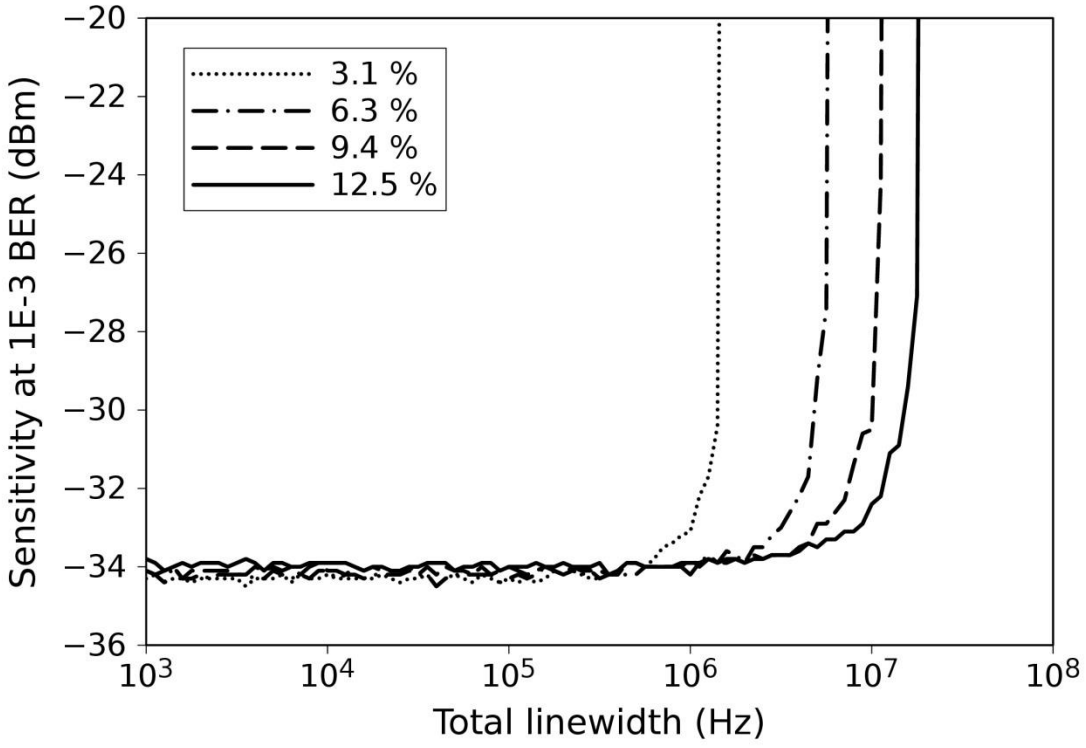

Figure 5.13. Linewidth tolerance for several overheads.

oscillator lasers) is varied from 1 kHz up to 100 MHz. Results are shown in Fig. 5.13, where we can see that 1 dB power penalties at a BER of 10^{-3} range from 800 kHz for ϵ_l = 3.1 % up to 8.9 MHz corresponding to ϵ_l = 12.5 %. As the proposed example of a tunable laser to be included at

each OFDM transceiver features linewidths of up to 5 MHz [S7500], the total laser linewidth is fixed at 10 MHz (5 + 5 MHz) and ϵ_l to 12.5 % for the rest of this paper.

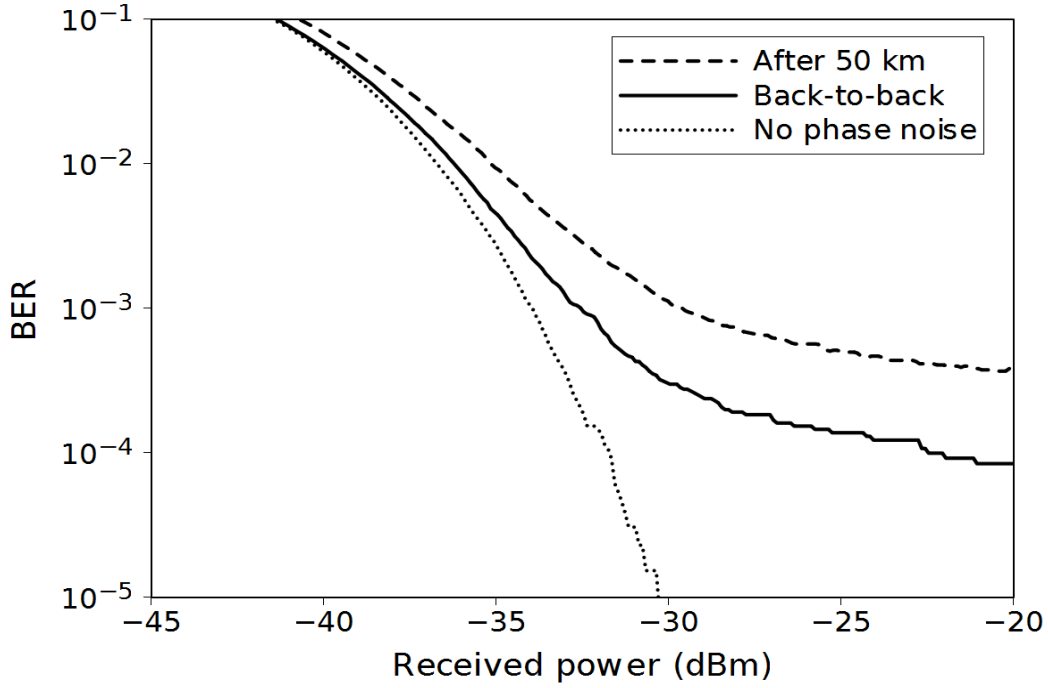

Figure 5.14. Sample sensitivity curves for back-to-back and transmission after 50 km cases with a total laser linewidth of 10 MHz. The no-phase-noise curve corresponds to a back-to-back configuration with total linewidth set to zero.

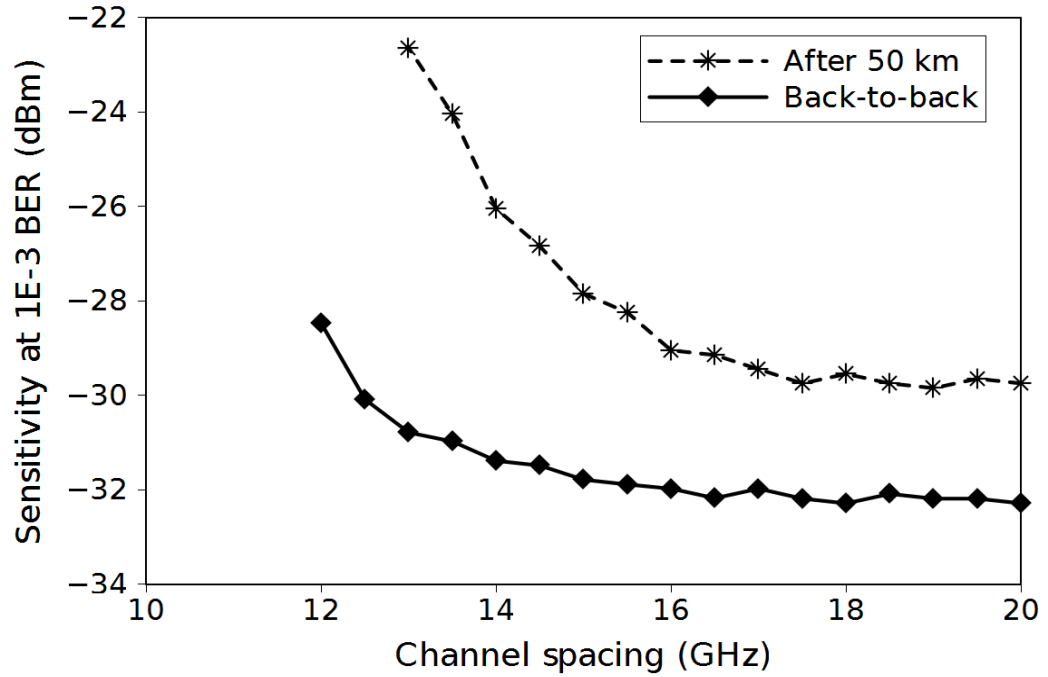

Figure 5.15. Sensitivity penalty at 10^{-3} BER versus the channel spacing.

For this case, sample sensitivity curves are shown in Fig. 5.14, where it can be observed that the sensitivity at 10^{-3} BER when including the linewidth is −32.4 dBm, only 1.6 dB away from the −33 dBm obtained when not considering phase noise.
The next step is to assess the channel spacing sensitivity penalties for the back-to-back case.
For that, a couple of identical interfering channels are considered and placed at each side of the channel of interest.
The transmission power of each interference signal has been set to the same power as the useful signal, assuming a worst case scenario, and only the spacing between both signals is varied. Results are shown in Fig. 5.15, where it can be seen that a limit is given at 14 GHz for a sensitivity penalty below 1 dB at a BER of 10^{-3}.

D.2. RAN overlay transmission

After these first considerations, a transmission over an optical distribution network is simulated. The transmission link includes a standard single mode fiber (SSMF) and a variable attenuator to emulate the power splitting elements at the outside plant. The split-step Fourier method [Agrawal07] is used to model the propagation through the SSMF. The parameters of the fiber model used are shown in Table 5.5 below.

OFDM reception	
Gain	27 dB
Output power	+5 dBm
Noise figure	6 dB
Output OSNR	29.8 dB
Fiber	
Effective area	80 μm^2
Dispersion	17 ps/(nm·km)
Dispersion slope	0.07 ps/(nm^2·km)
Loss	0.2 dB/km
Kerr coefficient	$2.35 \cdot 10^{-20}$ m^2/W

Table 5.5. Network simulation parameters.

An optical amplifier is included at the CO for compensating the losses of the M:1 power splitter and the coupler for including the TDM-PON signals. As the first limit of the channel spacing has been found at 14 GHz, a maximum of 312 channels (156 upstream and 156 downstream) is initially forecasted. Thus, the minimum splitting ratio to be employed at the CO is M = 256, introducing 24 dB of attenuation. When combined with the optical coupler, the total losses to be compensated by the optical amplifier of the CO are 27 dB to ensure a CO output power of +5 dBm per channel. A noise figure of 6 dB is assumed for the optical amplifier, meaning that the optical signal-to-noise ratio (OSNR) at the output of the CO is 29.8 dB.

Thus, the corresponding noise has been added before propagation over the transmission link in order to include this effect in the upcoming simulations. Under these conditions, the sensitivity and channel spacing of the proposed system are evaluated after transmission.
Additionally, nonlinear effects of the fiber are assessed at the variation of the launch power.
From the sensitivity measurements, the power budget for 10^{-3} BER is calculated as

$$B(dB) = P_t(dBm) - P_r(dBm) \tag{5.2}$$

where P_t is the transmitted power and P_r is the received power. These results are shown in Fig. 5.16 below, where it can be observed that the RAN budget obtained for 10^{-3} BER is 7.5 dB for back-to-back and 34.8 dB after 50 km. The sample sensitivity plot is shown in Fig. 5.14, corresponding to the transmission after 50 km, where it can be observed that the sensitivity at 10^{-3} BER is −29.8 dBm, which results in a power penalty of 2.6 dB with respect to the back-to-back case analyzed.

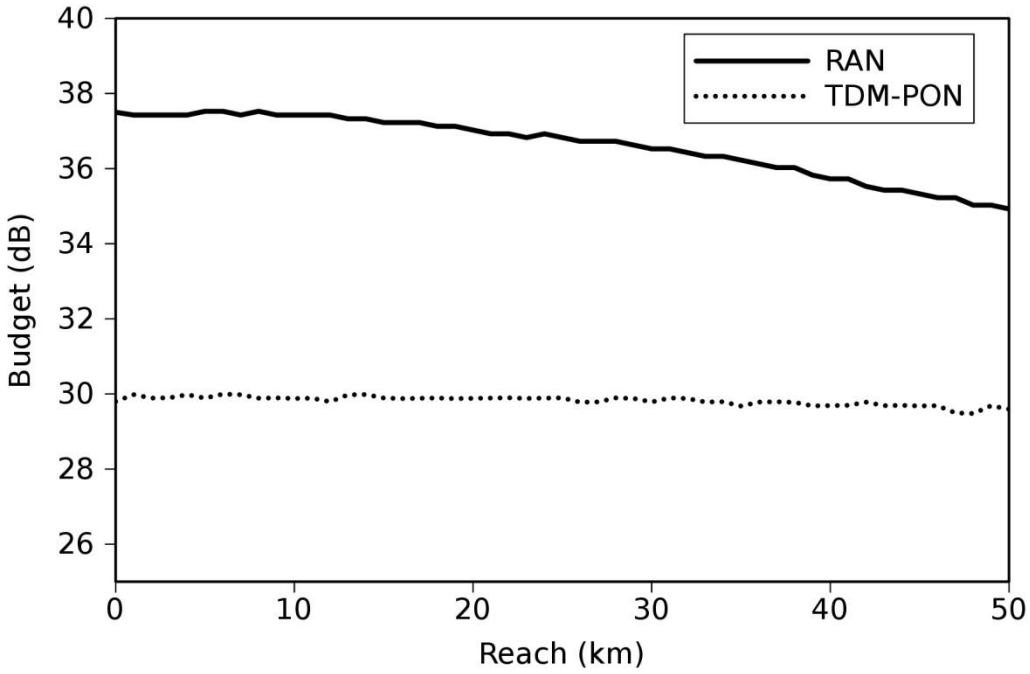

Figure 5.16. Radio access network and TDM-PON power budgets for 10^{-3} BER as a function of the reach.

Regarding the channel spacing, the interference signals have also been set to the same power as the useful signal while varying the spacing between them. Sensitivity at 10^{-3} BER is evaluated after transmission over a 50 km link. Results are shown in Fig. 5.15, where it can be seen that the behavior after 50kmis different from the back-to-back case. Besides the inherent power penalty of 2.6 dB with respect to the back-to-back, the performance of the system is degraded more rapidly, achieving a sensitivity of −26.1 dBm at 14 GHz spacing, 3.7 dB away from the −29.8 dBm reported when transmitting a single channel. This poses a trade-off between sensitivity and channel spacing at the maximum distance targeted. A good compromise is found at spacings of 15 GHz, which achieves a sensitivity of −27.7 dBm and is only 2.96 GHz higher than the signal bandwidth.

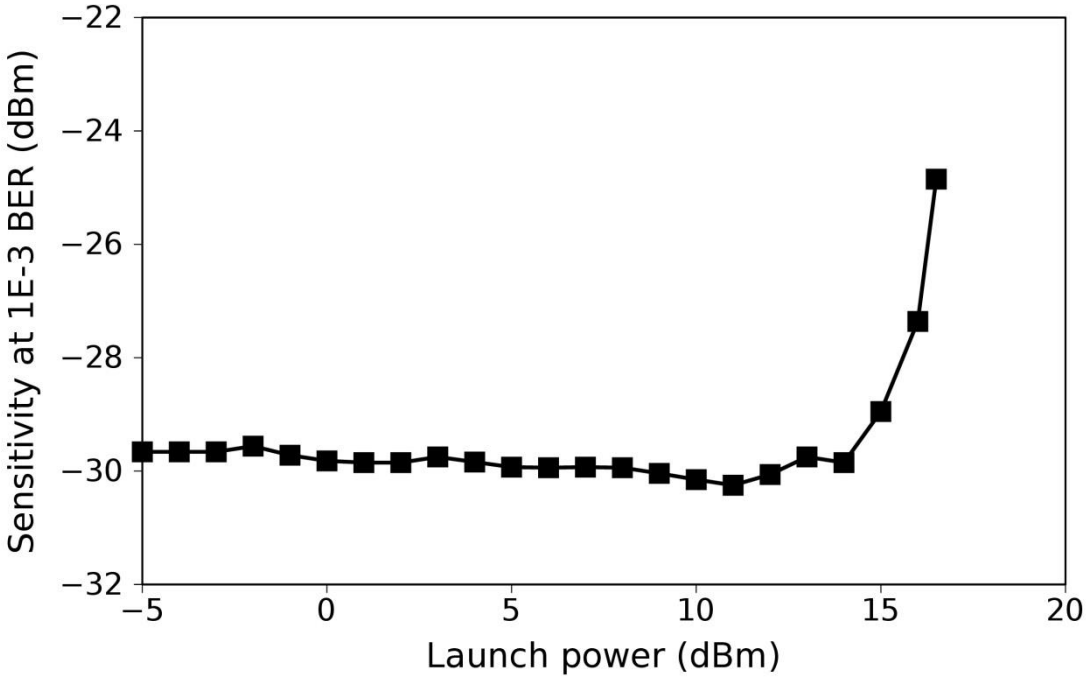

Figure 5.17. Sensitivity at 10−3 BER after 50 km SSMF versus the launch power.

Finally, fiber nonlinearity effects are evaluated after 50 km transmission. In the first step, no adjacent channels are considered, and the sensitivity at 10^{-3} BER is evaluated at several launch powers. Results are shown in Fig. 5.17 above. There, it can be observed that sensitivity at 10^{-3} BER fluctuates around −29.8 dBm within a range of ±0.4 dB for launch powers up to +14 dBm. Beyond that point, the sensitivity needed increases, and 10^{-3} BER is unachievable for launch power beyond 16.5 dBm. As a second step, nonlinearity effects are assessed in the presence of several adjacent channels whose launch power is varied while maintaining the channel of interest at +5 dBm. Two cases are evaluated, first placing one channel at each side of the channel of interest, and, second, when two consecutive channels are also at each side of the channel of interest. The spacing between channels is considered to be 15 GHz. Results are shown in Fig. 4.18 below, where it can be observed that at −5 dBm, a sensitivity of −29.8 dBm is obtained for a BER of 10^{-3}, as expected.

When increasing the power of adjacent channels, −28.7 dBm are needed when launching at _3 dBm for obtaining 10^{-3} BER, 0.9 dB away from the value obtained at −5 dBm. For the targeted output power of _5 dBm, the penalty is increased up to 2.1 dB, achieving a sensitivity of −27.7 dBm for 10^{-3} BER. At that point, the penalty difference between considering two or four adjacent channels is 0.2 dB in terms of sensitivity. Finally, it should be noted that because of fiber nonlinear effects, it is not possible to achieve a BER of 10^{-3} for powers of the adjacent channels beyond +8 dBm when considering only two of them and +6.6 dBm for the case of considering four channels.

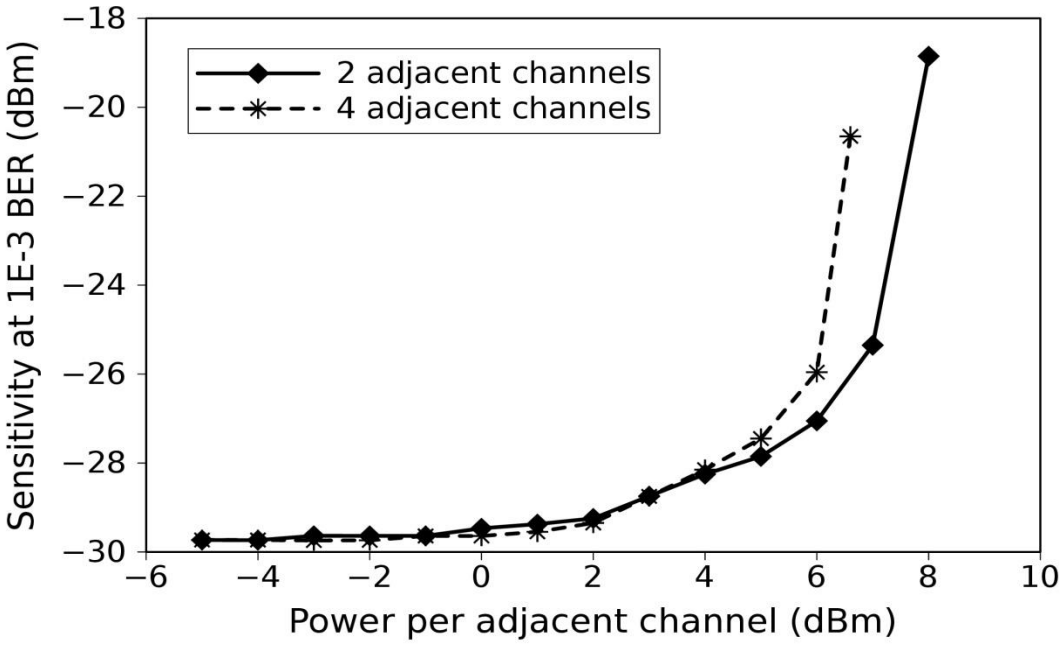

Figure 5.18. Sensitivity at 10−3 BER after 50 km SSMF versus the power of each of the adjacent channels.

D.3. TDM-PON transmission

Additionally, the TDM-PON power budget is analyzed. In fact, an XG-PON compliant transmission system is simulated using the same distribution network parameters as before. Thus, a data set of 2^{17} pseudo-random bits is generated using a sequence of $2^{15} - 1$.

Transmitter	
Extinction ratio	10 dB
Output power	+5 dBm
Receiver	
Photodiode type	APD
Responsivity	0.7 A⁄W
Avalanche gain	9
Ionization coefficient	1
Dark current	10 nA
Thermal noise	12 $pA/\sqrt{Hz}$
Electrical filter type	5th order Bessel–Thompson
Electrical filter bandwidth	8 GHz

Table 5.6. Simulation parameters for the standard IM/DD system corresponding to TDM-PON path.

The transmitter and receiver are modeled as an ideal nonreturn to zero (NRZ) intensity modulation direct detection (IM/DD) system running at 10 Gb⁄s, with the parameters provided in Table 5.6 above.
This combination provides a receiver sensitivity of −28 dBm for the proposed transmitter, leading to a transmission system fully compliant with the XG-PON standard [ITU-T G.987.2]. Moreover, 3 dB extra losses have been included for considering the optical filter, inserted to prevent crosstalk between radio delivery and PON equipment. Results are shown in the TDM-PON dotted line in Fig. 5.19. The power budget obtained for 10^{-3} BER is 30 dB for back-to-back and 29.6 dB at 50 km.

E. Results and Discussion

Based on the simulation results, four cases are analysed considering the losses inserted in the legacy PON path, which depend on the x:y coupling ratio at the selected CPEs incorporating the proposed transceiver. The x:y ratios analyzed are 99:1, 90:10, 80:20 and 50:50. In order to evaluate the feasibility of the RAN overlay, the main parameters to take into account are the OFDM channel spacing and the allowed splitting ratio N. According to the simulations, the OFDM channel spacing is fixed at 15 GHz. Thus, a maximum of 290 channels can be allocated in the C band, so 145 wavelengths can be used for downstream, while the other 145 are employed for upstream. Note that the splitting ratio N supported by the network (for TDM-PON and RAN paths) is expected to be higher than the number of channels to be deployed. Thus, a minimum splitting ratio of $N \geq 145$ has to be satisfied.
Regarding the achievable splitting ratio N, it is also a function of the network reach. It is evaluated for RAN and TDM-PON paths to ensure a power margin higher than 3 dB at 10^{-3} BER for both cases. The power margins are calculated as

$$M(dB) = B(dB) - L_f(dB) - 3\log_2(N) - 10\log_{10}(z) \tag{5.3}$$

where $L_f = \alpha \cdot d$ are the fiber losses, α is the attenuation coefficient of the fiber (dB⁄km), d is the reach (km), and z is the coupling ratio of the CPE assigned to the path.
According to the example in Section B, z = x for the OLT–ONU path and z = y for the the RRM–RRU path. Thus, from the power budget B obtained in the simulations, the maximum achievable splitting ratio for a minimum margin of 3 dB is calculated as a function of the reach for the two network paths. Results are shown in Fig. 4.19 for the four proposed x:y coupling ratios. Furthermore, a summary of the overall performance is provided in Tables 4.7 and 4.8, also taking into account the proposed channel spacing. Note that Table 4.7 shows the TDMPON reach for a splitting ratio $N \geq 256$ because the channel spacings for such values limit the RAN signal delivery.
In Fig. 5.19, it can be observed that very low losses in the OLT–ONU path severely limit the performance of the RAN delivery transmission system, whereas increasing the loss on the OLT–ONU path makes possible a better transmission of the RAN signals. Precisely, Fig. 5.19(a) shows the first limit, when only 0.04 dB extra losses are included in the TDM-PON path. This means that RAN signals have to cope with 20 dB extra losses, reducing the achievable path to very short distances (up to 12 km) and considering small splitting ratios (N = 32). Conversely, Fig. 5.19(d) shows the case when the RAN delivery path has the same extra losses as the TDM-PON path. In this case, the RAN path allows much higher splitting ratios (up to N = 2048 for 7 km), while the TDM-PON path is limited to ratios lower than those reported in Figs. 5.19(a)–5.19(c). Figure 5.19(c) shows the more balanced performance between TDM-PON and RAN.

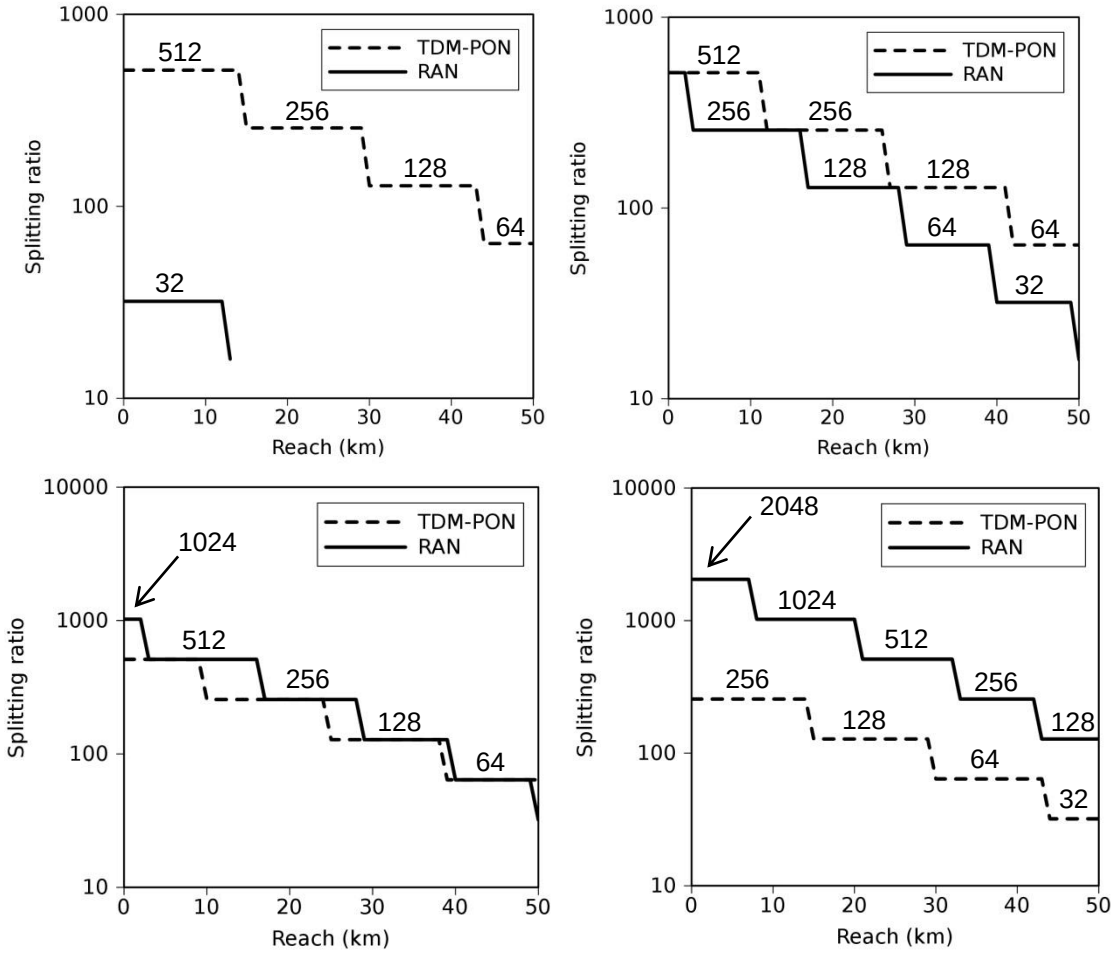

Figure 5.19. Optical distribution splitting ratio N achievable with the proposed RAN delivery and a standard TDM-PON for achieving a power margin higher than 3 dB and at different x∶y coupling ratios: (a) 99∶1, (b) 90∶10, (c) 80∶20 and (d) 50∶50.

This is the case for x:y = 80:20, which introduces 0.96 dB insertion losses on the OLT–ONU path and 7 dB additional loss in the RRM–RRUpath. For this case, the maximum splitting ratio achieved by the RAN is N = 1024 for distances up to 10 km, followed by a splitting ratio of N = 512, possible for a maximum reach of 12 km. On the other hand, the TDM-PON can achieve splitting ratios of up to N = 512 for a maximum distance of 9 km. When increasing the reach, the losses cumulate, and the splitting ratio has to be decreased for maintaining a power margin higher than 3dB in both paths. For distances below 24 km, $N \geq 256$ is guaranteed for both signal paths. This means that 145 RRUs can be supported if a 15 GHz channel spacing is used. According to the cases summarized in Section II, each RRU can serve a metro cell, whereas 3 RRUs are needed for supporting a macro cell. As each wavelength is providing a net data rate of 10 Gb⁄s, for distances below 24 km and employing 15 GHz of channel spacing, the network can support either 145 metro cells or 48 macro cells.

Coupling ratio	Insertion loss (dB)	Maximum split ratio	Maximum reach (km)[a]
x:y = 99:1	0.04	1:512	29
x:y = 99:10	0.46	1:512	26
x:y = 80:20	0.96	1:512	24
x:y = 50:50	3	1:256	14

[a] *For achieving a power margin higher than 3 dB with a minimum splitting ratio of 1:256*.

Table 5.7. OLT–ONU path performance.

Coupling ratio	Insertion loss (dB)	Max. no. macro cells	Max. no. metro cells	Max. reach[a]
x:y = 99:1	20	4	32	12
x:y = 99:10	10	48	145	16
x:y = 80:20	7	48	145	28
x:y = 50:50	3	48	145	42

[a] *For the maximum number of served macro and metro cells.*

Table 5.8. RRM–RRU path performance.

Even the CPRI standard specifies maximum distances >10 km, so latency may be a key issue when managing this kind of deployment, as LTE and LTE-advanced require round trip delays in a user plane lower than 5 ms and 2.5 ms, respectively [3GPP TR 25.912]. A simplified OFDM implementation based on Hartley transform and BPSK mapping has been proposed to reduce delays associated to the DSP of the transceiver. However, this may not be enough to cope with this stringent requirement. In that case, the maximum reach for the RAN deployment should be reduced.

5.2 Applications in Optical Transport Networks

5.2.1 Flexible Metropolitan Area Network

In this section, effects when cascading optical filters are investigated for a phase modulated coherent optical OFDM system based on Hartley transform. The system is applicable for a flexible metropolitan area network of up to 100 km where the traffic is aggregated/dropped by means of wavelength division multiplexing. The evaluation is performed by means of numeric simulations in a 10 Gb/s system with a total bandwidth of 10 GHz. First a back-to-back (no fiber) case is assessed. Results show a 3 dB power penalty after a single filter of only 68 % of the signal bandwidth. The same penalty is achieved when cascading 10 filters of 21.6 GHz

bandwidth. Additionally, the penalties associated to the introduction of fiber spans between filters are investigated.

A. Behind the research

Today, the existing optical transport infrastructure is mostly based on wavelength division multiplexing (WDM), meaning that each wavelength is used for setting a virtual point-to-point link to transmit data over the network. These WDM channels are mostly using the standard grid [ITU-T G.694.1] and featuring data rates up to 10 Gb/s and beyond. To improve the dynamicity and spectral efficiency while taking advantage of the intelligence inherent to the control plane of these networks, a flexible grid has been recently included in the ITU-T standard [ITU-T G.694.1]. One of its main features is that wavelength allocation and channel bandwidth will be variable, with bandwidth granularity of 12.5 GHz and nominal central frequency granularity of 6.25 GHz [ITU-T G.694.1]. So, low data rates (e.g. 10 Gb/s) will become highly affected when cascading these low bandwidth filters, bringing more destructive phenomena that significantly limits the maximum fiber distance, as it happens at higher data rates for the standard fixed grid [Pataca11].

In this scenario, one of the key enabling technologies for data plane will be the so-called optical orthogonal frequency division multiplexing (OFDM), thanks to its unique flexibility and scalability to high-speed transmission [Shieh10]. Among the existing optical OFDM techniques, those combining coherent detection with digital signal processing are the most promising to cope with the required flexibility while improving spectral efficiency. Furthermore, in these systems no electrical guard band is required, as it happens in intensity modulated with direct detection (IM/DD) optical OFDM systems. However, coherent optical OFDM systems still are quite sensitive to the system nonlinearities, related to the peak-to-average power ratio (PAPR) level of the signal [Jansen08a].

An interesting technique has been proposed to mitigate these non-linear effects by reducing the PAPR level of the OFDM transmitted signal [Thompson08]. Such a system has been ported to the optical domain: A discrete multi-tone (DMT) signal was modulated in the phase of the optical field (resulting in a PAPR of 0 dB) and further detected by means of an intradyne receiver with phase diversity [Huene11-Fabrega11]. Moreover, [Fabrega11] has demonstrated the feasibility of this system when obtaining the DMT signal using Hartley transform, with its inherent benefits on simplifying digital signal processing [Svaluto10].

In this paper, optical filtering effects are discussed for a phase modulated coherent optical OFDM system based on Hartley transform. As a small bandwidth granularity will be allowed in the new flexible grid, the cases studied are for a system featuring a standard data rate of 10 Gb/s, which occupies a total bandwidth of 10 GHz [Fabrega11]. Also, several cases are studied by means of numeric simulations. Optical filters are modeled as a low-pass equivalent Gaussian function, which has been shown to be a fair approximation for the transfer function associated to each channel [Roudas02]. Using this model, first a back-to-back (no fiber) case is investigated. Next the performance when placing fiber spans of several lengths between filters is assessed. Precisely, the cases for reaching a total transmission reach of 100 km are assessed, either using 10x10 km fiber spans or using 5x20 km fiber spans.

B. Transmission Scheme

The proposed model of transmission is shown in Fig. 5.20, where the OFDM signal is generated using pure optical phase modulation and Hartley transform. First, at the transmitter side, input data is parallelized and mapped into real binary phase shift keying (BPSK) symbols. A training symbol sequence is then inserted. OFDM modulation using inverse FHT (IFHT) and serialization are then performed, transferring the proper OFDM symbols to a digital-to-analog converter (DAC). Next, the resulting real OFDM signal is fed into the optoelectronic front-end. Here, the signal is optically phase modulated and adapted to be sent over the transmission link.
Three possible configurations are studied for the link. First, a back-to-back case for determining

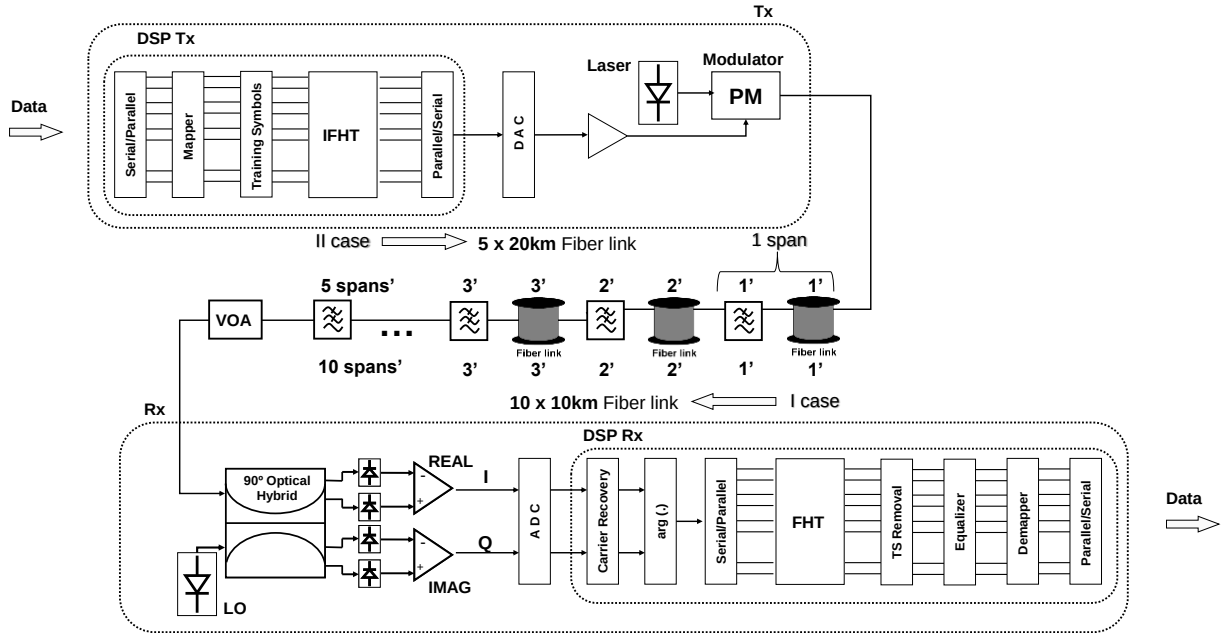

Figure 5.20. Schematic of the proposed transmission system.

the power penalty due to the concatenation of several optical filters. After that, the same penalty is studied but adding standard single mode fiber (SSMF) spans between the filters, searching for the effects of combining fiber and optical filter concatenation. Two cases are carried out, one with 10 spans of 10 km each, and another with 5 spans of 20 km.
At the receiver side, a 90º optical hybrid combines the received optical signal with the reference local oscillator (LO) and produces 4 different optical signals with 0º, 180º, 90º and 270º phase shifts respectively. These signals drive two pairs of photo-diodes (PD) acting as balanced detectors. Subsequently, the resulting I and Q outputs are digitized by analog-to-digital converter (ADC) and injected to digital signal processing (DSP) block. At DSP, first the carrier recovery and phase demodulation of the complex received signal are performed. The signal passing through the carrier recovery module compensated for mitigating phase and frequency errors. Next, the argument of the received signal for both I and Q components is extracted. Finally, the data are parallelized and OFDM demodulated using FHT. The training symbols are removed and equalization of the received signal is performed. Data is reconstructed by means of symbols demapping. Afterwards, serialization is executed.

C. *Filter Cascading Effect*

The performance of filter cascading has been evaluated by means of numeric simulations of the architecture shown in Fig. 5.20. All the simulations were performed using Matlab software. An input data stream operating at 10 Gb/s was created from a pseudorandom bit sequence (PRBS) of length 2^{15}-1. The resulting signal was mapped onto BPSK constellation and OFDM modulated to 64 carriers using the FHT. No cyclic prefix was used. The resulting signal was injected to the phase modulator with an amplitude featuring an standard deviation of $0.4V_{\pi}$. This value was found to be the optimum point after extensive numerical simulations. The laser driving the phase modulator was modeled as a standard continuous wave laser centered at 1550 nm, with output power of 0 dBm.

The transmission link was featured by a SSMF and the optical filters. A variable optical attenuator (VOA) was placed at the end of the line for sensitivity measurements. The transmission through SSMF was modeled using the split-step Fourier method (SSFM) [Agrawal07]. Fundamental fiber parameters used were attenuation of 0.2 dB/km, dispersion of 17 ps/nm·km and dispersion slope of 0.07 ps/nm·km^2. As the simulations were performed using low-pass equivalent models, the additional optical filters were emulated as low-pass gaussian filters [Roudas02]. The first analyzed configuration was without fiber link. Next, each one was placed after each fiber span, increasing the transmission distance until 100 km SSMF was reached. This was done using either spans of 10 km or spans of 20 km SSMF.

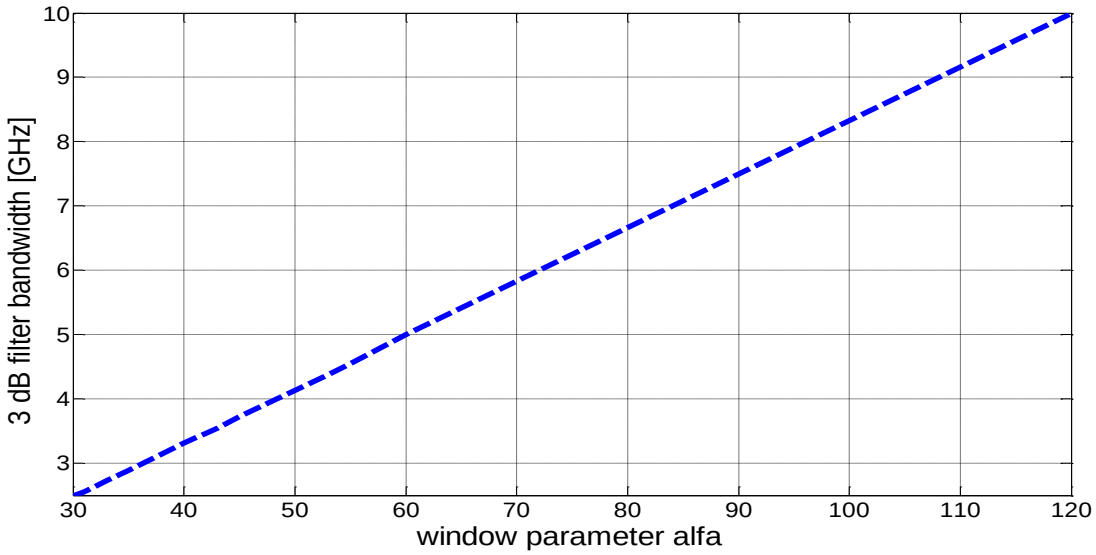

Figure 5.21. Low-pass gaussian filter with 3 dB filter bandwidth vs. window parameter α.

At the receiver, the local oscillator was also modeled as a continuous wave laser running at 1550 nm with output power of 1 mW, giving -6 dBm to each photo-detector after a 90º optical hybrid. The balanced photo-detectors were emulated as PIN diodes with responsivity of 0.7 A/W, impedance of 50 Ohm and dark current of 1 pA. After phase diversity detection, phase unwrapping and OFDM demodulation were performed. The final BER waterfall and sensitivity curves were estimated by counting the number of wrongly received bits. An enhanced forward error correction (FEC) was assumed. So, a target BER of 10^{-3} was established as a reference for all the simulations.

The optical filters were generated using a Gaussian window, which was further converted to a digital filter. Before the system analysis, the 3 dB filter bandwidth has been characterized as function of the gaussian window parameter α (defined as the reciprocal of the standard deviation). Results are shown in Fig. 5.21.
Precisely, in Fig. 5.21, 3dB bandwidths of the low-pass equivalent filters are plotted as function of α. As expected, this bandwidth ($3dB_{BW}$) behaves linearly with α:

$$3dB_{BW} = A \cdot \alpha \tag{5.4}$$

where, A stands for the slope of the function (0.833 GHz). Sample magnitude responses of filters at different α are plotted on Fig. 5.22.

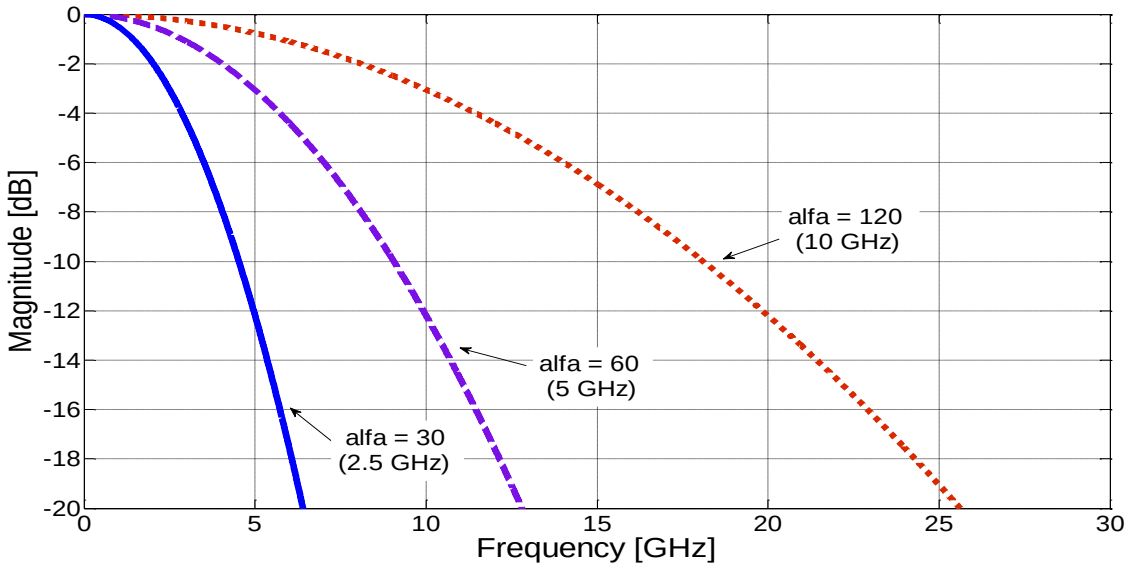

Figure 5.22. Magnitude response for α = 30, α = 60 and α = 120.

Next, the back-to-back configuration with only optical filters was simulated.
Hence, the fibers on Fig. 5.20 were not included. Gaussian optical filters, with equal bandwidth, were inserted one by one between transmitter and receiver. For each case, the total bandwidth of the filters was varied in the range of 5-33 GHz. Fig. (5.22-5.23) shows the results in terms of receiver sensitivity at 10^{-3} BER. This case was set as basis for further comparison when inserting the proposed fiber spans between the filters. The results with 10 km spans between filters are shown on Fig. 5.23 while Fig. 5.24 presents the curves corresponding to 20 km spans, both including the back-to-back results for comparison.

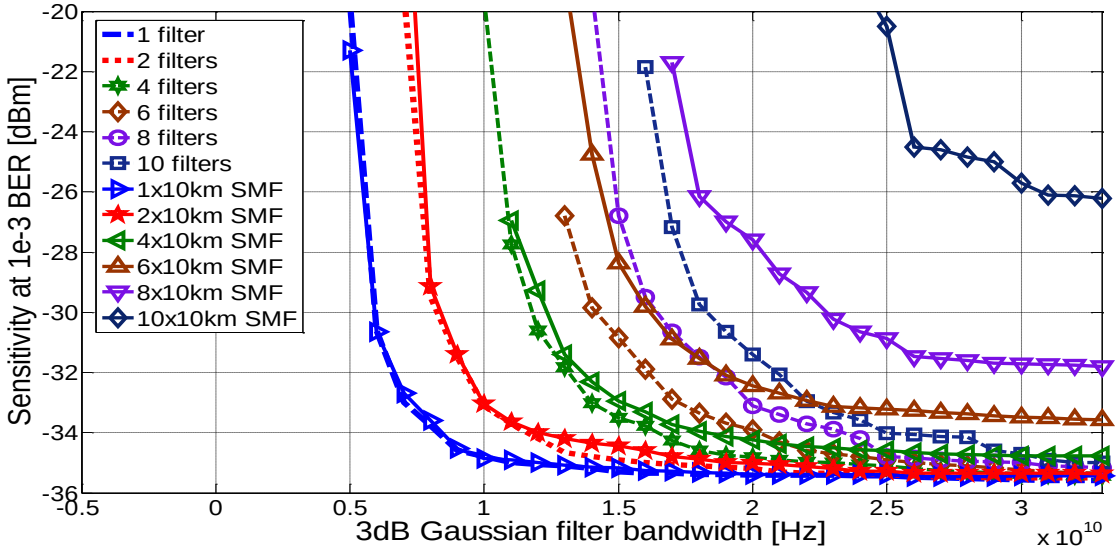

Figure 5.23. Filter concatenation w/o SSMF spans and based on 10 spans with 10km of SSMF each.

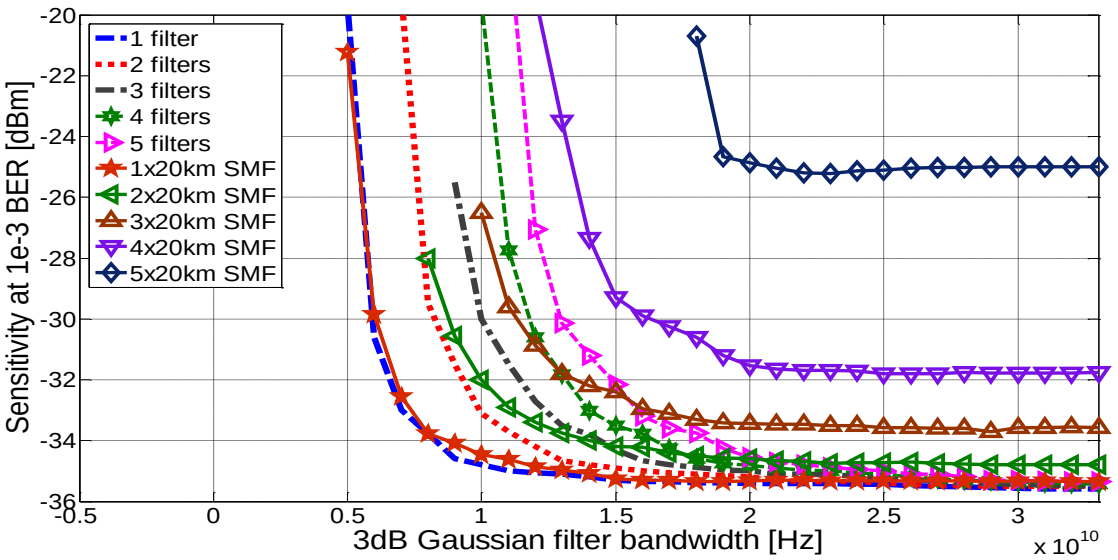

Figure 5.24. Filter concatenation w/o SSMF spans and based on 5 spans with 20km of SSMF each.

The 1 dB and 3 dB power penalties at BER 10^{-3} have been computed and are shown in Table 5.9 below.

filters	**1**		**2**		**3**		**4**		**5**	
penalty[dB]	1	3	1	3	1	3	1	3	1	3
b-to-b*	9	6.8	12.8	9.6	15.8	11.8	18	13.6	20.4	15.4
10kmSSMF*	9.2	6.8	16	9.8	17.2	12.2	25	14.4		17.3
20kmSSMF*	10.8	7	20	10.6		15.4				

filters	**6**		**7**		**8**		**9**		**10**	
penalty[dB]	1	3	1	3	1	3	1	3	1	3
b-to-b*	22	16.6	24	18.4	24.6	19.4	27.2	20.6	29	21.6
10kmSSMF*		20.6		26						
20kmSSMF*										

(*) filter bandwidths for b-to-b, 10km and 20km span are given in [GHz], painted boxes stand for non-captured values.

Table 5.9. Filter bandwidths in [GHz] at 1dB and 3dB power penalties at 10^{-3} BER for different cases tested.

Analyzing the values collected for the back-to-back case, The bandwidth for 1 dB penalty ranges from 9 GHz to 29 GHz bandwidth corresponding to the cases of 1 filter and 10 filters respectively. For the same scenario, the 3 dB penalty is obtained for bandwidths from 6.8 GHz to 21.6 GHz, also corresponding to the cases of 1 filter and 10 concatenated filters respectively.
Regarding the case of inserting a 10 km span of SSMF between filters, the minimum bandwidth needed for 1 dB penalty ranges from 9.2 GHz (after 1 filter) up to 25 GHz (after 4 filters). For that case, a 3 dB power penalty is obtained for 6.8 GHz with 1 filter up to 26 GHz with 7 filters. Beyond that number of filters, the obtained penalty was higher than 3 dB.
Finally, when introducing spans of 20 km of SSMF, the bandwidth needed for 1 dB penalty varies from 11 GHz after 1 filter to 20 GHz after 2 concatenated filters. A 3 dB penalty is obtained at bandwidths of 7 GHz (1 filter) and 15.4 GHz (3 filters). For a number of filters greater than 3, the power penalty was higher than 3 dB.
So, for the system proposed, the penalty introduced by the optical filters is non-negligible and strongly depends on the lengths of fiber spans introduced between them.
In case that standard 12.5 GHz filters are used, 1 dB sensitivity penalty can only be reached after 1 filter for all three scenarios. So, the cascade of two filters is not possible. Also for 12.5 GHz bandwidth filters, the maximum number of filters cascaded for obtaining a 3 dB penalty is 3 for the back-to-back and when using spans of 10 km, and 2 filters when employing spans of 20 km.
When standard 25 GHz filters are used, for 1 dB power penalty, a maximum of 8 filters can be introduced in a back-to-back system, 4 filters when considering 10 km spans, and 2 filters with 20 km spans. For the 3 dB penalty, 10 filters can be cascaded in back-to-back, 6 filters for inserting 10 km spans, and 3 filters for 20 km spans.

5.2.2 Metro/Regional National Network

At this subsection, for an application in metro/regional network, a reduced-complexity CO-OFDM transceiver is proposed for upgrading the existing core network infrastructure while enabling elastic functionalities. A potential deployment within the Telefónica I+D national network model is then briefly evaluated by means of numerical simulations stated below.

A. Behind the research

Today, the existing optical transport infrastructure is mostly based on dense wavelength division multiplexing (DWDM), meaning that each wavelength is used for setting a virtual point-to-point link to transmit data over the network using a standard grid [ITU-T G.694.1]. Nevertheless, this approach is inefficient when assigning wavelengths to a low rate signal that does not fill the entire channel. Furthermore, transmission systems under investigation target data rates beyond 100Gb/s, whose spectrum occupancy does not fit well into the standard grid. In order to overcome these problems, the spectrum-sliced elastic optical path network (SLICE) architecture [Jinno10] proposes to partition the optical spectrum into finer (e.g. 12.5 GHz) fixed-size slices and to adaptively allocate a number of contiguous slices to variable bit rate connections.
In this scenario, one promising technology for the data plane is the coherent optical orthogonal frequency division multiplex (CO-OFDM) based on digital signal processing (DSP), because of its unique flexibility, baud rate scalability and sub-GHz granularity [Shieh10]. Additionally, as CO-OFDM systems rely on strong DSP, it is easy to equalize and mitigate the channel impairments. This means that the external plant of a specific deployment can be simplified, as no inline compensation is needed.
However, one of CO-OFDM drawbacks is the sensitivity to the phase noise related to the optical sources, whose effects are mitigated by means of employing low linewidth lasers in combination with pilot tones and enhanced DSP [Shieh10].

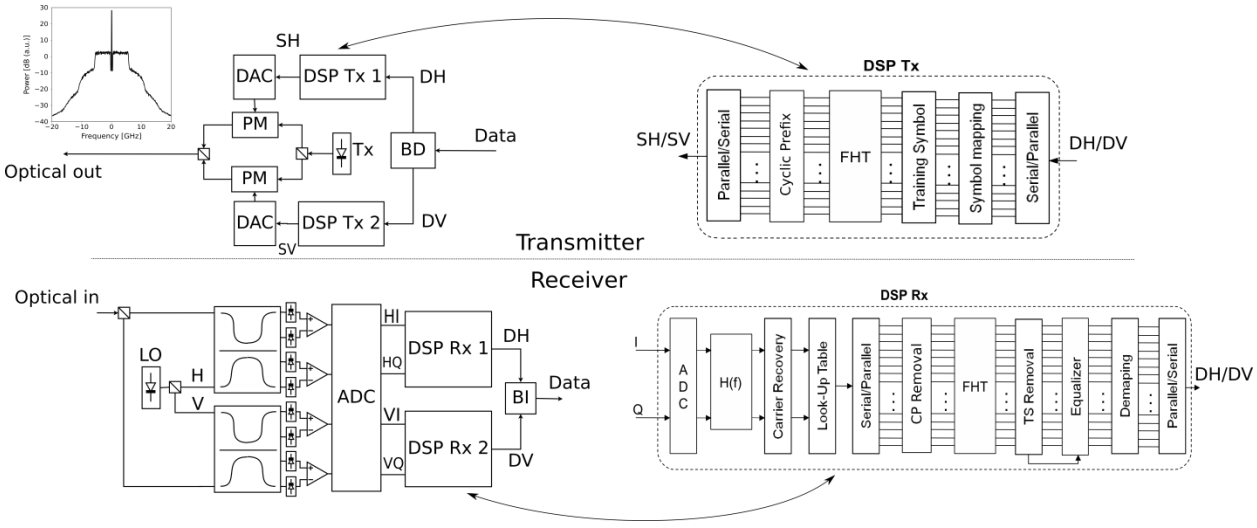

Figure 5.25. Transceiver scheme: transmitter, receiver and the corresponding DSP blocks. BI: bit interleave; BD: bit deinterleave.

Also, their high Peak-to-Average Power Ratio (PAPR) is a critical parameter [Jansen08a], reducing the tolerance to the system non-linearities.
Constant envelope optical OFDM has been proposed [Huene11, FabregaMCh13a, FabregaMCh13b] for significantly reducing the PAPR. Moreover, in these systems the optical phase noise turns to be additive (instead of multiplicative) to the baseband OFDM signal recovered, and its effects can be mitigated by suppressing the central subcarriers and without any specific digital processing [Huene11, FabregaMCh13a, FabregaMCh13b].
In this paper, a constant envelope CO-OFDM transceiver is proposed for upgrading the existing core network infrastructure. Its operation using polarization multiplexing (PolMux) is investigated. Also, its performance is evaluated by means of numerical simulations for a potential deployment within the Telefónica I+D national network model. Compared with existing fixed grid technologies, it shows reduced bandwidth occupancy and low OSNR requirements while avoiding the need for inline dispersion compensation.

B. Transceiver design

The proposed transceiver scheme is shown in Fig. 5.25, where details of the DSP blocks are depicted in the corresponding insets. The idea behind is to allow a robust transmission, featuring simple signal processing. PolMux is used for doubling the spectral efficiency. So, two different streams (DH, DV) can be transmitted at orthogonal states of polarization (SOP).
At the DSP blocks of the transmitter, each stream of data is first parallelized and mapped into a Binary Phase Shift Keying (BPSK) constellation, then a training symbol sequence (TS) is inserted. Next, the resulting symbols are OFDM modulated using the fast Hartley transform (FHT), which is equal to its inverse. Subsequently, the cyclic prefix (CP) is inserted and the obtained real-valued OFDM symbols are serialized. Finally, the digital signal is converted into the analog domain by a digital-to-analog converter (DAC), injected into a phase modulator (PM), and transmitted.
At the receiver side, a polarization diversity receiver is proposed. There, the local oscillator (LO) is linearly polarized at +45º and decomposed by a polarization beam splitter (PBS), while optical data signal is, in turn, splitted by passing through another PBS. Each of the outputs (H, V) are coupled with the corresponding LO signal in a 90º optical hybrid, driving two pairs of photo-diodes acting as balanced detectors. Next, the resulting In-phase (I) and Quadrature (Q) outputs for each orthogonal SOP are digitized by an analog-to-digital converter (ADC). At the DSP block of the receiver, the signal first passes through a digital filter H(f) which compensates for the chromatic dispersion [Savory08] and a carrier recovery block (for compensating phase and frequency errors). Note that in case of operating in PolMux an additional digital filter should be included at this point [Savory08]. The argument of the complex received signal recovered from the I and Q components is afterwards extracted. Then, CP is removed, the FHT is carried out, the training symbols are conveniently extracted, and equalization is performed. Finally, data are detected after demapping and serialization. Note that due to the nature of the transmitted signal (inset Fig. 5.25), a self-coherent detection is also possible.

C. Simulations and results

The performance of the proposed transceiver is assessed by means of numerical simulations using Matlab software. A data set of 2^{17} pseudo-random bits per polarization is generated using a sequence of 2^{15}-1. The target data rate is variable, according to the network demands. For each case, a total overhead of 38.2 % is considered. The resulting bit sequence is parallelized, BPSK

encoded and OFDM modulated using the FHT with 64 carriers. Up to 5 subcarriers are set to zero, for reducing the phase noise impact [FabregaMCh13], resulting in a 7.8% overhead, already taken into account. 16 training symbols are inserted every 2048 OFDM symbols for equalization, ensuing in a 0.8% of associated overhead. The resulting signal is injected to the phase modulator, excited by a continuous wave (CW) laser of 1 MHz linewidth running at 1550 nm. The modulation amplitude is varied until the standard deviation of the optical phase is set to the optimum of 0.36π [FabregaMCh13a]. The output power of the transmitter is set to 0dBm.
At the receiver, the LO is also modeled as a CW laser at 1550 nm, giving 0 dBm to each photodetector after the PBS and the 90º hybrid. The power of the received signal at each photodetector is of -6 dBm. The photodetectors are modeled as PIN diodes with responsivity of 0.7 A/W, dark current of 1 pA and thermal noise of 11.51 $pA/\sqrt{Hz}$. OFDM decoding and demodulation are done after intradyne detection.
The output parameter measured is the statistical counting of received bits, providing a measure of the system bit error ratio (BER). A target BER of $2\cdot10^{-2}$ is considered, as a soft decision FEC [Onohara11] can be used for a 20 % overhead, already taken into account in the total overhead.
First, a back-to-back evaluation is performed at different net data rates. Results are shown in Fig. 5.26. There it is shown that for the targeted BER, the OSNR requirement at 100 Gb/s is of 11 dB, 2.3 dB below the requirement of the 100 G PolMux-QPSK format, which is 13.3 dB [Nolle11].

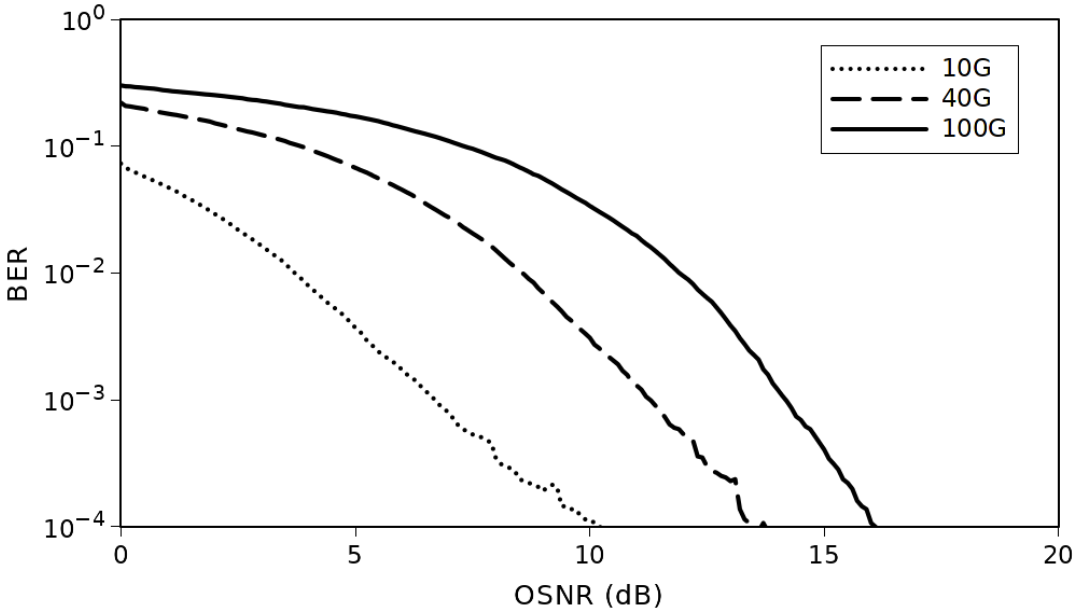

Figure 5.26. Back to back OSNR performance.

Afterwards, the performance for 56 different traffic demands is tested for the 30-node Telefónica I+D reference network for the spanish core (shown in Fig. 5.27a). These demands ask connections between two different nodes of the network and at different net data rates, ranging from 337.4 Mb/s up to 76.04 Gb/s. This is shown in Fig. 5.27b, dotted line, where the net data rate is plotted against the demand ID.

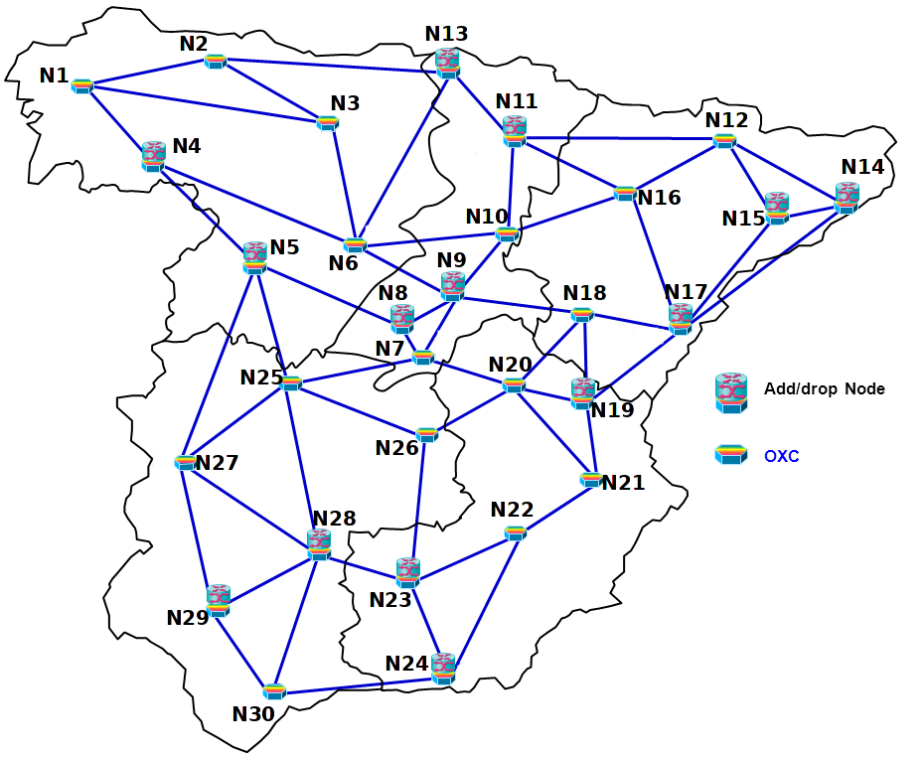

Figure 5.27a. National Spanish Network scheme deployed by Telefonica I+D.

First, the shortest path for each traffic demand is calculated, giving different path lengths (and number of hops), as shown in Fig. 5.27c, dotted line. There it can be seen that the distances range from 143 km up to 877 km. The number of hops depends on the specific traffic demand, with a maximum of 6.

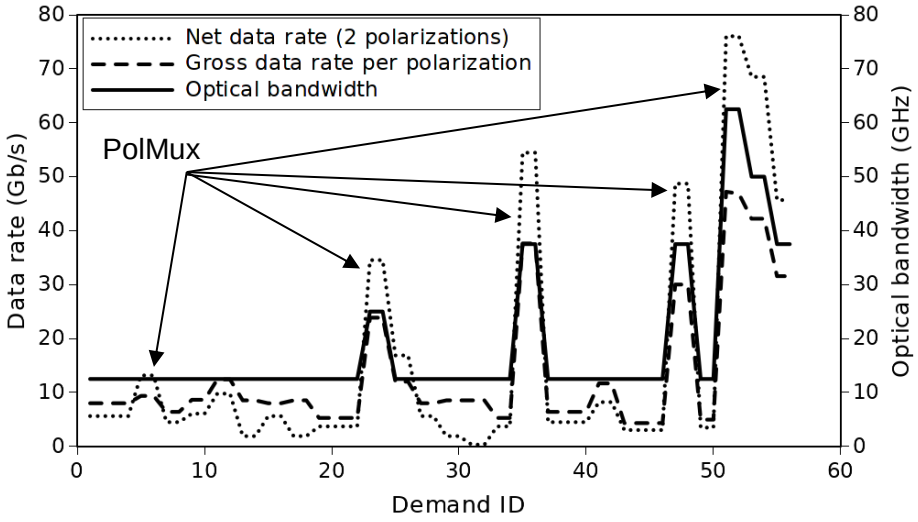

Figure 5.27b. Optical bandwidth use and data rate in the function of traffic demand.

The transmission links include standard single mode fiber (SSMF) and erbium doped fiber amplifiers (EDFAs) for compensating the transmission losses. The split-step Fourier method is

used to model the propagation through the SSMF. The fiber model has an effective area of 80 μm^2, nonlinear coefficient of $2.4 \cdot 10^{-20}$ m^2/W, dispersion of 16.5 ps/(km·nm), dispersion slope of 0.057 ps/(km·nm^2), and average loss of 0.29 dB/km. EDFAs locations are selected following common operator practices and modeled as standard amplifiers with constant output power per channel.

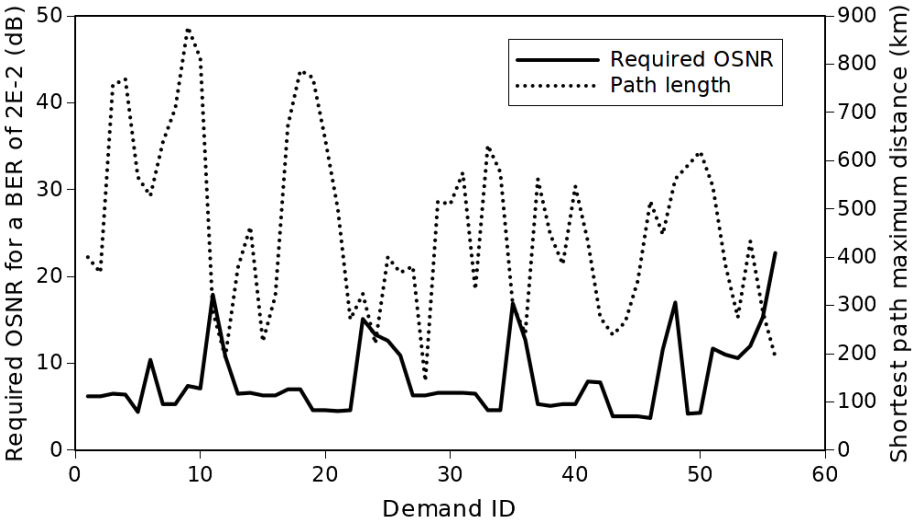

Figure 5.27c. OSNR required and distance for each traffic demand.

To emulate the filtering effects, a single optical filter is considered per node, modeled as a Gaussian filter of 3rd order with effective bandwidth of 86 % of the nominal value.
Results of the transmission simulations are shown in Fig. 5.27b-c in terms of required OSNR and optical bandwidth. Fig. 5.27b shows that the 78.6 % (44 out of 56) asks only for 12.5 GHz, while the maximum bandwidth (62.5 GHz) is required only for 2 traffic demands (51, 52). As the majority of the traffic demands are asking medium/low net data rates, simple phase modulation is used instead of PolMux. This is achieved by only using one of the branches of the transmitter depicted in Fig. 5.25.

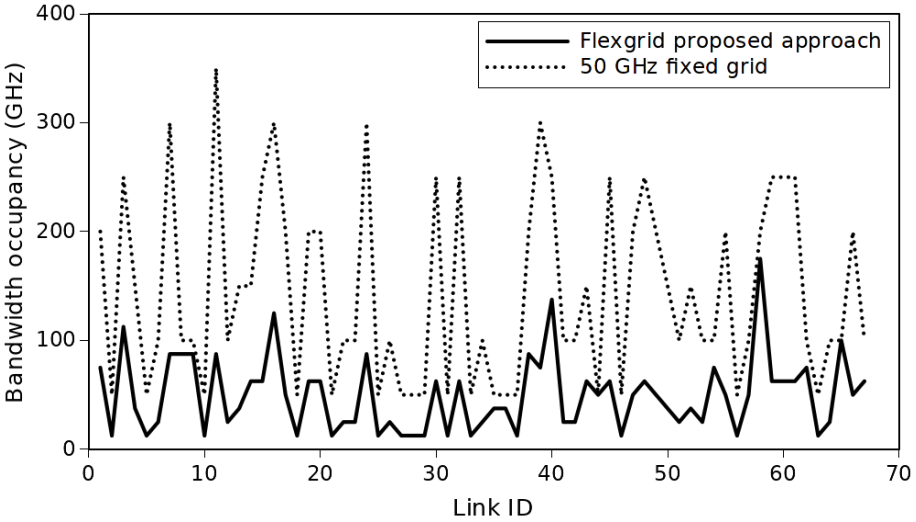

Figure 5.28. Bandwidth occupancy per link for flex and fixed grid of 50 GHz.

Only for a selected set of demands (5, 6, 23-26, 47, 48, 51-56) the transceivers are set to operate in PolMux, when there is a need for optimizing their optical bandwidth.
Fig. 5.27c shows the required OSNR at $2 \cdot 10^{-2}$ BER. The average required OSNR is 8.1 dB, with a maximum of 22.7 dB, necessary only by demand 56.
After the path transmission evaluation, the bandwidth occupancy per link is assessed and compared to a fixed grid of 50 GHz. Results are shown in Fig. 4.28 above.
There it can be observed that the average bandwidth occupancy is of 144 GHz for the fixed grid, while for the elastic approach is of 49.6 GHz, giving a reduction of 65.5 %.

5.3 Chapter Summary

At this chapter, the use cases applicable to access networks and optical transport networks were clearly investigated. The investigation through those applications was performed using Matlab environment. The following conclusions have been drawn.
First, the use cases for access networks were studied.
In case of full-duplex transmission, the feasibility of a colorless bidirectional 10 G/10 G PON, reusing downstream signal for upstream transmission, has been investigated. Upstream has been achieved saturating an RSOA and using it to modulate the optical phase with a DMT signal using low overhead (11.3 %). Coherent reception was used at the CO side, reusing the downstream laser source. After characterizing and including the bandwidth-limiting effects of the RSOA packaging parasitics, the phase noise tolerance has been evaluated, showing a power penalty of 1 dB at 6.4 MHz linewidth, at the expense of increasing overhead. For the 11.3 % overhead proposed, 1 MHz could be tolerated with less than 0.3 dB penalty.
The sensitivity performance in front of downstream back-reflections has been also investigated, obtaining 1 dB sensitivity penalty at 10^{-3} BER for only 9.5 dB OSRR.
Sensitivities reported implied power budgets of up to 30.4 dB after 50 km, matching clearly the typical values of PON deployments. Furthermore, the OSNR required at the output of the RSOA was found to be 17.7 dB after 50 km. As commercial RSOAs could achieve noise figures of up to 10~dB, the proposed system required a downstream signal of 27.7 dB OSNR that was easy to achieve in a non-amplified PON.
Next, the decomposed RAN over deployed PON infrastructure was discussed. WDM was used, assigning exclusive wavelengths per RRM–RRU pair. In order to cope with that, coherent optical OFDM technology was proposed. Thanks to it, the losses introduced in the path of the deployed infrastructure were reduced to the range of 0.04 – 3 dB and the decomposed RAN could be massively deployed in urban environments while ensuring compatibility with standard PONs. Furthermore, the case of a practical implementation has been analyzed by means of numerical simulations. Results showed that for TDM-PON path losses of only 0.96 dB, a maximum of 145 metro cells could be served at the same time, together with the PON customers and within a 24 km reach. Alternatively, 48 macro cells could be supported within the same reach.
Analysing the use cases for optical transport networks featured by long-haul, two cases were investigated. The first case concerned a flexible metropolitan area network of up to 100 km, on which the traffic is aggregated and dropped by means of WDM. The second case was about an elastic upgrade of the existing Telefonica model of the Spanish national core network applying novel polarization multiplexing constant envelope coherent OFDM transceiver.
Hence, regarding the first case for long-haul, optical filtering effects for the proposed optical CE-OFDM have been investigated. The considered cases were for a system featuring a standard data

rate of 10 Gb/s, which occupied a total bandwidth of 10 GHz. Filter cascading effect was studied by means of numeric simulations. First a back-to-back case was assessed, showing a 3 dB sensitivity penalty after a single filter of only 6.8 GHz (68 % of the signal bandwidth). For this case, 10 filters of bandwidth 21.6 GHz could be cascaded for a 3 dB penalty. The cases including fiber spans between filters were also analyzed for distances up to 100 km. Precisely, inserting 10 km spans, a maximum of 7 filters (with 26 GHz bandwidth) could be cascaded for a 3 dB power penalty. When inserting 20 km spans, the 3 dB penalty point has been found after 3 filters of 15.4 GHz.

Another relevant study for long-haul was an elastic upgrade for Spanish national core network equipped with a novel transceiver. At this case, a PolMux bandwidth/bitrate variable constant envelope CO-OFDM transceiver has been investigated as a solution for upgrading existing transport networks. Its performance has been evaluated by means of numerical simulations for a potential deployment within the 30-node Telefónica I+D national network model, with traffic demands of up to 76.04 Gb/s and coping with distances up to 877 km. Results showed an average OSNR requirement of 8.1 dB, and an average bandwidth occupancy reduction of 65.5 % per link respect to the 50 GHz fixed grid.

CHAPTER 6: CONCLUSIONS AND FUTURE WORK

In this chapter, the conclusions together with future plans for investigation in the research initiated by the thesis are given.

6.1 Conclusions

The idea of the PhD thesis was to find a technique to meet the requirements and cover the challenges opened by the extensive deployment of optical networks during last decade. Nowadays, the huge growth of demand for bandwidth along with continuous increase of data rate up to 100 Gb/s and beyond are to be coped by the next generation transmission systems. A solution is a system that is able to deal with such high rate, mitigate the optical impairments accumulated along the propagation link and guarantee the same level of high efficiency across long distances.

The constant-envelope optical OFDM system proposed and investigated in this thesis came up as a great novel approach that fully satisfies those needs for future optical networks. The technique is implemented by means of an optical phase modulator and non-complex DSP based on the Hartley transform. It significantly reduces the PAPR of the transmitted signal and, thus, nonlinear distortions are expected to affect less the system performance.

In the present thesis, 5 chapters were presented to cover the description and principles of the system itself, as well as its theoretical and numerical characterization along with several use cases. These ones where targeting a broad range of applications, from access to core networking, including the metro/aggregation segment.

Initially, the motivation, the state of the art, objectives and structure of the thesis were provided. Next, in chapter 3, a detailed explanation of the proposed optical CE-OFDM was given.
The mentioned explanation is based on the principle of operation and general description of the system, which is composed of the following basic elements: transmitter DSP, optoelectronic up-conversion front end, a phase diversity receiver and receiver DSP.

Next, in chapter 4, the theoretical and numerical characterization of the CE-OFDM system is performed. In fact, the impact of modulator driving in terms of additive noises associated to receiver sensitivity and optical amplification was discussed. Both models supported from the thermal noise analysis in case of sensitivity performance and ASE noise analysis in case of optical amplification noise performance. Additionally, the impact of the phase noise, frequency offset and IQ imbalance was studied. For all of those, system performances and the relation between the sensitivity and the standard deviation of the transmitted phase were investigated. The results provided a great contribution for an optical modulator, establishing the range of optimal driving voltage. Moreover, a baseband filtering was proposed in order to carry out the phase and carrier recovery and as a great alternative replacing the common moving average

filters. Additionally, supporting the cyclic prefix designed to mitigate the dispersion impact, a digital filter to combat dispersion turned out an especially important to deal with this distortion.

Afterwards, in chapter 5, the proposed optical CE-OFDM system was applied to different configurations ranging from access to long-haul. In case of applications for access, the system was initially employed for radio access network signals delivery by means of WDM overlay in deployed passive optical architecture. A decomposed radio access network was demonstrated giving a low cross talk between radio service delivery signals and fixed access clients. Furthermore, a narrow channel spacing was exhibited.
Next, full-duplex 10 Gb/s bidirectional transmission over a single wavelength with RSOA based ONU was demonstrated. Upstream transmission was originally featured by proposed CE-OFDM system, however downstream transmission was based on IM/DD. The reported sensitivity performances showed that a power budget matched the PON standards and an OSNR was easy to achieve in a non-amplified PON.
Considering applications for the metro-core, first a flexible metropolitan area networks of up to 100 km with traffic add/drop using WDM was examined. The filters concatenation revealed the narrowing effects of optical filters. Finally, an elastic upgrade of the existing Spanish national core network was proposed. The mentioned elastic upgrade featured a novel transceiver based on CE-OFDM configuration with polarization multiplexing. Furthermore, a flexible grid in respect to the existing ITU fixed grid was investigated in order to reduce bandwidth occupancy.

6.2 Future Work

At this section, a future work in respect to the proposed fully optical CE-OFDM system is explained in the following order,

- Polarization mismatch between local oscillator and received signal. As was implied, the local oscillator and the received signal are assumed to have the same state of polarization. Otherwise, a proper mixing in the 90º hybrid would not be possible. Thus, it would be desirable to have an idea of the impact of this mismatch.

- Residual amplitude modulation. For the specific case of using alternative devices to perform the phase modulation, some of them (e.g. DFB lasers) are expected to have a residual amplitude modulation together with the phase modulation. Controlling and evaluating the impact of this residual modulation will be important because it can cause an additional penalty when transmitting over fiber (e.g. increased dispersion penalty).

- Polarization mode dispersion effects. For long haul distances, one of the major problems is the so-called polarization mode dispersion, which is a dispersive effect due to the random variation of the fiber birefringence properties [Kaminow97]. Moreover, it is expected to have a high impact not only because of its effects on the optical phase and amplitude, but also due to its effects on the state of polarization of the signal. So it is proposed to characterize such an impact and search alternatives for compensating it.

- Fiber nonlinearities. The objective will be to investigate those which are critical to coherent systems: nonlinear phase noise induced by self phase modulation and cross phase modulation [Ho05, Kikuchi10].

BIBLIOGRAPHY

[3GPP TR 25.912] 3GPP TR 25.912: Feasibility Study for Evolved Universal Terrestrial Radio

[Abramowitz] M. Abramowitz et. al, "Inverse Circular Functions in Handbook of Mathematical Functions with Formulas, Graphs, and Mathematical Tables," *Dover*, pp. 79-83, 1972

Access (UTRA) and Universal Terrestrial Radio Access Network (UTRAN), V8.0, 2008

[Adhikari] S. Adhikari et. al, "Experimental investigation of self coherent optical OFDM systems using Fabry-Perot filters for carrier extraction," *ECOC*, 2010

[AnaDevweb] http://www.analog.com/static/imported-files/tech_docs/dsp_book_Ch15.pdf

[Agrawal02] G.P Agrawal, "Fiber Optic Communication Systems," *John Wiley & Sons*, 2002

[Agrawal07] G.P Agrawal, "Non-linear Fiber Optics," *Oxford: Elsevier*, 2007

[Armstrong06] J. Armstrong et. al, "Power efficient optical OFDM," *Electronics Letters*, 2006

[Armstrong06a] J. Armstrong et. al, "Performance of Asymmetrically Clipped Optical OFDM in AWGN for an Intensity Modulated Direct Detection System," *IEEE Global Telecomm.*, 2006

[Armstrong08] J. Armstrong et. al, "Comparison of asymmetrically clipped optical OFDM and DC-biased optical OFDM in AWGN," *IEEE Communications Letters*, 2008

[Armstrong09] J. Armstrong, "OFDM for Optical Communications," *Journal of Lightwave Technology*, February 2009

[Barros10] D.J.F. Barros et. al, "Comparison of orthogonal frequency-division multiplexing and on-off keying in amplified direct-detection single-mode fiber systems," *Journal of Lightwave Technology*, vol. 28, no. 12, June 2010

[Barry03] J.R. Barry et. al, "Digital Communications," *Springer*, pp. 727–736, 2003

[BBrown94] B. Brown, "Designing photodiode amplifier circuits with OPA128," *Burr Brown Corporation*, January 1994

[Benyuan10] Z. Benyuan et. al, "Ultra-Long-Haul Transmission of 1.2-Tb/s Multicarrier No-Guard-Interval CO-OFDM Superchannel Using Ultra-Large-Area Fiber," *Photonics Technology Letters*, vol. 22, no. 11, pp. 826-828, June 2010

[Berkleyweb] http://ptolemy.eecs.berkeley.edu/eecs20/week12/freqResponseRA.html

[Binh10] L.N. Binh "Optical Fiber Communications Systems," *CRC Press*, 2010

[Bracewell83] R.N. Bracewell, "Discrete Hartley transform," *OSA Letters*, 1983

[Bracewell00] R. N. Bracewell, "The Fourier Transform and Its Applications," *McGraw-Hill*, 2000

[Buchali09] F. Buchali et. al, "Optical OFDM: a promising high speed optical transport technology," *Bell Labs Technical Journal*, January 2009

[Bulakci08] O. Bulakci et. al, "Reduced complexity precoding based peak-to-average power ratio reduction applied to optical direct-detection OFDM," *ECOC*, September 2008

[Bulakci09] O. Bulakci et. al, "Wavelet transform based optical OFDM," *OFC/NFOEC*, February 2009

[Buus06] J. Buus and E. Murphy, "Tunable lasers in optical networks," *J. Lightwave Technol.*, vol. 24, no. 1, pp. 5–11, January 2006

[Caballero12] A. Caballero, et. al, "High-Capacity 60 GHz and 75–110 GHz Band Links Employing All-Optical OFDM Generation and Digital Coherent Detection," *Journal of Lightwave Technology*, vol. 30, no. 1, pp. 147-155, January 2012

[Cai12] A. Caballero, et. al, "High-Capacity 60 GHz and 75–110 GHz Band Links Employing All-Optical OFDM Generation and Digital Coherent Detection," *Photonics Technology Letters*, vol. 24, no. 19, pp. 1704-1707, October 2012

[Cao12] Z. Cao et. al, "A Synchronized Signaling Insertion and Detection Scheme for Reconfigurable Optical OFDM Access Networks," *Journal of Lightwave Technology*, vol. 30, no. 24, pp. 3972–3979, Dec. 2012

[Cartaxo11] A. Cartaxo, et. al, "A perspective on optical-wireless converged NG-FTTH networks using directly modulated lasers," in Proc. Int. Conf. Transparent Optical Networks *ICTON 2011*, paper Mo.B4.3, 2011

[Casas91] E.F. Casas et. al, "OFDM for data communications over mobile radio FM channels-part I: analysis and experimental results," *IEEE Trans. Communications*, May 1991

[Cincotti12] G. Cincotti et. al, "Coherent optical OFDM systems based on the fractional Fourier transform," in Proc. Int. Conf. Transparent Optical Networks *ICTON 2012*, July 2012

[Cisco11] Cisco, "Global mobile data traffic forecast update, 2011–2016," *Cisco Visual Networking Index*, 2011

[Ciscoweb] http://www.ciscopress.com/articles/index.asp?st=42081

[Clausen12] D. Clausen et. al, "Experimental Investigation of Bit and Power Loading in 10 Gbit/s Next Generation Optical OFDM Access Networks," in Proc. *17th International OFDM Workshop 2012*, August 2012

[Chandrasekhar09] S. Chandrasekhar et. al, "Transmission of a 1.2-Tb/s 24-Carrier No-Guard-Interval Coherent OFDM Superchannel over 7200-km of Ultra-Large-Area Fiber," *ECOC*, September 2009

[Chen07] C. Chen et. al, "Characterization of parasitics in to-packaged high-speed laser modules," *Advanced Packaging, IEEE Transactions on*, vol. 30, no. 1, pp. 97 –103, Feb. 2007

[Cho11] K. Y. Cho et.al, "Long-Reach Coherent WDM PON Employing Self-Polarization-Stabilization Technique," *Journal of Lightwave Technology*, vol. 29, no. 4, pp. 456–462, Feb. 2011

[Chochol12] M. Chochol et. al, "Characterization of a phase modulated coherent optical OFDM system based on Hartley transform," in Proc. of *17th European Conference on Networks and Optical Communications (NOC) 2012*, pp. 1 –5, June 2012

[Chochol12a] M. Chochol et. al, "Optical Filter Cascading Effects in a Phase Modulated Coherent Optical OFDM Transmission System Based on Hartley transform," In Proc. International Conference on Transparent Optical Networks *ICTON 2012*, Coventry, UK, paper Tu.P.3, June 2012

[Chochol12b] M. Chochol et. al, " Characterization and design of coherent optical OFDM transmission systems based on Hartley Transform," in Proc. of *Barcelona Forum on Ph.D. Research in Information and Communication Technologies*, 16 October 2012

[Chow08] C.W. Chow et. al, "Demonstration of high spectral efficient OFDM-QAM long reach passive optical network," *ECOC*, September 2008

[Chow10] C.W. Chow et. al, "Studies of OFDM signal for broadband optical access networks," *IEEE Journal On Selected Areas In Communications*, August 2010

[CPRI11] Common Public Radio Interface (CPRI), Interface Specification V5.0, 2011

[Cvijetic12] N. Cvijetic et. al, "OFDM for Next-Generation Optical Access Networks," *Journal of Lightwave Technology*, vol. 30, no. 4, pp. 384–398, Feb. 2012

[Davenport58] W. B. Davenport et. al, "An Introduction to the Theory of Random Signals and Noise," *John Wiley & Sons*, 1958

[Dischler09] R. Dischler et. al, "Transmission of 1.2 Tb/s continuous waveband PDM-OFDM-FDM signal with spectral efficiency of 3.3 bit/s/Hz over 400 km of SSMF," *the Optical Fiber Communication Conference*, San Diego, CA, paper PDP C2, 2009

[Domash02] L. Domash et. al, "Tunable thin-film filters based on thermo-optic semiconductor films," *Proc. SPIE*, vol. 4833, pp. 685–695, 2002

[Du12] L.B. Du et. al, "604-Gb/s coherent optical OFDM over 800 km of S-SMF with mid-span spectral inversion," *Opto-Electronics and Communications Conference (OECC)*, July 2012

[DSCR401HG] DSCR401HG: PIN Diode Datasheet, Discovery Semiconductor, 2011

[Fabrega10] J.M. Fabrega et. al, "Digital Phase Estimation Method Based on Karhunen-Loève Series Expansion for Coherent Phase Diversity Detection," *OFC/NFOEC*, March 2010

[Fabrega11qe] J. M. Fàbrega et. al, "Modulated grating Y-structure tunable laser for λ-routed networks and optical access," *IEEE J. Sel. Top. Quantum Electronics*, vol. 17, no. 6, pp. 1542–1551, Nov. 2011

[Fabrega11] J.M. Fabrega et. al, "Constant Envelope Coherent Optical OFDM Based on Fast Hartley Transform," In Proc. International Conference on Transparent Optical Networks *ICTON 2011*, Stockholm, Sweden, paper We.A1.6, July 2011

[FabregaMCh13a] J.M. Fabrega et. al, "Impact of Modulator Driving on Constant Envelope Optical OFDM based on Hartley Transform," *Photonics Technology Letters*, vol. 21, no. 5, pp. 5481-5486, 2013

[FabregaMCh13b] J.M. Fabrega et. al, "Decomposed Radio Access Network Over Deployed Passive Optical Networks Using Coherent Optical OFDM Transceivers," *Journal of Optical Communications and Networking*, vol. 5, no. 4, pp. 359-369, 2013

[FabregaMCh13c] J.M. Fabrega et. al, "Elastic Update of Transport Network with PolMux Constant Envelope Coherent Optical OFDM Transceivers," *in ECOC*, 2013

[Fyath11] R.S Fyath et. al, "Investigation of I/Q imbalance in coherent optical OFDM system," *WASET*, 2011

[Geng05] J. Geng, "Narrow Linewidth Fiber Laser for 100-km Optical Frequency Domain Reflectometry," *IEEE Photonics Technology Letters*, vol. 17, no. 9, September 2005

[Gerstel12] O. Gerstel, "Elastic Optical Networking: A New Dawn for the Optical Layer?," *IEEE Communications Magazine*, pp. 12-20, February 2012

[Ghanbarisabagh10] M. Ghanbarisabagh et. al, "Performance Analysis of Decision Feedback Time-Domain Equalizer for 20.48 Gb/s Direct-Detection Optical OFDM Transmission over 2560 km of SMF," *IEEE ICP-2010*, May 2010

[Giacoumidis12] E. Giacoumidis et. al, "100 Gb/s Coherent Optical Polarization Multiplexed Multi-Band-OFDM (MB-OFDM) Transmission for Long-Haul Applications," In Proc. International Conference on Transparent Optical Networks *ICTON 2012*, Coventry, UK, paper We.B1.2, July 2012

[Giacoumidis12a] E. Giacoumidis et. al, "Extensive Comparisons of Optical Fast-OFDM and Conventional Optical OFDM for Local and Access Networks," *Journal of Optical Communications and Networking*, vol. 4, no. 10, pp. 724-733, 2012

[Girard05] A. Girard, "FTTx PON Technology and Testing," *EXFO Electrical Engineering*, 2005

[Hae12] R.Y. Hae et. al, "Recent advances on node technologies in photonic networks," *Photonics Technology Letters*, vol. 24, no. 22, pp. 2064-2066, November 2012

[Hibino07] Y. Hibino et. al, "Recent advances on node technologies in photonic networks," *IEEE Photonics in Switching*, 2007

[Hillerkuss11] D. Hillerkuss, et al. "26 Tbit/s line-rate super-channel transmission utilizing all-optical fast Fourier transform processing," *Nature Photonics*, May 2011

[Huene11] J. H-Huene et. al, "Constant envelope optical OFDM for improved nonlinear and phase noise tolerance," *OFC/NFOEC*, 2011

[Hung03] W. Hung et.al, "System characterization of a robust re-modulation scheme with DPSK downstream traffic in a WDM access network," *in ECOC*, paper We.3.4.5, 2003

[Hussin13] S. Hussin et.al, "Analysis of Partial Pilot Filling Phase Noise Compensation for CO-OFDM Systems," *Photonics Technology Letters*, vol. PP, no. 99, pp. 1, April 2013

[Ho05] K.P. Ho, "Phase-Modulated Optical Communication Systems," *Springer* (New York), 2005

[IEEE 802.3ah] IEEE 802.3ah Standard: Media Access Control Parameters, Physical Layers, and Management Parameters for Subscriber Access Networks, 2004

[IEEE 802.3av] IEEE 802.3ah Standard: Physical Layer Specifications and Management Parameters for 10 Gb/s Passive Optical Networks, 2009

[Ip10] E. Ip, "Nonlinear Compensation Using Back-propagation for Polarization-Multiplexed Transmission," *Journal of Lightwave Technology*, vol. 28, no. 6, March 2010

[ITU-T G.694.1] ITU-T REC G694.1: Spectral grids for WDM applications: DWDM frequency grid, v 2.0, Feb. 2012

[ITU-T G.975.1] ITU-T Rec. G.975.1: Forward Error Correction for High Bit-Rate DWDM Submarine Systems, 2004

[ITU-T G.984.2] ITU-T Rec.G.984.2: Gigabit-Capable Passive Optical Networks (G-PON): Physical Media Dependent (PMD) Layer Specification, 2003

[ITU-T G.987.2] ITU-T G.987.2: 10G-capable PONs: Physical Media Dependent (PMD) Layer Specification, 2010

[Jan13] O. Jan et. al, "An Experiment of Coherent Optical DFT-spread OFDM with Laser Phase Noise," *in Proc. Symposium of Photonic Networks*, May 2013

[Jansen07] S. L. Jansen et. al, "16x52.5-Gb/s, 50-GHz spaced, POLMUX-COOFDM transmission over 4,160 km of SSMF enabled by MIMO processing," *the European Conference on Optical Communications*, PD1.3, 2007

[Jansen08a] S. L. Jansen et. al, "Coherent Optical 25.8-Gb/s OFDM Transmission Over 4160-km SSMF," *IEEE/OSA Journal of Lightwave Technology*, vol. 26, no. 1, pp. 6-15, January 2008

[Jansen08b] S. L. Jansen et. al, "Optical OFDM, a hype or is it for real?," *ECOC*, September 2008

[Jansen08c] S.L. Jansen et. al, "Optical OFDM – a candidate for future long haul optical transmission systems," *OFC/NFOEC*, February 2008

[Jansen08d] S.L. Jansen et. al, "10x121.9-Gb/s PDM-OFDM transmission with 2-b/s/Hz spectral efficiency over 1,000 km of SSMF," *the Optical Fiber Communication Conference*, San Diego, CA, paper PDP2, 2008

[Jansen09] S.L. Jansen et. al, "132.2 Gb/s PDM 8-QAM OFDM transmission at 4 b/s/Hz spectral efficiency," *IEEE Photonics Technology Letters*, June 2009

[Jansen09a] S.L. Jansen et. al, "Effect of Hybrid IQ Imbalance Compensation in 27.3-Gbit/s Direct-Detection OFDM Transmission," *OFC/NFOEC*, March 2009

[Jansen10] S.L. Jansen et. al, "Optical OFDM for ultra-high capacity long-haul transmission applications," *International Conference on Optical Network Design and Modeling (ONDM)*, 2010

[Jaworski07] M. Jaworski et. al, "Split-step Fourier-Method in Modeling Wavelength-Division-Multiplexed Links," in Proc. Int. Conf. Transparent Optical Networks *ICTON 2007*, paper Mo.P.13, 2007

[Jinno10] M. Jinno et. al, "Distance-adaptive spectrum resource allocation in spectrum-sliced elastic optical path network," *IEEE Communications Magazine*, vol. 48, no. 8, pp. 138-145, 2010

[Jinno12] M. Jinno et. al, "Multiflow Optical Transponder for Efficient Multilayer Optical Networking," *IEEE Communications Magazine*, pp. 56-65, 2012

[Jung09] S. P. Jung et. al, "Demonstration of RSOA-based WDM PON Employing Self-Homodyne Receiver with High Reflection Tolerance," *in OFC/NFOEC*, paper JWA69, 2009

[Kaminow97] I. P. Kaminow, and T. L. Koch (eds.) "Optical Fiber Telecommunications III A-B," *Academic Press*, San Diego, CA, 1997

[Kaneda10] N. Kaneda et. al, "Real-Time 2.5 GS/s Coherent Optical Receiver for 53.3-Gb/s Sub-Banded OFDM," *Journal of Lightwave Technology*, vol. 28, no. 4, February 2010

[Kang11] Z. Kang et. al, "Seamless Amalgamation of Full Duplex 2.5gbps Wireless and 10gbps Wired Optical Access Networks based on QAM-OFDM Technology," in Proc. of *ICCTA 2011,* October 2011

[Karaki12] J. Karaki et. al, "Frequency offset estimation in a polarization-multiplexed coherent OFDM system stressed by chromatic dispersion and PMD," *Conference on Lasers and Electro-Optics (CLEO),* May 2012

[Kawanishi02] T. Kawanishi et. al, "Electrically tunable delay line using an optical single-side-bandmodulator," *IEEE Photon. Technol. Lett.*, vol. 14, no. 10, pp. 1454–1456, Oct. 2002

[Khaleghi13] H. Khaleghi "Experimental Validation of Numerical Simulations and Performance Analysis of a Coherent Optical-OFDM Transmission System Employing a Semiconductor Optical Amplifier," *Journal of Lightwave Technology,* vol. 31, no. 1, pp. 161-170, January 2013

[Kikuchi10] K. Kikuchi "Ultra-long-haul optical transmission characteristics of wavelength-division multiplexed dual-polarisation 16-quadrature-amplitude-modulation signals," *IET Electronics Letters*, vol. 46, no. 6, pp. 433-434, June 2010

[Kikuchi10a] K. Kikuchi "Coherent Optical Communications," *Springer*, 2010

[Kobayash08] T. Kobayash et. al, "Electro-optically subcarrier multiplexed 110 Gb/s OFDM signal transmission over 80 km SMF without dispersion compensation," *Electron. Lett*., vol. 44, pp. 225–226, 2008

[Koonen08] A. M. J. Koonen, "Perspectives of radio over fiber technologies," *in Proc. Optical Fiber Communication Conference*, paper OThP3, 2008

[Koonen09] A.M.J. Koonen et. al, "Radio over fiber techniques for advanced in building networks," *ECOC*, September 2009

[Lazaro07] J. A. Lazaro, C. Arellano, V. Polo, and J. Prat "Rayleigh Scattering Reduction by Means of Optical Frequency Dithering in Passive Optical Networks With Remotely Seeded ONUs," *IEEE Photonics Technology Letters,* vol. 19, no. 1, pp. 64-66, January 2007

[Lei13] C. Lei et. al, "1-Tb/s WDM-OFDM-PON System with Subband Access Scheme and Flexible Subcarrier-Level Bandwidth Allocation," *IEEE Photonics Journal*, vol. 5, no. 1, February 2013

[Leibrich09] J. Leibrich et. al, "Impact of modulator bias on the OSNR requirement of direct detection optical OFDM," *IEEE Photonics Technology Letters*, August 2009

[Li10] A. Li et. al, "Wavelet packet transform-based OFDM for optical communications," *Journal of Lightwave Technology*, December 2010

[Li11] A. Li et. al, "Reception of Mode and Polarization Multiplexed 107-Gb/s COOFDM Signal over a Two-Mode Fiber," *OFC/NFOEC,* paper PDPB8, 2011

[Li12] C. Li et. al, "Investigation of Coherent Optical Multiband DFT-S OFDM in Long Haul Transmission," *IEEE Photonics Technology Letters*, vol. 24, no. 19, October 2012

[Lin12] C. Lin et. al, "Nonbinary LDPC-Coded Mode-Multiplexed Coherent Optical OFDM 1.28-Tbit/s 16-QAM Signal Transmission Over 2000 km of Few-Mode Fibers with Mode-Dependent Loss," *IEEE Photonics Journal*, vol. 4, no. 5, pp. 1922-1929, October 2012

[Linglong09] D. Linglong et. al, "Spectrum-Efficient Coherent Optical OFDM for Transport Networks," *IEEE Journal on Selected Areas in Communications,* vol. 31, no. 1, pp. 62-74, January 2013

[Liu10] Xu. Liu et. al, "Inline Dispersion Compensation Effect for 100gb/S PDM-CO-OFDM Long-Haul Transmission Systems," in *Proceedings of IC-NIDC2010*, 2010

[Liu11] S. Liu et. al, "A 25 Gb/s(/km^2) urban wireless network beyond IMT-advanced," *IEEE Communications Magazine*, vol. 49, no. 2, pp. 122–129, 2011

[Liu11a] X. Liu et. al, "448-Gb/s Reduced-Guard-Interval CO-OFDM Transmission Over 2000 km of Ultra-Large-Area Fiber and Five 80-GHz-Grid ROADMs," *Journal of Lightwave Technology*, vol. 29, no. 4, February 2011

[Llorente12] R. Llorente et. al, "Cost and Energy Efficient Multi-Standard OFDM Integrated Optical Access and In-Building Network Architecture," In Proc. International Conference on Transparent Optical Networks *ICTON 2012*, Coventry, UK, paper Mo.C3.1, July 2012

[Lobato12] A. Lobato et. al, "Performance comparison of single carrier and OFDM in coherent optical long-haul communication systems," in Proc. *of SPIE-OSA-IEEE*, vol. 8309, 2011

[Lowery06] A. J. Lowery et. al, "Orthogonal frequency division multiplexing for dispersion compensation of long haul optical systems," *OSA/Optics Express*, March 2006

[Ma10] Y. Ma et. al, "1-Tb/s Single-Channel Coherent Optical OFDM Transmission With Orthogonal-Band Multiplexing and Subwavelength Bandwidth Access," *Journal of Lightwave Technology*, vol. 28, no. 4, pp. 308-315, February 2010

[Madamopoulos12] N. Madamopoulos, et. al, "A fully distributed 10G-EPON-based converged fixed mobile networking transport infrastructure for next generation broadband access," *Journal of Optical Communications and Networking*, vol. 4, no. 5, pp. 366–377, 2012

[Manning94] R. J. Manning et. al, "Three-wavelength device for all-optical signal processing," *Optics Letters*, vol. 19, no. 12, pp. 889–991, Jun. 1994

[Matlab10] MATLAB, Version 7.10.0 (R2010a). The MathWorks Inc., Natick, MA, USA, 2010

[Mayrock07] M. Mayrock et. al, "OFDM in optical long haul transmission," *12th International OFDM Workshop*, August 2007

[Mehedy10] L. Mehedy et. al, "Frequency interleaved directly detected optical OFDM for next generation optical access networks," *IEEE MWP*, October 2010

[Millane94] R.P. Millane et. al, "Analytical Properties of the Hartley Transform and their Implications," in Proc. of *IEEE*, vol. 82, no 3, March 1994

[Milosavljevic11] M. Milosavljevic et. al, "Next generation PONs with wireless backhauling," in Proc. Int. Conf. Transparent Optical Networks *ICTON 2011*, paper Mo.B4.1, 2011

[Mirnia12] S.E. Mirnia et. al, "System Tolerance of NRZ-DQPSK All-Optical OFDM in Long-Haul Transmission System using DCF," in Proc. *3rd International Conference on Photonics 2012*, Penang, October 2012

[Murano08] R. Murano et. al, "Tunable 2.5 Gb/s receiver for wavelength-agile DWDM-PON," *in Proc. Optical Fiber Communication Conf.*, paper PDP32, 2008

[Nadal11] L. Nadal, M. Svaluto Moreolo, J. M. Fabrega, and G. Junyent "Comparison of peak power reduction techniques in OFDM systems based on FFT and FHT," In Proc. International Conference on Transparent Optical Networks *ICTON 2011*, Stockholm, Sweden, July 2011

[Nolle11] M. Nolle et. al, "Experimental investigation of 84-Gb/s and 112-Gb/s polarization-switched quadrature phase-shift keying signals," *Optics Express*, vol. 19, no. 26, pp. B667-672, 2011

[Omella09] M. Omella et. al, "Driving requirements for wavelength shifting in colorless ONU with dual-arm modulator," *J. Lightwave Technol.*, vol. 27, pp. 3912–3918, 2009

[Onohara11] K. Onohara et. al, " Soft-decision forward error correction for 100Gb/s digital coherent systems," *Optical Fiber Technology*, vol. 17, pp. 452-455, 2011

[Othman11] M. Othman et. al, "MIMOOFDMWDM PON with DM-VCSEL for femtocells application," *Optics Express*, vol. 19, no. 26, pp. B537–B542, 2011

[Painchaud09] Y. Painchaud et. al, "Performance of balanced detection in a coherent receiver," *Optics Express*, vol. 17, no. 5, pp. 3659-3672, 2009

[Papoulis02] A. Papoulis et. al, "Probability, Random Variables and Stochastic Processes," *McGraw-Hill*, 2002

[Pataca10] D. M. Pataca, et. al, "Transmission of a 20 Gb/s NRZ OOK Signal Throughout a 390 km Fiber Link and a Cascade of 11 x 50 GHz Filters and 9 x EDFAs," *Journal of Microwaves, Optoelectronics and Electromagnetic Applications*, vol. 10, no. 1, June 2011

[Peng08] W.R. Peng et. al, "The limit of transmission distance for an inter-symbol-interference-free optical OFDM system," *OFC/NFOEC*, February 2008

[Peng09] W.R. Peng et. al, "Theoretical and experimental investigations of direct detected RF tone assisted optical OFDM systems," *IEEE Photonics technology Letters*, May 2009

[Plant12] D.V. Plant et. al, "Optimal Design of Dispersion Filter for Time-Domain Split-step Simulation of Pulse Propagation in Optical Fiber," *Journal of Lightwave Technology*, vol. 30, no. 10, pp. 1405-1421, May 2012

[Proakis89] J. G. Proakis, "Digital Communications," *Prentice Hall*, 1989

[Puntsri13] K. Puntsri et. al, "Theoretical and experimental investigations of direct detected RF tone assisted optical OFDM systems," *in Proc. Symposium of Photonic Networks*, May 2013

[Qi09] Y. Qi et. al, "Experimental Demonstration and Numerical Simulation of 107-Gb/s High Spectral Efficiency Coherent Optical OFDM," *Journal of Lightwave Technology*, vol. 27, no. 3, pp. 168-176, February 2009

[Qian08] D. Qian et. al, "11.5 Gb/s OFDM transmission over 640km SSMF using directly modulated laser," *ECOC*, September 2008

[Qian09] D. Qian et. al, "Optical OFDM transmission in metro/access networks," *OFC/NFOEC*, 2009

[Qiao10] Y. Qiao et. al, "Fiber Nonlinearity Post-compensation via Spectral Inversion for 40Gb/s Long-haul CO-OFDM System," *IEEE-OSA*, 2010

[Qiu11] K. Qiu et. al, "OFDM-PON Optical Fiber Access Technologies," *Proc. SPIE-OSA-IEEE*, vol. 8309, 2011

[Qunbi13] Z. Qunbi et. al, "Experimental Study of the Intra-Channel Nonlinearity Influence on Single-Band 100G Coherent Optical OFDM Systems," *Photonics Technology Letters*, vol. 26, no. 6, pp. 553-555, January 2013

[Qunbi13a] Z. Qunbi et. al, "Low Overhead Intra-Symbol Carrier Phase Recovery for Reduced-Guard-Interval CO-OFDM," *Journal of Lightwave Technology*, vol. 31, no. 8, pp. 1158-1169, April 2013

[Raharimanitra11] F. Raharimanitra et. al, “40 Gb/s NG-PON system using low electrical bandwidth tunable receiver and emitter at 10 Gb/s,” *in Proc. European Conf. Optical Communications (ECOC)*, paper Mo.1.C.2, 2011

[Ramirez12] http://www.slideshare.net/fernandomireles/multi-carrier-modulation-and-single-carrier-modulation

[Roerich13] D. Roerich et. al, “Optimal Modulation Index of the Mach-Zehnder Modulator in a Coherent Optical OFDM System Employing Digital Predistortion,” *in Proc. Symposium of Photonic Networks*, May 2013

[Rosenkranz09] W. Rosenkranz et. al, “Orthogonal frequency division multiplexing (OFDM) in optical communications with direct detection for metro networks,” *ICTON 2009*, July 2009

[Roudas02] I. Roudas et. al, “Accurate Modeling of Optical Multiplexer/Demultiplexer Concatenation in Transparent Multiwavelength Optical Networks,” *IEEE/OSA Journal of Lightwave Technology*, vol. 20, no. 6, pp. 921-936, 2002

[Rushdi07] A. Rushdi et. al, “PAPR reduction in trigonometric-based OFDM systems,” *IEEE*, 2007

[S7500] S7500 Tunable Laser Datasheet, Finisar, 2011

[Sano09] A. Sano et. al, “Long haul WDM transmission using no-guard-interval coherent optical OFDM”, *ECOC*, September 2009

[Savchenkov09] A. A. Savchenkov et. al, “Tunable optical single-sideband modulator with complete sideband suppression,” *Optics Letters*, vol. 34, no. 9, pp. 1300–1302, May 2009

[Savory08] S. Savory et. al, “Digital filters for coherent optical receivers,” *Optics Express*, vol. 16, no. 2, pp. 804-817, 2008

[Schmidt08] B. Schmidt et. al, “Experimental demonstrations of electronic dispersion compensation for long haul transmission using direct detection optical OFDM,” *Journal of Lightwave Technology*, January 2008

[Schrenk11] B. Schrenk et. al, “SOA/REAM as Vector Modulator for QAM Upstream,” *in OFC/NFOEC*, paper OThK, 2011

[Schwartz66] M. Schwartz et. al, “Communication Systems and Techniques,” *McGraw-Hill*, 1966

[Segel11a] J. Segel et. al, “Alcatel-Lucent LightRadio Portfolio: White Paper 1. Technical Overview,” p. 16, 2011

[Segel11b] J. Segel et. al, “Alcatel-Lucent LightRadio Portfolio: White Paper 3. Customer Solutions,” p. 17, 2011

[Seimetz09] M. Seimetz, “High-Order Modulation for Optical Fiber Transmission,” *Springer*, 2009

[Shen07] G. Shen et. al,, “Translucent optical networks: the way forward,” *IEEE Commun. Magazine*, February 2007

[Shieh07] W. Shieh et. al, “Transmission experiment of multi-gigabit coherent optical OFDM systems over 1000 km SSMF fibre,”*Electron. Lett*., vol. 43, pp. 183–185, 2007

[Shieh08] W. Shieh et. al, “Coherent optical OFDM: theory and design,” *Optics Express*, January 2008

[Shieh08a] W. Shieh et. al, "107 Gb/s coherent optical OFDM transmission over 1000-km SSMF fiber using orthogonal band multiplexing," *Opt. Exp*., vol. 16, pp. 6378–6386, 2008

[Shieh09] W. Shieh, "High spectral efficiency coherent optical OFDM for 1 Tb/s ethernet transport," *the Optical Fiber Communication Conference*, San Diego, CA, paper OWW1, 2009

[Shieh10] W. Shieh and I. Djordjevic, "OFDM for Optical Communications", *Elsevier*, 2010

[Soliman09] N.F. Soliman et. al, "Peak power reduction of OFDM signals using trigonometric transforms," *ICCES*, December 2009

[Sorensen85] H.V. Sorensen et. al, "On Computing the Discrete Hartley Transform," *IEEE Transactions on Acoustics, Speech, and Signal Processing*, vol. 33, vo 4, October 1985

[Silva10] J.A.L. Silva et. al, "Experimental demonstration of a direct detection constant envelope OFDM system," *OSA/SPPCom*, 2010

[Simon00] M.K. Simon et. al, "Digital Communications over Fading Channel," *John Wiley & Sons*, 2000

[Svaluto08] M. Svaluto Moreolo et. al, "Fiber optics transforms," *ICTON 2008*, June 2008

[Svaluto10] M. Svaluto Moreolo et. al, "Novel power efficient optical OFDM based on Hartley Transform for intensity-modulated direct detection systems," *Journal of Lightwave Technology*, March 2010

[Svaluto11] M. Svaluto Moreolo et. al, "Performance analysis of DHT-based optical OFDM using large-size constellations in AWGN ", *IEEE Communications Letters*, May 2011

[Svaluto12] M. Svaluto Moreolo et. al, "Experimental demonstration of a cost-effective bit rate variable IM/DD optical OFDM with reduced guard band," *Optics Express,* vol. 20, is 26, pp. B159-B164, 2012

[Tang09] Y. Tang et. al, "Coherent Optical OFDM Transmission Up to 1 Tb/s per Channel," *Journal of Lightwave Technology*, vol. 27, no. 16, August 15, 2009

[Thompson05] S.C. Thompson et. al, "Constant envelope OFDM phase modulation," *PhD dissertation*, UCSD, San Diego, 2005

[Thompson08] S.C. Thompson et. al, "Constant envelope OFDM," *IEEE Transactions On Communications*, August 2008

[VanDeventer96] M. O. van Deventer, "Fundamentals of Bidirectional Transmission over a Single Optical Fibre," *Kluwer academic press*, 1996

[Wang00] C.L. Wang et. al, "Discrete Hartley Transform based Multicarrier Modulation," in Proc. of *IEEE ICASSP 2000*, vol. 5, pp. 2513-2516, 2000

[Wang05] D. Wang et. al, "A Novel DHT-based Ultra-Wideband System," in Proc. of *IEEE ISCIT*, 2005

[Wei10] J. L. Wei et. al, "Wavelength reused bidirectional transmission of adaptively modulated optical OFDM signals in WDM-PONs incorporating SOA and RSOA intensity modulators," *Optics Express*, vol. 18, no. 10, p. 9791, Apr. 2010

[Weisstein] E.W. Weisstein et. al, "Inverse Tangent, MathWorld-A Wolfram Web Resource," http://mathworld.wolfram.com/InverseTangent.html

[wiki12] http://en.wikipedia.org/wiki/Electro-optic_modulator

[Wu10] Z. Wu et. al, "Phase Modulated Coherent Optical OFDM by Phase Restoration of Optical Field," *IEEE topical meeting in Microwave Photonics*, September 2010

[Xiao12] X. Xiao et. al, "A 240 Gb/s self-coherent CO-OFDM transmission applying real-time reception over 48 KM SSMF," *Photonics Global Conference (PGC)*, December 2012

[Zhang11] L. Zhang et. al, "A Novel MAMSK-OFDM Technology for Next-Generation Optical Access Networks," *Photonics Technology Letters*, vol. 23, no. 1, pp. 60-62, January 2011

[Zhang13] S. Zhang et. al, "Transoceanic Transmission of 40 117.6 Gb/s PDM-OFDM-16QAM Over Hybrid Large-Core/Ultralow-Loss Fiber," *Journal of Lightwave Technology*, vol. 31, no 4, pp. 498-505, February 2012

[Zhanyu12] Y. Zhanyu et. al, "Constant Envelop Minimum-Shift Keying OFDM Coherent Optical Communication System," *Journal of Lightwave Technology*, vol. 30, no 23, pp. 3627-3632, December 2012

[Zhao10] J. Zhao et. al, "A novel optical fast OFDM with reduced channel spacing equal to half of the symbol rate per carrier," *OFC/NFOEC*, February 2010

[Zhou12] X. Zhou et. al, "A simple and efficient frequency offset estimation algorithm for high-speed coherent optical OFDM systems," *Optics Express*, vol. 20, no. 7, March 2012

[Zhu05] N.H. Zhu et. al, "Extraction of intrinsic response from s-parameters of laser diodes," *IEEE Photonics Technology Letters*, vol. 17, no. 4, April 2005

[Zwillinger95] D. Zwillinger et. al, "Inverse Circular Functions in CRC Standard Mathematical Tables and Formulae," *Boca Raton, FL: CRC Press*, pp. 465-467, 1995